INFORMATION TO USERS

This manuscript has been reproduced from the microfilm master. UMI films the text directly from the original or copy submitted. Thus, some thesis and dissertation copies are in typewriter face, while others may be from any type of computer printer.

The quality of this reproduction is dependent upon the quality of the copy submitted. Broken or indistinct print, colored or poor quality illustrations and photographs, print bleedthrough, substandard margins, and improper alignment can adversely affect reproduction.

In the unlikely event that the author did not send UMI a complete manuscript and there are missing pages, these will be noted. Also, if unauthorized copyright material had to be removed, a note will indicate the deletion.

Oversize materials (e.g., maps, drawings, charts) are reproduced by sectioning the original, beginning at the upper left-hand corner and continuing from left to right in equal sections with small overlaps.

ProQuest Information and Learning
300 North Zeeb Road, Ann Arbor, MI 48106-1346 USA
800-521-0600

SC

RECTANGULAR PRESTRESSED CONCRETE SECTIONS UNDER SHORT TERM LOADING OF COMBINED BENDING AND AXIAL THRUST.

by

SYED IMTIAZ RASUL

A thesis submitted to the Faculty of Graduate Studies, University of Ottawa, in partial fulfillment of the requirement for the degree of Master of Applied Science in Civil Engineering.

OTTAWA, ONTARIO,

CANADA

November, 1969

TABLE OF CONTENTS

SYNOPSIS

Both experimental and analytical investigation of fifty five partially prestressed concrete rectangular specimens under the combined action of bending moment and axial thrust were carried out. Tests were conducted under short term loading. Sectional dimensions of the specimens, concrete mix design and stress in the prestressing tendons have been kept constant. The variables were the amount and arrangement of longitudinal steel and total prestressing force.

These fifty five specimens were divided into eleven series of five specimens each. Five of these series, PC1 to PC5 were symmetrically prestressed; the steel ratio, A_s/bd varied from .0191 to .0066. The remaining six series, PB1 to PB6 were unsymmetrically prestressed with the steel ratio varying from .0136 to .0033. Each of the five specimens within a series has been tested to failure under different transverse loads - the axial load ranged from 0 to 95 kips. Three 6 in. x 12 in. control cylinders and two 3 in. x 3 in. x 12 in. control prisms have been used to determine the concrete strength, the initial tangent modulus of elasticity and the dynamic modulus of elasticity of the concrete for each series.

Analytical expressions for ultimate load, moment and curvature have been derived from the fundamental relations of equilibrium of forces, moments and compatibility of strains. A computer programme

was used to calculate the moment-axial thrust interactions and the eccentricity-curvature relationship at ultimate load. These results have been presented in graphical form.

From the experimental work, moment-curvature and transverse load-deflection at midspan relations have been plotted. Correlation of experimental and analytical values of moment and curvature at ultimate load has been good.

LIST OF FIGURES

FIGURES

FIGURES

LIST OF TABLES

LIST OF PHOTOGRAPHIC PLATES

LIST OF FLOW CHARTS

CHAPTER 1

INTRODUCTION

1.1 GENERAL:

Beam-columns are structural members subjected to the combined action of flexural and axial loading. Columns in multi storey buildings are usually eccentrically loaded due to unequal live load distribution as well as wind or earthquake forces. They are therefore acted upon by bending moments in addition to axial thrust. Since plain concrete has very little tensile strength, concrete columns are usually reinforced with steel bars. These bars become effective when the concrete cracks in tension. But for structural safety, fire-proofing or sometimes for aesthetic reasons, these cracks have to be eliminated. Concrete columns prestressed with high tensile steel reinforcement provide a solution. They have the advantages noted:

(i) It may increase the ultimate load carrying capacity of eccentrically loaded sections.

(ii) For precast columns subjected to transportation and erection stresses, prestressing supplies a higher resistance to cracking during handling.

(iii) Prestressing eliminates cracks. These sections therefore have better fire and corrosion resistance. Should the section becomes cracked due to over-loading, the cracks will disappear as soon as this over-load is removed.

(iv) Prestressing yields a homogeneous member with a reliable buckling capacity. This is important for slender columns.

(v) Prestressed sections are usually smaller in cross-section as compared to reinforced concrete. This results in a saving of material and also is aesthetically more pleasing.

1.2 OBJECT:

The strength and deformation characteristics of rectangular prestressed concrete beam-column sections under combinations of axial and transverse loads were the principal objects of this investigation. Both analytical and experimental study have been undertaken. Specific problems treated were the moment - curvature relationship, the load-deflection characteristics, the moment-axial thrust interaction behaviour and the variation of curvature at ultimate load with eccentricity. Short term loading has been used.

Fifty five beam-columns, each 6 in. x 8 in. in cross section, 62 in. long and prestressed by high tensile strands were tested to failure. Sectional dimensions of the specimens, concrete mix design and stress in the prestressing tendons were kept constant. Variables used were amount and position of longitudinal reinforcements and amount of total prestressing forces. These fifty five specimens were divided into eleven series. Five series were symmetrically prestressed and the remaining six series were unsymmetrically prestressed. Each specimen within a particular series was tested to failure under transverse load. The axial load level was varied

from zero to 95 kips. At each transverse load increment, the moment-curvature and the load-deflection relations were computed.

From the equilibrium of forces and moments and the compatibility of strains, analytical expressions have been developed for the ultimate load, moment and curvature. Ultimate load capacity and ductility of symmetrically and unsymmetrically prestressed sections have been compared. Also the effect of reinforcement area on these properties have been studied. The influence of ultimate strain of concrete on the ductility of members has been investigated. Finally, analytical and experimental results have been compared.

1.3 EARLIER INVESTIGATIONS:

(a) Reinforced concrete beam columns:

The reinforced concrete beam-column members are compressed by external forces. The prestressed concrete beam-columns are subjected to internal compressive force in addition to external compressive force. It is expected that the strength and deformational characteristics of the reinforced concrete and the prestressed concrete beam-column members will be similar. Most of the investigators in prestressed concrete beam-columns have used Jensen or Hognestad stress-blocks as used in the reinforced concrete beam-columns. Earlier investigations in reinforced concrete beam-columns have therefore been included here.

An earlier study of rectangular reinforced concrete sections failing in tension under combined bending and axial load was carried

out by the Structural Bureau of Portland Cement Association[1]* using Jensen's[2] basic assumptions of ultimate strength analysis.

Whitney[3,4] developed semi-empirical formulae for the ultimate load of rectangular reinforced concrete sections failing in compression under combined bending and axial load. He had assumed that there is always sufficient reinforcement to prevent tension failure. Taking moments about the tension reinforcement, he obtained:

$$P = \frac{2A'_s f'_{yp}}{\frac{2e}{d'} - 1} - \frac{bt f'_c}{\frac{3te}{d^2} - \frac{6dt - 3t^2}{2d^2}}$$

where P = axial load

A'_s = area of compression reinforcement

f'_{yp} = yield stress of compression reinforcement

e = eccentricity of load from centroidal axis

b = width of section

t = total depth of section

f'_c = compression strength of 6 in x 12 in cylinder

d = distance from centroid of tension reinforcement to the compression edge

d' = distance between centroid of tension and compression steel.

For tensile failure of rectangular reinforced concrete sections, Whitney assumed rectangular stress block and developed expressions for ultimate load and moment. Whitney also deduced

---

* Numbers in parentheses refer to References in Appendix.

equations for rectangular and cylindrical columns with round cores on semi empirical basis. His deductions in general gave quite good agreement with experimental values.

Eivind Hognestad[5] did detailed investigation on reinforced concrete members subjected to combined bending and axial load. He introduced assumed stress-strain diagram for concrete in flexure which comprises of initial parabolic and then straight line variation. This stress-strain relationship seems to agree fairly well with experimental studies and has been used quite frequently by later investigators. For the initial tangent modulus of elasticity of concrete, he used Inge-Lyse's equation:

$$E_c = 1800000 + 460\, f'_c \qquad \text{where } f'_c \text{ is in psi.}$$

Hognestad found that a constant average value of 0.0038 in/in was quite satisfactory as the ultimate strain for the concrete he had used. He had neglected tensile strength of concrete and assumed that there was no slip in between concrete and reinforcement and that Bernoulli-Navier hypothesis of linear distribution of strain was found reasonably accurate. His study covered both rectangular and circular eccentrically loaded reinforced concrete columns. Considering the equilibrium of forces and moments, he developed basic expressions for ultimate load of eccentrically loaded columns failing in the modes of tension failure, compression failure and balanced failure. Tests were conducted at the University of Illinois on 120

reinforced concrete columns of which 90 were square tied columns and 30 were cylindrical spiral columns. Main variables used were amount of reinforcement, quality of concrete and eccentricity of load. His experimental values seem to agree reasonably well with theoretical predictions.

Ernst, Hromadik and Riveland[6] in 1953 obtained expressions for axial thrust, bending moment and rotations for hinged reinforced concrete columns using assumed stress-strain relationship of concrete and steel. Hognestad stress-block for concrete with 0.0038 ultimate strain and elasti-plastic stress-strain relation of steel was used. Deflection of column was determined from Cosine wave assumption proposed by Westergard and Osgood.[7]

In 1958, Broms and Viest[8,9] obtained analytical solutions for strength and deformation characteristics of both hinged and restrained columns. They used Hognestad stress-block of concrete with 0.0038 ultimate strain and elastic-plastic stress-strain relationship of steel. Restraining moments produced by the adjoining members were assumed proportional to the end rotations of columns. Their recommendation formed the basis of 1963 ACI Code on eccentrically loaded reinforced concrete columns.

At the University of Illinois, an analytical study of ultimate strength and behaviour of restrained and unrestrained reinforced concrete columns under combined bending and axial thrust was undertaken by Pfrang and Siess[10,11]. The column and its adjoining members were supposedly removed from actual structure and then

by reasonable assumptions and selection of a realistic model, laboratory testing conditions were simulated. Unlike previous investigators, their method of analysis did not include any predetermined shape of deflected column and did not require extensive simplifying assumptions as to the character of the structural system or the cross-sectional properties of the members. Numerical solutions for three hundred specific cases were obtained using a computer program. The variables investigated were slenderness ratio, ratio of maximum end eccentricity to depth of column, ratio of maximum to minimum end eccentricity, degree of end restraint and percentage of reinforcement. Hognestad stress block for concrete with 0.004 ultimate strain, elasti-plastic stress-strain relationship of steel, restraining moments produced by the adjoining members and numerical integration procedure were used to determine the lateral deflection of columns. From this study they concluded that increasing the coefficient of end restraint always increases capacity of a given column. Decreasing the ratio of end eccentricities effectively increases the stiffness of column. Increasing eccentricity of load decreases column capacity and the slenderness ratio is quite significant in determining the ultimate capacity of restrained and unrestrained columns.

(b) Prestressed concrete beam-columns:

An early investigation of prestressed-concrete columns under axial load was made by Breckenridge[12] at the University of Southern California in 1953.

The object of his investigation was to determine the effect of prestressing on the ultimate superimposed axial load of long columns and the loss of prestress due to the superimposed load. The column sizes used in his tests were $1\frac{5}{8}$ in x 2 in and 3 in x 3 in in cross-section. Nine of the columns were post tensioned and one pretensioned, all with 1 - 1/4" dia wire. The h/r ratio varied from 24.4 to 44.9 where h is the length and r is the minimum dimension of the specimen. Electrical resistance strain gages were installed on the four faces of the columns at mid height to measure the strain produced by the superimposed load. The loss of prestress was obtained from another gauge installed on the prestressing wire. Based on these tests,an expression was derived for the loss of prestress due to superimposed axial load. Formulae for the stresses in an axially prestressed and eccentrically loaded column were developed. It was concluded that prestressing with a single unbonded concentrically placed tendon had no effect on the critical superimposed load.

At the University of Florida, Ozell and Jernigan[13] conducted tests on 41 full size prestressed concrete columns and 6 reinforced concrete columns. Nominal column sizes were 7-3/4" x 7-3/4" and 6" x 6". There were 16 groups determined by the h/r ratio and the amount of reinforcement. The prestressed concrete columns were pretensioned with the percentage of steel varying from 0.53 to 2.50. The slenderness ratio ranged from 10 to 32. Based on these test results, the authors obtained an empirical formula for the ultimate load capacity of prestressed concrete columns. Theoretical studies

were made of the initial curvature of columns as computed from the test results. It was observed that in the columns tested, the maximum initial curvature was about h/417. Lateral ties were found to have a beneficial effect on the lateral buckling of these columns. The optimum value of p, ratio of reinforcement area to the area of concrete, for h/r ratios of 20 and 30 was found to be 1.25 percent for the type of wire used. Under axial load, the prestressed concrete columns with h/r ratio of 20 had a lower ultimate strength than reinforced concrete columns. But for h/r ratio of 30, prestressed and reinforced concrete columns had the same strength.

Paul Zia[14] at the University of Florida made a theoretical investigation of the ultimate strength of slender prestressed concrete columns. Analytical expressions for the stress distribution and the plastic equilibrium at the ultimate load by means of Jensen's hypothesis were developed. Since the expressions were mathematically complicated, the author prepared a set of curves to facilitate the analysis. His results compared favourably with the experimental results obtained by Ozell and Jernigan[13]. It was observed that for h/r less than 25, prestressing penalizes the strength of column. Optimum prestressing for h/r between 25 and 35 appeared to be between p = 0.5 percent to p = 1 percent. Too little prestressing was detrimental to the flexural resistance of the column whereas too much prestressing reduced the axial load carrying capacity.

At the University of California, Berkeley, Lin and his associates have conducted both analytical and experimental investiga-

tions of prestressed concrete columns under eccentric loading. In 1957, Lin and Itaya[15,16] tested a single prestressed concrete column under eccentric loading as a demonstration for delegates to World Conference on Prestressed Concrete. The column was a 16 in. octagonal shaped cross-section, 25 ft. long and was prestressed by 13 - 3/8 in. dia 7 wire strands. Spiral ties were used. Elasti-plastic stress-strain relation of steel and Jensen's stress-block for concrete were used. The elastic and plastic behaviour of the column were determined both experimentally as well as analytically.

Lee[17] applied the simplified Von Karman's theory[18] for eccentrically loaded columns and Jensen's stress-strain relationship of concrete to partially prestressed concrete columns with end restraint. Elasti-plastic stress-strain curve of steel was used and it was assumed that prestressed concrete was capable of taking tensile stress of upto 0.12 f_c' .

Lin and Lakhwara[19] investigated the elastic and plastic behaviour of two partially prestressed concrete columns under eccentric load. Both analytical and experimental study was done and the results were compared. The columns were 6 in. x 6 in. and 10 ft. long. 4-1/2 in dia mild steel bars at the four corners were used. The columns were centrally post-tensioned by 1-5/8" dia high tensile bar. The two columns were tested to failure by loading with end eccentricities of 2 in. and 3 in. The elastic analysis was found to be satisfactory upto the cracking load and thereafter a plastic analysis was used.

Harold Tai[20] developed expressions for the ultimate analysis of partially prestressed concrete columns under eccentric load. A computer solution was achieved. Two different column sections were used. One column section was 6 in. x 6 in. with $A_s = 0.8$ sq.in., $A_{sp} = 0.306$ sq.in. and $P_p = 34884$ lbs. The second column section was 12 in. x 12 in. with $A_s = 1.76$ sq.in., $A_{sp} = 0.5752$ sq.in. and $P_p = 86280$ lbs. Both these columns were concentrically prestressed and eccentricity ratios of load were 1/12 and 8/12 .

Sandrini[21] developed a computer solution for partially prestressed concrete columns under eccentric load. Strength and deformational characteristics of eccentrically loaded partially prestressed concrete columns were investigated. A modified form of Jensen's stress block with the ultimate compressive strain of 0.003 for concrete was used. Results were compared with Lin and Lakhwara's experimental values and good agreement was obtained.

Zia and Moreadith[22] conducted an analytical investigation of the load carrying capacity of rectangular prestressed concrete columns with hinged ends. The effect of concrete strength, steel percentage, slenderness ratio and eccentricity on the strength of columns were investigated. On the basis of results, a simple design procedure was proposed.

Zia and Guillermo[23,24] investigated the influence of the variation of column cross-section, amount and location of prestressing reinforcement and concrete strength on the ultimate strength of

prestressed concrete columns under combined bending and axial thrust. Nine widely different AASHO-PCI pile sections with slight modifications were analysed. Dimensionless interaction diagrams were found to resemble those of reinforced concrete sections, but the mode of failure was different.

At the University of Melbourne and later on at the University of California, Berkeley, Aroni[25] conducted analytical and experimental investigations of the behaviour of slender prestressed concrete columns under eccentric load. A total of 36 slender eccentrically loaded, hinged, axially prestressed concrete columns were tested. The variables studied were eccentricity, slenderness and prestress. Columns were 2.02 in. x 3 in. in cross section and pretensioned by 4 high tensile steel wires of 0.198 in. diameter. The analytical solution was based on the cotangency criterion, the finite element technique and the successive approximation method.

Thirty prestressed concrete columns were tested by Brown and Hall[26,27] at the University of New South Wales, Australia. The main variables examined were the degree of prestress and the eccentricity of the loading. Five different degrees of prestress ranging from zero to a little above 0.5 f'_c were used. Eccentricity ratios were varied from 0 to 2. From the results obtained, it was observed that for axially loaded columns with slenderness ratio of about 33, small prestress of up to 0.3 f'_c would decrease load carrying capacity. But for large eccentricities, the presence of prestress affects the capacity of a column only slightly. Capacity

of columns were increased by large prestress of up to 0.6 f'_c .

Kabaila and Hall[28] presented a computer analysis of rectangular, symmetrically reinforced unrestrained prestressed concrete columns. Continuous stress-strain relationship of concrete as proposed by Rusch[29] has been used. The analytical results were compared with Brown and Hall's experimental values. The accuracy and range of validity of two other approximate analyses were also discussed.

At the University of London, U.K., K.J. Brown[30] developed a theoretical inelastic analysis to determine the ultimate load carrying capacity of hinged prestressed concrete columns under short term loading. This study included the effects of slenderness ratio, magnitude and position of prestress and eccentricity of load.

Tests of earlier investigators have been mainly confined to the concentric prestressing[19,20,23,24]. The important variables studied were the amount of prestress, the eccentricity of load and the slenderness ratio. Lin and his associates[19,20] have mainly used a single concentric tendon with varying amounts of prestress. Additional mild steel bars were used at the four corners of the beam-column sections. Nine widely different AASHO-PCI pile sections under concentric prestress were investigated by Zia and Guillermo[23,24]. Buckling of the slender prestressed concrete beam-column sections were studied by Zia and Moreadith[22] and also by Kabaila and Hall[28]. Using Jensen stress-block, Tai[20] obtained analytical values of the ultimate load of rectangular prestress concrete beam-column

sections under concentric prestress. But his results differed by 25% from the experimental values of Lakhwara[19] . Sandrini[21] modified the value of ultimate strain of concrete in Jensen stress-block to get better correlation with experimental results. Lee[17] has concluded that the Hognestad stress-block gives a better approximation of the actual stress-strain relationship of concrete.

In the test series reported here, a comparative study of the merits and demerits of a wide range of concentric and eccentric prestressing has been done. The amount of longitudinal steel reinforcement has been varied from 0.1598 sq.in. to 0.9186 sq.in. The eccentricity of the load ranged from 0 to 27 inches. The sectional dimensions of the specimens, the concrete mix design and the prestressing stress in the tendons have been kept constant.

1.4 IMPORTANCE OF STUDY:

Compression members in most of the concrete structures as well as some flexural members may be subjected to combined bending and axial thrust due to unsymmetrical loading, wind or earthquake forces. A thorough investigation of the strength and deformational characteristics of compression members under combined bending and axial thrust is therefore needed.

Although the ultimate strength of prestressed concrete sections under concentric load as well as combined bending and axial thrust have been investigated both experimentally and analytically,

comparatively little work has been done to verify rotations at ultimate load. In the limit analysis of concrete structures, rotation capacity of the hinging sections are important for complete redistribution of moments.

Moment-axial load interaction diagrams can be quite conveniently used to investigate ultimate load capacity and mode of behaviour for material failure of beam-column sections. Any combination of load and moment inside the interaction envelope may be considered as less than ultimate capacity. Thus the interaction diagram represents ultimate capacities for material failure under short term loading. Loads higher than balanced load, P_b would initiate failure in compression mode; whereas loads lower than P_b would lead to tension mode failure. In the compression mode, either compression hinge or compressive hinge may occur. In the compression hinge, both tensile and compressive stresses are present in the section. In compressive hinge only compressive stresses are present throughout the section It is however quite important to find out whether compression and compressive hinges are admissible for beam-column sections and if not, how to prevent their occurrence.

Limit analysis of concrete structures allow redistribution of moment among the different hinging sections in a structure at high loads. But redistribution of moments is controlled by rotation capacity of the different hinges. In case of reinforced and prestressed concrete, the ultimate compressive strain, ε_u may range

from 0.003 to 0.007. Hinge rotation therefore must be limited to a certain range in order to avoid excessive flexural cracking and deflections. An attempt has been made in this thesis to derive analytical expressions for rotations at ultimate load for the different types of hinges occuring in prestressed concrete beam-column members. A number of factors might influence curvature at ultimate load in prestressed concrete beam-column sections— the ultimate concrete stress and strain, the yield stresses of reinforcement, the amount and position of longitudinal reinforcement, the amount of stirrups, the cross-sectional dimensions, bending moment, axial thrust, the amount and position of precompression. Some of these variables have been studied in this investigation to find out their influence on rotational ductility.

1.5 ACKNOWLEDGEMENTS:

The tests were performed in the Structures Laboratory of the Civil Engineering Department, University of Ottawa. To his supervisor, Professor Carl Berwanger, the writer expresses his sincere gratitude for suggesting the problem and for his guidance during the project. The research was made possible through funds held by Professor Carl Berwanger as grantee of the National Research Council of Canada. Funds were used to obtain equipment and also to employ summer students to assist with the experimental work. A part of the cost of the specimens was covered by the Civil Engineering Department

of the University of Ottawa.

To his fellow graduate student, Ronald Ernest Brown, the writer extends his warm appreciation for cooperation and assistance. Messrs. Paul Moreau, Dennis Mackinnon and Jean Poirier assisted with the experimental work; their help is sincerely acknowledged. Mention must also be made of the generous facilities of the Computing Centre of the University of Ottawa.

Finally, the writer wishes to thank the Ministry of Education, Government of Pakistan, the Canadian International Development Agency and the Canadian Commonwealth Scholarship and Fellowship Committee for nominating and sponsoring him for this study.

1.6 NOTATION:

Symbols have been defined where they first appeared in this thesis. However, in this chapter, all the symbols have been arranged in the alphabetical order for ready reference.

a	=	depth of stress block
A_s	=	area of steel reinforcement
A_{s1}, A_{s2}	=	area of first and second layer of compression reinforcement
A_{s3}, A_{s4}	=	area of first and second layer of tension reinforcement
A'_s	=	area of compression reinforcement
b	=	width of specimen
CC	=	cover to the first layer of compression reinforcement
CT, k_b	=	cover to the first layer of tension reinforcement

C_M = moment contributed by concrete

C_U = compressive force in concrete

d = distance of centroid of first layer of tension reinforcement from the extreme compression edge of the specimen

d' = distance between centroid of tension and compression reinforcement

e = eccentricity of the load from the centroidal axis of the section

E_c = initial modulus of elasticity of concrete

E_d = resonance modulus of elasticity of concrete

E_s = modulus of elasticity of prestressing tendons

f'_c = compressive strength of concrete from cylinder test

f_{sp} = prestressing stress in the tendons

f_{su} = steel stress at ultimate load

f_{sy} = yield stress of prestressing tendons

f'_{yp} = yield stress of compression reinforcement

h = actual length of specimen

HC = distance between first and second layer of compression steel

HT = distance between first and second layer of tension steel

k_1, k_2, k_3 = stress block parameters

M_b = ultimate moment at balanced failure

M_o = ultimate moment at zero axial load

M_p = plastic moment capacity

M_u = ultimate moment

M_y = moment at the commencement of yielding of tensile steel

P = load

P_{Axial} = axial load

P_b = axial load at balanced failure

P_u = ultimate axial load

P_1 = A_{s1}/bd

P_2 = A_{s2}/bd

P_3 = A_{s3}/bd

P_4 = A_{s4}/bd

q_u = $p\, f_{su}/f'_c$ (tension reinforcement index)

r = minimum dimension of the section

R_1d, R_2d, R_3d, R_4d = section parameter

t = total depth of section

T_M = moment contributed by the steel

T_U = total force contributed by the steel

T_1, T_2, T_3, T_4 = forces at different layer of steel

$\varepsilon_1, \varepsilon_2, \varepsilon_3, \varepsilon_4$ = strain in the different layers of steel

ε_{cu} = concrete strain at the level of tension steel

ε_{st} = strain in steel

ε_u = ultimate strain in concrete

ϕ_o = ultimate curvature at zero axial load

ϕ_u = ultimate curvature

θ_o = unit rotation at the commencement of yielding of steel

θ_p = total concentrated rotation at the yielding section

θ_u = unit rotation

CHAPTER 2

INELASTIC BEHAVIOUR OF CONCRETE AND STEEL

2.1 INELASTIC BEHAVIOUR OF REINFORCED AND PRESTRESSED CONCRETE MEMBERS:

Ever since the publication of notes by M. Koenen,authors have argued that classical elastic theory does not clearly guarantee safety and economy of reinforced and prestressed concrete sections. The consideration of the inelastic character of concrete near ultimate load is therefore necessary. The basic assumptions of these writers may be summarised as follows:

(a) Distribution and magnitude of concrete compressive stresses.

(b) Ultimate strain of concrete or limiting depth of neutral axis.

(c) Tensile stresses in concrete may be ignored.

(d) Bernoulli-Navier hypothesis of linear distribution of strain.

(e) Absence of slip between concrete and steel, that is, perfect bond.

(f) Stress-strain relationship of steel.

Most of the earlier investigators have assumed that concrete does not resist tension, that Bernoulli's hypothesis is valid and that there is perfect bond between concrete and steel. Hognestad[5,32,33] has summarised the results of these earlier investigators in his assumptions for an analytical solution of eccentrically loaded reinforced concrete columns. In June 1963, American Concrete Institute[34] published Building Code Requirements for Reinforced Concrete which confirmed the inelastic analysis in the ultimate strength design of reinforced and prestressed concrete members.

To illustrate the extent to which quantitative expression of inelastic concrete stress distribution is of importance for practical design purposes, the basic equations for flexural strength of the rectangular prestressed concrete beams may be presented. It is assumed that tensile stresses carried by concrete may be neglected

in sections subject to bending. As shown in Fig. 2.1 **, properties of inelastic concrete stress distribution are represented by the following coefficients:

k_1 = ratio of average stress to maximum stress

k_2 = ratio of depth to resultant of compressive stress and depth to neutral axis.

k_3 = ratio of maximum stress to cylinder strength, f'_c

The equilibrium of forces and moments for bending of a section with only tension reinforcement gives:

$C_u = T_u$ where C_u = compressive force of concrete

T_u = total tensile force of steel

$$\therefore \quad k_1 k_3 f'_c b a = A_s f_{su} \qquad (2.1.1)$$

where b = width of the section

a = depth of stress block

f_{su} = stress in tensile steel at the ultimate load

$$\therefore \quad M_u = A_s f_{su} (d - k_2 a) \qquad (2.1.2)$$

where M_u = ultimate moment

d = distance from the centroid of tensile steel to the compression edge

** Figures have been presented in Appendix A.

For the under-reinforced sections, ultimate strength is controlled by the tensile stress of steel. The steel stress at the ultimate moment, f_{su} is then equal to the yield stress, f_y:

$$\therefore M_u = bd^2 f'_c q_u \left(1 - \frac{k_2}{k_1 k_3} q_u\right) = A_s f_y d \left(1 - \frac{k_2}{k_1 k_3} q_u\right) \quad \ldots\ldots\ldots \quad (2.1.3)$$

where q_u = tension reinforcement index $= p \frac{f_{su}}{f'_c}$

If there are several layers of steel with different values of stress at ultimate load, f_{su}, steel area, A_s and effective depth, d_n, equation (2.1.3) becomes:

$$M_u = bd^2 f'_c \left(\Sigma q_u\right) \left[1 - \frac{k_2}{k_1 k_3} \left(\Sigma q_u\right)\right]$$

$$= A_s f_y d \left[1 - \frac{k_2}{k_1 k_3} \left(\Sigma q_u\right)\right] \quad (2.1.3a)$$

where $\Sigma q_u = \Sigma \left(\frac{A_s f_{su}}{bdf'_c}\right)$ and $d = \frac{\Sigma (A_s f_{su} d_n)}{\Sigma (A_s f_{su})}$

It is observed that when the ultimate strength of the section is controlled by the tensile stress in steel, the effect of the assumed concrete stress distribution is represented by the ratio $\frac{k_2}{k_1 k_3}$.

When the ultimate strength of the prestressed concrete section is governed by compression, concrete crushes without the yield of the tension reinforcement. Linear distribution of the strain then may be assumed in computing the stress in tension and compression reinforcement. From Fig. 2.1

$$k_u = \frac{a}{d} = \frac{\varepsilon_u}{\varepsilon_u + \varepsilon_{cu}} \qquad (2.1.4)$$

where ε_u = ultimate concrete strain

ε_{cu} = concrete strain at the level of tension steel

By combining equation (2.1.4) with equations(2.1.1) and (2.1.2), the stress f_{su} as well as the ultimate moment, M_u may be obtained. It is then necessary to know the ultimate concrete compression strain, ε_u and independent values of k_2 and $k_1 k_3$.

To illustrate this, the balanced steel ratio, p_b for which yielding of steel and crushing of concrete in compression zone take place simultaneously at ultimate strength may be computed by solving equations (2.1.1) and (2.1.4):

$$p_b = k_1 k_3 \frac{\varepsilon_u}{\varepsilon_u + \varepsilon_{cy}} \cdot \frac{f'_c}{f_y} \qquad (2.1.5)$$

where ε_{cy} = strain in concrete at the level of tension steel, when the steel yields.

For balanced reinforcement:

$$M_u = bd^2 f'_c k_1 k_3 \frac{\varepsilon_u}{\varepsilon_u + \varepsilon_{cy}} \left(1 - k_2 \frac{\varepsilon_u}{\varepsilon_u + \varepsilon_{cy}}\right) \qquad (2.1.6)$$

It is therefore found that reliable information regarding the values of k_2, $k_1 k_3$ and ε_u in the inelastic stress distribution are essential for understanding the behaviour of prestressed concrete sections.

For design, it is convenient to consider a rectangular stress distribution as shown in Fig. 2.2 This has been proposed in the ACI Building Code 318-63. Use of the rectangular stress distribution tacitly assumes that $k_2 = k_1/2$. This corresponds closely to the geometry of the actual inelastic concrete stress distribution. If the depth of the equivalent rectangular stress-block is chosen as k_1 times the depth of neutral axis, all equations for the ultimate strength of rectangular cross-sections are identical to those obtained by Fig. 2.1 for $k_2 = k_1/2$.

In case of the non-rectangular sections and for non-symmetrical bending of rectangular sections such simple mathematical expressions are difficult to obtain. In many practical cases, and particularly when ultimate strength is controlled by tensile stresses of steel, the errors involved in the use of rectangular stress

distribution is small.

2.2 PLASTIC DESIGN IN STEEL:

Plastic design is a structural steel design method which takes into consideration the inelastic behaviour of structural steel and defines the limit of structural usefulness as the load attained when a sufficient number of plastic hinges have formed to transform the structure into a mechanism.

To trace the origins of plastic design, it may be noted that as early as 1914, Kazinczy[35] suggested the development of plastic hinges in continuous structures near ultimate load. In the United Kingdom, Baker[36], Neal[37], Symonds[38], Horne[39] and Heyman[40] have made considerable contributions in developing plastic design into a full-fledged structural design method. In the United States, plastic design has been accepted through experimental work and publications of Beedle and his associates[41], Prager[42] and Hodge[43].

Approaches of the various authors have been different, but all of them recognised the following conditions as essential requirements for collapse of a structure:

(a) Bending moment distribution must be in equilibrium with external loads.

(b) A sufficient number of plastic hinges must exist to transform either the entire or part of the structure into a mechanism.

(c) Full plastic moment capacity of the section would nowhere be exceeded.

2.3 LIMIT DESIGN:

Limit design is an inelastic theory of statically indeterminate concrete structures in which readjustments in the relative magnitude of the internal moments and forces at various sections are recognised at high loads. Individual sections may be designed either by ultimate strength design or by straight-line theory. However, it would appear to be logical and consistent to use inelastic methods of design both for the whole structure and for the individual sections.

The moment-curvature relationship for a structural concrete section, before yield of reinforcing steel, is a curve similar to a part of stress-strain curve for concrete. When the reinforcing steel yields, the curvature increases rapidly with little increase in moment. The resulting moment-curvature curves are as shown in Fig. 2.3. The bending moment at which the curvature increases rapidly is usually referred to as the plastic moment, M_u .

In a statically indeterminate structure the stiffness of a member at any particular critical section will be considerably reduced when the bending moment at that section reaches the plastic moment capacity of the section, M_u. This reduction in stiffness results in a redistribution of the bending moments in the structure. Full redistribution of moments is said to occur if the ultimate moment

capacity of all the critical sections in a structure are developed before the collapse of all or part of the structure.

To simplify calculations, it is convenient to represent the moment-curvature relationship of an under reinforced beam by two straight lines, shown by idealized dotted line in Fig. 2.3. This idealized curve implies constant stiffness of the section until the plastic moment is reached, and then increasing deformation without further increase in moment. The ultimate strength of the section, based on the yield point stress of the steel, may be used as the plastic moment. This idealized moment-curvature relationship can be used to establish the load-moment relationships for any of the critical sections in a statically indeterminate structure in concrete.

Use of the idealized curve implies that the hinging section will continue to maintain its full plastic moment while developing sufficient rotation to enable full redistribution of moments to occur. Whether or not full redistribution of moments will occur in a particular concrete structure, therefore, depends upon the rotational capacity of the hinging sections.

Four theories of limit design for concrete structures will be reviewed briefly, as being representative of the many theories which have been developed.

Ernst[44] modified the moment-area theorems to include the behaviour of structures in the inelastic range. Unit rotation

diagram instead of the conventional M/EI diagram was used. At a section developing its ultimate strength, the unit rotation θ_u is given by:

$$\theta_u = (\varepsilon_u + \varepsilon_{st})/d \quad \text{where}$$

ε_u = maximum concrete compressive strain at ultimate load

ε_{st} = maximum steel strain at ultimate load

d = effective depth of the section.

The unit rotation diagram with the definite yield length and with localised yield would be as shown in Fig. 2.4a and 2.4b. In the second case the yield is considered to be spread over a length λ, the total concentrated rotation at the yielding section, θ_p is therefore

$$\theta_p = \lambda(\theta_u - \theta_o) \quad \text{where } \theta_o \text{ is unit rotation at the commencement of yield of steel.}$$

In the analysis of continuous reinforced concrete beams, Ernst has applied this adaptation of the moment-area theorems to check the concentrated rotations necessary at all the hinging sections if full redistribution of moments is to occur. In this calculation, the concentrated plastic rotations are considered to act as concentrated loads on the conjugate beam. The concentrated rotations so calculated are compared with experimentally determined values to check whether they are admissible.

Sawyer[45] replaced the idealized moment curvature diagram by the nonideal one(Fig. 2.3) in which moment in the plastic region increases linearly from the moment at the commencement of steel yield, M_y upto the ultimate moment of the section, M_u .

Continuous beams and single-bay portal frames are analyzed by a trial and error adaptation of the elastic centre method. In this analysis the total plastic rotation in any particular region of maximum moment is considered to be concentrated at the point of maximum moment. All parts of the beam or frame away from the points of maximum moment are assumed to have constant stiffness. The trial and error process is continued until the components of the movement of the elastic centre due to the effect of both elastic and plastic deformations is zero.

Baker[46] stated that a structure 'n' times statically indeterminate would develop 'n' yielding hinges under increasing load prior to failure. For the purpose of calculation, the yielding is considered to be concentrated at 'n' points. The rest of the members between these 'n' points are assumed to behave elastically. The ultimate strength of the structure is reached when a very small additional increment of load would cause the formation of one or more additional hinges, thus producing collapse of the structure.

It is considered that the plastic moments at each yielding section (x_1 , x_2...) remain constant under increasing load. Therefore, on the formation of the 'nth' hinge, the structure becomes

statically determinate. Using the standard influence coefficient equations it is then possible to calculate the plastic rotations of the hinging sections (θ_1 , θ_2 ...) if full redistribution is to take place.

Berwanger[47] has applied the idealized moment-curvature diagram, normally assumed in the plastic design of steel,to continuous concrete beams and single or double storey framed structures in reinforced concrete. Initially, the value of the ultimate load, the bending moments at ultimate load, the hinge locations and their plastic moment capacities are determined by the plastic moment distribution method. The relative moments of inertia of the critical sections are determined as being directly proportional to their plastic moment capacities. Once the distribution factors, carry-over factors and the fixed end moments have been determined from an appropriate assumption for the variation of the flexural rigidity of the structure, a conventional elastic moment distribution is performed. From the consideration of this initial elastic moment distribution and the plastic moment capacities of the hinges, the location of the first hinge is determined, and the load at which it is formed is calculated. A subsequent elastic moment distribution is performed considering a modified elastic structure having a hinge of zero moment capacity where the plastic hinge is located and being loaded with the increment of loads beyond the load required to produce the first hinge. The second hinge location is found from a consideration

of the summed elastic moments and the plastic moment capacities from which the load at which it forms is computed. Additional elastic moment distributions, using successively modified elastic structures such that hinges of zero moment capacity occur at points where plastic hinges have been located, are performed for successive load increments until all hinges and their loads have been determined. From the information provided by the successive elastic moment distributions, the required ductilities or rotations are computed at the early forming hinges. The critical sections can be designed for their plastic moment capacities and adequate rotation capacities. The working loads and moments can be determined from the ultimate loads by the application of a suitable factor of safety.

2.4 PLASTIC AND LIMIT DESIGN COMPARED:

Though similar in approach, plastic design of structural steel and limit design of concrete differ in two important respects:

(1) Rotation capacity: Plastic design emphasizes the formation of a sufficient number of plastic hinges to transform the structure into a mechanism. Ultimate rotation needed at the first hinge for the formation of all other necessary hinges is not of much concern. Under normal conditions, ultimate strain of mild steel is greater than 15 percent and far exceeds the strain required by moment distribution in any section.

In the case of structural concrete, ultimate strain in flexural

compression ranges from 0.3 to 0.7 percent; the ultimate strain in tension reinforcement, depending on the amount and position of reinforcement varies from less than 0.5 percent to over 2 percent. The rotation capacity is an important consideration in the limit design of concrete. Moreover, to avoid excessive flexural cracking, hinge rotations must be limited to certain limits even when considerable rotation capacity is present after cracking.

(2) Distribution of moment resistance: Unless cover plates or variable depth sections are used, the positive and negative moment resistance of structural steel members are equal and constant along the entire length of a member. Plastic design of steel is thus more economic than elastic design. On the other hand, inelastic structural analysis must ensure that all three design conditions, namely, equilibrium, collapse mechanism and yield condition are fulfilled.

In case of structural concrete, the positive and negative moment resistance may be made different by changing the amount and location of reinforcement. It is quite possible in a concrete structure to bring the distribution of moments at ultimate load reasonably close to moment distribution corresponding to elastic behaviour. All plastic hinges necessary to form a mechanism will then form at practically the same load, thus reducing the amount of hinge rotations necessary.

CHAPTER 3

METHOD OF ANALYSIS

3.1 MOMENT-THRUST-CURVATURE RELATIONSHIP:

When a prestressed concrete section is subjected to combined bending and axial thrust, equilibrium of forces and moments would give ultimate load and moment; and from the compatibility of strains, the value of ultimate curvature may be computed. The interaction diagrams may be conveniently used to investigate these properties in a prestressed concrete beam-column section. The interaction diagram is defined as the envelope of all combinations of load and moment which may exist without material failure of the cross-section. The boundary of interaction diagram represents all possible combinations of axial load and bending moment which constitute material failure as limited by crushing of the concrete at ultimate compressive strain which may vary from 0.003 to 0.007 in/in. The interaction diagram is thus a convenient means of studying the structural behaviour and computing the ultimate strength of prestressed concrete sections under combined bending and axial thrust. As seen in Fig. 3.1, the interaction diagram may be divided into four distinct regions - each producing a different type of hinge action:

(1) Region A-B - Tensile hinge with large rotation; failure resulting primarily from yielding of tensile steel and then secondary compression failure of concrete.

(2) Region B-C - Compression hinge in which both compressive

and tensile stresses are present in the section. Failure initiated primarily by crushing of concrete under compressive stresses.

(3) Region C-D - Compressive hinge in which the entire section is in compression.

Compatibility and servicebility conditions must be taken into consideration before allowing the formation of any of the above types of hinges. Thus it is evident that if the load varies so does the mode of failure and the ultimate curvatures would be similarly influenced. The ultimate curvature in general would be affected by ultimate concrete stress and strain, stress block, yield stress and strain of reinforcement, amount and location of reinforcement, axial load, bending moment, cross sectional dimensions and time dependant stresses such as creep and shrinkage and by the amount of prestress.

From the above discussion, it is evident that, a series of possible strain configurations may exist inside the interaction envelope. When additional bending moment is applied to a section already subjected to constant axial thrust, an unique set of strain distribution is defined all the way up to failure. Therefore, points on the interaction diagram define a family of curves which relate moment-curvature relationship at different axial load levels (Fig.3.2). These relationships may be computed by means of programming of a high speed digital computer when the following procedure is adopted.

(1) Specific strain distribution over the depth of section is assumed i.e., position of neutral axis is fixed.

(2) A realistic stress-strain relationship of concrete and steel is taken and from this assumption the stress distribution over the section is computed.

(3) The resultant axial load and bending moment about the centroidal axis is calculated.

(4) The curvature is computed from the assumed strain distribution.

A computer programme in FORTRAN IV was written for the University of Ottawa IBM 360-65 digital computer to compute the ultimate moment-axial thrust-curvature relationship. This programme is explained in detail at a later stage in this thesis.

3.2 TYPES OF FAILURE:

The following five types of failures may be encountered in a prestressed concrete beam-column section:

(1) Tension Failure:

Tension failure occurs when the stresses in prestressing tendons used as tension reinforcement exceed the yield level (in this case determined by 0.2% offset method). The neutral axis moves rapidly towards the compression face and ultimately the concrete at the compression face reaches the ultimate strain, ε_u and crushes. Here failure is initiated by yielding of tension reinforcement though final failure is complete when the concrete crushes. This type of failure is associated with extensive cracking and large

deflection and is often preferred due to large rotation capacity.

(2) Compression Failure:

This type of failure is initiated by the crushing of extreme compression fibres in concrete. The stresses in the tensile reinforcement are usually within the elastic range whereas the compressive strain in the concrete exceeds ultimate strain, ε_u . Failure here is quite sudden, violent and without much warning and should usually be avoided.

(3) Balanced Failure:

Balanced failure is that type of failure in which the extreme concrete compression fibre reaches the ultimate strain simultaneously as the tensile reinforcement reaches the yield point. It is the transition point between tension and compression failures. As both the steel and concrete fail at the same time, this type of failure makes maximum utilization of the materials.

(4) Brittle Failure:

This type of failure usually occurs in specimens with a very small amount of tensile reinforcement. Failure is initiated by rupture of the tensile steel immediately after the formation of tension cracks and is quite sudden and most unwarranted.

(5) Buckling Failure:

In case of a section under combined bending and axial thrust, this type of failure may be initiated by instability. It results when the rate of change of moment caused by

lateral deflection due to applied eccentric load is equal to the rate of change of the resisting moment. At this load, the deflections would increase rapidly without any further increase in the load and and finally the concrete would crush.

3.3 BASIC ASSUMPTIONS:

The following were the basic assumptions used by the writer to develop analytical expressions for prestressed concrete sections subjected to combined bending and axial thrust under short time loading:

(a) Concrete Strain Distribution:

Bernoulli-Navier hypothesis of plane section remaining plane after bending has been extended to sections under combined bending and axial thrust. The linear distribution of strain was assumed up to failure. Many previous studies as well as experimental strain measurements by writer showed that this assumption was realistic.

(b) Bond between concrete and Prestressing Tendons:

It was assumed that there was no slip between concrete and prestressing strands and therefore the strain in the steel at any level due to loading may be taken equal to strain in concrete at the same depth. Though local loss of bond may occur near tension crack regions, this assumption seems to be reasonably accurate.

(c) Stress-Strain Relationship of Steel Reinforcement:

The usual trapezoidal elasti-plastic stress-strain relationship of steel (as shown in Fig. 3.3) was used. Yields stress was assumed by 0.2% offset method. For the modulus of Elasticity E_s, value supplied by manufacturers was used.

(d) Stress-Strain Relationship of Concrete:

Stress block as proposed by Hognestad (Fig. 3.4) has been used. However in some computations the rectangular stress block as proposed by ACI code 318-63 has been used for simplifying computations. For ultimate strain, ε_u, experimentally obtained values have been substituted. It was further assumed that for all practical purpose, tensile strength of concrete may be ignored.

(e) Shrinkage and Creep:

No detailed measurements of shrinkage and creep losses have been made. However, it was assumed that loss of prestress due to these factors was complete at the time of testing.

(f) Type of Loading:

Short time loading has been assumed.

(g) Deflection due to Shear has been neglected.

3.4 DEVELOPMENT OF ANALYTICAL EXPRESSIONS FOR RECTANGULAR PRESTRESSED CONCRETE SECTIONS UNDER COMBINED BENDING AND AXIAL THRUST.

(a) Tensile Hinge:

From the equilibrium of forces (Fig. 3.5)

$$P_u = k_1 k_3 f'_c\, ab - A_{s1} f_{s1} - A_{s2} f_{s2} - A_{s3} f_{s3} - A_{s4} f_{s4} \qquad \text{.....(3.4.1)}$$

where k_1 and k_3 are two factors depending on concrete strength, as given by ACI 318-63.

$k_1 = 0.85 - 0.05(f'_c - 4)$, where f'_c is in k.s.i.

$k_3 = 0.85$

Substituting: $p_1 = \frac{A_{s1}}{bd}$; $p_2 = \frac{A_{s2}}{bd}$;

$p_3 = \frac{A_{s3}}{bd}$; $p_4 = \frac{A_{s4}}{bd}$

Dividing both sides of equations by bd:

$$\frac{P_u}{bd} = k_1 k_3 f'_c \frac{a}{d} - p_1 f_{s1} - p_2 f_{s2} - p_3 f_{s3} - p_4 f_{s4} \qquad (3.4.2)$$

Taking moments about the plastic centroid, (anticlockwise moment positive):

$$M_u = k_1 k_3 f'_c\, ab\,(d - R_4 d - k_2 a) - A_{s1} f_{s1} R_1 d - A_{s2} f_{s2} R_2 d + A_{s3} f_{s3} R_3 d + A_{s4} f_{s4} R_4 d$$

$$\therefore \frac{M_u}{bd} = k_1 k_3 f'_c \frac{a}{d}(d - R_4 d - k_2 a) - p_1 f_{s1} R_1 d - p_2 f_{s2} R_2 d + p_3 f_{s3} R_3 d + p_4 f_{s4} R_4 d$$

Substituting $w = k_1 k_3 f'_c$

$$\frac{P_u}{bd} = w\left(\frac{a}{d}\right) - p_1 f_{s1} - p_2 f_{s2} - p_3 f_{s3} - p_4 f_{s4} \qquad (3.4.3)$$

and

$$\frac{M_u}{bd} = w\left(\frac{a}{d}\right)(d - R_4 d - k_2 a) - p_1 f_{s1} R_1 d - p_2 f_{s2} R_2 d + p_3 f_{s3} R_3 d + p_4 f_{s4} R_4 d \qquad (3.4.4)$$

Now $$e = \frac{M_u}{P_u} = \frac{M_u}{bd} \cdot \frac{bd}{P_u}$$

$$\therefore \quad e \cdot \frac{P_u}{bd} = \frac{M_u}{bd} \qquad (3.4.5)$$

Substituting values of $\frac{P_u}{bd}$ and $\frac{M_u}{bd}$:

$$e\left[w\left(\frac{a}{d}\right) - p_1 f_{s1} - p_2 f_{s2} - p_3 f_{s3} - p_4 f_{s4}\right] = w\left(\frac{a}{d}\right)(d - R_4 d - k_2 a) - p_1 f_{s1} R_1 d - p_2 f_{s2} R_2 d + p_3 f_{s3} R_3 d + p_4 f_{s4} R_4 d$$

$$\therefore \quad w\left(\frac{a}{d}\right)^2 k_2 d - w\left(\frac{a}{d}\right)\left[e - d(1 - R_4)\right] - p_1 f_{s1}(e - R_1 d) - p_2 f_{s2}(e - R_2 d) - p_3 f_{s3}(e - R_3 d) - p_4 f_{s4}(e - R_4 d) = 0 \qquad (3.4.6)$$

Let $S = e - R_1 d$

$T = e - R_2 d$

$X = e - d(1 - R_4)$

$Y = e + R_3 d$

$Z = e + R_4 d$

$$w\left(\frac{a}{d}\right)^2 k_2 d - wX\left(\frac{a}{d}\right) - p_1 f_{s1} S - p_2 f_{s2} T - p_3 f_{s3} Y - p_4 f_{s4} Z = 0$$

Dividing through by $wk_2 d$

$$\left(\frac{a}{d}\right)^2 + \frac{X}{k_2 d}\left(\frac{a}{d}\right) - \frac{1}{wk_2 d}\left[p_1 f_{s1} S + p_2 f_{s2} T + p_3 f_{s3} Y + p_4 f_{s4} Z\right] = 0$$

Substituting back $w = k_1 k_3 f'_c$

$$\left(\frac{a}{d}\right)^2 + \frac{X}{k_2 d}\left(\frac{a}{d}\right) - \frac{1}{k_1 k_2 k_3 d}\left[p_1 \frac{f_{s1}}{f'_c} S + p_2 \frac{f_{s2}}{f'_c} T + p_3 \frac{f_{s3}}{f'_c} Y + p_4 \frac{f_{s4}}{f'_c} Z\right] = 0$$

Let $m = 1/k_1 k_2 k_3$

$$\left(\frac{a}{d}\right)^2 + \frac{X}{k_2 d}\left(\frac{a}{d}\right) - \frac{m}{d}\left[p_1 \frac{f_{s1}}{f'_c} S + p_2 \frac{f_{s2}}{f'_c} T + p_3 \frac{f_{s3}}{f'_c} Y + p_4 \frac{f_{s4}}{f'_c} Z\right] = 0$$

Solving this quadratic equation:

$$\frac{a}{d} = -\frac{1}{2}\frac{X}{k_2 d} \pm \frac{1}{2}\left[\left(\frac{X}{k_2 d}\right)^2 + \frac{4m}{d}\left(p_1 \frac{f_{s1}}{f'_c} S + p_2 \frac{f_{s2}}{f'_c} T + p_3 \frac{f_{s3}}{f'_c} Y + p_4 \frac{f_{s4}}{f'_c} Z\right)\right]^{1/2}$$

Ignoring negative sign:

$$\frac{a}{d} = -\frac{X}{2k_2 d} + \frac{X}{2k_2 d}\left[1 + \frac{k_2^2 d^2}{X^2}\frac{4m}{d}\left(p_1 \frac{f_{s1}}{f'_c} S + p_2 \frac{f_{s2}}{f'_c} T + p_3 \frac{f_{s3}}{f'_c} Y + p_4 \frac{f_{s4}}{f'_c} Z\right)\right]^{1/2}$$

$$= \frac{X}{2k_2 d}\left[-1 + \left\{1 + \frac{V}{X^2}\left(p_1 \frac{f_{s1}}{f'_c} S + p_2 \frac{f_{s2}}{f'_c} T + p_3 \frac{f_{s3}}{f'_c} Y + p_4 \frac{f_{s4}}{f'_c} Z\right)\right\}^{1/2}\right]$$

where $V = 4 k_2^2 d m$

Let $a = k_u d \quad \therefore \frac{a}{d} = k_u$

$$k_u = \frac{X}{2k_2 d}\left[-1 + \left\{1 + \frac{V}{X^2}\left(p_1 \frac{f_{s1}}{f'_c} S + p_2 \frac{f_{s2}}{f'_c} T + p_3 \frac{f_{s3}}{f'_c} Y + p_4 \frac{f_{s4}}{f'_c} Z\right)\right\}^{1/2}\right] \qquad (3.4.8)$$

From compatibility of strains:

$$\frac{a}{d} = \frac{\varepsilon_u}{\varepsilon_u + \varepsilon_4}$$

$$\frac{a}{d}(\varepsilon_u + \varepsilon_4) = \varepsilon_u \quad \text{or,} \quad \varepsilon_4 = \varepsilon_u \left(\frac{1 - \frac{a}{d}}{\frac{a}{d}}\right) = \varepsilon_u \left(\frac{1 - k_u}{k_u}\right)$$

Substituting value of k_u :

$$\varepsilon_4 = \varepsilon_u \left[\frac{1 - \frac{X}{2k_2 d}\left[-1 + \left\{1 + \frac{V}{X^2}\left(p_1 \frac{f_{s1}}{f'_c} S + p_2 \frac{f_{s2}}{f'_c} T + p_3 \frac{f_{s3}}{f'_c} Y + p_4 \frac{f_{s4}}{f'_c} Z\right)\right\}^{1/2}\right]}{\frac{X}{2k_2 d}\left[-1 + \left\{1 + \frac{V}{X^2}\left(p_1 \frac{f_{s1}}{f'_c} S + p_2 \frac{f_{s2}}{f'_c} T + p_3 \frac{f_{s3}}{f'_c} Y + p_4 \frac{f_{s4}}{f'_c} Z\right)\right\}^{1/2}\right]}\right]$$

From the strain diagram

Curvature, $\phi_u = \frac{\varepsilon_u}{a} = \frac{\varepsilon_u + \varepsilon_4}{d} = \frac{\varepsilon_u}{d}\left(1 - \frac{\varepsilon_4}{\varepsilon_u}\right)$

$$\phi_u = \frac{\varepsilon_u}{d}\left[1 + \frac{1 - \frac{X}{2k_2 d}\left[-1 + \left\{1 + \frac{V}{X^2}\left(p_1 \frac{f_{s1}}{f'_c} S + p_2 \frac{f_{s2}}{f'_c} T + p_3 \frac{f_{s3}}{f'_c} Y + p_4 \frac{f_{s4}}{f'_c} Z\right)\right\}^{1/2}\right]}{\frac{X}{2k_2 d}\left[-1 + \left\{1 + \frac{V}{X^2}\left(p_1 \frac{f_{s1}}{f'_c} S + p_2 \frac{f_{s2}}{f'_c} T + p_3 \frac{f_{s3}}{f'_c} Y + p_4 \frac{f_{s4}}{f'_c} Z\right)\right\}^{1/2}\right]}\right]$$

$$= \frac{\varepsilon_u}{d}\left[\frac{1}{\frac{X}{2k_2 d}\left[-1 + \left\{1 + \frac{V}{X^2}\left(p_1 \frac{f_{s1}}{f'_c} S + p_2 \frac{f_{s2}}{f'_c} T + p_3 \frac{f_{s3}}{f'_c} Y + p_4 \frac{f_{s4}}{f'_c} Z\right)\right\}^{1/2}\right]}\right]$$

$$\therefore \phi_u = \frac{2 k_2 \varepsilon_u}{\left[X^2 + V\left(p_1 \frac{f_{s1}}{f'_c} S + p_2 \frac{f_{s2}}{f'_c} T + p_3 \frac{f_{s3}}{f'_c} Y + p_4 \frac{f_{s4}}{f'_c} Z\right)\right]^{1/2} - X}$$

..... (3.4.10)

(b) Compressive Hinge:

From the equilibrium of Forces (Fig. 3.6):

$$P_u = k_1 k_3 f'_c \, bd \, (1 + k_b) - A_s f_{s1} - A_{s2} f_{s2} - A_{s3} f_{s3} - A_{s4} f_{s4}$$

..... (3.4.11)

$$\frac{P_u}{bd} = w\,(1 + k_b) - p_1 f_{s1} - p_2 f_{s2} - p_3 f_{s3} - p_4 f_{s4} \quad \text{where} \quad w = k_1 k_3 f'_c$$

$$M_u = wbd\,(1 + k_b)\,(d - R_4 d - k_2 a) - A_{s1} f_{s1} R_1 d - A_{s2} f_{s2} R_2 d + A_{s3} f_{s3} R_{s3} d + A_{s4} f_{s4} R_4 d \qquad (3.4.12)$$

$$\therefore \frac{M_u}{bd} = w(1 + k_b)\,(d - R_4 d - k_2 a) - p_1 f_{s1} R_1 d - p_2 f_{s2} R_2 d + p_3 f_{s3} R_3 d + p_4 f_{s4} R_4 d$$

$$= w(1 + k_b)\, d(1 - R_4) - w(1 + k_b) k_2 a - p_1 f_{s1} R_1 d - p_2 f_{s2} R_2 d + p_3 f_{s3} R_3 d + p_4 f_{s4} R_4 d$$

$$e = \frac{M_u}{p_u} = \frac{M_u}{bd} \cdot \frac{bd}{p_u} \qquad \therefore\ e \cdot \frac{p_u}{bd} = \frac{M_u}{bd} \qquad (3.4.13)$$

$$e\left[w(1+k_b) - p_1 f_{s1} - p_2 f_{s2} - p_3 f_{s3} - p_4 f_{s4}\right] = w(1 + k_b)\, d\,(1 - R_4) - w(1 + k_b)\, k_2 a - p_1 f_{s1} R_1 d - p_2 f_{s2} R_2 d + p_3 f_{s3} R_3 d + p_4 f_{s4} R_4 d$$

or $$w(1 + k_b)\left[e - d(1 - R_4)\right] - p_1 f_{s1}(e - R_1 d) - p_2 f_{s2}(e - R_2 d) - p_3 f_{s3}(e + R_3 d) - p_4 f_{s4}(e + R_4 d) = - w(1 + k_b)\, k_2 a$$

Let $S = e - R_1 d$; $T = e - R_2 d$; $X = e - d(1 - R_4)$;

$Y = e + R_3 d$; $Z = e + R_4 d$

$$\therefore \quad wX(1 + k_b) - p_1 f_{s1} S - p_2 f_{s2} T - p_3 f_{s3} Y - p_4 f_{s4} Z = - w(1 + k_b) k_2 a$$

..... (3.4.14)

Dividing althrough by $w(1 + k_b)k_2$:

$$- a = \frac{X}{k_2} - \frac{1}{w(1 + k_b)k_2}\left[p_1 f_{s1} S + p_2 f_{s2} T + p_3 f_{s3} Y + p_4 f_{s4} Z\right]$$

Substituting value of w:

$$- a = \frac{X}{k_2} - \frac{1}{k_1 k_3 (1 + k_b) k_2}\left[Sp_1 \frac{f_{s1}}{f'_c} + Tp_2 \frac{f_{s2}}{f'_c} + Yp_3 \frac{f_{s3}}{f'_c} + Zp_4 \frac{f_{s4}}{f'_c}\right]$$

If $\quad \mu = \frac{1}{k_1 k_3 (1 + k_b)}$

$$- a = \frac{X}{k_2} - \frac{\mu}{k_2}\left[Sp_1 \frac{f_{s1}}{f'_c} + Tp_2 \frac{f_{s2}}{f'_c} + Yp_3 \frac{f_{s3}}{f'_c} + Zp_4 \frac{f_{s4}}{f'_c}\right]$$

..... (3.4.15)

From the strain diagram:

$$\text{Curvature, } \phi_u = \frac{\varepsilon_u}{a} = - \frac{\varepsilon_u}{\frac{X}{k_2} - \frac{\mu}{k_2}\left[Sp_1 \frac{f_{s1}}{f'_c} + Tp_2 \frac{f_{s2}}{f'_c} + Yp_3 \frac{f_{s3}}{f'_c} + Zp_4 \frac{f_{s4}}{f'_c}\right]}$$

$$\phi_u = - \frac{k_2 \varepsilon_u}{X - \mu\left[Sp_1 \frac{f_{s1}}{f'_c} + Tp_2 \frac{f_{s2}}{f'_c} + Yp_3 \frac{f_{s3}}{f'_c} + Zp_4 \frac{f_{s4}}{f'_c}\right]} \quad \cdots (3.4.16)$$

3.5 SCOPE OF ANALYTICAL EXPRESSIONS:

The analytical expressions developed in this chapter enable rapid computation of the ultimate load, the ultimate moment and the ultimate curvature of rectangular prestressed concrete sections under short-term loading of combined bending and axial thrust. These expressions may be extended to other prestressed concrete sections, such as I-section, T-section, channel section etc. These sections are frequently used in present day construction. The unique feature of these expressions lie in the fact that the strength and the deformation characteristics of plastic hinges in prestressed concrete sections may be predicted easily when sectional and stress-block parameters along with concrete and steel properties are known. In general it can be observed from the expressions that ultimate curvature is influenced by - the ultimate concrete stress and strain, yield stress and strain of prestressing tendons, percentage of reinforcement, amount of prestress, cover for reinforcement, bending moment and axial load. By judicious manipulation of these variables, ultimate curvature may be regulated within permissible limits.

In the case of reinforced concrete beam-column members, some of these variables have been studied by Pfrang and Siess[10,11]. In the case of prestressed concrete sections, Lin and Lakhwara[19], have made an investigation. During their research on ductility of concrete structures, Corley[48] and Mattock[49] observed that the presence of shear stress and rectangular or helical stirrups increase the ultimate

strain of concrete and therefore the ultimate curvature is also increased. As may be seen from Chapter 2, numerous investigators have worked on the ultimate strain of concrete, but it is observed that Hognestad's[5] suggestion of 0.0038 as the value of ultimate strain has been accepted by other investigators. The stress block parameters have been investigated experimentally and Hognestad[33] has reported that by measuring the ultimate moment and depth of neutral axis and assuming a value of k_2, k_1k_3 may be evaluated from the expression:

$$k_1k_3 = \frac{3000 + \frac{1}{2} f'_c}{f'_c + 1500} \quad , \quad f'_c \text{ is in psi.}$$

From the results of 364 reinforced concrete beam tests done in the United States and Canada, Hognestad[33] deduced that a value of $k_2/k_1k_3 = 0.59$ could be obtained and this value correlates with Whitney's[3] expression.

From the analytical expressions, it is quite evident that ratio of the ultimate moment - axial load or the ultimate eccentricity influences significantly the ultimate curvature value. At loads below the balanced load, that is, for tension failures, a considerable amount of ductility is present in the structure. The amount of ductility decreases gradually as the axial load level increases towards balanced load level. For limit design techniques, where built in ductility is assumed for redistribution of moments, axial load should be kept at fairly low level so that ductile failure is ensured. This may sometimes result in uneconomical designs. The designer has to meet the

dual criterion of strength and rotation in a plastic hinge. In the case of a purely flexural failure the variation of only the steel reinforcement could ensure ductile hinge.

It may be observed that comparatively little research has been done on yield-interaction diagrams. As mentioned earlier the yield interaction diagrams may be defined as the locus of all combinations of ultimate moments and axial thrusts for first yield of tension reinforcement. This apparent lack of interest may be ascribed to the acceptance of ultimate strength design method. In the ultimate strength design method, the ultimate capacity of the section is determined. This load is then divided by the load factor to obtain the design load. Yield load of the section is ignored altogether. Also problems of creep and shrinkage make it difficult to ascertain concrete stress distribution at yield of tensile reinforcement in plastic hinges.

CHAPTER 4

MATERIALS, FABRICATION AND TESTING

4.1 MATERIALS:

(i) Cement:

Lake Ontario 'Pronto' cement was used for all the beam-column specimens, control cylinders and prisms.

(ii) Fine and Coarse Aggregates:

Regular fine and coarse aggregates for precasting work were used and they satisfied the specifications. Two types of fine aggregates having Fineness Modulus respectively of 2.53 and 2.79 were used. Dirt content of the two types were 2.50 and 2.43 percent and specific gravity were 2.60 and 2.63 respectively. For the two types of coarse aggregates Fineness Modulus were 6.41 and 6.80 and specific gravity were 2.65 and 2.66 respectively. Maximum size of coarse aggregate used were 5/8". Sieve analysis of the aggregates are shown in Figs. 4.1 to 4.4.

(iii) Concrete Mix:

The concrete mix used was designed to have a cylinder strength of 5000 psi at 28 days. All concrete was mixed in the standard mixing machine of Wilson concrete Products at Belleville, Ontario.

For 3/4 cubic yard of concrete, the amount of cement, coarse and fine aggregates, water and admixtures used are given below:

coarse aggregate	1460 lbs
fine aggregate	1070 lbs
water	135 lbs
cement	445 lbs
maracon	37 lbs
NVX for required air content	

(iv) Prestressing tendons and Stirrups:

All longitudinal prestressing tendons used were 270 K grade 7-wire strands manufactured by the Steel Company of Canada and supplied by Conenco Canada Ltd. This particular grade has a guaranteed minimum ultimate strength of 270,000 psi.

Three different sizes of tendons were used for prestressing:

Diameter	Area in sq.in.
1/2 in.	0.1531
7/16 in	0.1167
3/8 in	0.0794

The actual stress-strain relationship of the tendons have been shown in Figs. 4.5 to 4.7. The idealized curves shown by the dotted lines were used in the computations. The experimental modulus of elasticity for the individual tendons were used in all calculations. Stirrups of 3/8" ϕ mild steel were used as ties.

4.2 METHODS OF FABRICATION:

(i) Types of Specimens:

All together 55 beam-column specimens of 6 in. x 8 in. dimension and varying reinforcement were designed for experimental investigation; these were divided into 11 groups of 5 each. Among these 11 groups,series PC1 to PC5 were meant to represent column sections and were symmetrically reinforced; and series PB1 to PB6 were unsymmetrically reinforced as beam sections. The amount of longitudinal reinforcement in the two groups ranged from 0.3196 sq. in. to 0.9186 sq. in. and 0.1598 sq. in. to 0.6534 sq. in. respectively.

This investigation was confined to the effect of combined bending axial load on the prestressed concrete sections and the material failure was assumed as the failure criterion. The span of the specimens was made 62 inches in order to avoid instability failures. Also in addition to normal stirrups, special precautions were taken to avoid shear or diagonal tension failure. This was done by providing extra outside clamps to the specimens as shown in plate 4.1. Concrete strength was designed to be 5000 psi at 28 days for all the specimens and all the tendons were stressed to 80,000 psi effective prestress. The total prestressing force varied in the different series due to the variation in the amount of reinforcement. Different dimensions and properties of the sections are shown in Figs. 4.8 to 4.18 and Table 4.1.

(ii) Prestressing, Casting and Curing:

Two 30 feet long steel forms with heavy end blocks were used for prestressing. Tendons were pulled from one end to the other end of the form through holes provided in the end blocks at the specific

depths and passing through the ties. The ties were then properly secured to the tendons by means of wires. One end of the tendons were anchored to the bulkhead by means of wedge-shaped split-cone anchors and at the other end, tendons were stressed one by one by a double acting hydraulic jack. The strands were designed to carry final effective prestress of 80,000 psi. Amount of losses were calculated according to the Canadian code and jacking stress was found out to be 99,800 psi. This was ensured both by the actual measurement of the elongation of wires and by the hydraulic pressure of the jack. After stressing each tendon, jacking end was securely fixed to the bulk head by means of the wedge type split-cone anchor.

Mixing of concrete was done in the standard mixer of Wilson Concrete Products and was brought by means of overhead crane to the casting formwork. All the specimens were cast in a horizontal position because of prestressing formwork and also to avoid differential quality of concrete along the length of the specimen. During casting, concrete was compacted by means of electrically driven pipe vibrators. Casting of 2 series, that is, 10 specimens were done in one day. Along with the specimens, 3 control cylinders (6 in by 12 in) and 2 prisms (3 in x 3 in x 12 in) were cast for each series; also slump test and percentage of entrained air were measured as shown in Table 4.2. After casting was finished, top surface of the specimens, control cylinders and prisms were finished with wooden and steel trowels.

Immediately after the completion of casting and finishing,

the specimens, control cylinders and prisms were covered with wet gunny bags and in about 8 hours time steam curing started. Usually after 48 hours, stressed tendons were cut by means of a cutting torch. Form was then dismantled and specimens were taken out and placed for normal curing under room temperature.

4.3 EQUIPMENT:

(i) Strain Measuring Devices:

At the mid-section of the beam-column specimens, where only flexural stresses were present, strain measurements were taken at six different depths. Since after formation of tension cracks, strains differ appreciably between cracked and uncracked sections at the same depth, thereby inducing some error in strain readings at the tensile zone, it was decided to take four strain measurements above the centre-line of the depth of beam-column section , and only two strain measurements below the centre-line. Hence a grid as shown in Fig. 4.19 was chosen and previously marked on the specimens.

Different equipment used for measuring deformation of the specimens are shown in schematic diagram in Fig. 4.20. Description of the various components are given below:

Displacement transducers were used to measure strain at various depths of the beam-columns at each increment of loading. The Particular model used was 7DCDT-100.

Altogether 10 transducers were mounted at the midsection of the specimens - one on top and 5 and 4 respectively on the front and back sides at different depths. Except transducer number 10 which was mounted on top and number 4, all others were paired at the same depth on both sides in order to have a check on their performance. However, their performance was quite satisfactory all along except for odd ones.

A DCDT consists of a coil assembly and a core. The coil assembly comprises of a differential transformer coil, a DC - exited solid state oscillator and a phase-sensitive demodulator (Fig. 4.21). When the core is displaced linearly along the axis of bore of coil assembly, voltage change proportional to displacement takes place in the output - actually the oscillator converts the DC input to AC which excites the primary winding, whereas actual core position fixes the amount of voltage induced in secondary windings; each of the two secondary circuits contains a secondary winding, a full-wave bridge and a R.C filter. These secondary circuits are connected in series opposition so that the resultant output is a DC voltage proportional to the core displacement from electrical centre.

Special aluminium blocks were devised for fitting the transducers on to the specimens. These were 3/4 in x 3/4 in x 1/2 in aluminium blocks and a 6 in long aluminium rod small enough to fit into the groove of Transducer core. Two types of blocks were used - one had inner hole just sufficient to contain the transducer coil and

the other had a smaller groove to fit the aluminium rod. Both the coil and aluminium rod could be held in position by means of two screws in the two aluminium blocks. The transducer core was fixed onto one end of the aluminium rod and slide' inside the coil When this was properly positioned, both the coil and the rod were fixed in position by means of brass screws.

The position of the aluminium blocks were earlier marked on the specimens. These markings and the base of the blocks were properly cleaned and then a solution of epoxy resin was spread over the markings as well as base of the aluminium blocks, and then the blocks were gently pressed against proper marking on the specimen. The particular type of adhesive used was an Armstrong A-2 type whose two main components are epoxy type resin formulation with an inorganic filler and an amine type catalyst. Curing of the adhesive starts as soon as the two parts are mixed. This particular type of adhesive produced excellent bond between the blocks and concrete; this was quite evident by large chunks of concrete coming along with the blocks when these were removed after completion of test.

A DC Power Supply unit was used for the constant DC voltage input to the transducers. The particular model used was 6204 B. This was a dual range, compact, regulated, constant voltage/current limiting supply unit. Different features of this instrument is shown in table 4.3. Its principle of operation is as follows:

Input line voltage passes through power transformer to a rectifier-filter which converts AC input to raw DC which is fed into the positive terminal via a regulator and current sampling resistor network. The regulator is made to alter its conduction to maintain a constant output voltage.

The Switching Unit was used to connect output of transducers to the readout device - one at each time. Particular model used was BLH model 220. The front panel contains an input bridge selector switch, a channel selector switch and a set of 5 output terminals. Rear panel consists of 10 groups of 5 terminals - each group for connecting to each transducer. The input bridge selector switch selects either two or four arm bridge input. The channel selector switch contains an off position and positions for each of the ten channels. Each channel is wired through this selector switch such that capacitive currents from channels not in use do not affect the channel in use.

The Voltage to Frequency Converter unit converts the output DC voltage from the transducers to corresponding frequency values. The model 2212A voltage-to-frequency converter (VFC) produces an output pulse train whose pulse rate is directly proportional to the magnitude of DC voltage applied to its input terminal by the transducers. Full scale output is 100 kH_z for switch selected ranges in decade steps from 1 volt down to 10 mv full scale. An optional range vernier multiplies full scale up to 3.5 times. Signal polarity is shown by front panel lamps.

Counter readings of 2212A output frequency may be converted to voltage decided by selected range of 2212A. For 1 volt multiplication factor is 0.01. During testing, range used was 1 volt and in addition 5 turns of vernier was added, so that

$$R_m = 1 + 0.25\ V_s = 2.25$$

Therefore, counter readings were multiplied by 0.01 x 2.25 in order to get output results in volts.

The Frequency Counter was used in conjunction with the 2212A voltage to frequency converter to measure the output from DCDT transducers. Model 5221A frequency counter measures frequency or repetition rate of periodic signals by totalising the events during gate times of 0.1, 1 or 10 seconds. The gate times are selected by a front panel switch. An internal control allows counting of either positive or negative input pulses. The readout storage provides continuous display of the most recent measurement, which is held even when the instrument is gated for a new count. If the new count differs from the stored count, the display shifts automatically to the new one. A sample rate control sets the period of time following a gate closure until the gate may be opened again.

(ii) Loading and Load Measuring Devices:

Schematic diagram of loading and load measuring devices have been shown in Fig. 4.21.

Vertical and Horizontal rams are hydraulically operated loading device which have a maximum stroke of 6 inches. The vertical ram

was mounted on top of the loading frame in a vertical position and was capable of transmitting up to 100000 lbs load. The horizontal ram was mounted on the left abutment.

Hand operated hydraulic pump was used to regulate the rate and amount of loading by the vertical ram. This was quite a handy tool and the amount of load transmitted could be roughly checked from the oil pressure indicator. A pressure of about 2460 psi would amount to a load of 100000 lbs.

The hydraulic Power Package unit was used to supply the necessary hydraulic pressure needed to operate the PUV5 horizontal ram. Essential components of this unit were a 10 gallon reservoir, 5 HP 1200 RPM 550 V 3-phase AC splash proof motor, PVB 5-pump. It operated at a pressure of 3000 psi and rated flow was 3 GPM.

The Power and Failsafe Panel was a safety device to protect the power package. When the oil level is too low or temperature is too high, the 'Pump Failure' light would be on and pump would stop operating. Any other abnormal operating condition such that servo amplifier alarm, exceeding force, pressure, position or other safely limits would make the 'Alarm' light on and the pump would stop operating, thereby relieving oil pressure. In such cases, usually 'reset' buttons have to be pushed to bring the pump into working once again. All these control relays are incorporated in this unit.

The Servo Amplifier was a DC operational, solid state amplifier of a modulur plug in type construction. It operated by means

of a number of external controls. 'Power Switch' turned power on and off for the servo amplifier. 'Static Set Point' was used to predetermine the direction of force transmitted by the ram. It consisted of a toggle switch with a plus, centre off and minus position as well as duo-dial calibrated 0 - 1000. With a load cell as the feed back transducer, the toggle switch in the positive direction and duo-dial off zero, the Servo valve was opened to produce compression load on the load cell of a magnitude determined by duo-dial setting; whereas negative direction would induce tension force. 'Range Switch' fixed the range of load to be transmitted; it had four positions - 10, 20, 50 and 100 percent. Range switch at 10 percent meant total load transmitted would be 10 percent of 100,000 lbs or 10,000 lbs in that particular setting. 'Velocity Limiter' governed the limiting of maximum current to the servo valve and limited actuator velocity. 'Gain control' was a 10 turn potentiometer with a duo-dial calibrated from zero to 1000.

MOOG 73-103 type servo valve was provided to regulate the amount and direction of flow of hydraulic oil from the pump to the ram. It connected the ram with the hydraulic power package and also was connected to the servo amplifier. Flow rate of the particular valve was 10 GPM.

Two load cells were used to pick up reaction of the vertical load at the two supports of the beam-column specimens. Total capacity of each was 50,000 lbs. One 100,000 lbs capacity load cell was used to record the reaction of the horizontal ram. These particular load

cells were in fact a short column with small l/r ratio to ensure freedom from buckling. Strain gauge attachments in it were done in such a way that it was very sensitive to axial loading. This was done by attaching four strain gauges arranged around the circumference of cylinder surface. Load cells were properly calibrated before testing was started.

Gilmore model 471-210 millivolt indicator was used for load cell readout. This unit read directly the loads recorded in the strain gauges of load cells. The front panel had a digital readout and power on-off switch plus instrument zero switch. Before the experiment, this unit was zeroed by means of instrument zero switch. It is capable of reading a load of up to 100000 lbs at an interval of 10 lbs. It had a continuous display and updated 3 readings per second.

Since one horizontal and two vertical load cells had to be read, one switching and selection unit was needed to connect the different load cells, one at a time, to the millivolt indicator. Hence, an Ellis BSG-6 switch and channel selection unit was used for this purpose. Rear panel of this instrument had six input connections and one output connection, whereas the frontpanel had six each of gain control, balance and channel selection switches. First one channel at a time was connected through the channel selection switch and gain control switch was used to properly set this channel. This was then followed for all the channels and load cell readouts taken through the millivolt indicator.

(iii) Deflection Measuring Devices:

At each increment of load, vertical deflection of beam-column specimen was measured at seven different points along longitudinal axis by means of a deflection bridge, as shown in Fig. 4.22 and Plate 4.2. This deflection bridge consisted of seven mechanical deflection gauges fitted at previously marked positions on top of the base of loading frame.

Dial indicators were used to measure deflection of the test specimens. The operation of these dial gauges are very simple. In this instrument, the movement of a plunger placed in contact with the test piece is transmitted by a rack and pinion arrangement to a gear train which in turn operates a pointer in a graduated dial. The smallest division on the dial corresponds to a spindle movement of 0.0001 inch.

(iv) Electrodynamic Materials Tester:

SCT-5 type electrodynamic materials tester was used to compute dynamic modulus of elasticity of concrete from control prisms shown in Plate 4.5 SCT 5 is a convenient laboratory instrument for measuring the resonant frequency of regularly shaped materials. It is composed of an accurately calibrated oscillator, which may be coupled to a vibrator for excitation of the specimen, and an amplifier feeding a meter which measures the signal from the crystal pick up in contact with the vibrating specimen. This meter reading may later on be converted into corresponding frequency from a chart supplied by the manufacturers.

(v) Cylinder Testing Machine:

Forney Testing Machine was used for compression and deformation test of control cylinders. This unit is an electrically operated hydraulic press type testing machine. In it, load is applied by the hydraulic press and is measured by the pressure developed within the hydraulic cylinder. It has a capacity of 300000 lbs with a minimum graduation of 50 lbs. Testing of a typical cylinder is shown in Plate 4.6.

4.4 TEST PROCEDURE:

(i) Beam-Columns:

Beam-column specimens were designed to be put under constant horizontal axial load and then loaded to failure by two point symmetrical vertical short duration loading, as shown in Figs. 4.19 and 4.22. Some special modification was made to the existing loading frame in order to facilitate horizontal axial loading. These were two triangular frames, composed of I-sections and added to both sides of the loading frame to act as vertical abutments. A hydraulically operated loading ram was attached to the left-side abutment. A load cell was attached to the right side abutment to pick-up the load transmitted from the ram. On the bed of the existing frame, longitudinal centre-line as well as two longitudinal edges and transeverse centre-line of the specimens along with the position of two supports were marked. Two 50000 lbs capacity load cells were properly positioned as the vertical supports. Then supporting plates and rollers were placed on the two load-cells to simulate hinged ends.

The specimen was then brought and lowered on the supports by means of a manually operated chain block and its position was properly adjusted so that marking of supports on the specimen coincided with the supporting plates on the load cells. Also longitudinal edges of the specimen were aligned with the markings on the bed of the test block and the transeverse centre-line of the specimen was aligned with the centre line of the vertical loading ram.

A plumb bob was used for all these alignments. Next the loading plates and rollers were properly positioned on the specimen and the I-beam used to transfer vertical load was properly positioned.

Two special end-connections as shown in Plates 4.3 and 4.4 were then mounted onto the two ends of the specimen. The purpose of these end connections were to transmit horizontal load on to the specimen axially and without any end-restraint. This was done by means of 1" ϕ rollers and 1/4" ϕ ball bearings with end plates as shown in Fig. 4.23 and Plates 4.3 and 4.4.

Special external clamps (as shown in Plate 4.1) were then mounted on to the specimens to avoid shear and diagonal tension failure. Next the displacement transducers were attached to small aluminium blocks which were previously mounted on the specimens at predetermined depths and 4 in. gauge length. The deflection bridge (Plate 4.2) was then set up in proper position. All these features are explained in detail at a later stage in this thesis.

Once all the necessary adjustments were done and all electrical circuits properly checked, horizontal axial load was gradually transmitted and kept constant at a predetermined level with the help of servo valve and servo amplifier. The load level was checked both by servo amplifier and load cell read out. Then the vertical load was transferred slowly at an increment of 1000 lbs initially and then 500 lbs at later stages and the specimen loaded to failure. At each increment load, strains and deflections were

read through proper read out system which is described in detail at a later stage.

(ii) Control Prisms:

For each series of 5 beam-column specimens, 2 prisms were cast to determine the dynamic modulus of elasticity. The prisms were 3in x 3in x 12in. in dimension. First the central point of the two ends and a centrally located transverse strip of 1 in were marked on the prisms. Then their individual weights were recorded. Each specimen was then mounted on an Electrodynamic Materials Tester (Plate 4.5) in such a manner that it was centrally located on the bridge and that both the transmitter and receiver of sonic wave were lightly touching the central points of the two ends. Maximum reading was noted and this was later converted into frequency from the chart supplied with the instrument. Dynamic modulus of elasticity was then calculated from the following formula as given by ASTM Designation C215-60:

$E_R = DW(n')^2$ where

E_R = longitudinal resonance modulus of elasticity (psi)

W = weight of specimen (lbs)

n' = fundamental longitudinal frequency (cps)

$D = 0.01035 \frac{L}{bt}$ for prism (sec^2/sq in)

L = length of prism (in)

t, b = dimensions of x-section of prism (in)

(iii) Control Cylinders:

Along with the 2 prisms, 3 control cylinders (6 in dia. x 12 in) were also cast for each series in order to determine ultimate concrete strength and static modulus of elasticity. A deformation test was conducted on 2 of the cylinders (Plate 4.6) whereas the third cylinder was loaded to failure in compression to obtain ultimate concrete strength. All three cylinders were capped with standard sulphur compound. For the deformation tests, a special steel frame with 2 gages of 9 in. gage length were mounted on the cylinders. The cylinder was placed on the loading table and properly centred. This was done by putting on small load and noting deformation of the two gages. Once properly positioned, each cylinder was loaded up to 50,000 lbs in increments of 500 lbs and deformation of the 2 gages recorded at each increment. Load was then brought down all the way to zero at 500 lbs interval and similar deformation readings taken. Then the gages were dismounted and cylinder loaded to failure recording ultimate load. Data from Sonic tests and deformation and compression tests were fed into a computer programme to calculate dynamic and static modulus of elasticity.

CHAPTER 5

PRESENTATION AND ANALYSIS OF TEST RESULTS

Test results as obtained from experimental investigations and analytical work are presented in this chapter in a concise form. In view of the volume of data involved, it was considered unnecessary to write each and every reading taken, instead important data are supplied in the form of tables, graphs and photographic plates. Typical test results are shown in Tables 5.1 to 5.3.

5.1 STRESS-STRAIN RELATIONSHIP OF CONCRETE:

For each series of 5 test specimens, 2 deformation and 1 compression test have been conducted on the 6" x 12" test cylinders casted and cured under the same condition as the test specimens. From the load-deformation readings, the Initial Tangent Modulus of Elasticity, E_c has been computed by means of a computer programme. This programme fits the experimental points to a straight line. Accordingly stress-strain curves of concrete in each series was plotted in graphical form in Figures 5.1 to 5.11. From the ultimate loads attained in both the deformation and compression tests, ultimate cylinder strength f'_c has been calculated.

Two 3" x 3" x 12" concrete prisms for each series of 5 test specimens have been used to find out the Dynamic Modulus of Elasticity of concrete by means of resonance method. Comparative results of Initial Modulus of Elasticity, Dynamic Modulus of Elasticity, Modulus

of Elasticity as obtained from Inge Lyse's equation $E_c = 1800 + 460f'_c$ are all entered in tabular form along with ultimate concrete strength f'_c in tables 5.4 and 5.5.

5.2 STRESS-STRAIN RELATIONSHIP OF PRESTRESSING TENDONS:

Stress-strain relationship of high tensile steel strands along with Modulus of Elasticity and Yield Stress for the various diameter of strands used are presented in graphical form in Figs. 4.5 to 4.7. For the sake of simplicity of computation, slightly modified stress-strain relationship as shown in dotted line in these figures have been used.

5.3 TEST SPECIMENS:

Fifty-five beam-column test specimens in 11 series have been tested to failure under different axial-transverse load combinations. Dimensions of all the test specimens have been kept same within 1/8" of variation whereas amount of steel and therefore prestressing force and the concrete strength have been assumed to be same within each series. Arrangement and position of steel in the various cross-section are shown in the Figures 4.8 to 4.18, whereas different parameters such as top and bottom steel, amount of prestress, top and bottom cover, concrete strength etc. are illustrated in Table 4.1.

During testing of each specimen, strains as indicated by 10 transducers fixed at different depths on the two faces and on top of the compression edge (Fig. 4.19), deflection of 7 dial gauges placed

along the length of the test specimen (Fig. 4.22) and readings of vertical as well as horizontal load cells have been recorded usually at load interval of 1000 lbs initially and 500 lbs at later stage. All these data have been processed with the help of several computer programmes as detailed below:

(i) Programme A:

In view of the large number of data involved, this programme has been devised simply to obtain a write-up of all the data punched along with the difference of load, strain and deflection at each increment of load, so that any error in punching or in recording could readily be detected.

(ii) Programme B:

Once checking of the data was completed, they were fed in this master programme which accomplished several computations at different stages as stated below:

I. From the cross-sectional properties, the centroidal axis was computed for each test specimen.

II. Stresses induced by the prestressing tendons at top and bottom of cross section were calculated.

III. Stresses produced at top and bottom of cross section due to axial loading were then computed. These were then added to prestressing stresses and by means of Hognestad stress-strain relationship, strains at top and bottom were calculated. Principle of linear variation of strain was then applied to find out strains at the level of the different transducers.

IV. From the load cell readings, left and right reactions were obtained and average moment was calculated. To this moment, moment due to self weight was added.

V. From the dial gauge readings, deflection profile of the test specimen was obtained; maximum additional moment due to deflection was then calculated by multiplying axial thrust with central deflection. This moment added to the moment obtained in phase IV gave total maximum average moment at midpoint of the specimen.

VI. Operations IV and V were then repeated for each increment of load. Next load, moment and deflections at each gage level were recorded in tabular form for each increment of load.

VII. From the transducer readings, average strains at six different depths were obtained. Then strains due to axial loading and prestressing were added. Average curvature and depth of neutral axis were then obtained by fitting strains to a straight line variation.

VIII. Step VII was then repeated for each set of reading. Here it may be noted that once the specimen was cracked, top four strain readings instead of all six were fitted to straight line variation in order to avoid any discrepancy due to erratic behaviour of transducers placed in tension zone. This has been explained in details earlier in chapter 4.

IX. Load, moment, strains at each depth, average curvature and depth of neutral axis were recorded in a tabular form. A Flow

Chart attached in Appendix D explains all these steps in detail.

(iii) Programme C:

The purpose of this programme was to define axial thrust-moment-curvature interactions of the different sections with the help of the analytical approach shown in Chapter 3. This approach is unique in the sense that axial load-moment-curvature interactions are defined when certain sectional and stress-block parameters are only known. Average strength and average strain of concrete in each series with Hognestad stress-strain relationship have been used in these computations. Different operations are stated below:

I. From the sectional properties, ultimate capacity of the section considered as an axially loaded short prestressed concrete column has been calculated.

II. Depth of neutral axis for balanced failure was then computed from section properties.

III. From the expressions developed in Chapter 3, ultimate axial thrust, ultimate moment and ultimate curvature have been computed for balanced failure. Also forces and moments contributed by concrete and steel were calculated to investigate the behaviour of different components.

IV. Next depth of neutral axis was reduced by 0.1 inch at each step and operation III repeated until depth of neutral axis reached within top cover; then step III was repeated by increasing depth of neutral axis from balanced failure position with equal increment of

0.1 inch. This was repeated up to the full depth of cross-section. Again, details of this programme has been presented in Appendix D in the form of Flow Chart.

(iv) Presentation of Beam-Column Test Results in Graphical Form:

Beam-column test results have been plotted in Figs. 5.15 to 5.58. For each series of beam-column specimens, results are presented in the shape of four graphs as stated below:

I. First of these four graphs shows the axial load-moment interaction characteristics as computed from programme C. Experimental axial thrust-moment values have been superimposed on this graph to indicate the correlation.

II. Second graph of each series presents experimental moment-average curvature relationship up to failure at different axial load levels.

III. Third graph depicts load-central deflection relationship of each specimen at different axial load level.

IV. Fourth curve plots ultimate eccentricity against ultimate curvature for different position of neutral axis. Ultimate curvatures as obtained from writer's expressions have been plotted against the ratio of the ultimate moment to the ultimate load. Measured curvature values as obtained from test results are superimposed on the theoretical curves.

CHAPTER 6

DISCUSSION

6.1 GENERAL BEHAVIOUR:

Due to sectional properties, most of the specimens exhibited compression mode of failure, though a few failed in tension.

Typical compression failure may be studied in the behaviour of test specimen PB1D (Plate 6.1). It cracked at a late stage of loading and finally very few tension cracks of small height were developed. From the strain measurements of the different transducer levels, it was observed that the neutral axis gradually moved towards the compression face until the compression strain in compression face reached ultimate concrete strain, ε_u and concrete crushed. It may be mentioned here, since high tensile prestressing tendons have high yield strain, compression steel did not yield before crushing of concrete and therefore compressive strains near failure loads did not increase as fast as is typical of concrete reinforced with structural grade steel.

Test specimen PB6A (Plate 6.2) exhibited typical tension failure. Tension cracks developed at an early stage of loading and as loading continued extensive tension cracks could be observed and neutral axis gradually moved towards the compression face. Near failure load, the specimen showed considerable ductility and large deformation took place at small increment of load.

6.2 AXIAL THRUST-MOMENT INTERACTION:

In each series of interaction behaviours, axial thrust-moment interaction curve is the first graph presented (Figs. 5.15, 5.19, 5.23, 5.27, 5.31, 5.35, 5.39, 5.43, 5.47, 5.51, 5.55). Average values of concrete cylinder strengths and experimental average ultimate strains of concrete were substituted in analytical expressions (developed in Chapter 3) to obtain these interaction diagrams. The five experimental values of axial thrusts and bending moments have been superimposed on these graphs. Though only five experimental points were obtained in each series, good correlation of experimental values with analytical results showed that in general analytically obtained moment-axial thrust interaction diagrams give a good indication of the locus of different combinations of axial thrusts and moments for material failure. The expected and the observed ultimate moments along with the axial load levels have been presented in Tables 6.1 and 6.2. A look at these tables indicate extremely good correlation.

Due to the sectional parameters and the amount of prestressing force, only two series namely PC5 and PB6 (Figs. 5.31 and 5.55) have shown positive axial thrust for balanced failure condition . In all other series, the entire locus comprised of compression failure only. Here it may be mentioned that although only amount and arrangement of prestressing tendons were meant to be the only variables, cylinder strength of concrete varied in the different series, despite of the fact that the same mix design was used althrough.

In order to study the effect of the variation of steel reinforcement area on the strength of prestressed concrete beam-column sections, moment-axial thrust, interaction diagrams for the symmetrically prestressed and unsymmetrically prestressed sections have been drawn in Figs. 6.1 and 6.2. In Fig. 6.1, moment-axial thrust interaction diagram of series PC1 to PC5 have been drawn with $f'_c = 6$ k.s.i, $E_c = 5000$ k.s.i, $E_s = 30000$ k.s.i and $\varepsilon_u = 0.003$ in/in. From this figure, it may be observed that as the total reinforcement area changes from 0.9186 sq. in to 0.3196 sq. in in series PC1 to PC5, the ultimate moment capacity at zero axial load, M_o reduced from 369 kip-in. to 243 kip-in. But at the same time, the axial load carrying capacity, P_o increased from 200 kips to 229 kips. Around an eccentricity of 1.363 inches, the five interaction diagrams have intersected each other. It may therefore be observed that increase in symmetrical prestressing increases the load carrying capacity of beam-columns beyond an eccentricity of 1.363 inches.

In Fig. 6.2, similar trend has been observed for unsymmetrically prestressed specimens, series PB1 to PB6. In this case, the ultimate moment capacity at zero axial load, M_o increased from 2 52 kip-in to 376 kip-in as the steel reinforcement area was increased from 0.1598 sq. in to 0.6534 sq. in, whereas the axial load capacity, P_o reduced from 236 kips to 213 kips. From these curves, it may be noted that beyond an eccentricity of 1.45 inches, increase in unsymmetrical prestressing increases the ultimate load carrying capacity of the beam-column sections. From the moment-axial thrust interaction curves of rectangular prestressed concrete

sections, the following observations may be made:

(1) In reinforced concrete sections, the magnitude of balanced point load, for symmetrically reinforced sections, is independent of the amount of reinforcement because in reinforced concrete, compression steel always yields. But in case of prestressed concrete sections balanced load is not constant, because high tensile steel used as compression reinforcement does not yield and therefore the force contributed by compression steel is not constant (Table 6.3).

(2) However, unsymmetrically prestressed sections have more section capacity than symmetrically prestressed sections. This may be quite evident from Fig. 6.3. Here, though PB6 (unsymmetrically prestressed), has only half the total reinforcement of PC5 (symmetrically prestressed), their section capacity is more or less same.

(3) Though similar in shape, interaction diagram of reinforced and prestressed concrete sections differ in one important aspect. In case of reinforced concrete sections, maximum moment capacity is achieved at balanced load level, but for prestressed concrete beam-column sections this is not so. This apparent difference in behaviour could easily be explained from Fig. 6.4. Here the force contributed by concrete, C_u increased at a much faster rate than the decrease in the force contributed by the steel, T_u as the depth of neutral axis is increasing. This may be explained by the fact that the change in force caused by steel strain is quite small compared to initial prestressing force. Hence, rapid increase in C_u causes concrete moment, C_M curve to rise sharply until the

neutral axis reaches up to a depth of 4 in. Thereafter, the force C_u continues to increase at the same rate but by now the moment arm has been reduced significantly and therefore C_M curve flattens out and gradually decreases after neutral axis has crossed a depth of 5 in. Since the ultimate moment capacity is given by the expression:

$$M_u = C_M + T_M$$

and the contribution of T_M is very small, M_u is mainly influenced by concrete moment, C_M. Thus, ultimate moment, M_u continues to increase beyond the balance point up to a depth of neutral axis of 5 in. when it reaches the peak and then gradually decreases.

(4) In Figs. 6.5 and 6.6, the variation of the ultimate load with the area of longitudinal steel reinforcement have been compared for $\frac{e}{t}$ ratios of zero and 1, where e is the eccentricity of the load and t is the total thickness of the section. From these two figures, it is evident that for both symmetrically and unsymmetrically prestressed sections, the ultimate load decreases with the increase of longitudinal steel at $\frac{e}{t} = 0$. For 6000 psi concrete in Fig. 6.5 as the longitudinal reinforcement area reduces from 0.9186 sq. in. to 0.3196 sq. in. in series PC1 to PC5, the ultimate load capacity decreases from 229 kips to 199 kips for $\frac{e}{t} = 0$. In case of 4000 psi concrete, the corresponding reduction is from 145 kips to 113 kips. But when the $\frac{e}{t}$ ratio is increased to 1, there is a slight increase in the ultimate load capacity of

both symmetrically and unsymmetrically prestressed sections with the increase of the area of longitudinal reinforcement. For 6000 psi concrete in Fig. 6.5, as the longitudinal reinforcement area reduces from 0.9186 sq. in. to 0.3196 sq. in. in series PC1 to PC5, the ultimate load capacity increases from 32 kips to 45 kips for $\frac{e}{t}$ ratio of 1. For 4000 psi concrete corresponding increase in from 25.3 kips to 33.5 kips. In Fig. 6.6, similar trend for unsymmetrically prestressed sections, PB1 to PB6 has been noticed.

(5) Reduction of the load capacity of beam columns as compared to the load carrying capacity of axially loaded columns, P_u/P_{Axial} may be estimated both for symmetrically and unsymmetrically prestressed sections for different values of $\frac{e}{t}$ ratios from the Figs. 6.7 and 6.8.

6.3 MOMENT-CURVATURE-AXIAL THRUST RELATIONSHIP:

The second graph in each series presents the variation of moment-curvature relationship at various axial load levels (Figs. 5.16, 5.20, 5.24, 5.28, 5.32, 5.36, 5.40, 5.44, 5.48, 5.52, 5.56). A study of these figures indicate the manner in which axial load influences the ductility in the different series. The experimental and analytical values of ultimate moments and the curvatures at ultimate load for the different axial load levels of the different series have been presented in tabular form in Tables 6.1 and 6.2.

In Series PC1 (Fig. 5.16) all the axial load levels have been higher than the balanced load. Curvature at ultimate load varied from 0.001002 rad./in at zero axial load to 0.000627 rad/in at the axial load of 95 kips (Table 6.1).

The ratio of ultimate curvature at different axial load levels to the ultimate curvature at zero axial load, ϕ_u/ϕ_o varied from 1 to 0.6146 as the ratio of ultimate moments at different axial loads to the ultimate moment at zero axial load, M_u/M_o was varied from 1 to 0.9443. From Fig. 5.16, it may be observed that the specimens became gradually stiffer as the axial load was increased. At the axial load of 95 kips, the section was initially stiffer than the other members of the same series (PC1), but near the ultimate moment value, it became less stiff. From Table 6.1, it may be observed that from PC1C to PC1D, reduction in M_u/M_o was 0.0279 whereas the reduction in ϕ_u/ϕ_o was 0.1265. But from PC1D to PC1E, reduction of M_u/M_o was 0.0379 as compared to the reduction of 0.0470 in ϕ_u/ϕ_o. Thus it is seen that the reduction in M_u/M_o increased from PC1D to PC1E whereas the reduction in ϕ_u/ϕ_o decreased and therefore there was little loss in stiffness in PC1E.

Series PC2 and PC3 (Figs. 5.20, 5.24 and Table 6.1) showed similar trend in behaviour, that is, the value of the ultimate curvature gradually reduced as the axial load level was increased from zero to 95 kips and a slight loss of stiffness at the axial load level of 95 kips was observed. In PC4E, (Fig. 5.28) axial load of

95 kips was not much higher than the balanced load, therefore the loss of stiffness at this axial load level was not noticeable. In series PC5 (Fig. 5.32), due to the decrease in the area of longitudinal reinforcement tensile failure was observed at zero axial load level (PC5A) and the value of ultimate curvature of 0.001751 rad/in was quite high. But as the axial load level was increased to around balanced load (PC5B), the value of ultimate curvature dropped to 0.001484 rad./in. This value was further reduced to 0.000678 rad./in as the axial load level was increased to 95 kips.

In case of unsymmetrically prestressed sections, series PB1 to PB6, same general trend has been observed. In series PB1 (Fig. 5.36), since the axial load level was much higher than the balanced load, the value of ultimate curvature of 0.000953 rad./in at zero axial load (Table 6.2) was quite low. This value was further reduced to 0.000521 rad./in as the axial load level was increased to 95 kips and there was a slight loss of stiffness at near the ultimate load of 95 kips (Fig. 5.36) due to the reason explained above. From Fig. 5.36, it may be observed that as the range of axial load levels were very close and much higher than the balanced load level, the moment-curvature relations were located in a narrow band. Series PB2 to PB5 (Figs. 5.40, 5.44, 5.48, 5.52 and Table 6.2) showed the same general characteristics. But as the amount of longitudinal steel reinforcement was reduced from 0.6534 sq. in. in PB2 to 0.3196 sq. in. in PB5, the value of ultimate curvature at

zero axial load level increased from 0.001101 rad./in in PB2 to 0.001254 rad./in in PB5. Same trend was observed at other axial load levels. In case of series PB6 (Fig. 5.56 and Table 6.2) the amount of longitudinal steel reinforcement reduced to 0.1598 sq. in. and therefore tensile failure was observed at low axial load levels, PB6A and PB6B. The value of the ultimate curvature at low axial load levels were correspondingly quite high (0.001669 and 0.001628 rad/in respectively for PB6A and PB6B), but as the axial load level was increased to 95 kips (PB6E), the value of the ultimate curvature reduced to 0.000736 rad./in.

6.4 TRANSVERSE LOAD VS. DEFLECTION AT MIDPOINT:

The third graph in each series (Figs. 5.17, 5.21, 5.25, 5.29, 5.33, 5.37, 5.41, 5.45, 5.49, 5.53 and 5.57) exhibits variation of the mid-point deflection with the transeverse load at different axial load levels.

In series PC1 (Fig. 5.17), at zero axial load, PC1A, deflection at mid-point was 0.43 inches at the ultimate load. But the amount of deflection at mid-point gradually reduced to 0.17 inches as the axial load level was increased to 75 kips. However, at the axial load level of 95 kips (PC1E), final deflection at the mid-point of the specimen was slighty increased to 0.175 inches and the section showed slight loss of stiffness. For the rest of the symmetrically prestressed series, PC2 to PC5, similar trend of increasing stiffness with the increase in axial load was observed.

For the unsymmetrically prestressed sections, PB1 to PB6 (Figs. 5.37, 5.41, 5.45, 5.49, 5.53 and 5.57) similar trend was observed. However, as the amount of longitudinal reinforcement was reduced from 0.6534 sq. in. in PB1 to 0.1598 sq. in. in PB6, the final value of mid-point deflection at failure load increased from 0.34 inches to 0.85 inches (Figs. 5.37 and 5.57).

From these observations, it may be concluded that:

(1) Both symmetrically and unsymmetrically prestressed sections gain stiffness against deflection as the axial load level is increased.

(2) Increase in the longitudinal reinforcement and therefore in the prestressing force reduces mid-point deflection in both symmetrically and unsymmetrically prestressed sections.

6.5 ECCENTRICITY VS CURVATURE AT THE ULTIMATE LOAD:

As explained in the Chapter 5, theoretical values of the curvatures at ultimate load have been plotted against the eccentricities at ultimate load, as obtained from computer programme C, as the fourth graph in each series (Figs. 5.18, 5.22, 5.26, 5.30, 5.34, 5.38, 5.42, 5.46, 5.50, 5.54 and 5.58). From these curves and also from Tables 6.1 and 6.2, it may be noted that the curvature at ultimate load increased rapidly with the increase of eccentricity at low values of eccentricity but the rate of increase was gradually reduced as the eccentricity was increased to higher values and became

almost flat at very high eccentricities. This same trend has been shown by all the series. However, in series PC5 and PB6 (Figs. 5.34 and 5.58) which exhibited balanced failure at positive axial thrust, there was an apparent break in the curve at balanced failure point. From tables 6.1 and 6.2, and Figs. 6.9 and 6.10 it may be observed that both for symmetrically and unsymmetrically prestressed rectangular sections, ultimate curvature increases with the decrease in the amount of longitudinal reinforcement.

Fig. 6.11 shows the comparison of variation of curvature with eccentricity at ultimate load of unsymmetrically prestressed series PB1 with symmetrically prestressed series PC2. These two series have same total amount of longitudinal reinforcement of 0.6534 sq.in., but PC2 exhibits about 1.5 times higher curvature than PB1 at the same eccentricity levels of 20 inches and higher.

The four experimental values of eccentricity and curvature at ultimate load in each series have been superimposed on the theoretical curves and in general good correlation has been obtained (Table 6.1 and 6.2). Little amount of scatter in some cases, specially at low axial load level may be ascribed to the sensitivity of the curves to the variation of ultimate strain (Fig. 6.12). Since average experimental ultimate strains have been used in the compilation of these curves, little bit of scatter is naturally expected, specially when ultimate strain varied from 0.00357 to 0.004559 in some cases. Although only 4 points have been compared in each series, which does

not allow to make any conclusive statement, the general trend may be summarised as follows:

(1) Analytical expressions as obtained from writer's analysis give a satisfactory indication of the relationship of curvature with eccentricity at ultimate load for prestressed concrete beam-column sections.

(2) Ultimate curvature is greatly sensitive to the amount of prestressing tendons. Both in symmetrically and unsymmetrically prestressed sections, increase in longitudinal reinforcement decreases curvature at ultimate load (Tables 6.1 and 6.2).

(3) Curvature at ultimate load is also quite sensitive to ultimate compressive strain of concrete, ε_u. An increase in ultimate concrete strain increases curvature at ultimate load significantly (Fig. 6.12).

(4) Symmetrically prestressed sections are more ductile than unsymmetrically prestressed sections, especially at high eccentricity of loads (Fig. 6.11).

6.6 VARIATION OF ϕ/ϕ_o WITH P_U/P_{Axial} :

Nondimensional load-curvature relationship has been presented both for the symmetrically and the unsymmetrically prestressed series in Figs. 6.13 to 6.16.

In Fig. 6.13, average curves have been drawn for the five experimental points of P_U/P_{Axial} VS. ϕ/ϕ_o relationship for the five symmetrically prestressed series, PC1 to PC5. It may be observed that PC1 ($p = 0.0191$) has 50 percent more ϕ/ϕ_o value than PC5 ($p = 0.0066$) for P_U/P_{Axial} ratio of 0.4. That means, for the

same ratio of axial load level of 0.4, the reduction in ductility from zero axial load level in PC5 was about 50 percent more than in PC1. Similar trend has been observed in the unsymmetrically prestressed series, PB1 to PB6 (Fig. 6.14). In this case at the same P_U/P_{Axial} ratio of 0.4, the reduction in ductility from zero axial load level was about 75 percent more in PB6 ($p = 0.0033$) than PB1 ($p = 0.0136$). These values of 50 and 75 percent reduction (Figs. 6.13 and 6.14) however gradually decreased as the axial load level approached zero.

In Figs. 6.15 and 6.16, correlation of the experimental and theoretical values of P_U/P_{Axial} VS. ϕ/ϕ_o relationship have been shown. In both the figures, the firm line indicates theoretical values obtained from Programme C by using average values of experimental ultimate strain, ε_u, whereas the dotted line has been drawn by using the ACI value of $\varepsilon_u = 0.003$. From the figures, it may be observed that the correlation of experimental points with the theoretical curves has been extremely good. In both the figures, it is also evident that ACI value of $\varepsilon_u = 0.003$ gives conservative estimate of ductility, especially at high axial load levels and for higher reinforcement ratios (PC1 and PB1).

6.7 POSSIBLE ERRORS IN TEST AND ANALYSIS:

Both the experimental tests and the analytical methods reported in this thesis are liable to be subjected to some inadvertent errors. Despite of best efforts, the components of variables in the tests could not be perfectly controlled and some of the assumptions of the analytical work may not be strictly true. Therefore, possible

sources of error are indicated in the following discussion:

(1) Three 6 inches long control cylinders were used as a measure of concrete strength in the specimens in each series. Although the specimens as well as the control cylinders were cast from the same batch of concrete and cured under identical condition, they showed some variation in strength and therefore average value of f'_c had to be used.

(2) The sectional dimension of the test specimens were found to vary up to 1/8 inches which contributed to some variation in ultimate loads.

(3) Yield points of prestressing tendons of same diameter varied a little bit in the different lots.

(4) Position of prestressing tendons might possibly have differed little bit from intended position due to some minor fault in formwork and casting.

(5) The amount of prestressing force was determined by measuring hydraulic pressure in prestressing jack as well as by the measurement of actual elongation with the help of a measuring scale. Both of these methods being very crude, it is expected that some error might have been introduced here.

(6) Final prestressing force was calculated by subtracting expected losses from initial prestress, which has probably led to some error.

(7) Due to the amount of prestress on concrete for about a month, stress-strain relationship of test specimens might be little

bit different from plain concrete cylinders.

(8) Although horizontal pins used to transfer axial thrust performed satisfactorily, sometimes it was observed that on application of axial thrust, the specimens tended to move vertically due to rotation at the bearings. In most cases corrective measures were successful while in others new elevation of test specimen had to be considered.

(9) Some error might have crept into due to unsymmetrical positioning of load plates about longitudinal axis. This was evident by difference in strain shown from transducers at same depth placed on front and rear face.

(10) In order to avoid damage to the transducers, they had to be removed sometimes before the final crushing of concrete. This obviously led to incomplete moment-curvature relationship.

CHAPTER 7

CONCLUSION

In view of the number of specimens tested and the analytical results obtained, it is quite evident that the general trend shows good agreement and therefore following conclusions may be made:

(1) The mode of behaviour and failure pattern of the prestressed concrete beam-column sections are quite similar to the reinforced concrete sections under combined bending and axial load. Final failure in the specimens is caused by crushing of concrete at an ultimate compressive strain, ε_u ranging from 0.003570 to 0.005857 in/in. After crushing, load capacity suddenly falls.

(2) However, there is one important deviation in the moment-axial thrust interaction diagram of the prestressed concrete beam-columns from those of the reinforced concrete sections. Unlike reinforced concrete, moment capacity in prestressed concrete sections increase even beyond balanced load (Fig. 6.4).

(3) Unlike structural grade steel in the reinforced concrete beam column sections, high tensile tendons used as compression steel in prestressed concrete sections do not yield when concrete crushes. This results in varying balanced load in prestressed concrete beam-columns (Table 6.3).

(4) In the prestressed concrete beam-column sections, considerable amount of ductility is exhibited for tension failures and this decreases as axial load level is increased to balanced load and

beyond. However, as the axial thrust is further increased, an apparent slight increase in ductility is evident. This is because rate of reduction of moment capacity is greater than rate of reduction in curvature at that axial load level (Tables 6.1 and 6.2).

(5) Stiffness of prestressed concrete beam-column sections against rotation increases with increased axial load level up to certain axial thrust and then it falls (Fig. 5.16).

(6) Curvature of the prestressed concrete beam-column sections at ultimate load is greatly influenced by the ultimate compressive strain of concrete, prestressing force and axial thrust (Fig. 6.12, Tables 6.1 and 6.2).

(7) Ductility of the prestressed concrete sections are increased with decreasing longitudinal reinforcement (Figs. 6.9 and 6.10).

(8) The strength capacity of unsymmetrically prestressed sections are higher than symmetrically prestressed beam-column sections (Fig. 6.3).

(9) On the other hand, symmetrically prestressed sections are more ductile than unsymmetrically prestressed beam-column sections, especially at high values of eccentricity (Fig. 6.11).

SUGGESTIONS FOR FUTURE RESEARCH:

In view of the experimental and analytical work done, some suggestions for future investigations may be made:

(1) Analytical expressions developed for moment-curvature-axial thrust interactions have been verified by limited number of experimental data. Hence, some more experimental work in this direction specially at higher values of eccentricity would be quite beneficial.

(2) Many investigators have found out variation in the stress-strain relationship of plain concrete and concrete which has been prestressed under load for sometime. This has been attributed to creep effect. The creep characteristics of concrete will play an important part in determining not only the effects of prestressing but also rate of loading.

(3) Research in the field of yield interaction characteristics would certainly be helpful in understanding the behaviour of prestressed concrete beam-column sections.

APPENDIX A: FIGURES

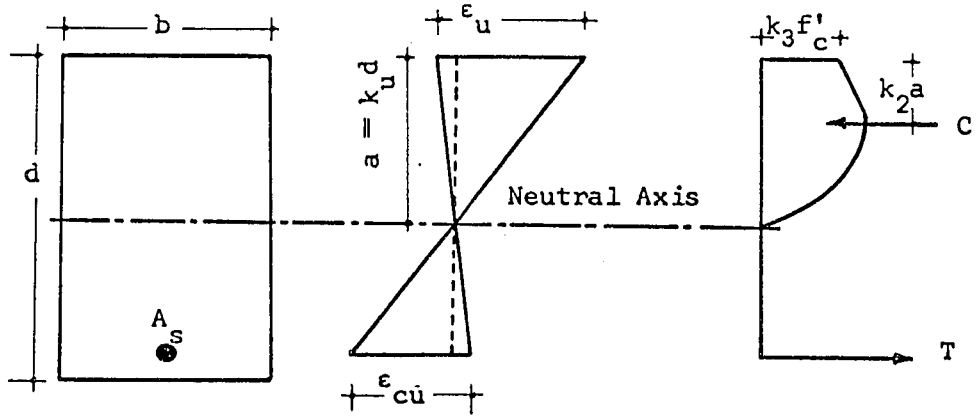

FIG. 2.1: BEHAVIOUR AT ULTIMATE LOAD

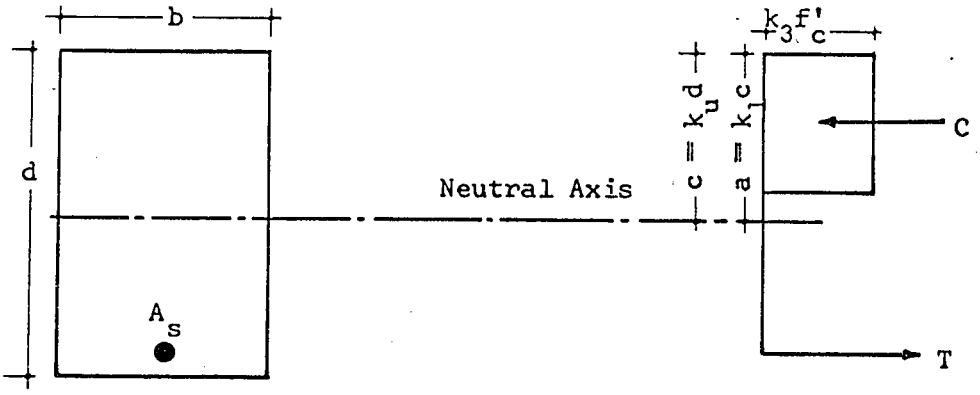

FIG. 2.2: RECTANGULAR STRESS DISTRIBUTION

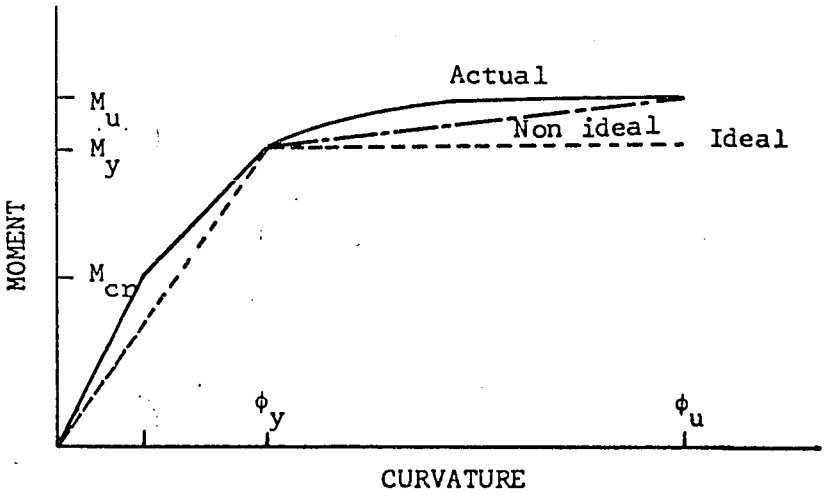

FIG. 2.3: MOMENT-CURVATURE RELATIONSHIP

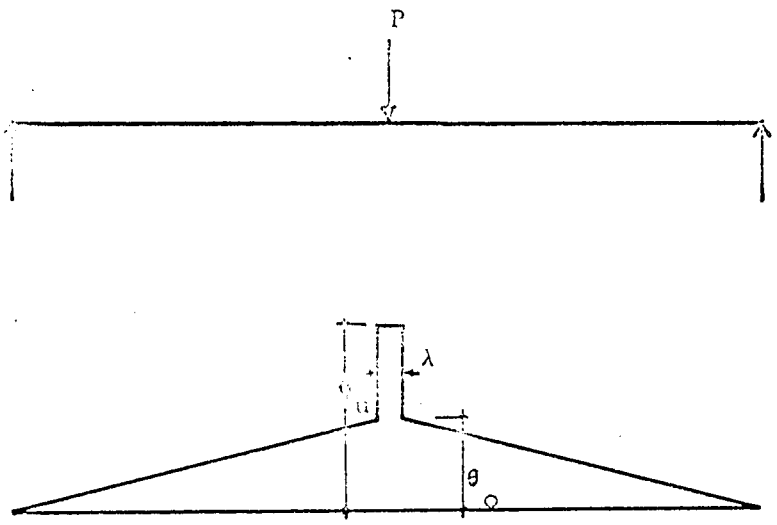

(a) BEAM WITH LOCALIZED YIELD

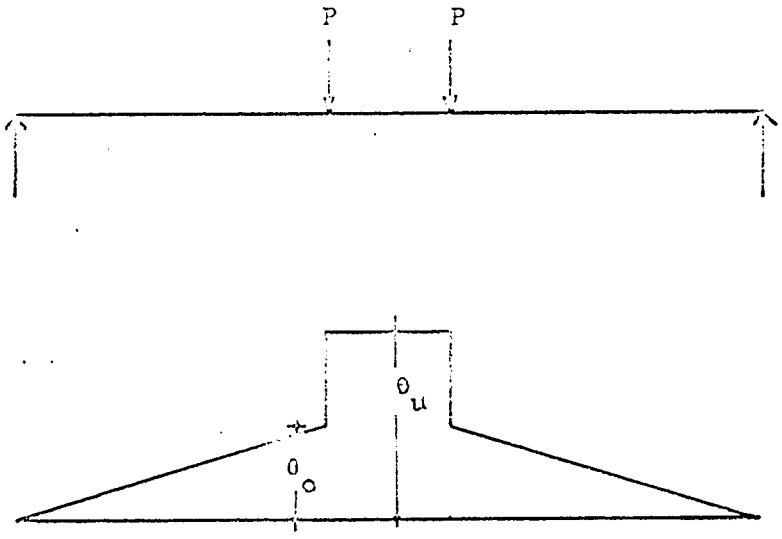

(b) BEAM WITH FINITE YIELD LENGTH

FIG. 2.4 UNIT ROTATION DIAGRAM

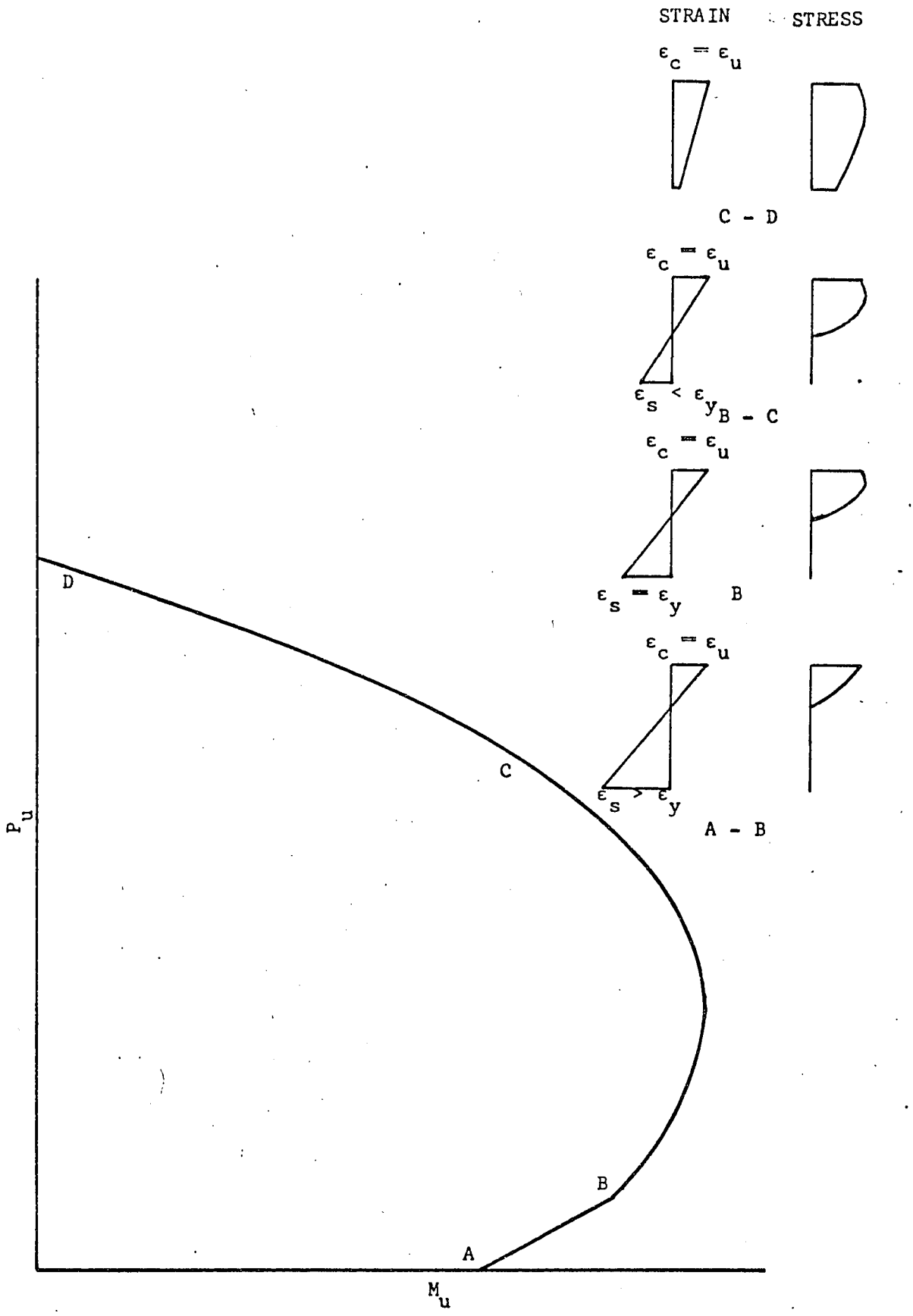

FIG. 3.1 - INTERACTION DIAGRAM WITH STRESS BLOCK AND STRAIN DISTRIBUTION AT DIFFERENT LOADING STAGES.

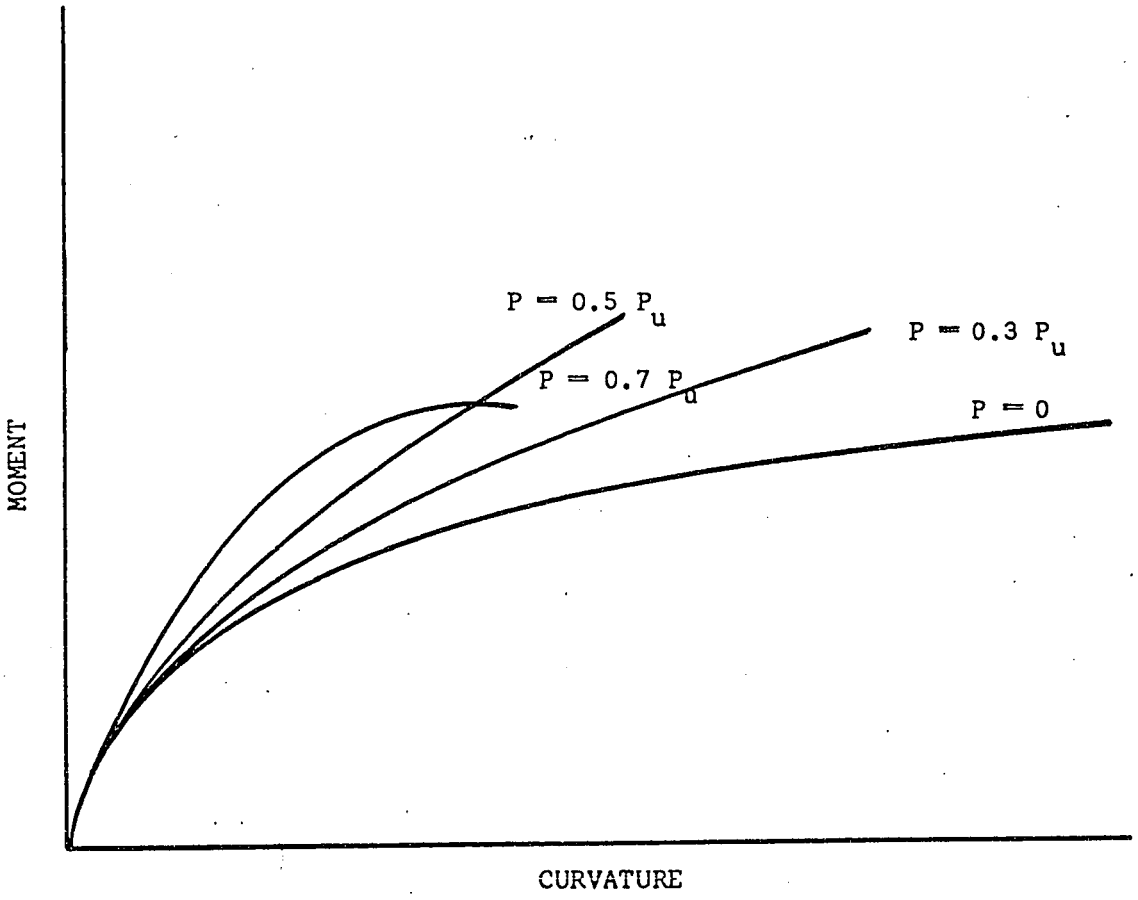

FIG. 3.2: TYPICAL MOMENT-CURVATURE-AXIAL LOAD RELATIONSHIP

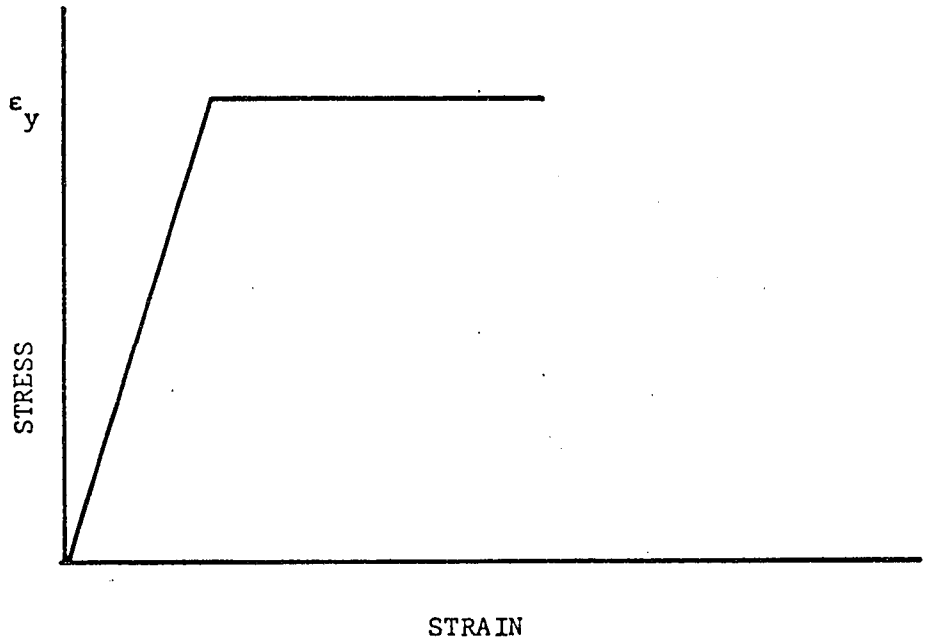

FIG. 3.3: IDEALISED ELASTI-PLASTIC STRESS-STRAIN RELATIONSHIP OF PRESTRESSING TENDONS.

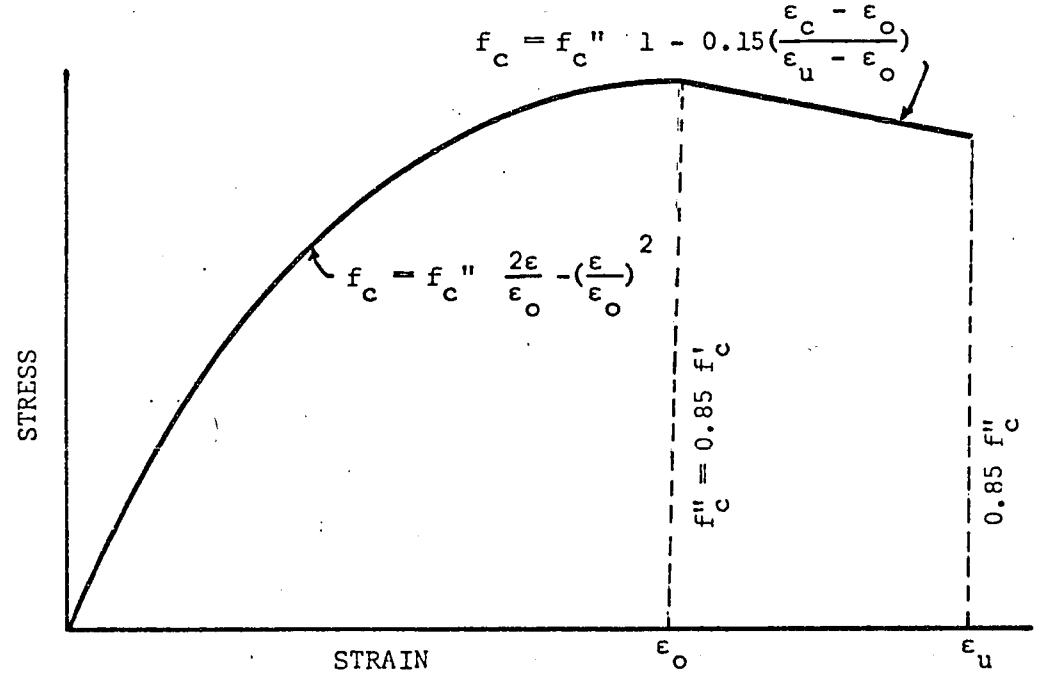

FIG. 3.4: STRESS-STRAIN RELATIONSHIP OF CONCRETE AS PROPOSED BY HOGNESTAD.

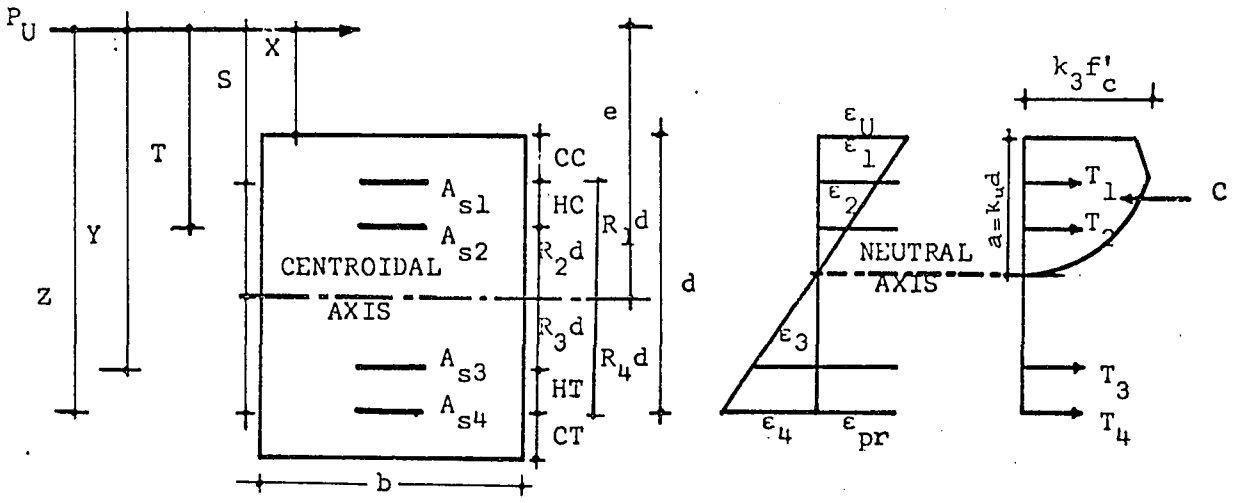

FIG. 3.5: STRESS AND STRAIN DISTRIBUTION AND SECTION PARAMETERS FOR TENSILE HINGE IN PRESTRESSED CONCRETE BEAM-COLUMN SECTIONS.

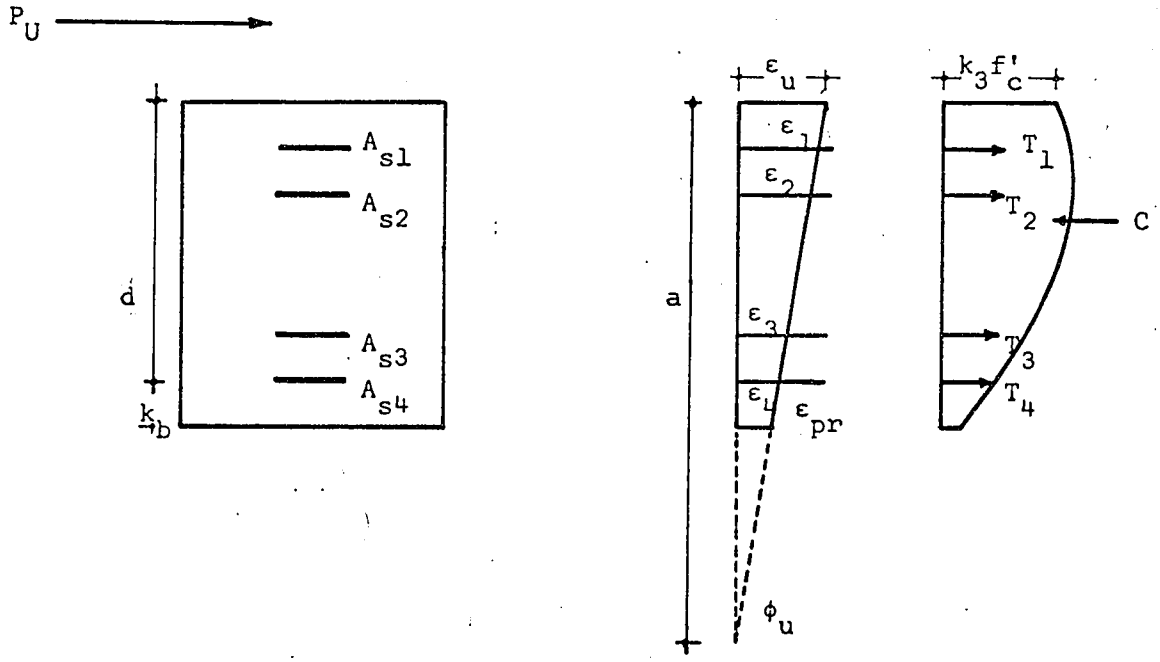

FIG. 3.6: STRESS AND STRAIN DISTRIBUTION AND SECTION PARAMETERS FOR COMPRESSIVE HINGE IN PRESTRESSED CONCRETE BEAM-COLUMN SECTIONS.

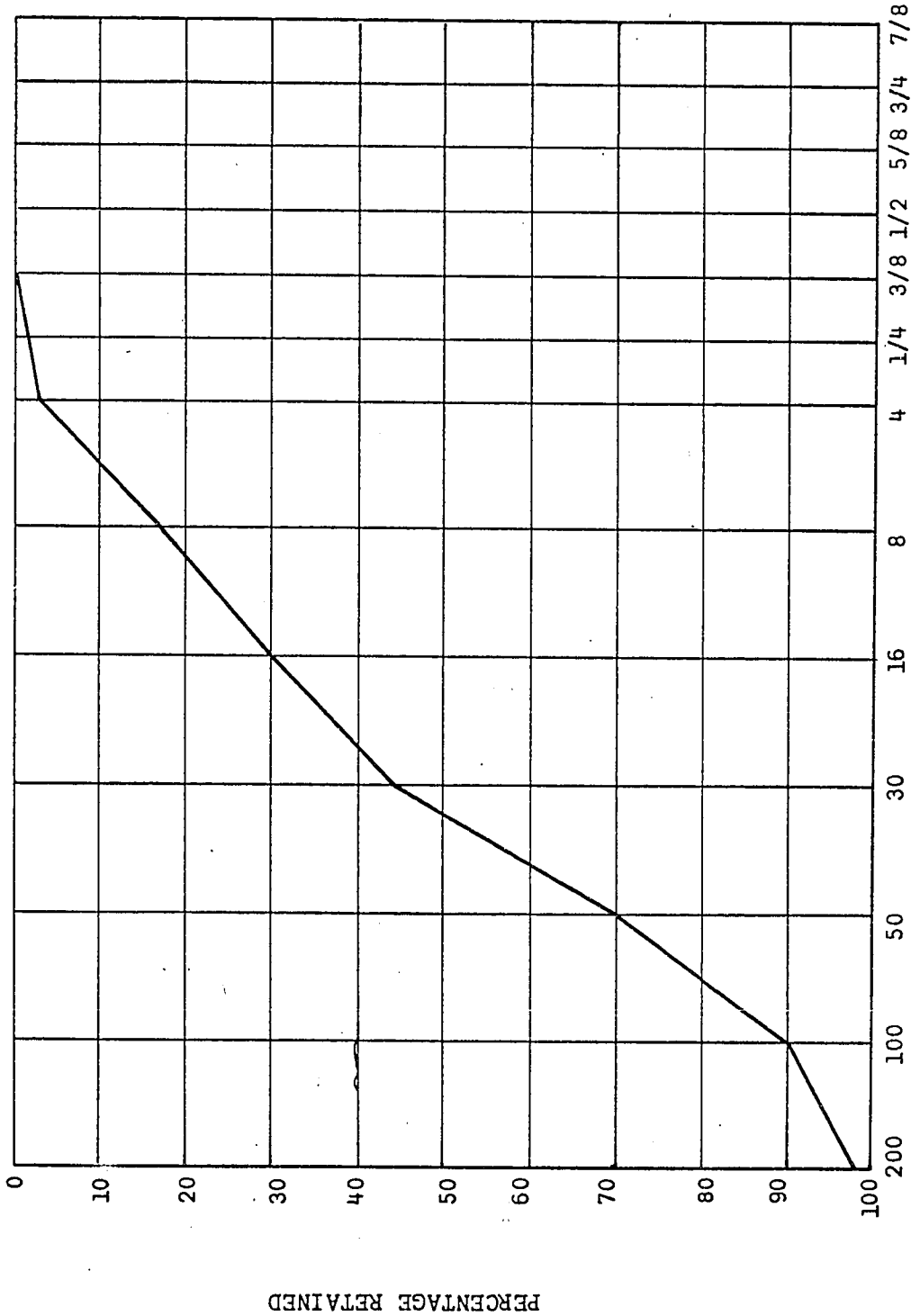

FIG. 4.1: SIEVE ANALYSIS OF TYPE ONE SAND

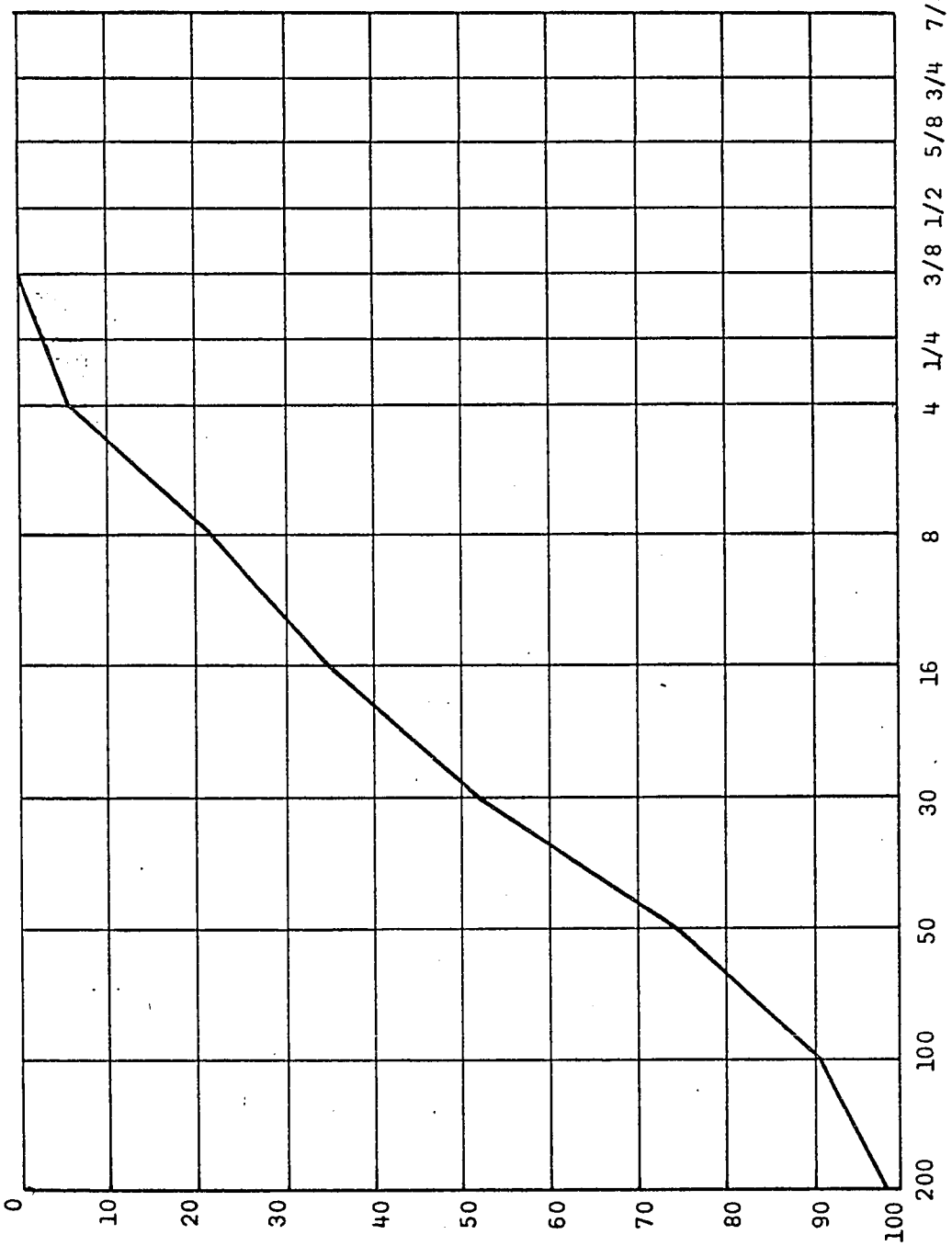

FIG. 4.2: SIEVE ANALYSIS OF TYPE TWO SAND

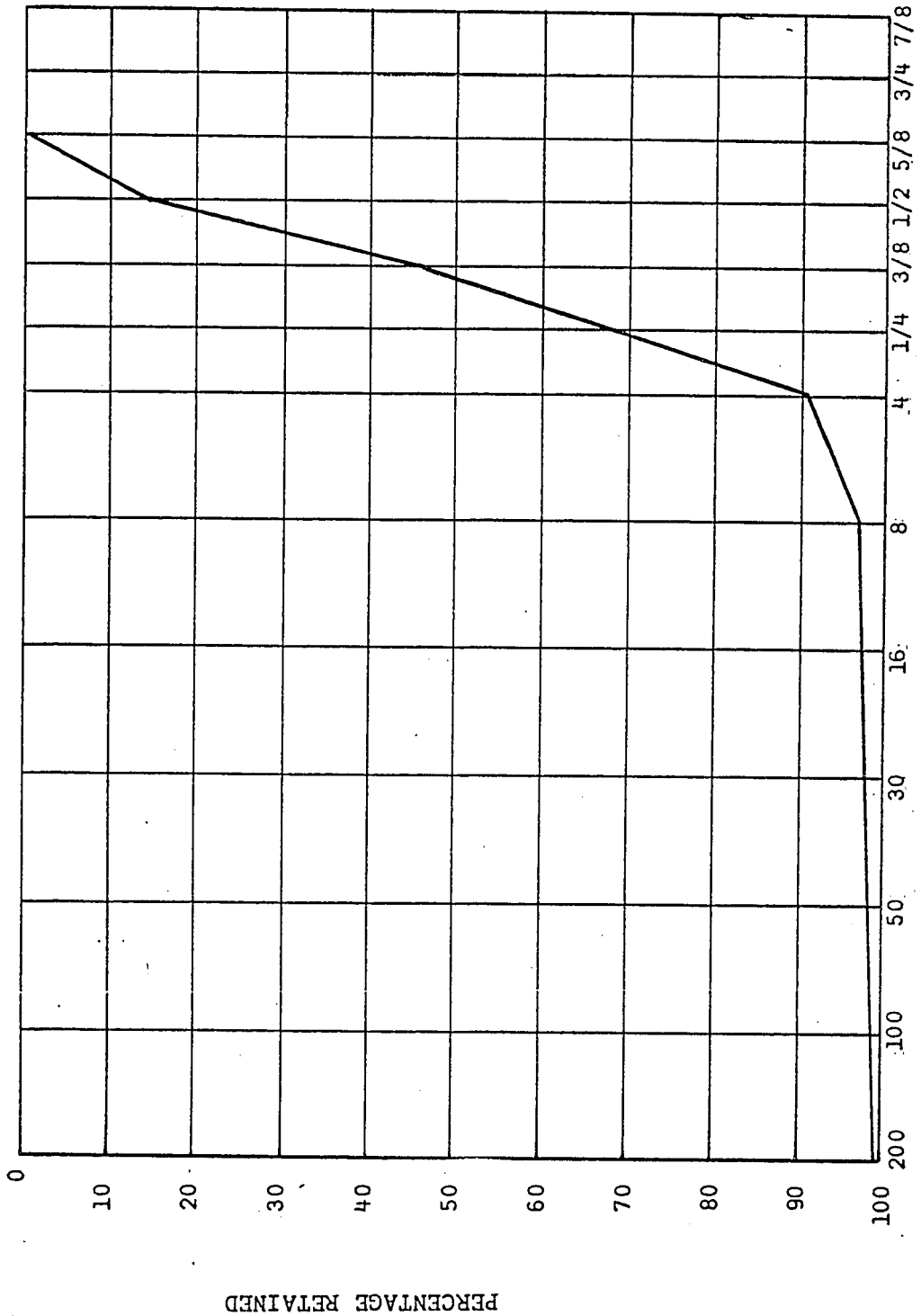

FIG. 4.3: SIEVE ANALYSIS OF TYPE ONE STONE

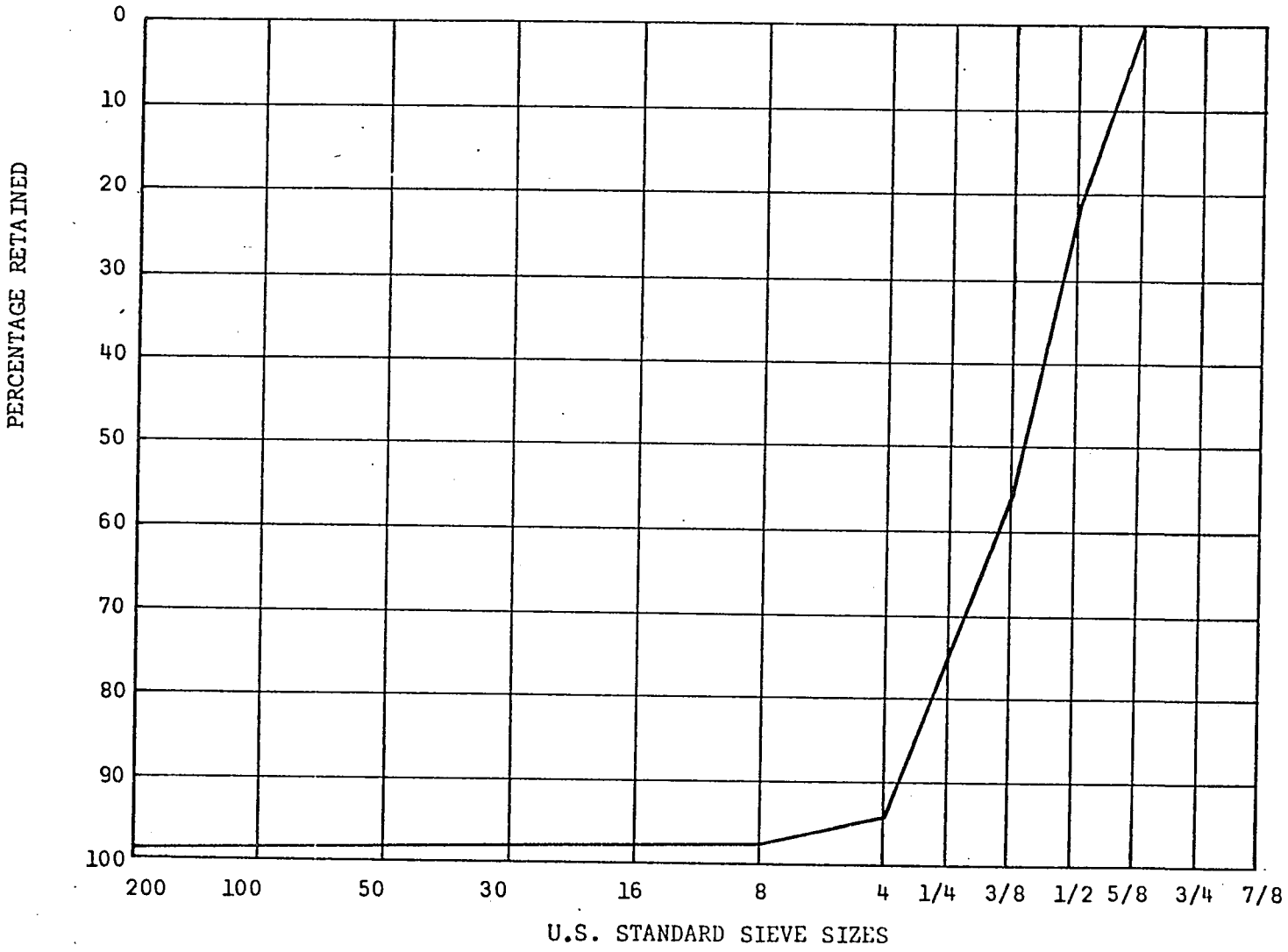

FIG. 4.4: SIEVE ANALYSIS OF TYPE TWO STONE

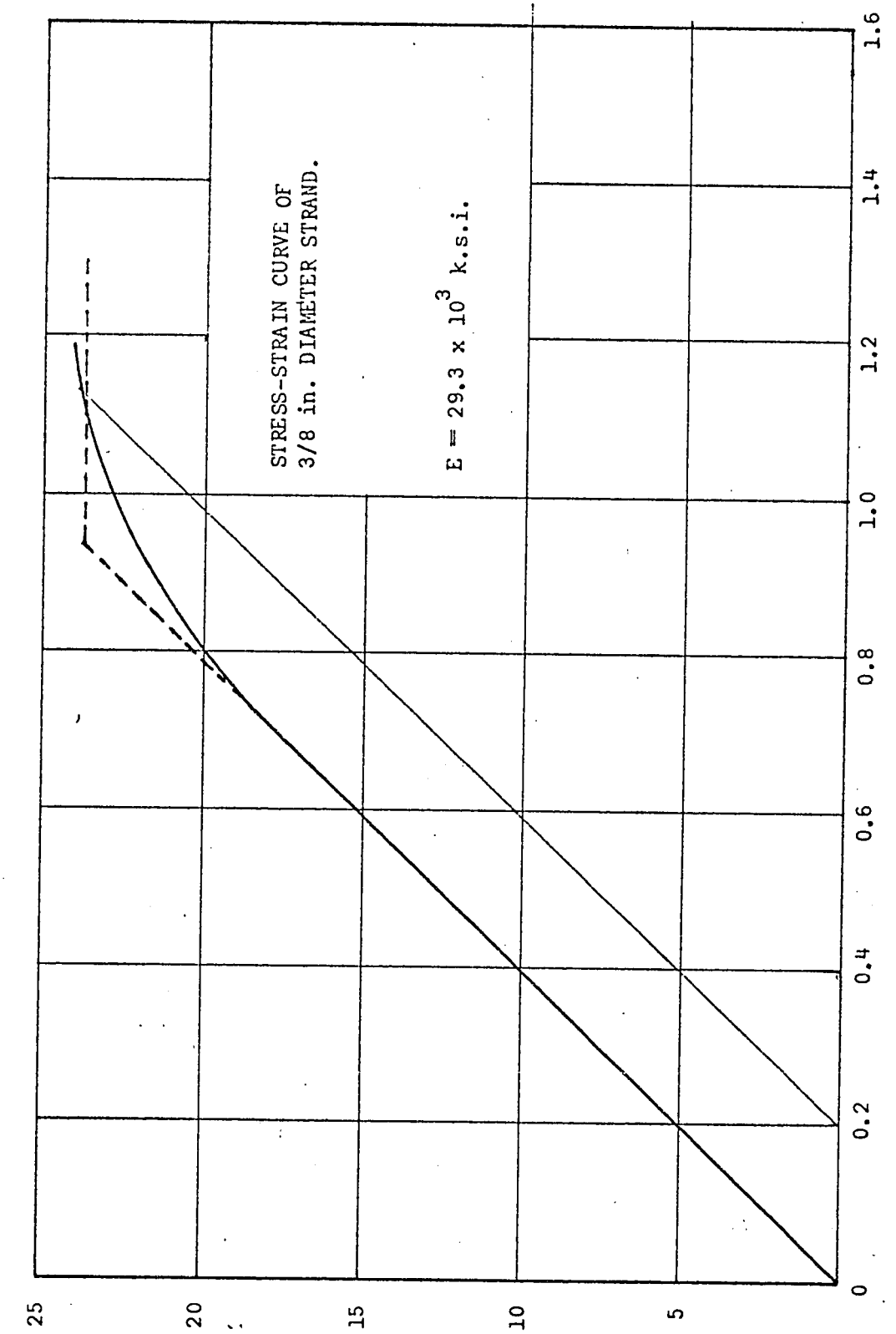
STRESS-STRAIN CURVE OF
3/8 in. DIAMETER STRAND.
E = 29.3 x 10^3 k.s.i.
LOAD IN KIPS
25
20
15
10
5
0
0.2
0.4
0.6
0.8
1.0
1.2
1.4
1.6
PERCENT EXTENSION

FIG. 4.5

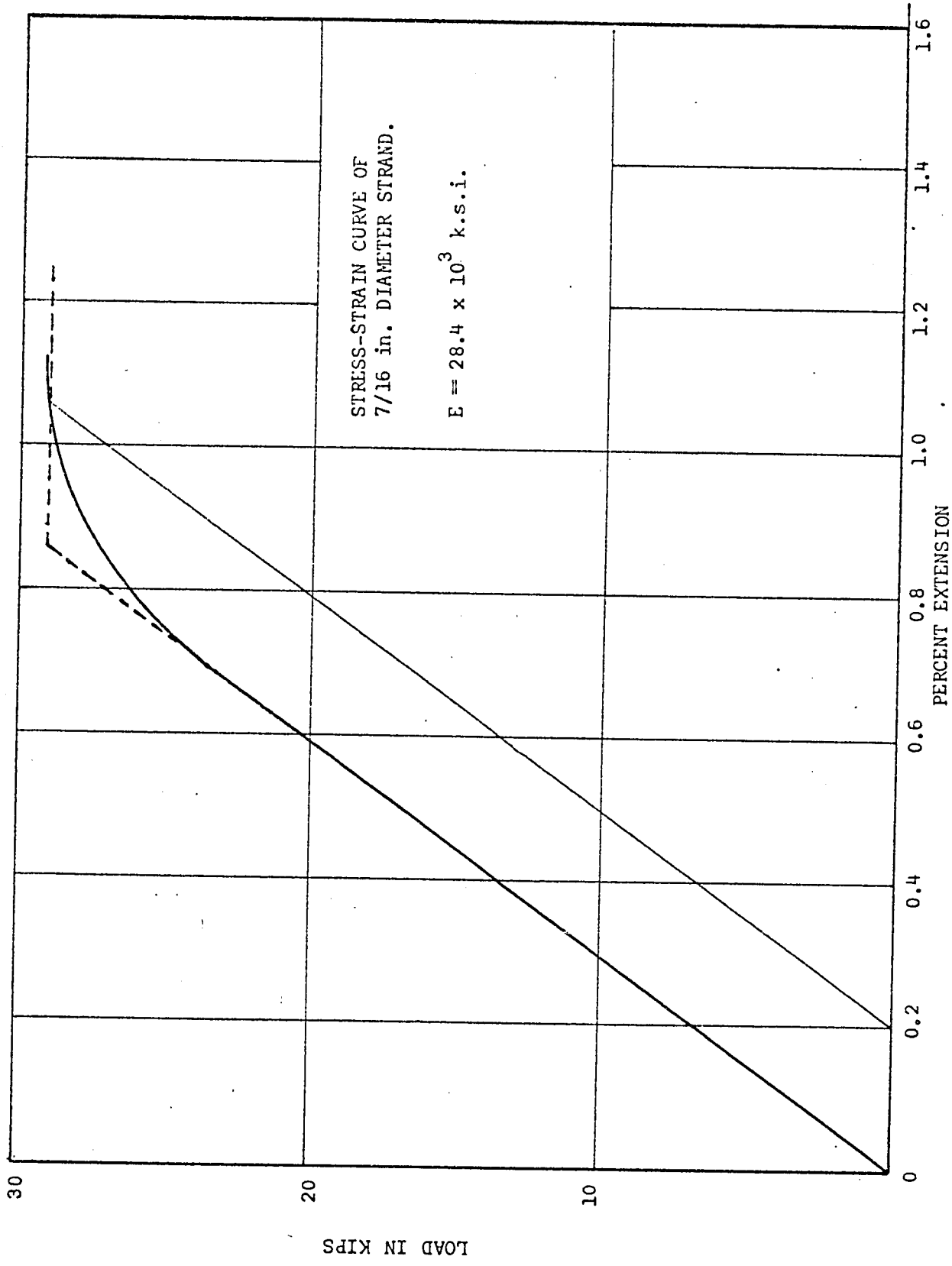
STRESS-STRAIN CURVE OF
7/16 in. DIAMETER STRAND.
E = 28.4 x 10^3 k.s.i.
LOAD IN KIPS
30
20
10
0
0.2
0.4
0.6
0.8
1.0
1.2
1.4
1.6
PERCENT EXTENSION

FIG. 4.6

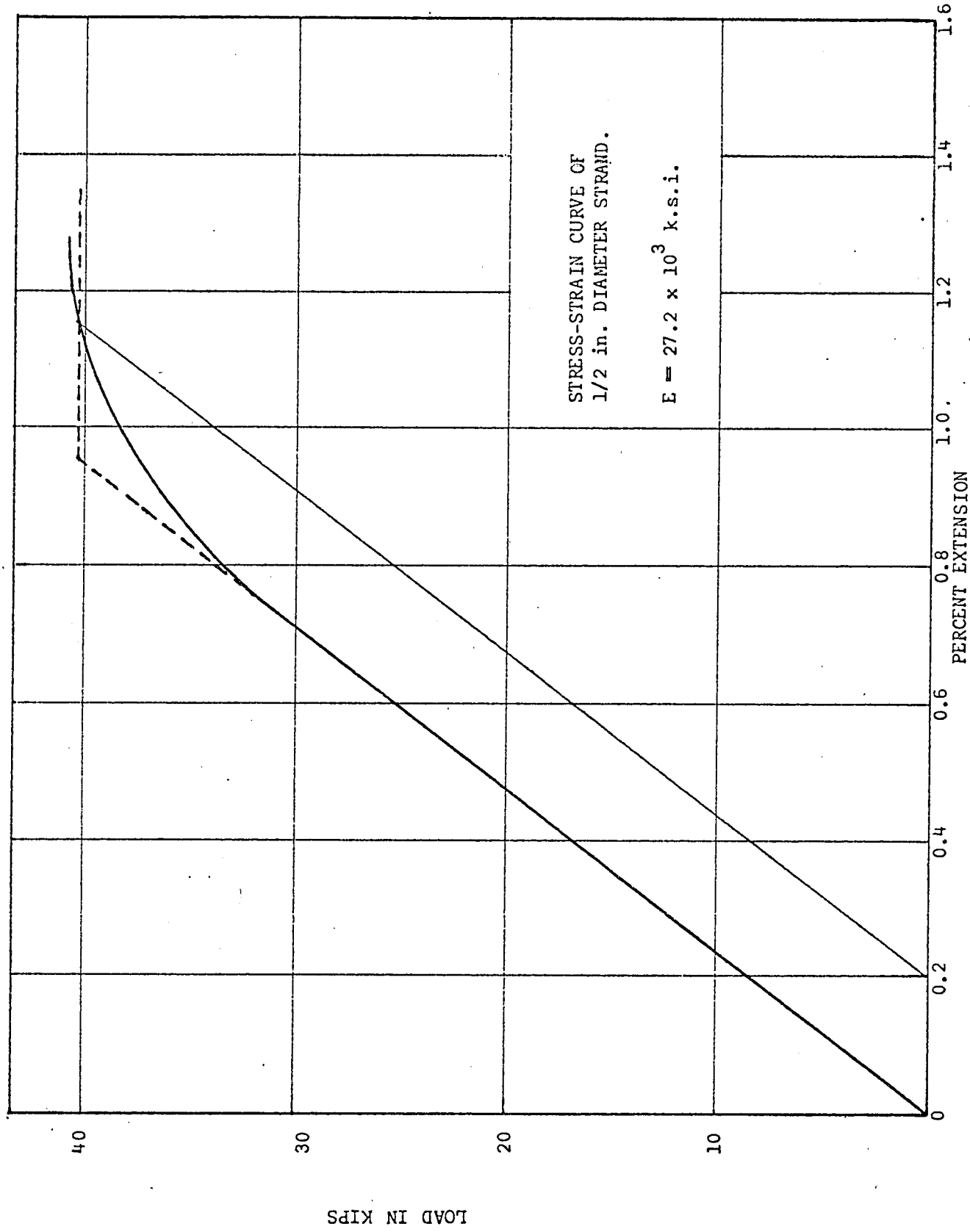
STRESS-STRAIN CURVE OF
1/2 in. DIAMETER STRAND.
E = 27.2 x 10^3 k.s.i.
LOAD IN KIPS
PERCENT EXTENSION
0
10
20
30
40
0.2
0.4
0.6
0.8
1.0
1.2
1.4
1.6

FIG. 4.7

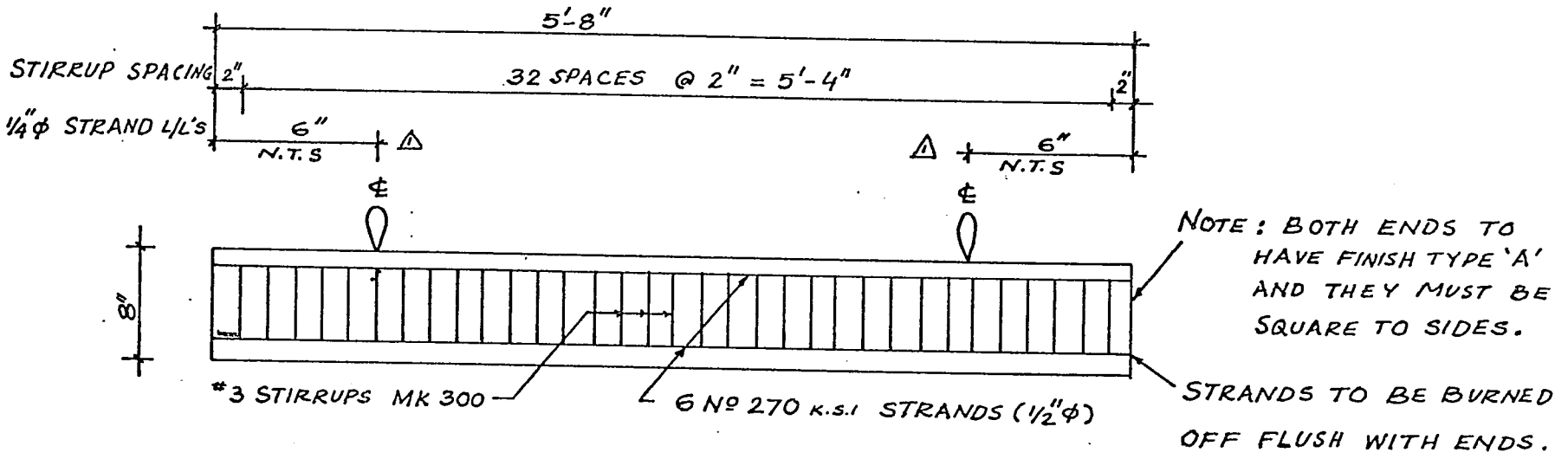

ELEVATION.

NOTES:

1. f_c' 5,000 P.S.I
2. f_y 270 K.S.I

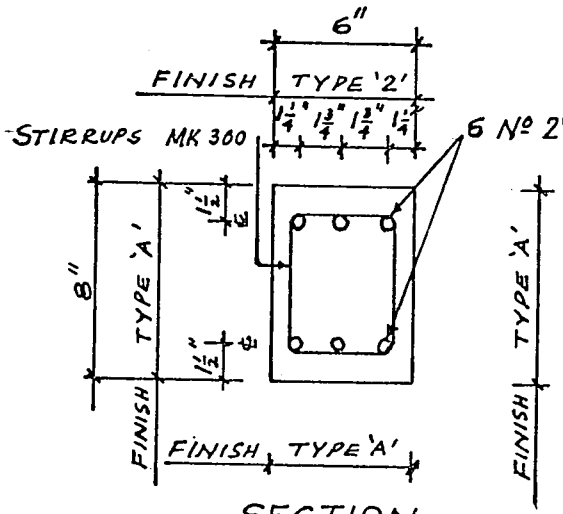

SECTION.

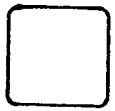

INS. DMS.

DETAIL OF #3 STIRRUPS
MK 300 x 2'-1" LG.
33 No THUS REQD.

FIG. 4.8: FABRICATION DRAWING OF PC1.

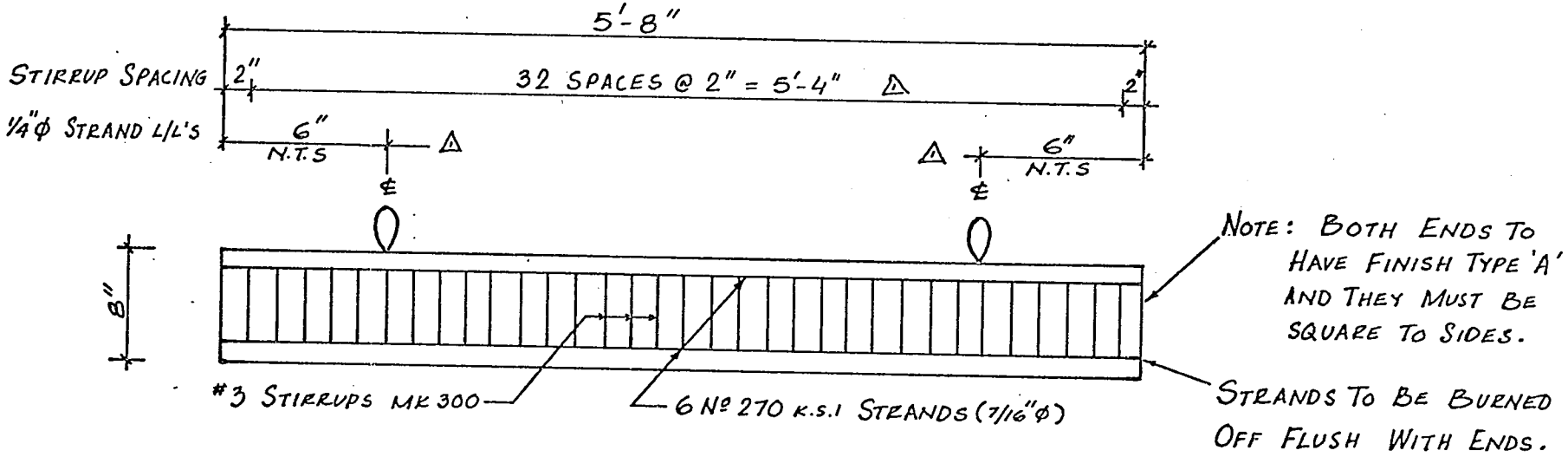

ELEVATION.

NOTES:

1. f'_c 5,000 P.S.I
2. f_y 270 K.S.I

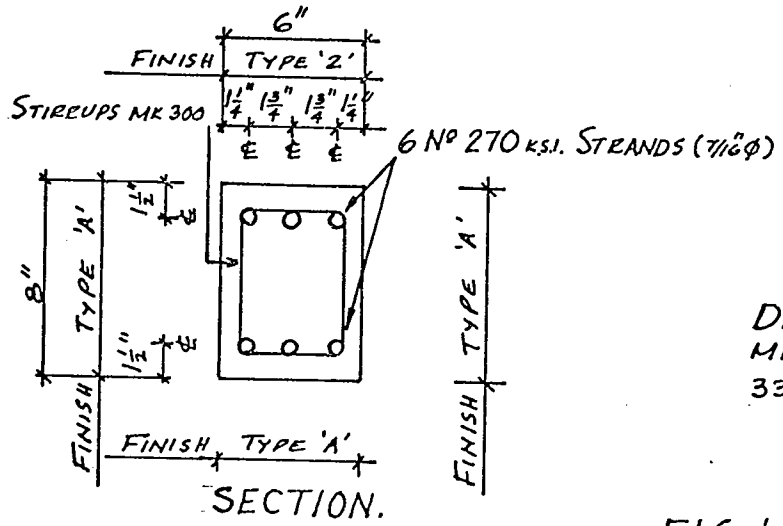

SECTION.

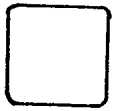

INS. DMS.

DETAIL OF #3 STIRRUPS
MK 300 x 2'-1" LG.
33 Nº THUS REQ'D.

FIG. 4.9: FABRICATION DRAWING OF PC2.

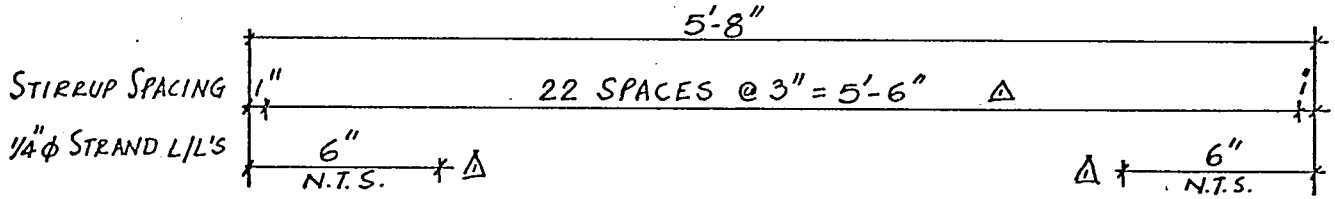

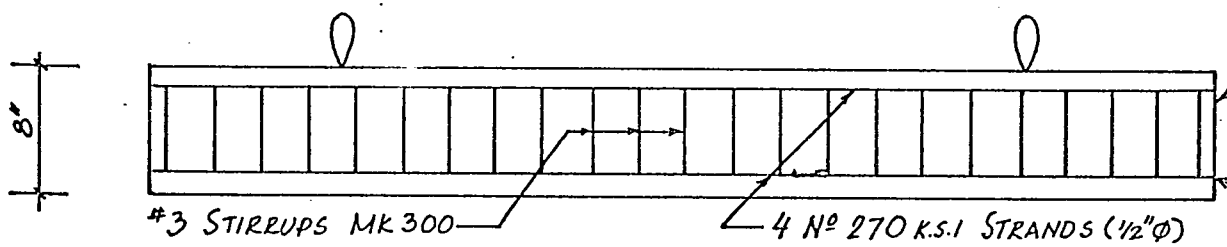

NOTE: BOTH ENDS TO HAVE FINISH TYPE 'A' AND THEY MUST BE SQUARE TO SIDES.

STRANDS TO BE BURNED OFF FLUSH WITH ENDS.

ELEVATION.

NOTES:

1. f'_c 5,000 P.S.I
2. f_y 270 K.S.I

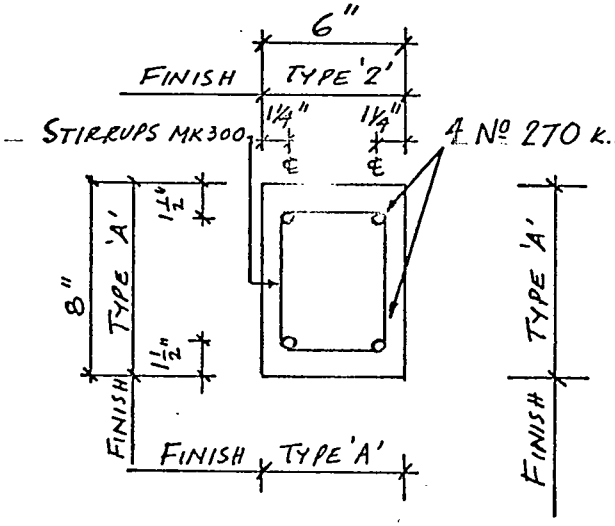

INS. DMS.

DETAIL OF #3 STIRRUPS MK 300 × 2'-1" LG.
△ 23 Nº THUS REQD.

SECTION.

FIG. 4.10 : FABRICATION DRAWING OF PC3.

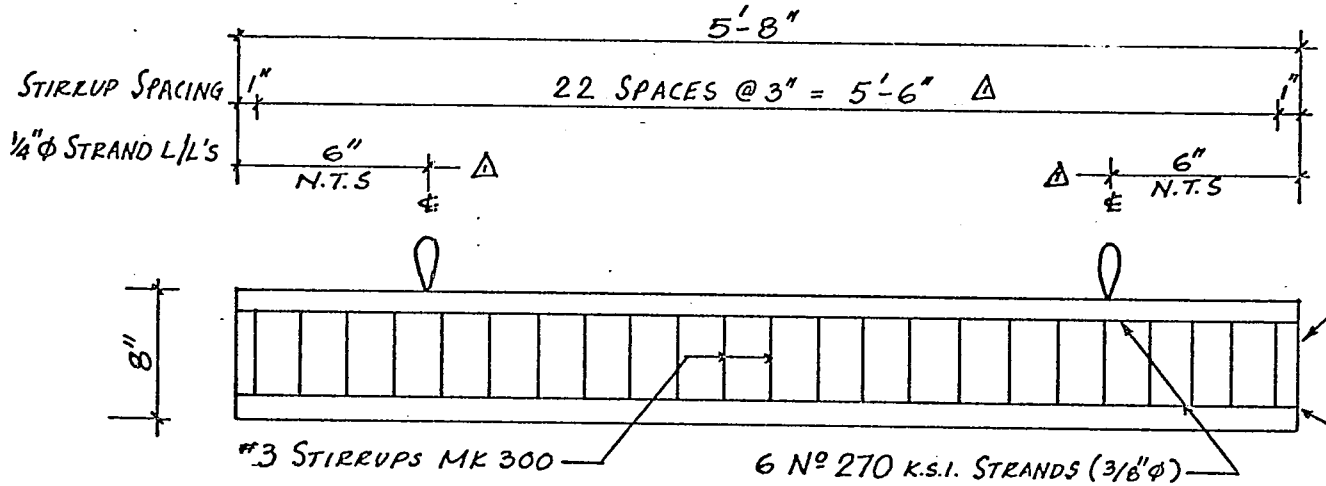

ELEVATION.

NOTES:

1. f'_c 5,000 P.S.I.
2. f_y 270 K.S.I.

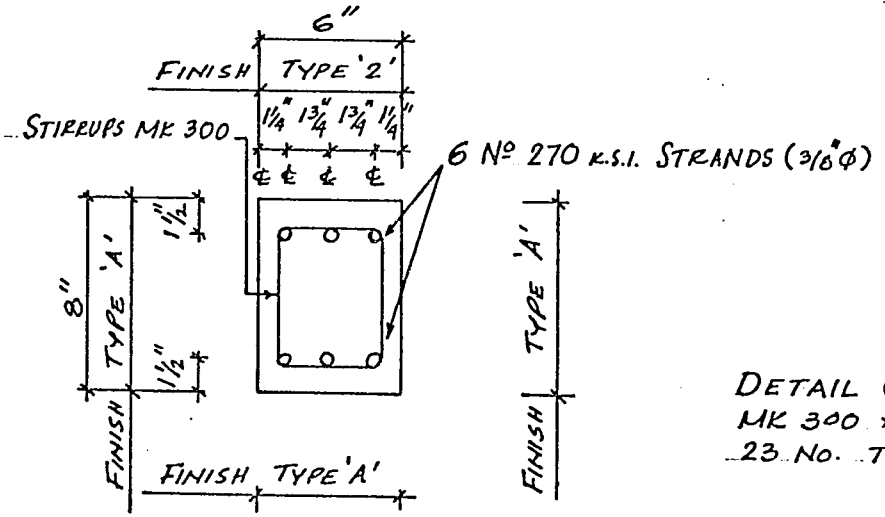

SECTION.

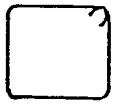

DETAIL OF #3 STIRRUP
MK 300 x 2'-1" LG.
23 No. THUS REQD.

FIG. 4.11: FABRICATION DRAWING OF PC4.

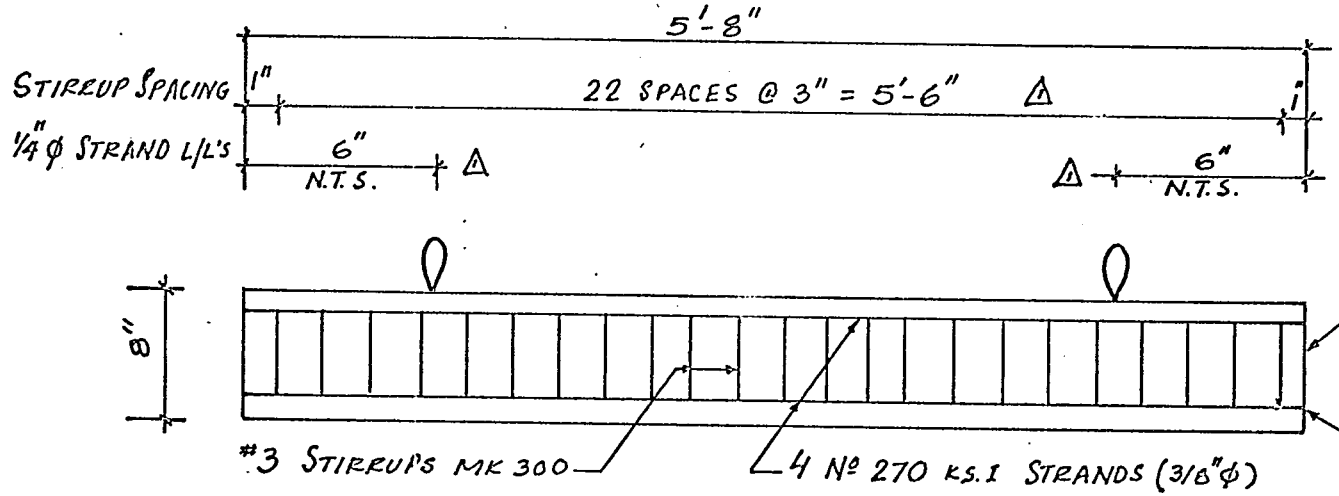

ELEVATION.

NOTES:

1. f'_c 5,000 P.S.I
2. f_y 270 K.S.I

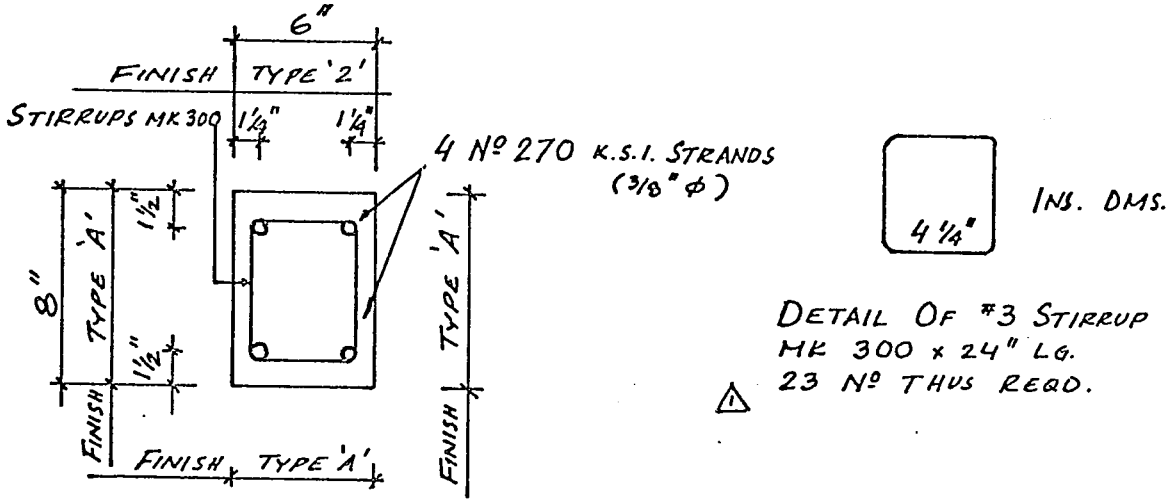

SECTION.

INS. DMS.

DETAIL OF #3 STIRRUP MK 300 x 24" LG. 23 Nº THUS REQD.

FIG. 4.12: FABRICATION DRAWING OF PC5.

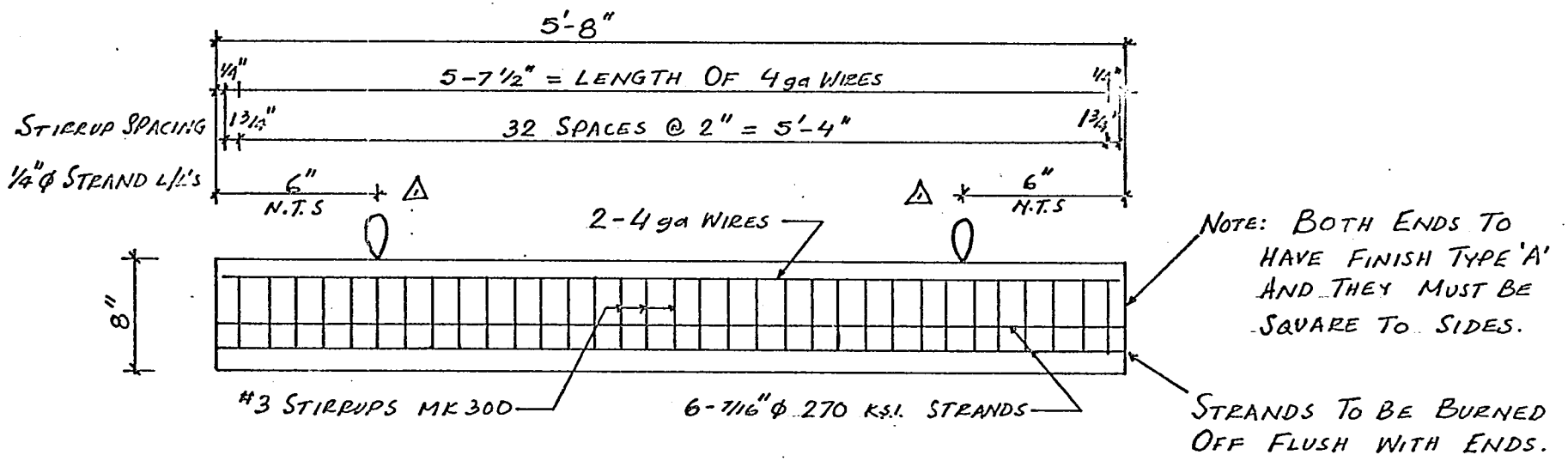

ELEVATION.

NOTES :

1. f'_c 5,000 P.S.I
2. f_y 270 K.S.I

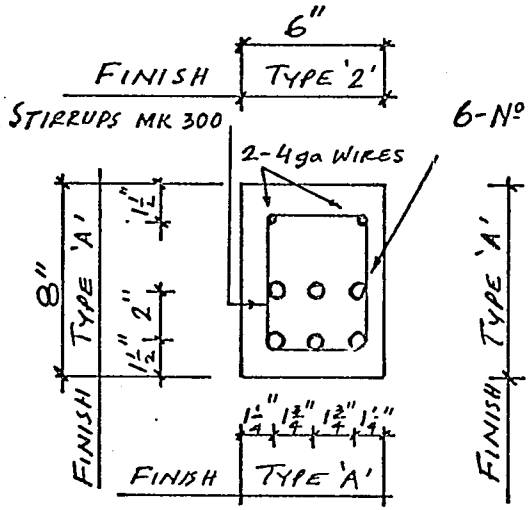

SECTION.

DETAIL OF #3 STIRRUP
MK 300 x 2'-1" LG
33 Nº THUS REQD.

FIG. 4.13 : FABRICATION DRAWING OF PB1.

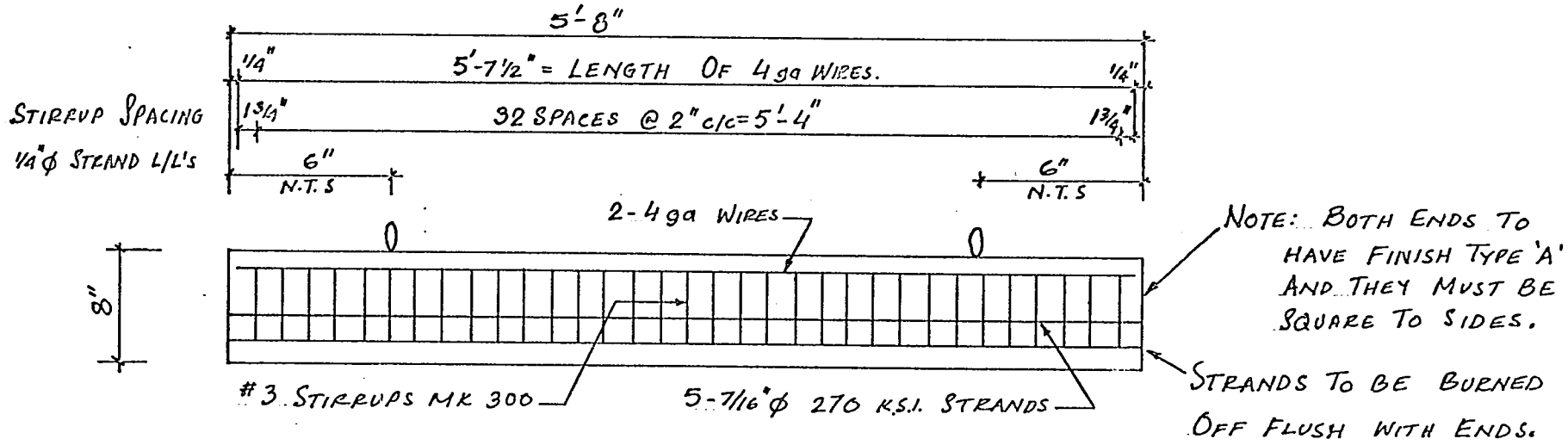

ELEVATION.

NOTES:

1. f'_c 5,000 psi
2. f_y 270 KSI

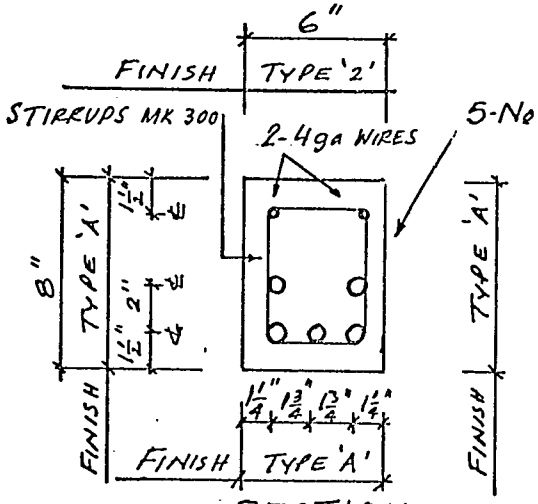

SECTION.

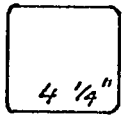

INS. DMS.

DETAIL OF #3 STIRRUP MK 300 x 2'-1" LG. 33 Nº THUS REQD.

FIG. 4.14: FABRICATION DRAWING OF PB2.

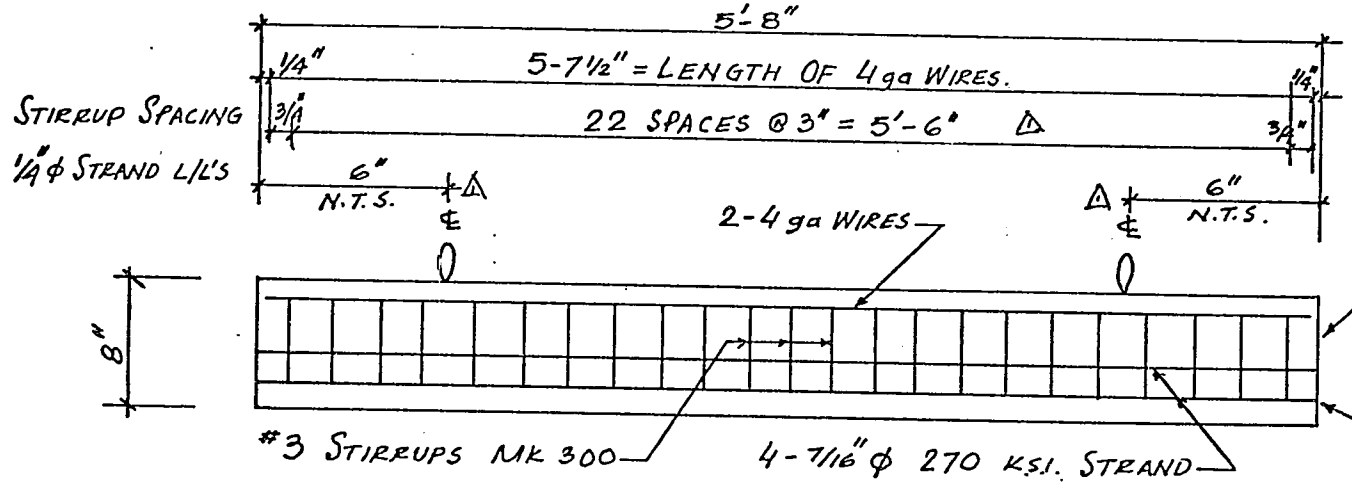

ELEVATION.

NOTES:

1. f'_c 5,000 P.S.I.
2. f_y 270 K.S.I.

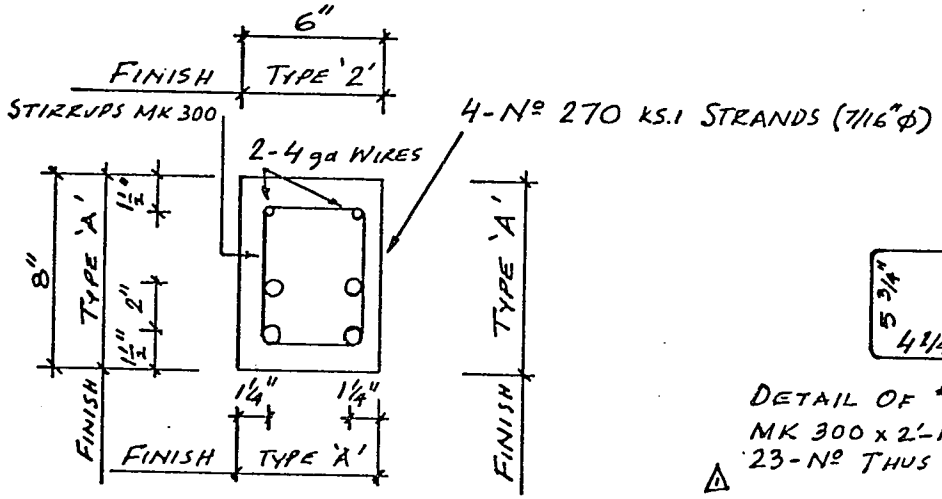

SECTION.

DETAIL OF #3 STIRRUP MK 300 x 2'-1" LG.
23-Nº THUS REQD.

FIG. 4.15 : FABRICATION DRAWING OF PB3.

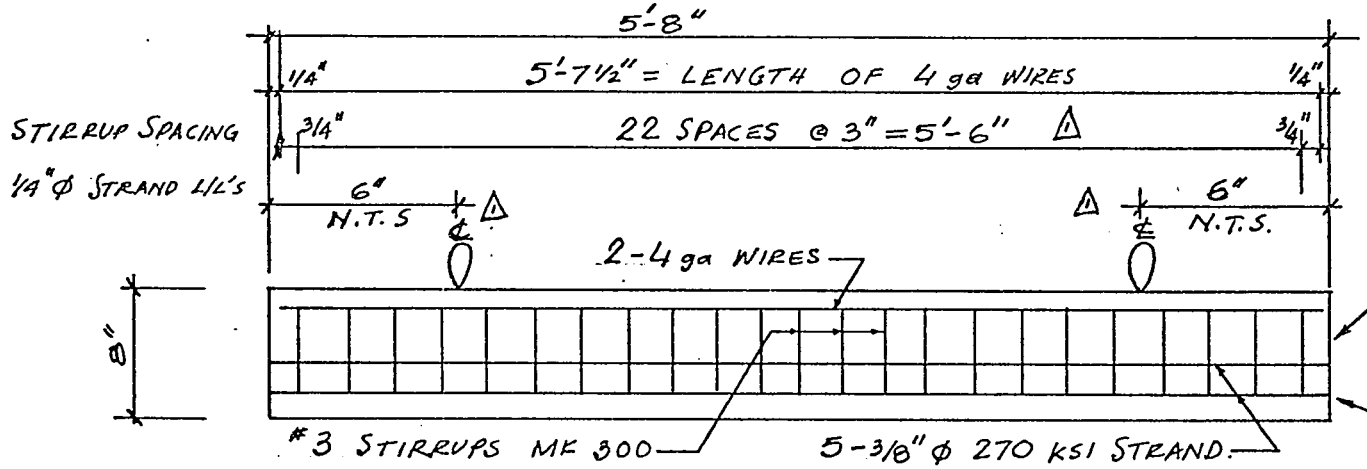

ELEVATION.

NOTES:

1. f'_c 5,000 p.s.i
2. f_y 270 k.s.i

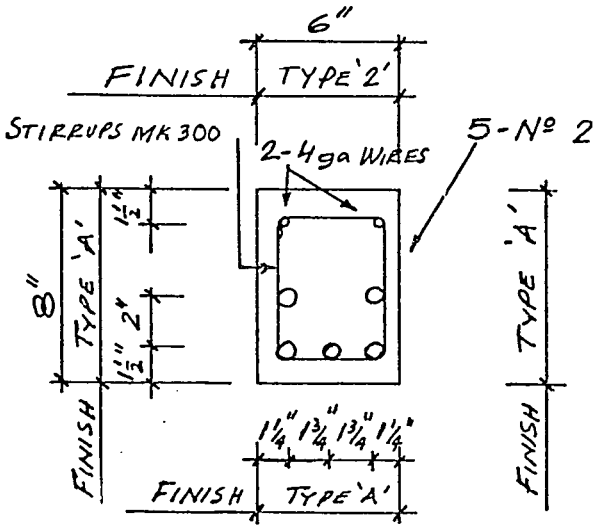

SECTION.

INS. DMS.

DETAIL OF #3 STIRRUP MK 300 x 2'-1" LG. 23-Nº THUS REQD.

FIG. 4.16 : FABRICATION DRAWING OF PB4.

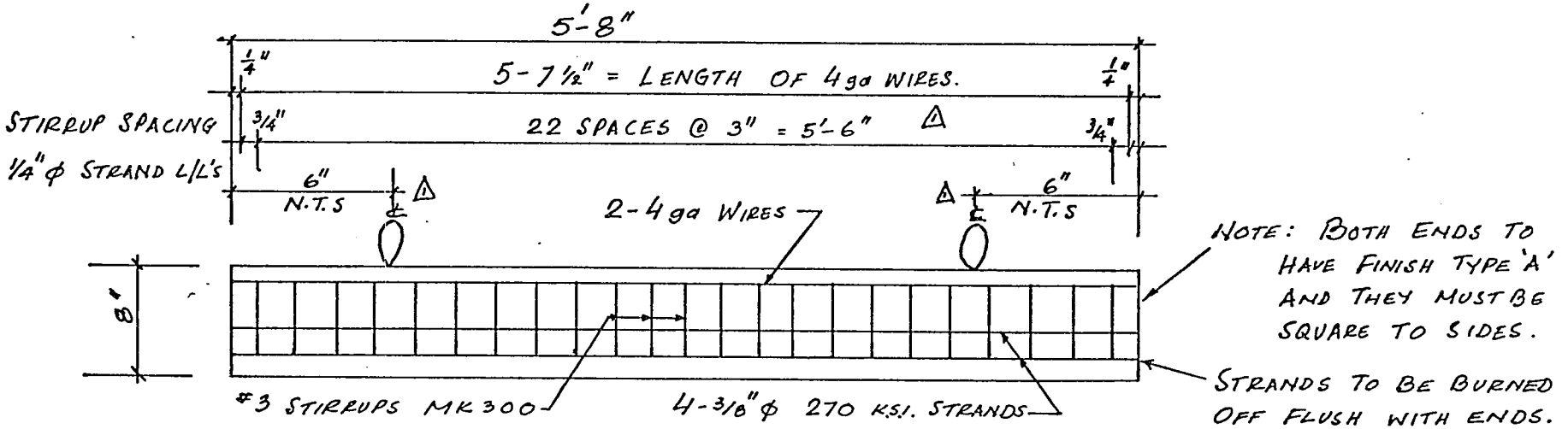

ELEVATION.

NOTES:

1. f'_c 5,000 p.s.i.
2. f_y 270 k.s.i.

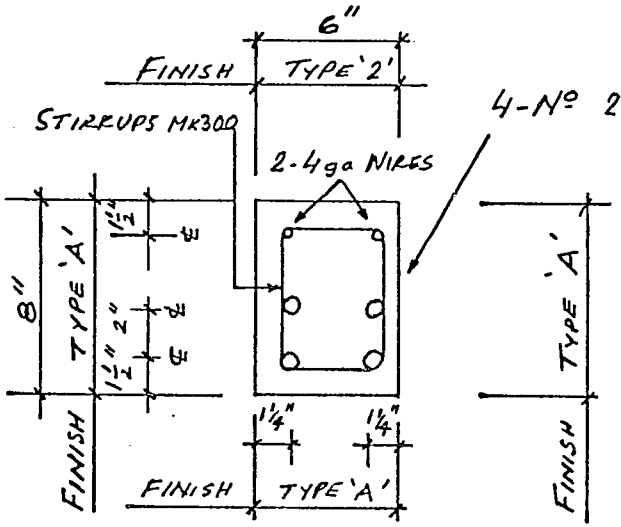

SECTION.

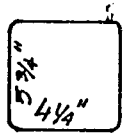

INS. DMS.

DETAIL OF #3 STIRRUP MK 300 = 2'-1" LG.
23-Nº THUS REQD.

FIG. 4.17 : FABRICATION DRAWING OF PB5.

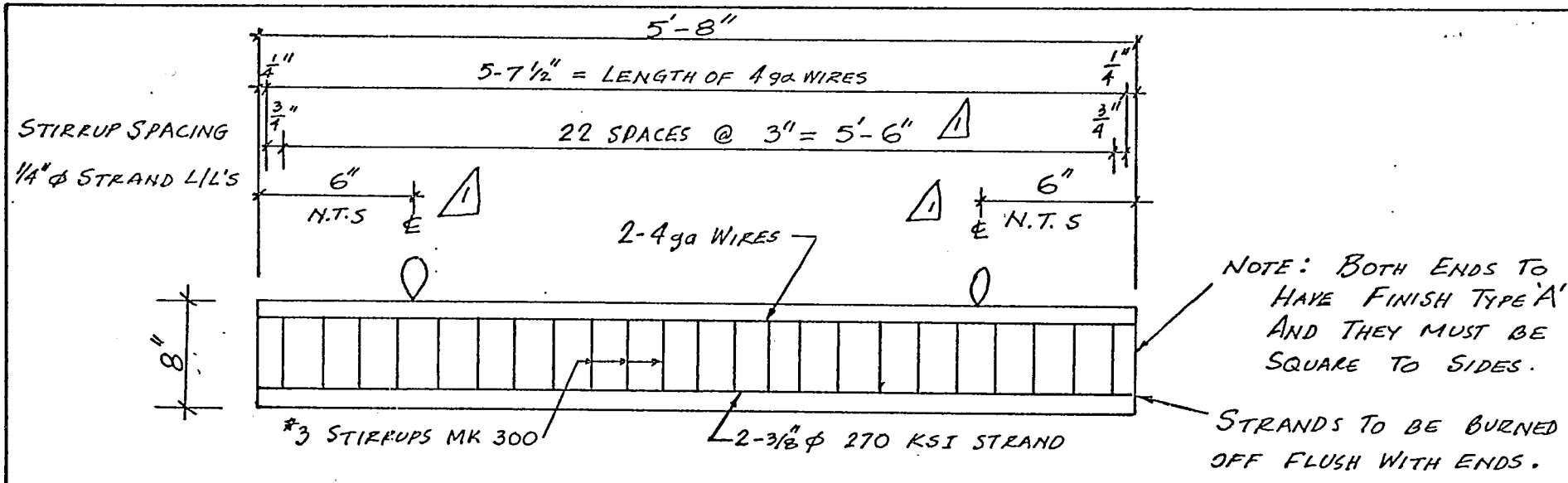

ELEVATION.

NOTES:

1. f'_c 5,000 psi
2. f_y 270 ksi

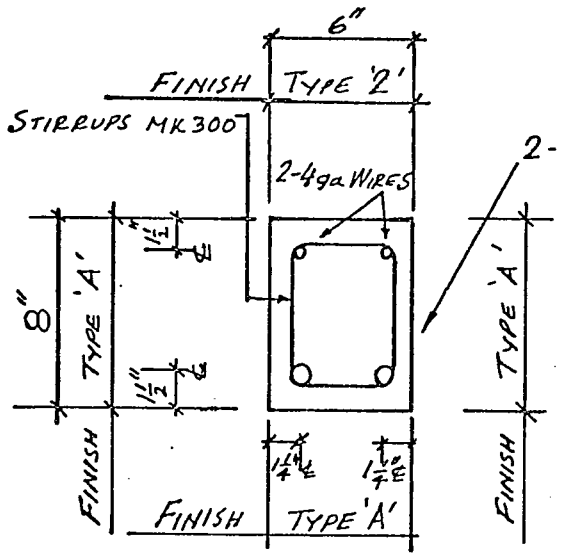

SECTION.

INS. DMS.

DETAIL OF #3 STIRRUP MK 300 = 2'-1" LG.
23-Nº THUS REQD.

FIG. 4.18 : FABRICATION DRAWING OF PB6.

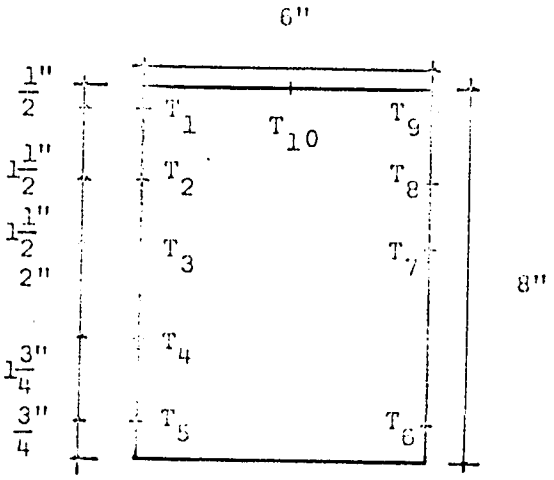

FIG. 4.19 TRANSDUCER LAYOUT.

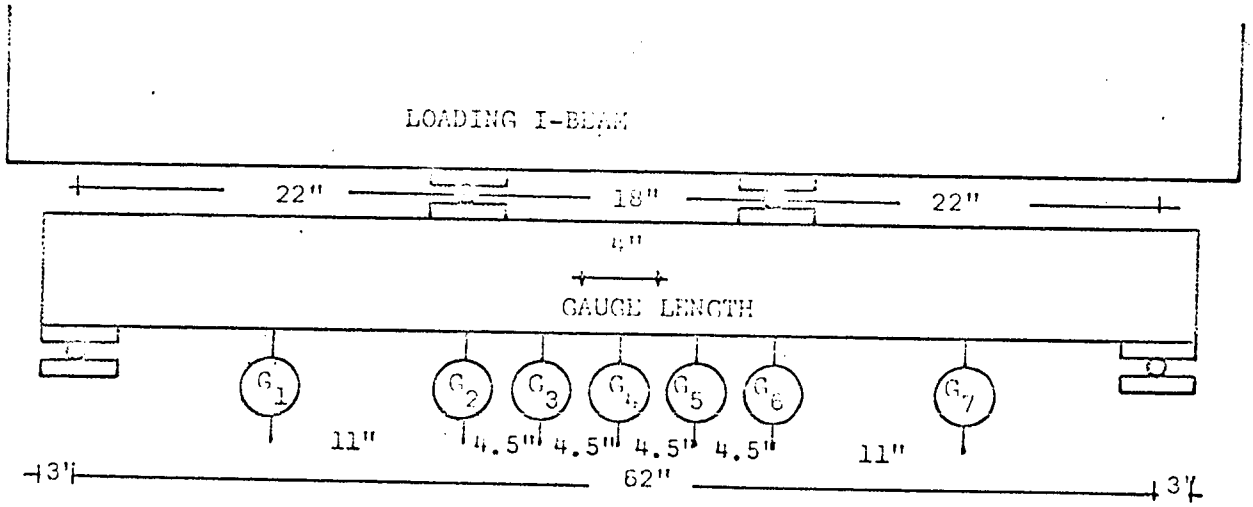

FIG. 4.22: POSITION OF PLATES FOR VERTICAL LOADING AND SUPPORT, TRANSDUCER GAUGE LENGTH AND DEFLECTION BRIDGE.

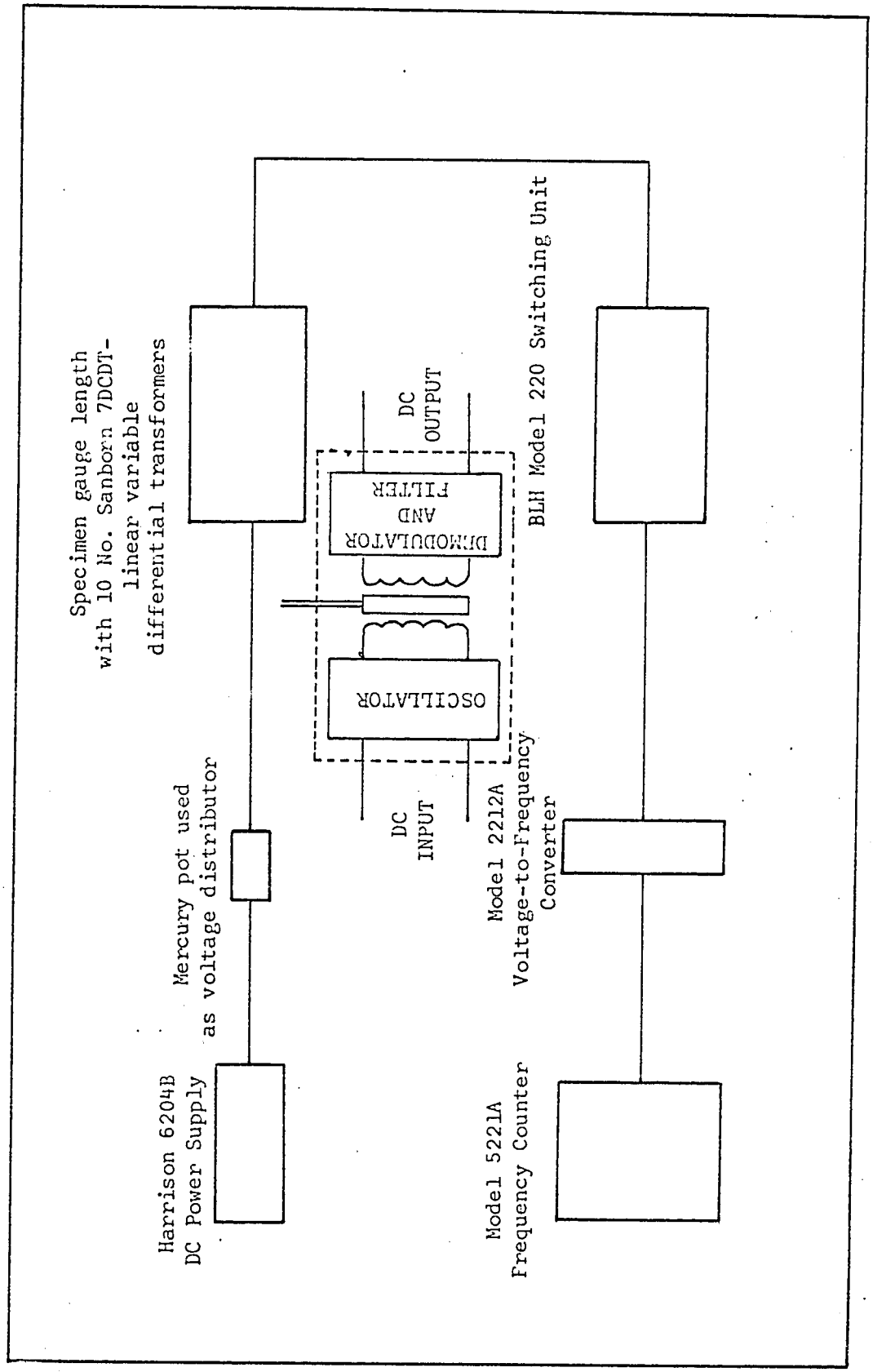

FIG. 4.20: SCHEMATIC LAYOUT OF STRAIN MEASURING DEVICES

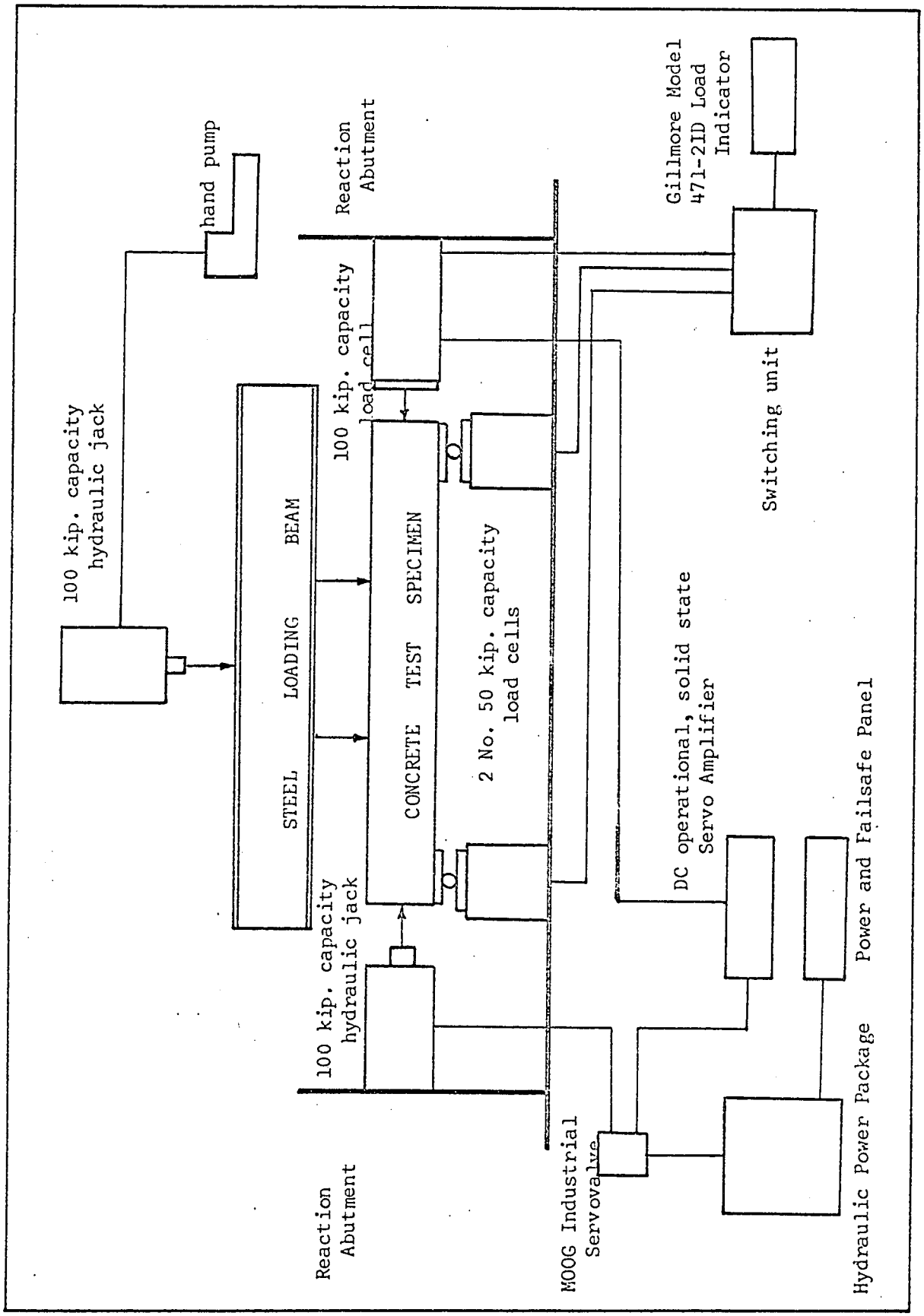

FIG. 4.21: SCHEMATIC DIAGRAM OF LOADING AND LOAD MEASURING DEVICES.

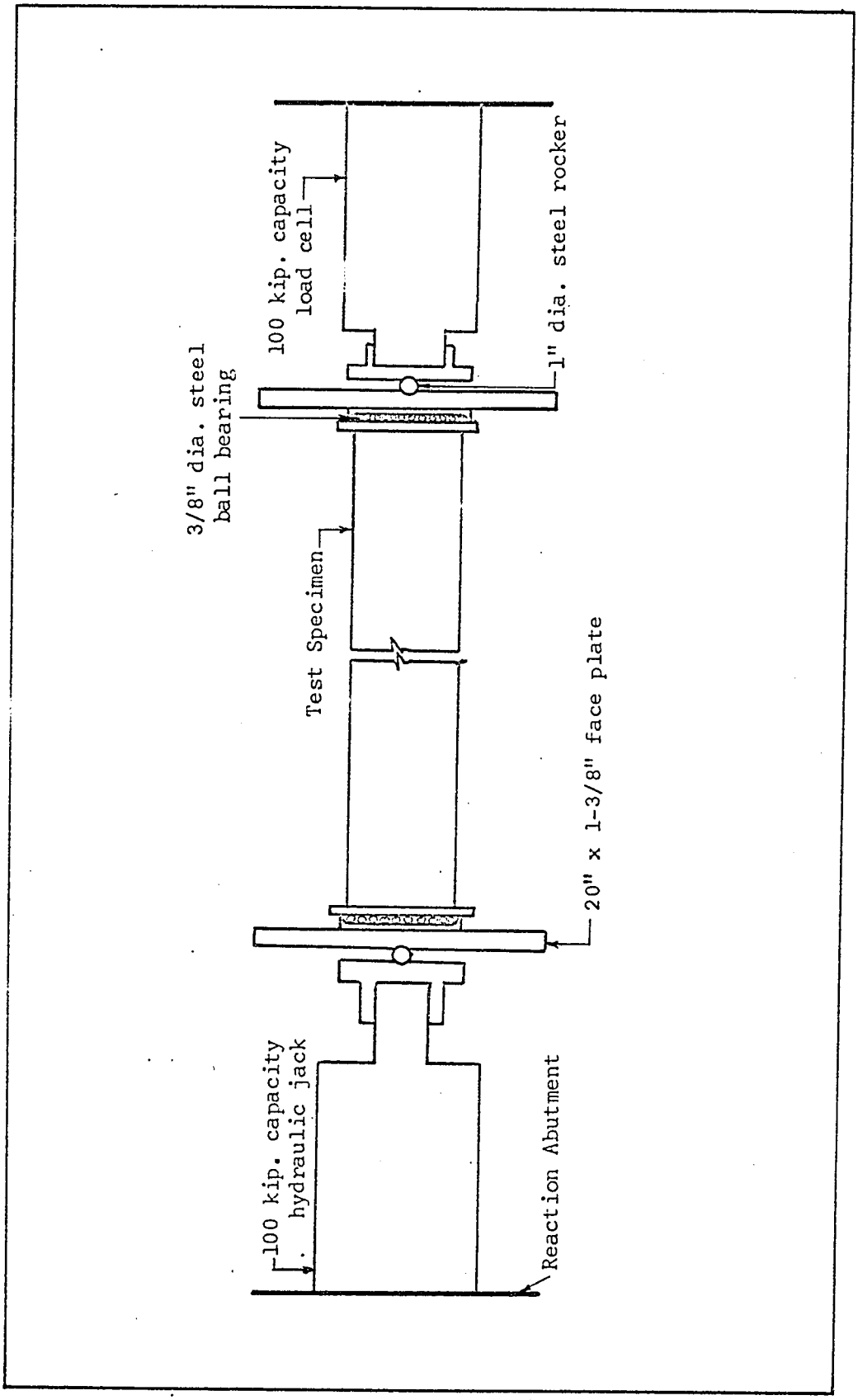

FIG. 4.23: AXIAL LOADING AND DETAILS OF HORIZONTAL PINS.

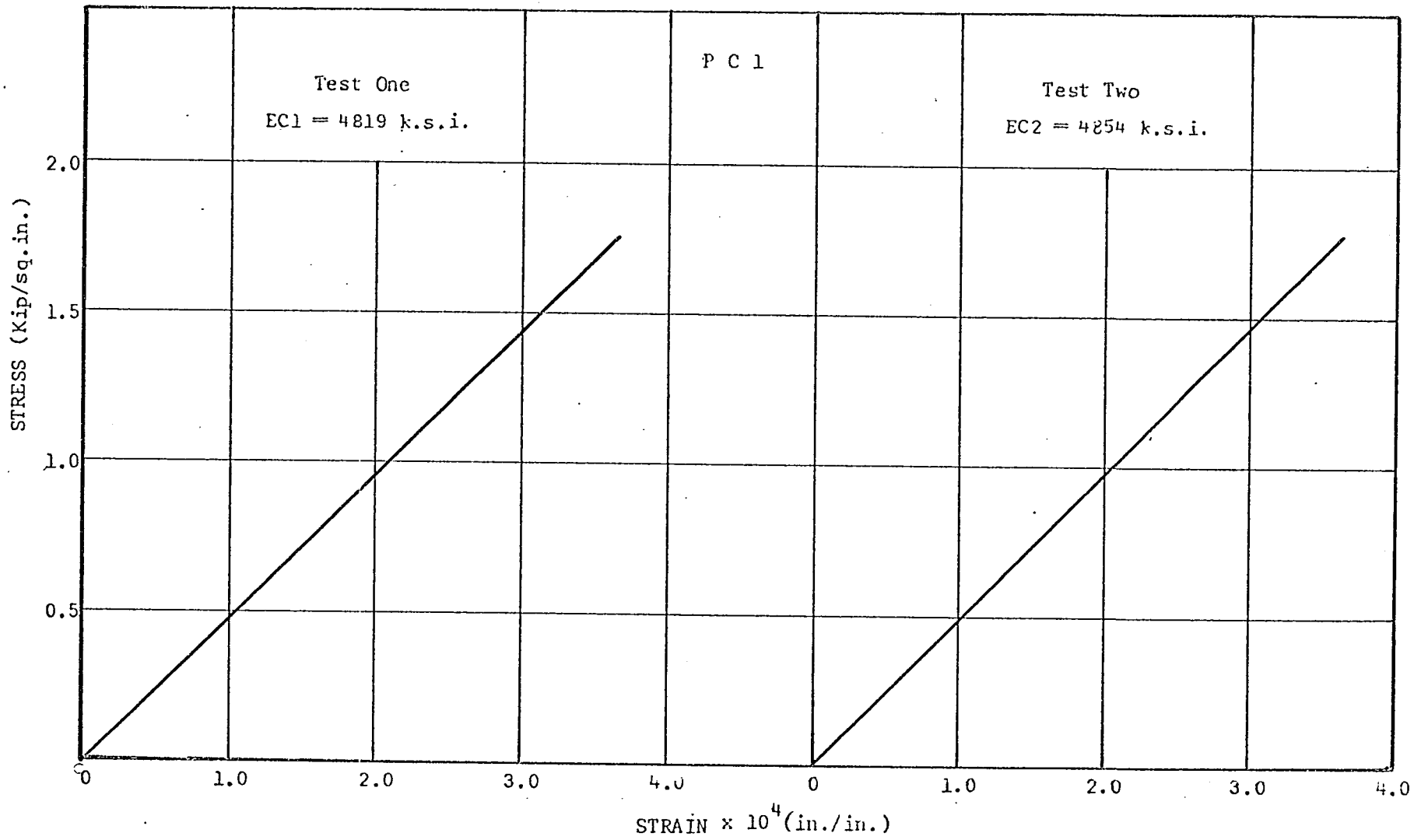

STRESS-STRAIN CURVE FOR CONCRETE

FIG. 5.1

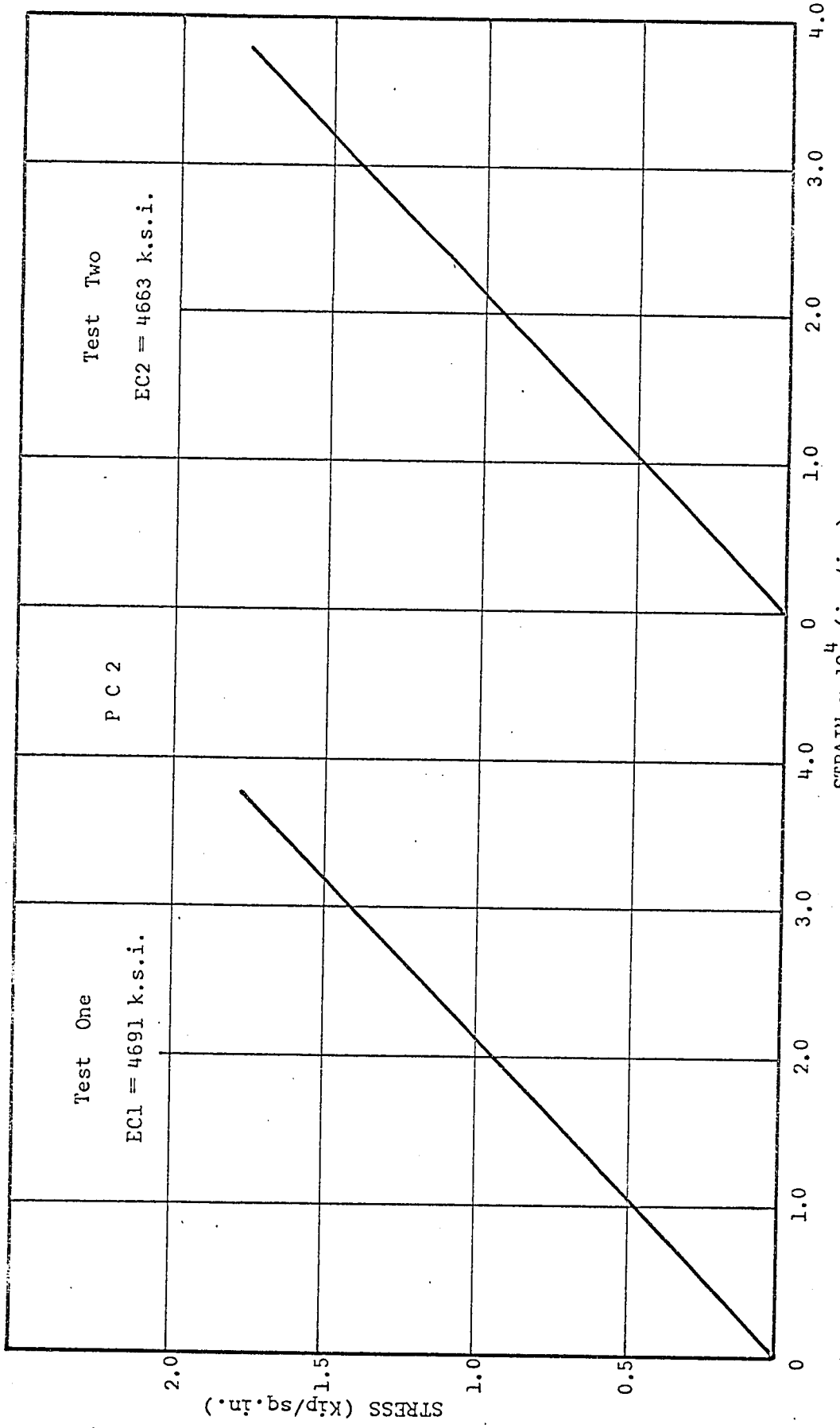

STRESS-STRAIN CURVE FOR CONCRETE

FIG. 5.2

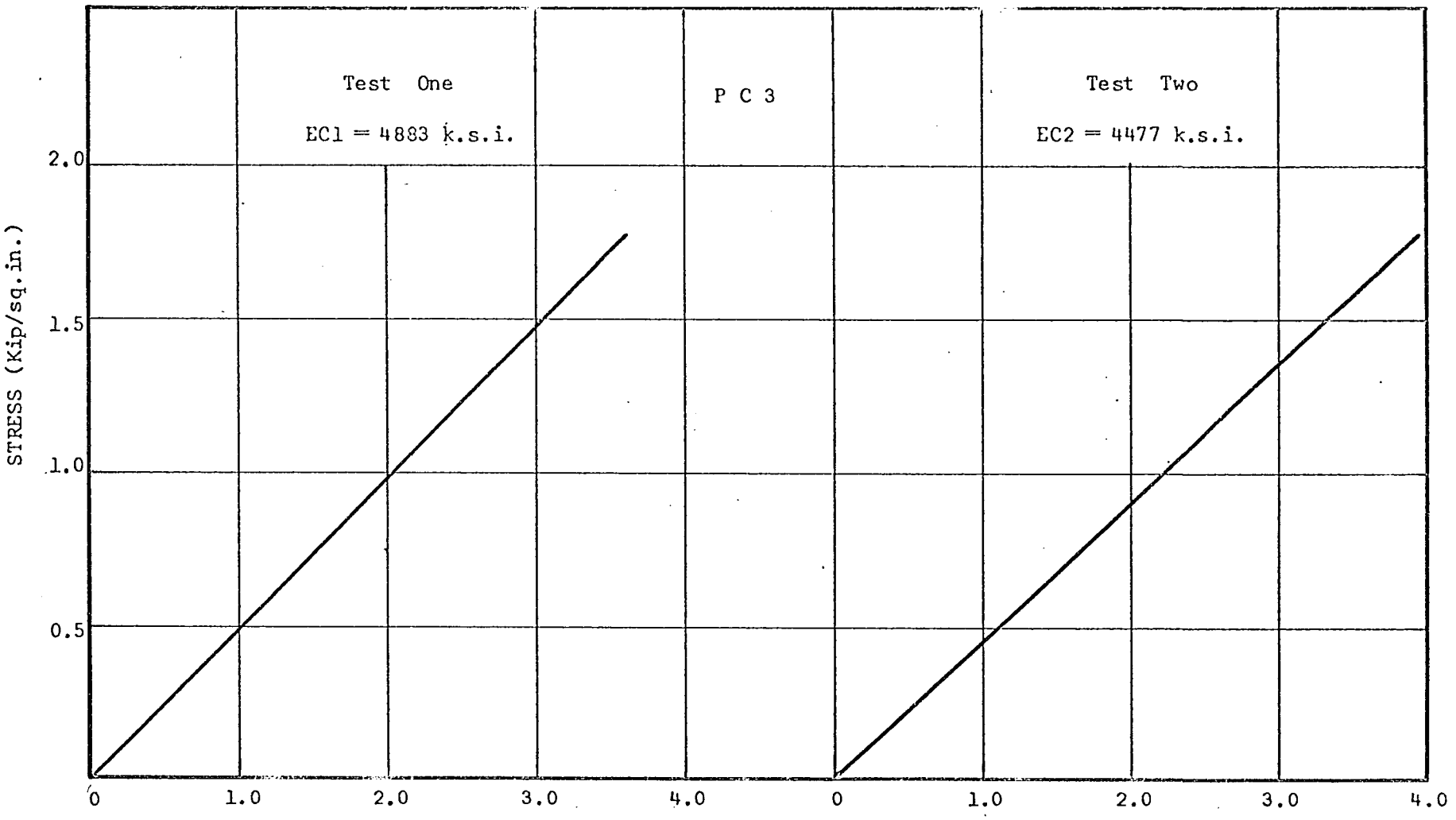

STRESS-STRAIN CURVE FOR CONCRETE

FIG. 5.3

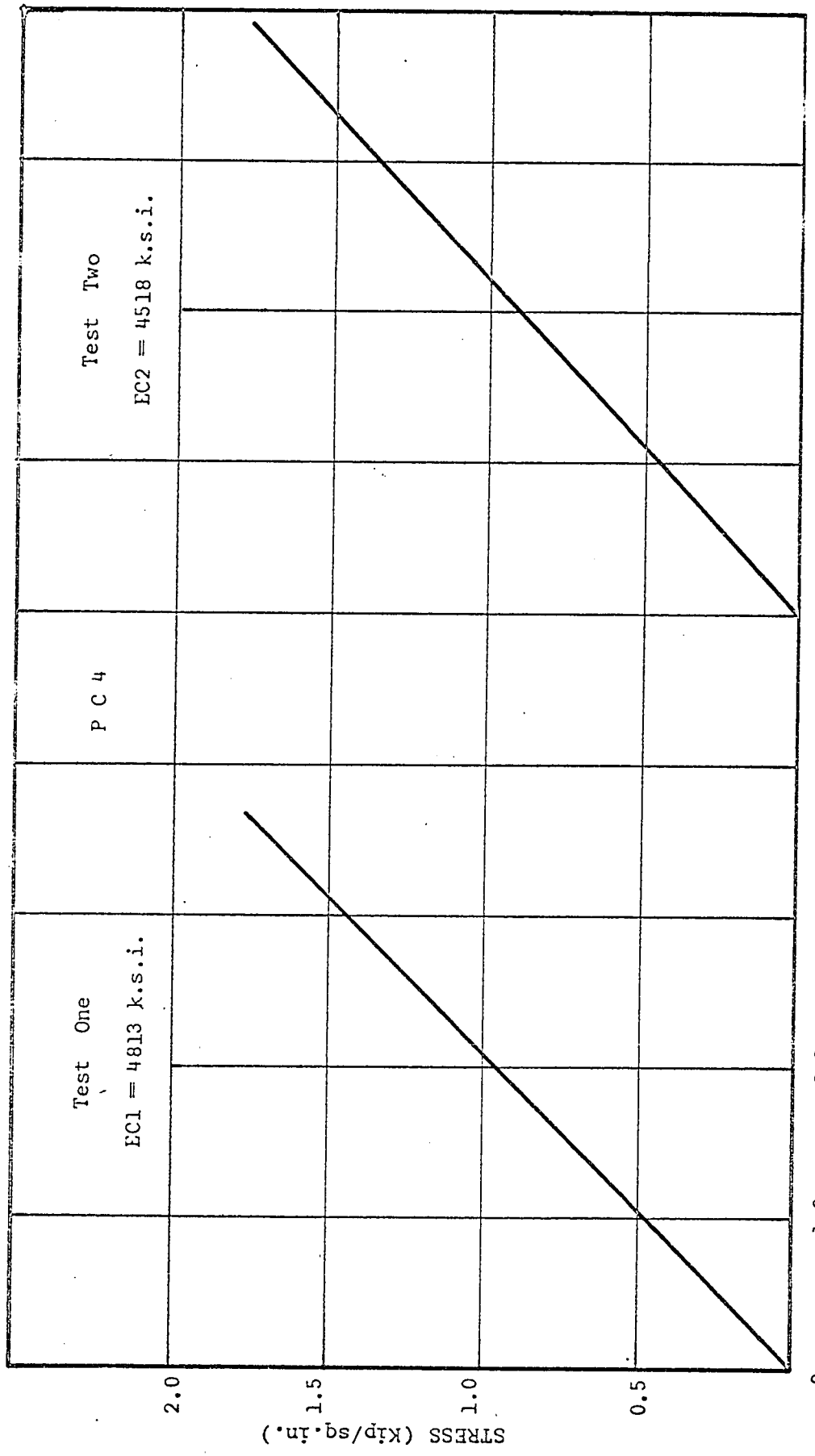

STRESS-STRAIN CURVE FOR CONCRETE

FIG. 5.4

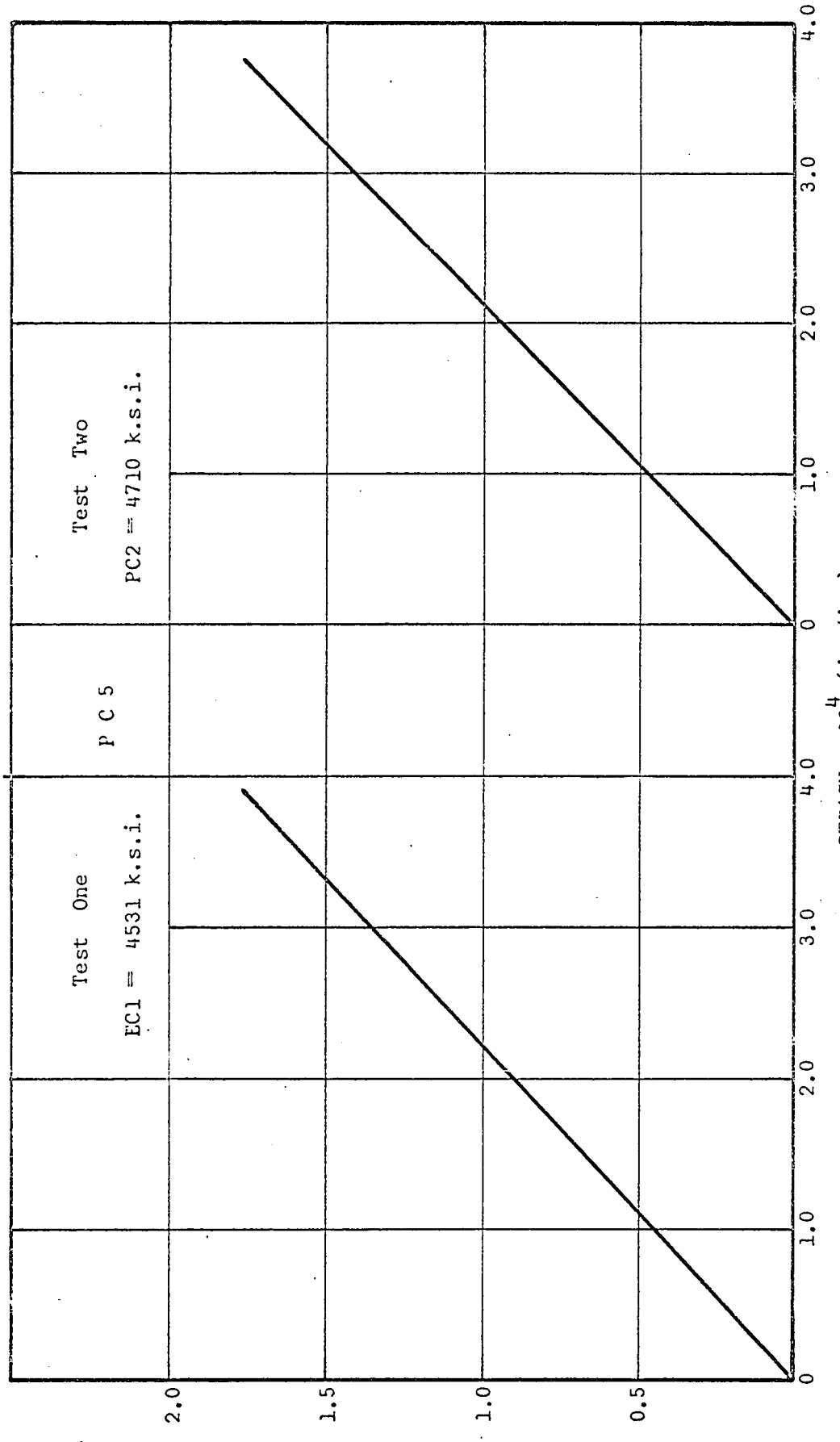

STRESS-STRAIN CURVE FOR CONCRETE

FIG. 5.5

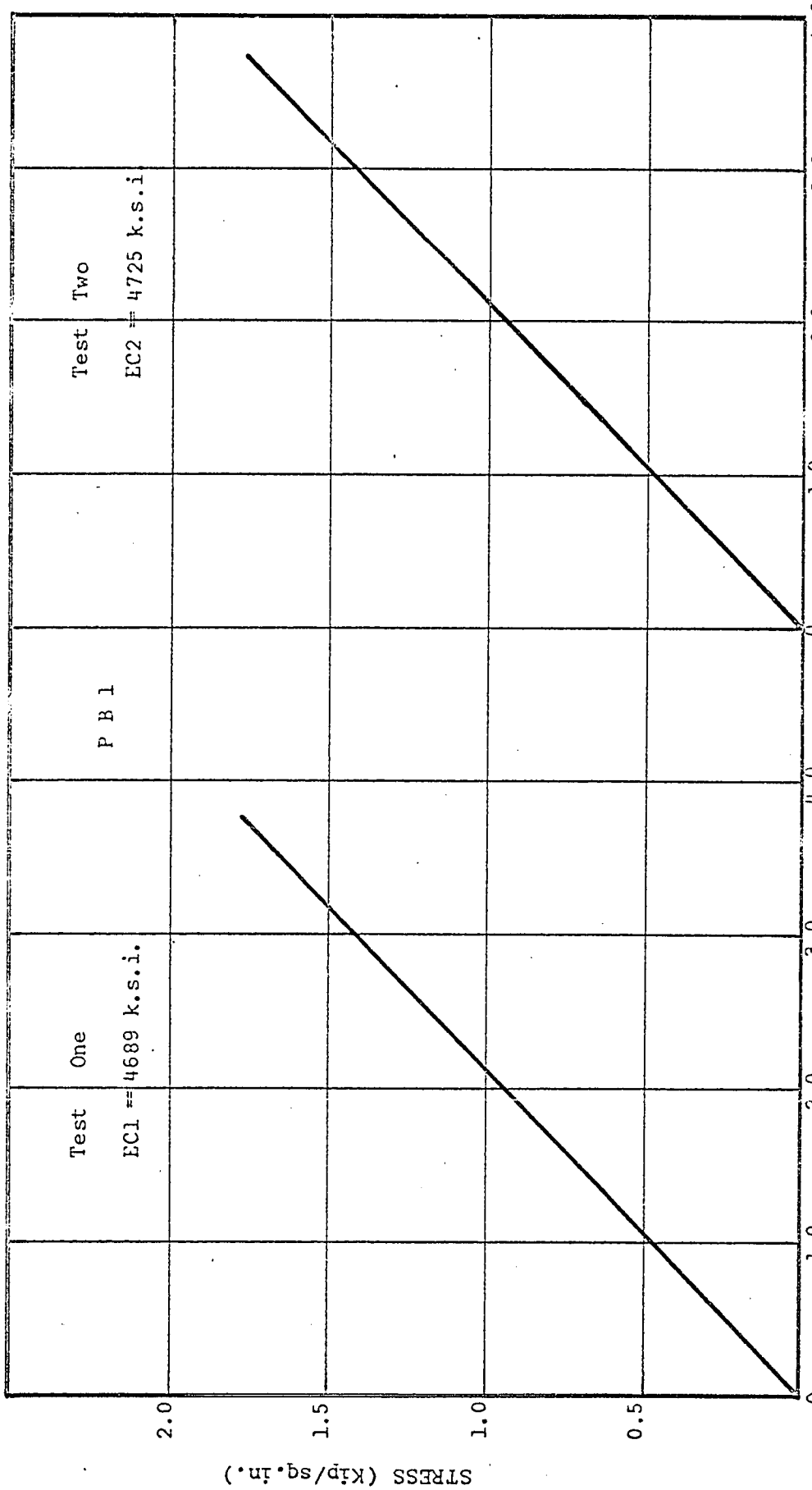

STRESS-STRAIN CURVE FOR CONCRETE

FIG. 5.6

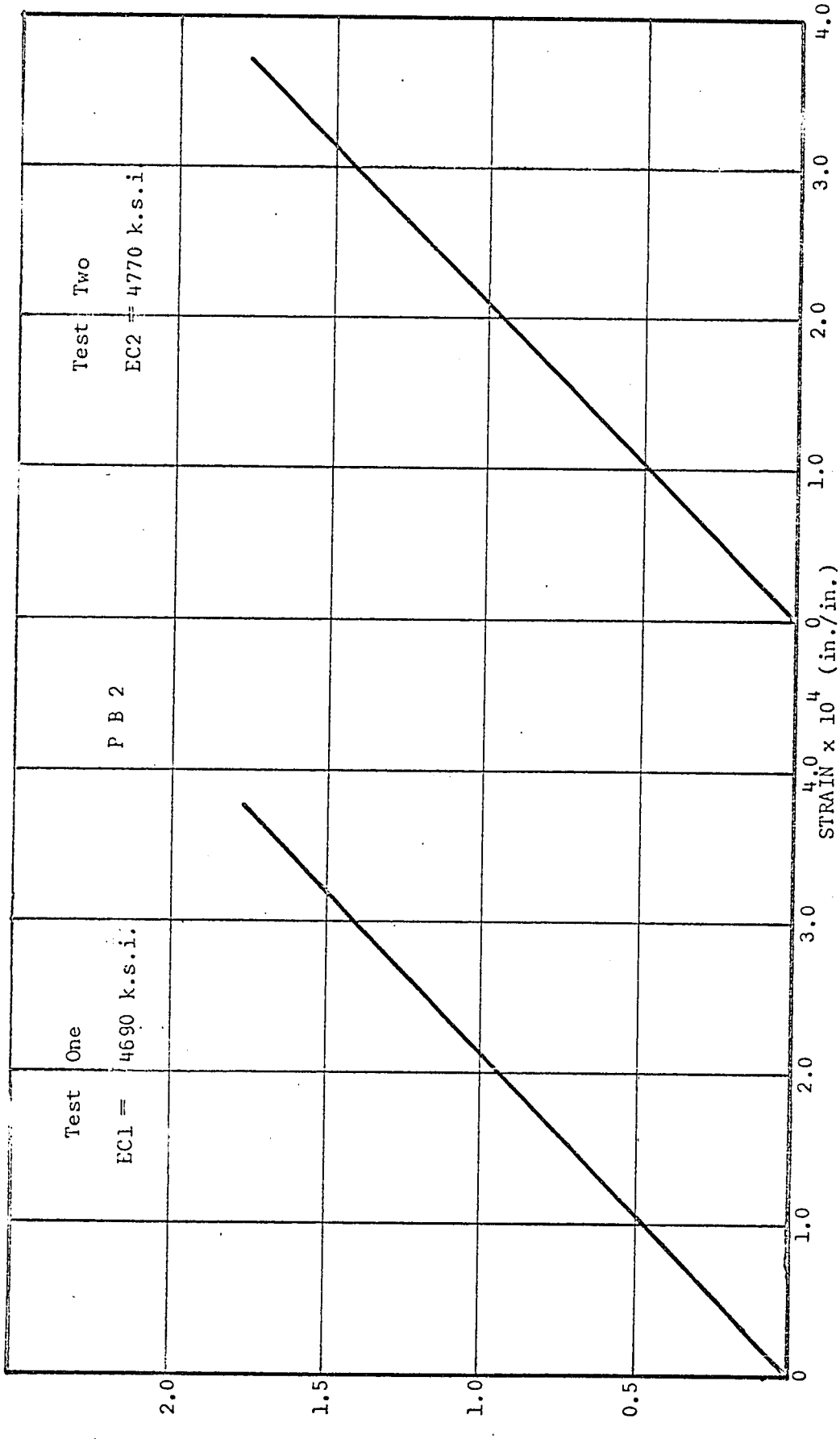

STRESS-STRAIN CURVE FOR CONCRETE

FIG. 5.7

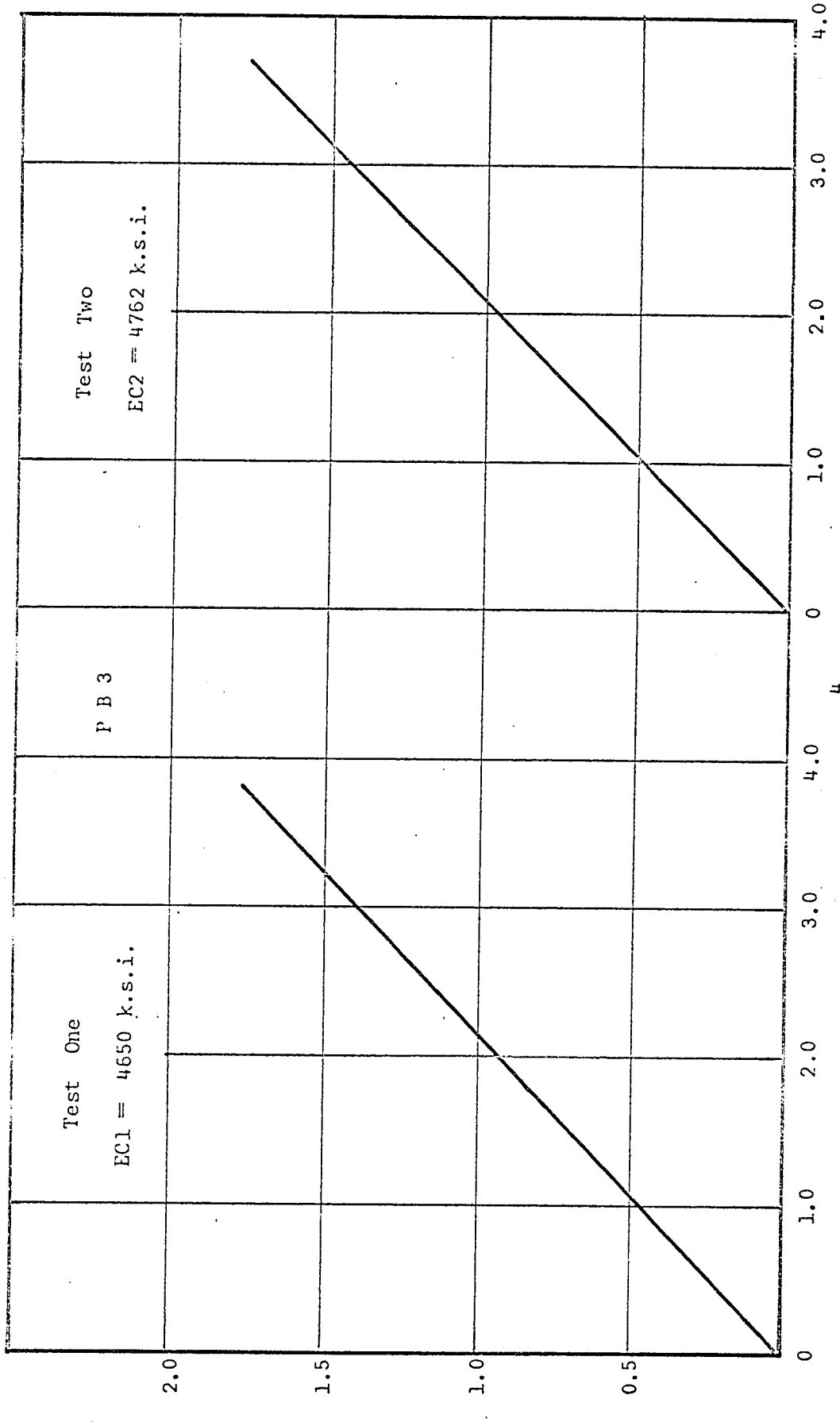

STRESS-STRAIN CURVE FOR CONCRETE

FIG. 5.8

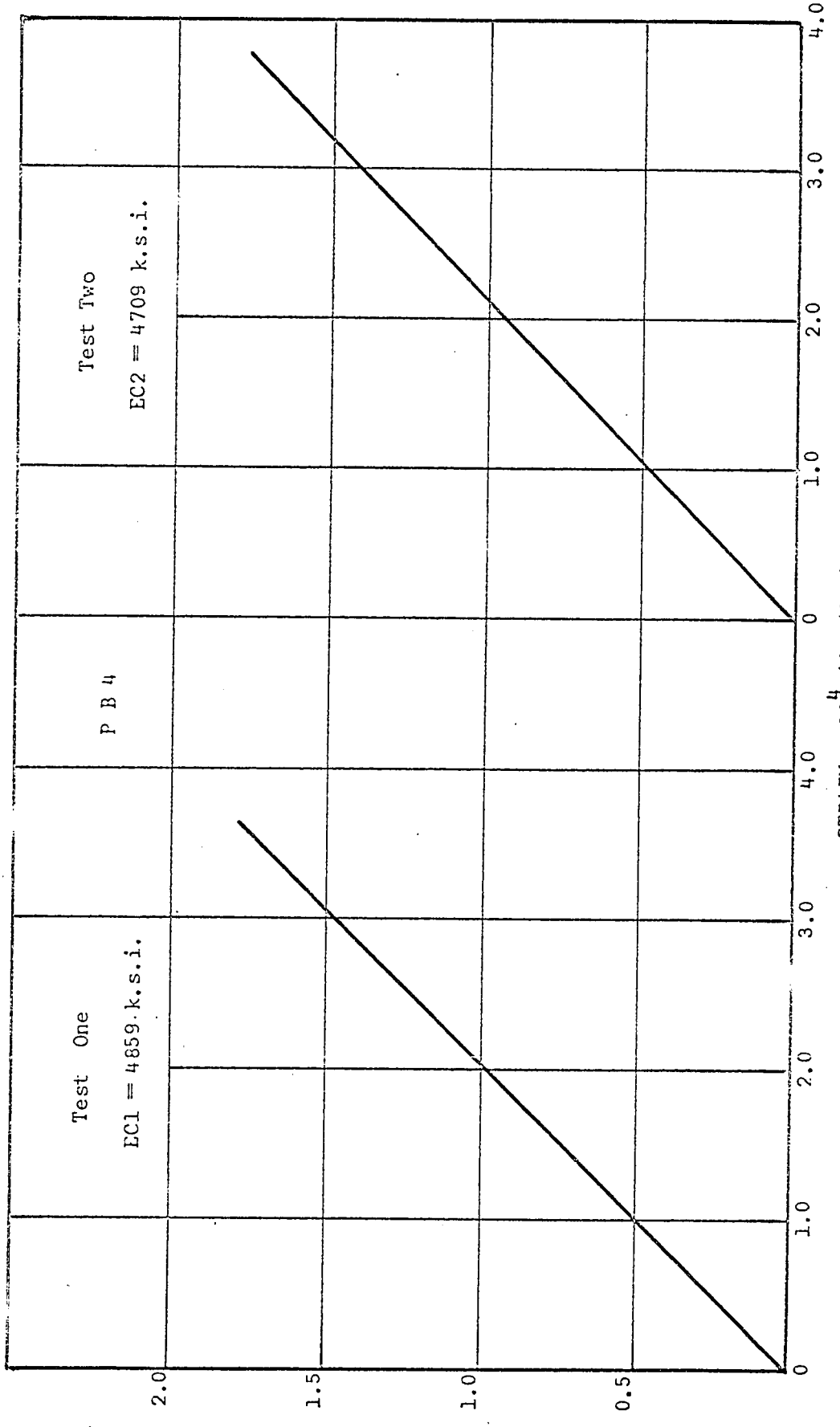

STRESS-STRAIN CURVE FOR CONCRETE

FIG. 5.9

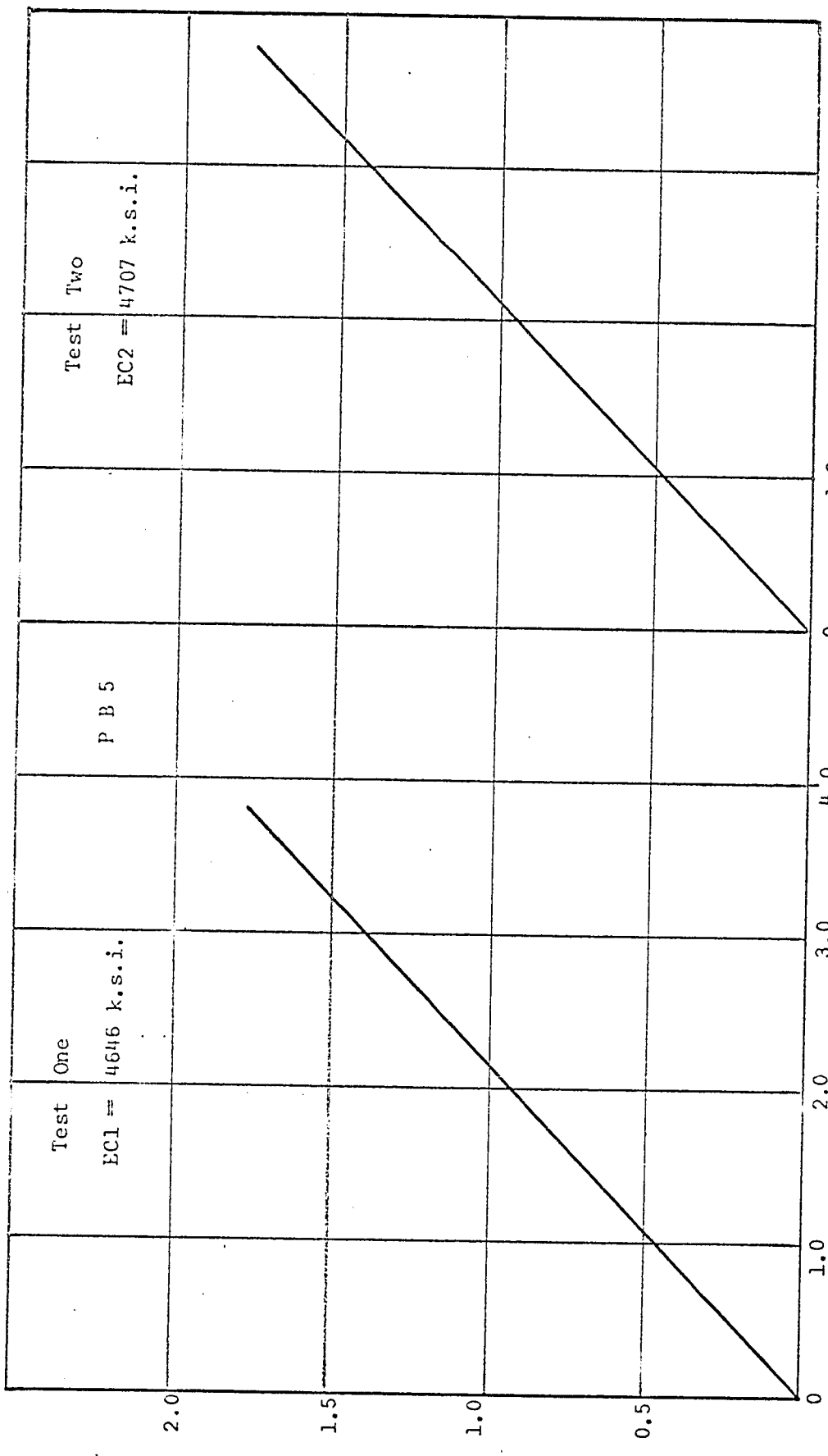

STRESS-STRAIN CURVE FOR CONCRETE

FIG. 5.10

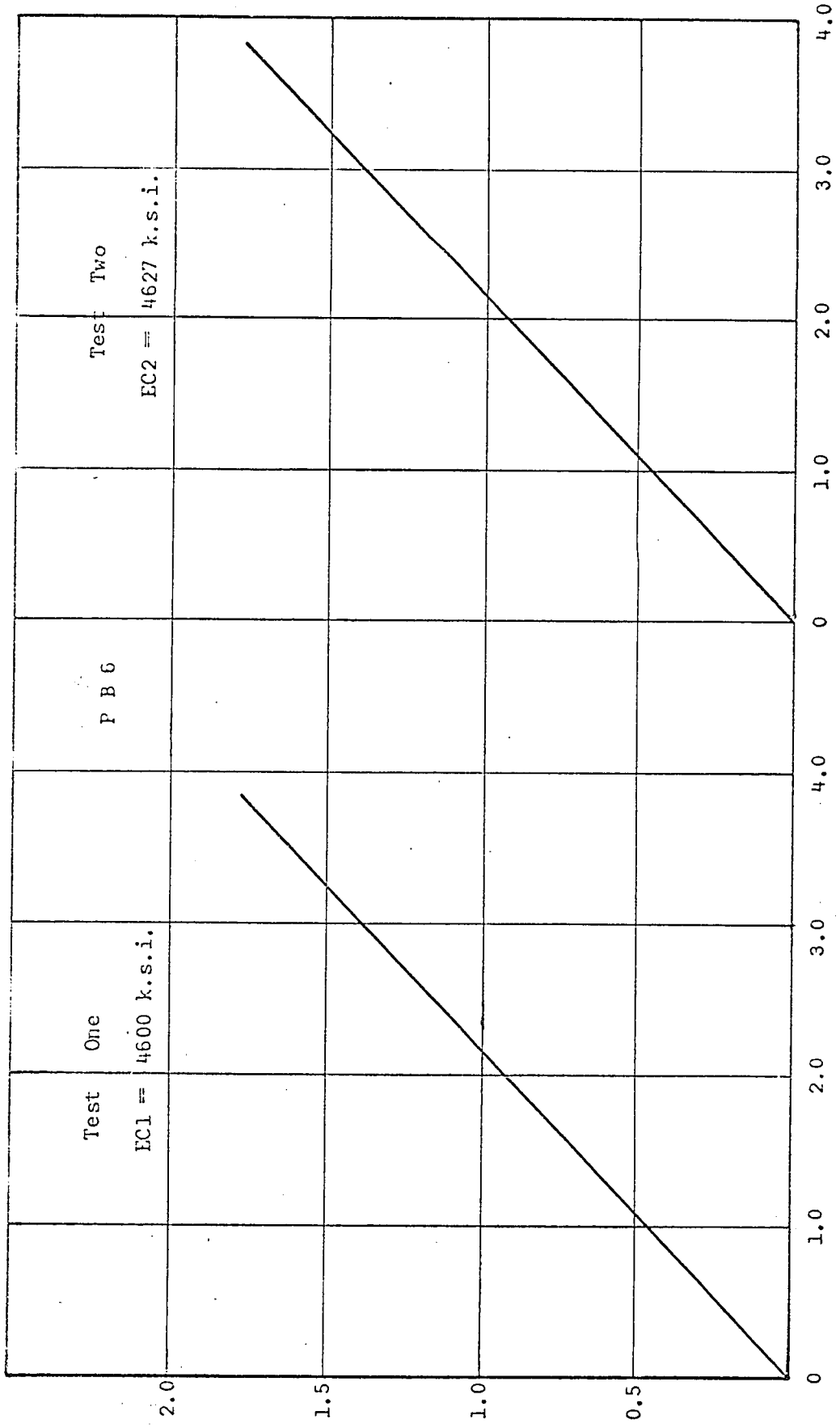

STRESS-STRAIN CURVE FOR CONCRETE

FIG. 5.11

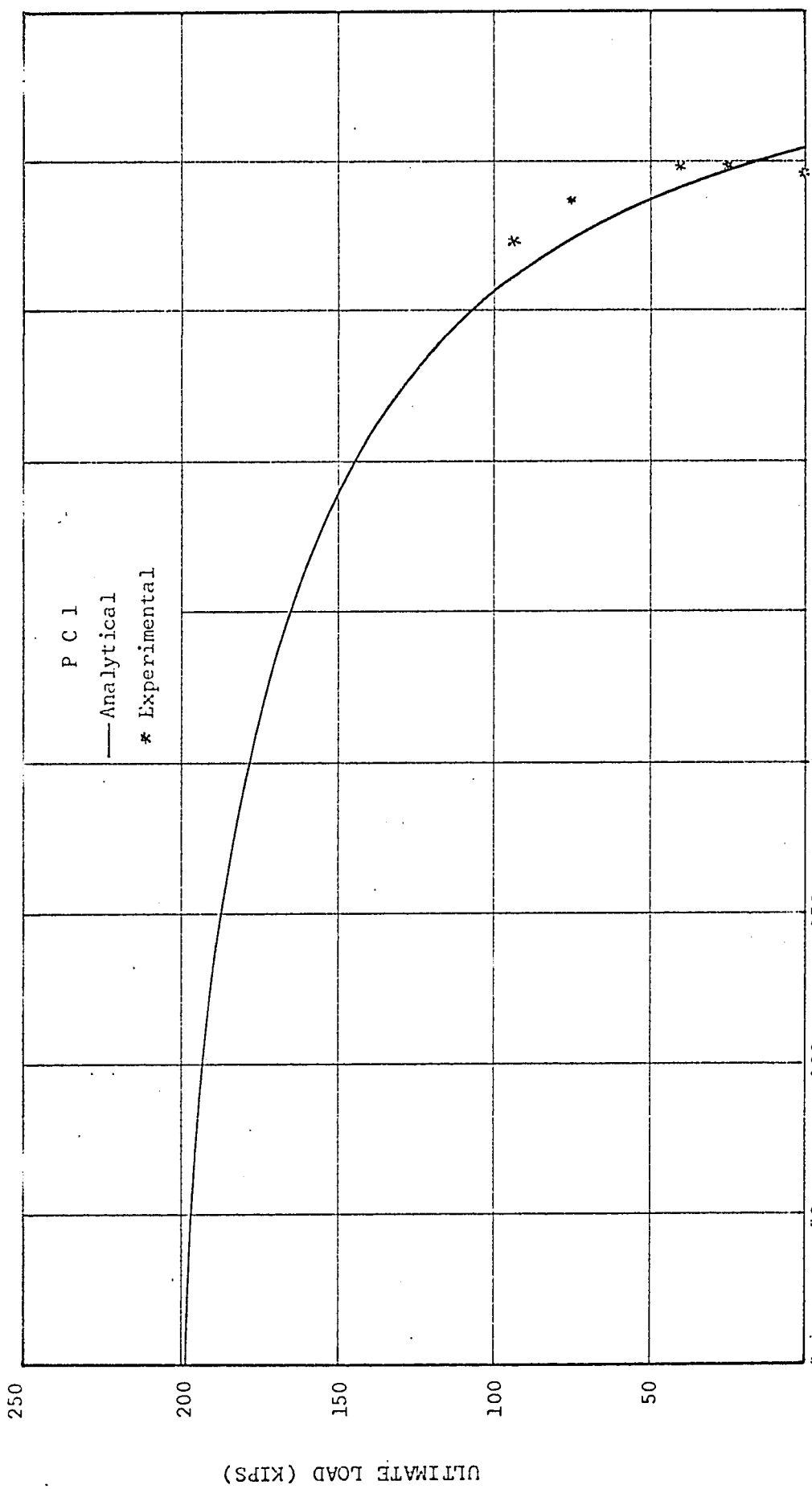

AXIAL THRUST-MOMENT INTERACTION

FIG. 5.15

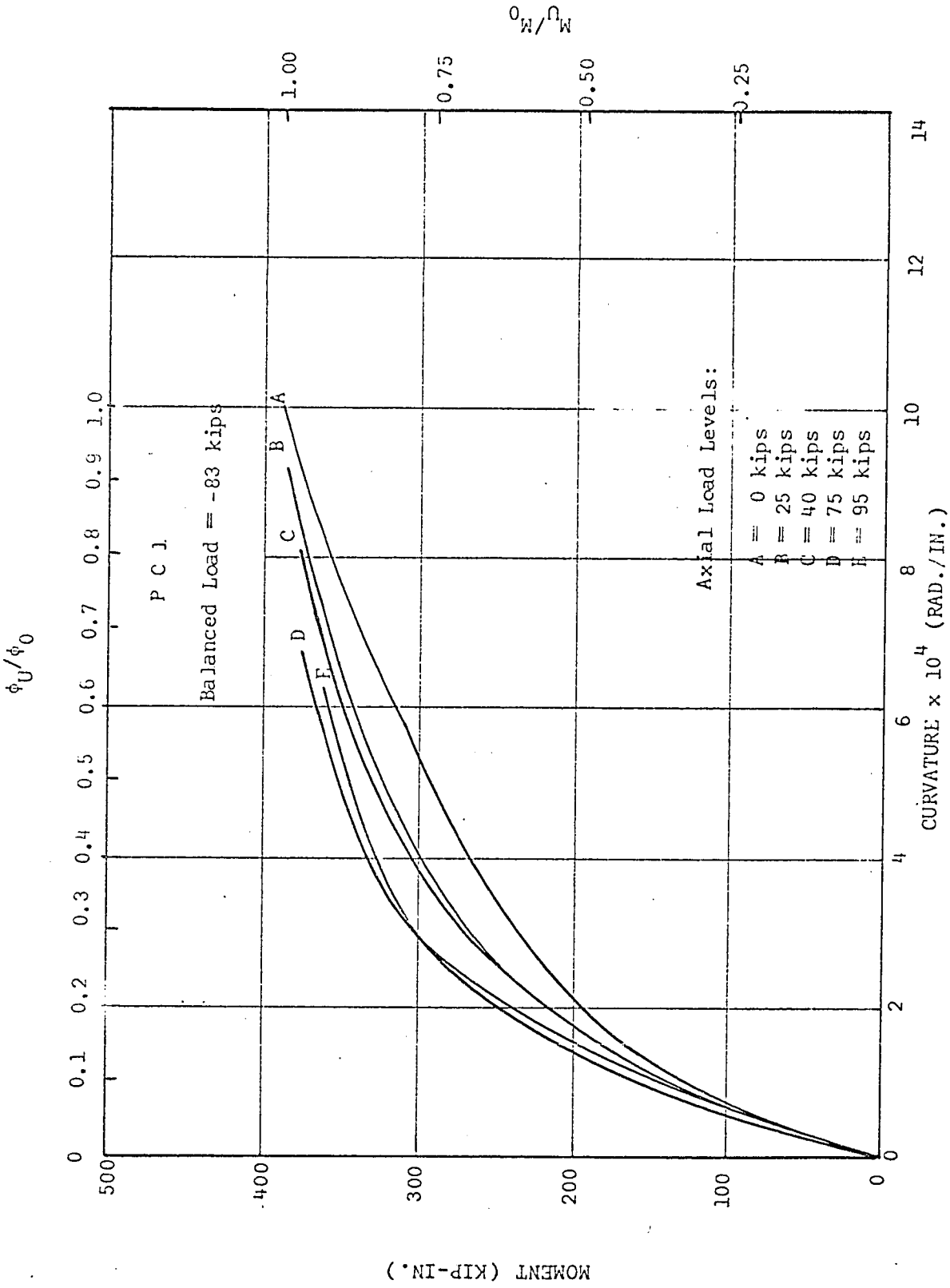

MOMENT-CURVATURE RELATIONSHIP

FIG. 5.16

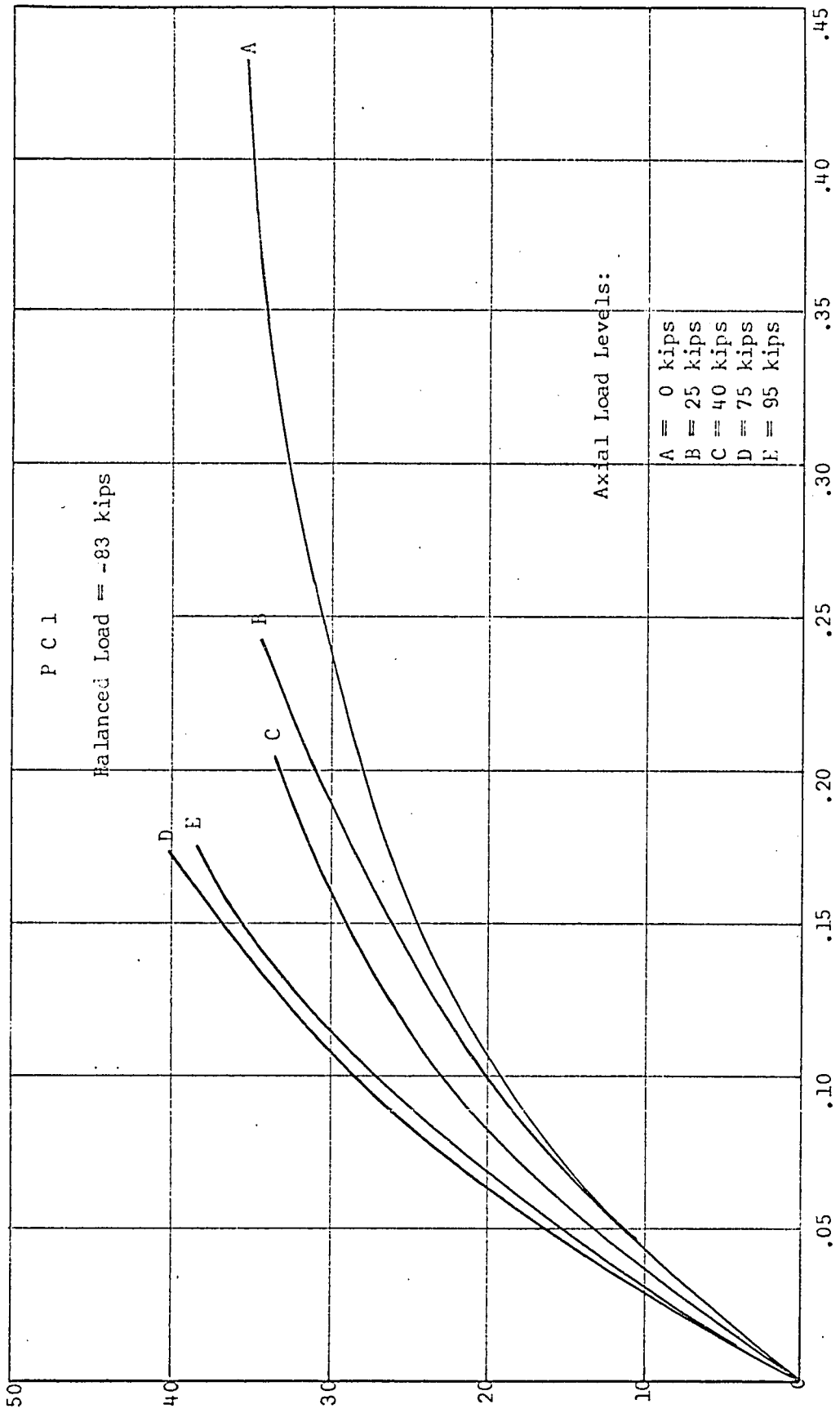

LOAD VS. DEFLECTION AT MIDPOINT RELATIONSHIP

FIG. 5.17

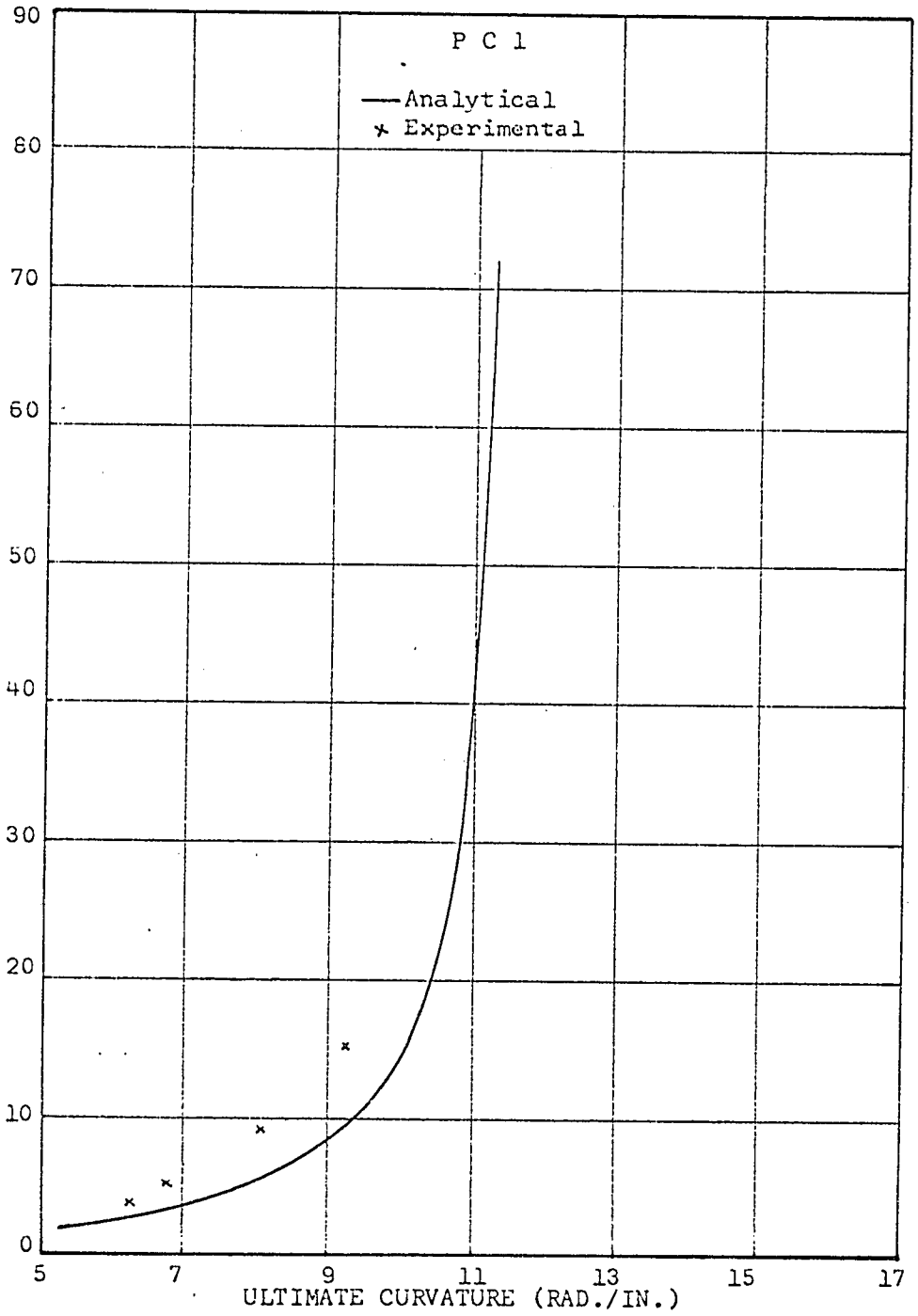

ECCENTRICITY VS. CURVATURE AT THE ULTIMATE LOAD

FIG. 5.18

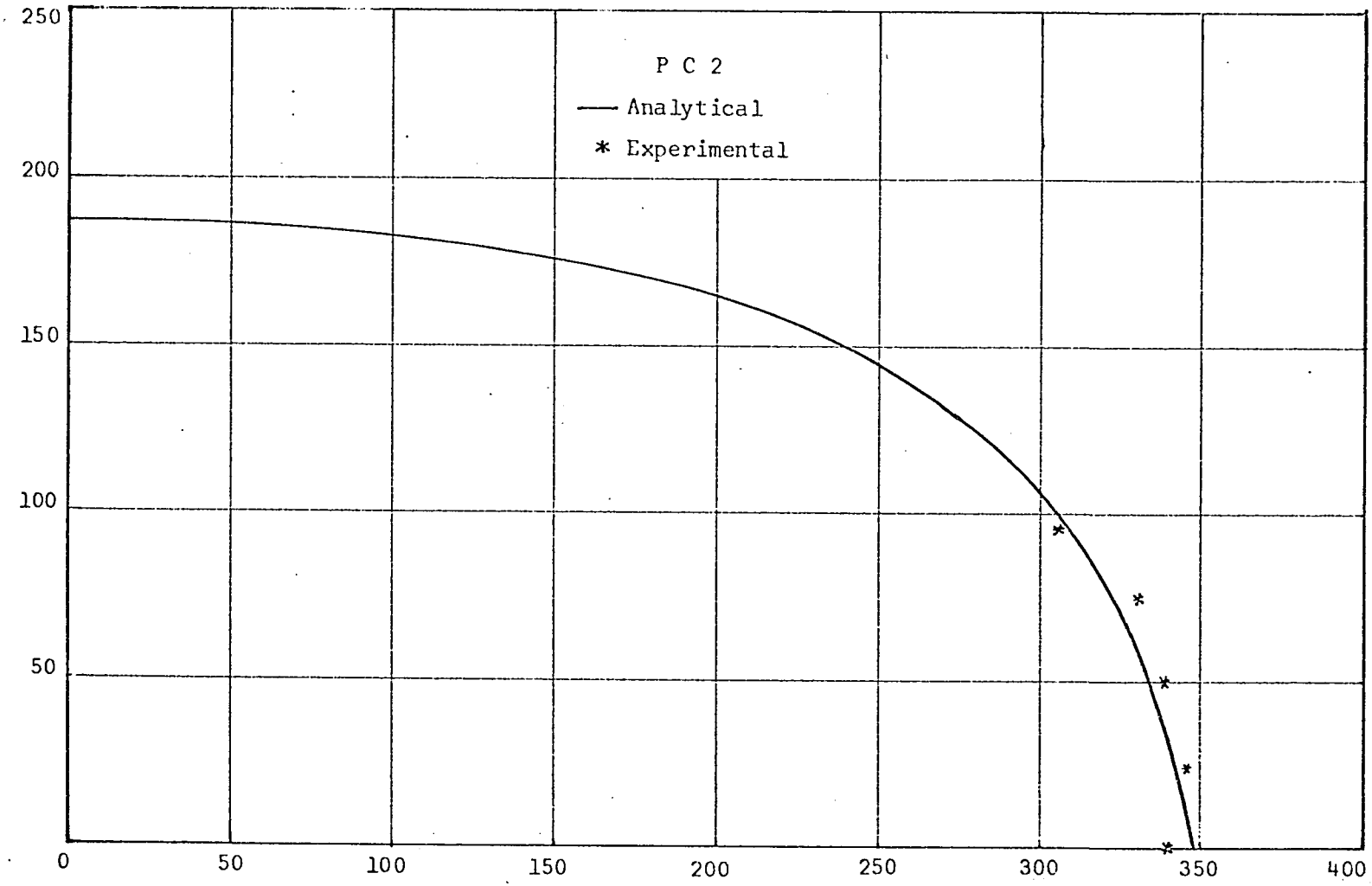

AXIAL THRUST-MOMENT INTERACTION

FIG. 5.19

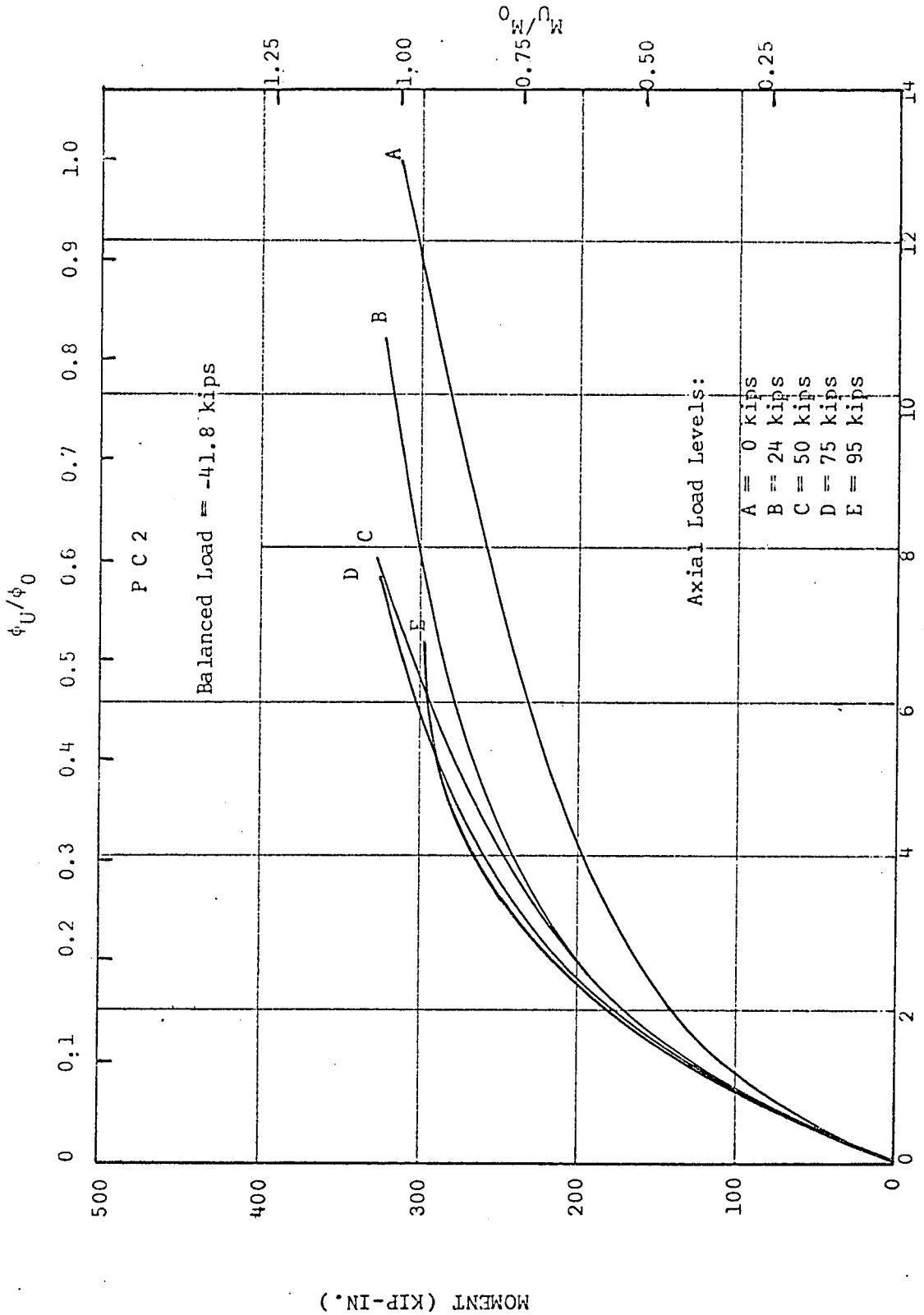

MOMENT-CURVATURE RELATIONSHIP
FIG. 5.20

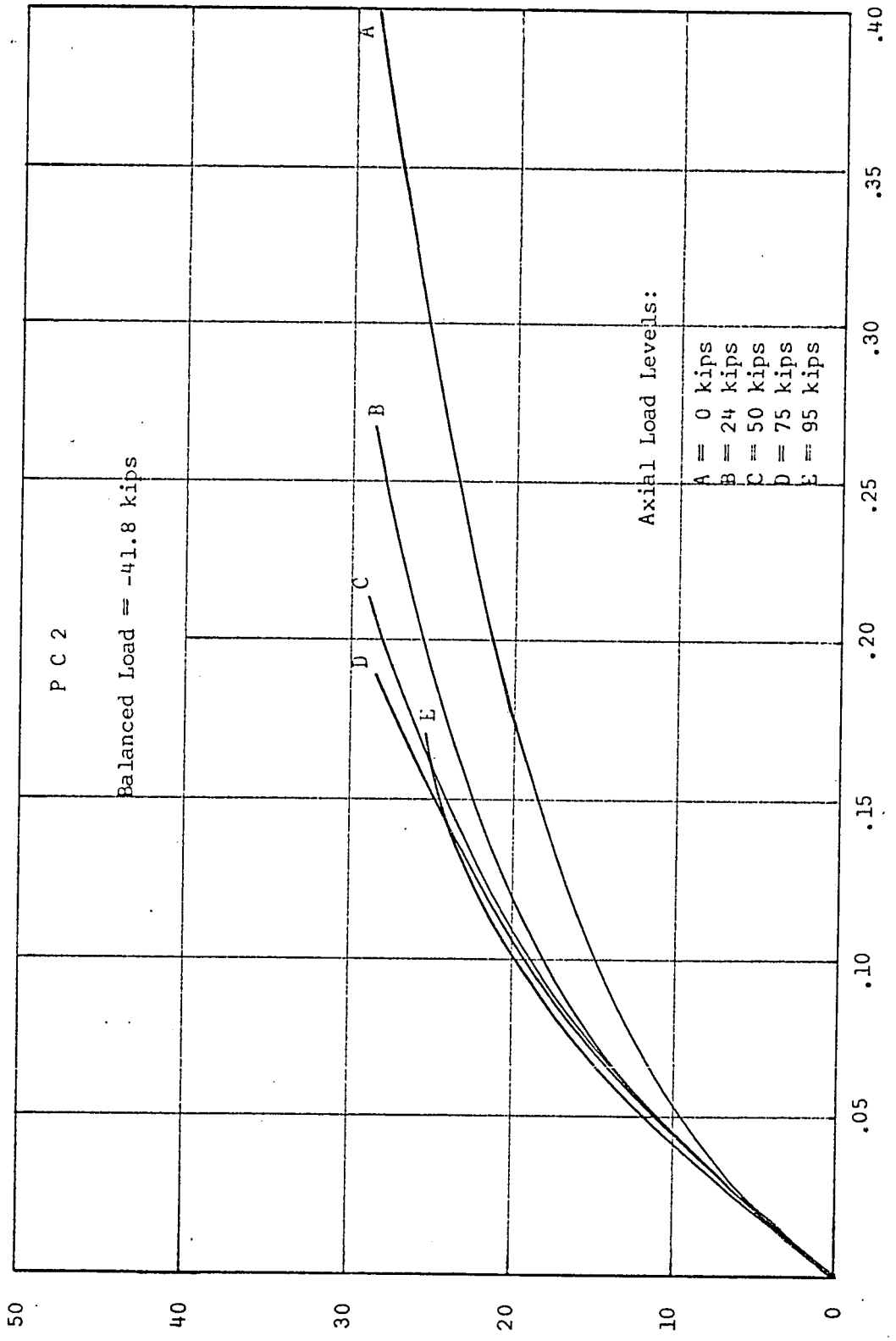

LOAD VS. DEFLECTION AT MIDPOINT RELATIONSHIP

FIG. 5.21

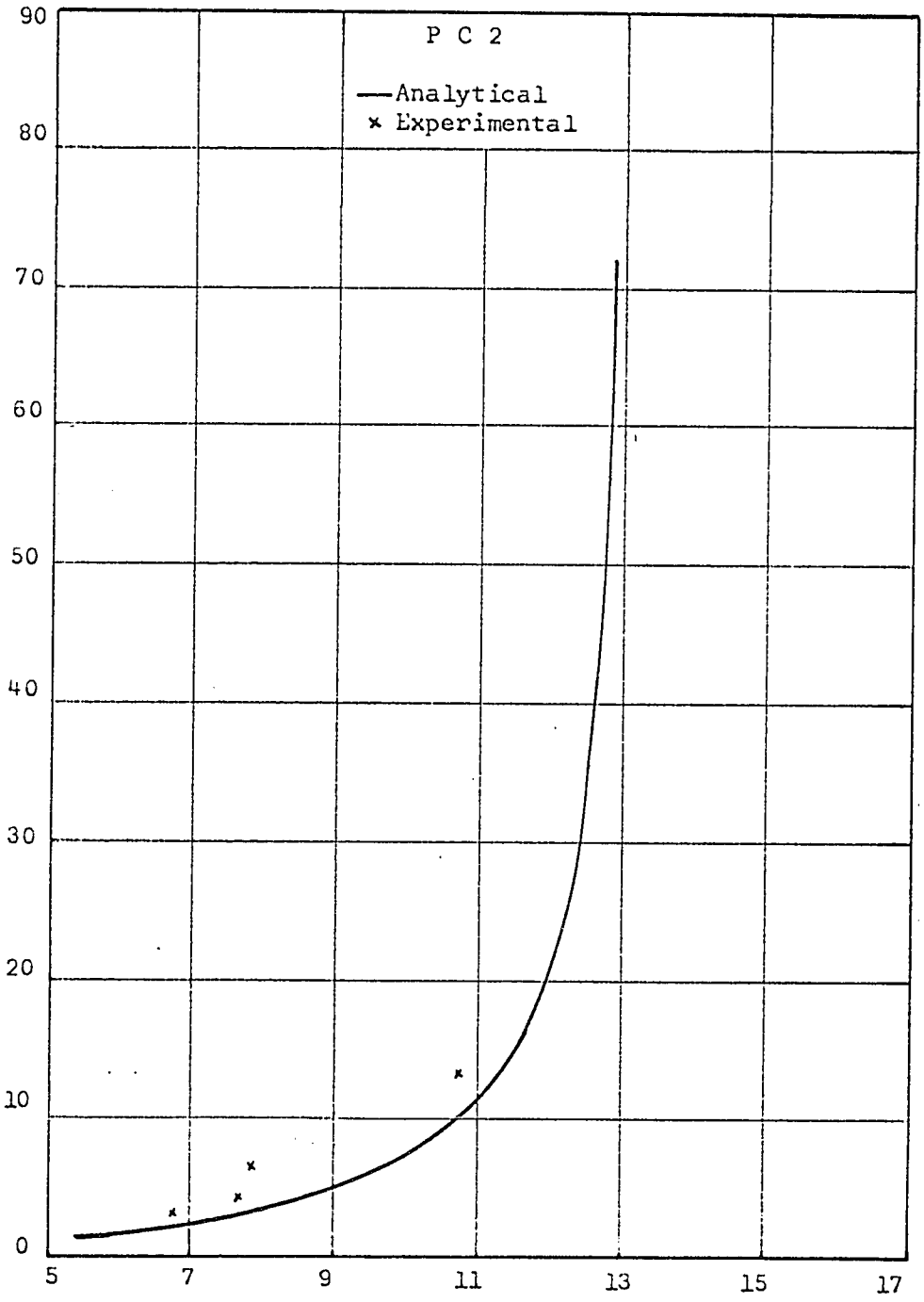

ECCENTRICITY VS. CURVATURE AT THE ULTIMATE LOAD

FIG. 5.22

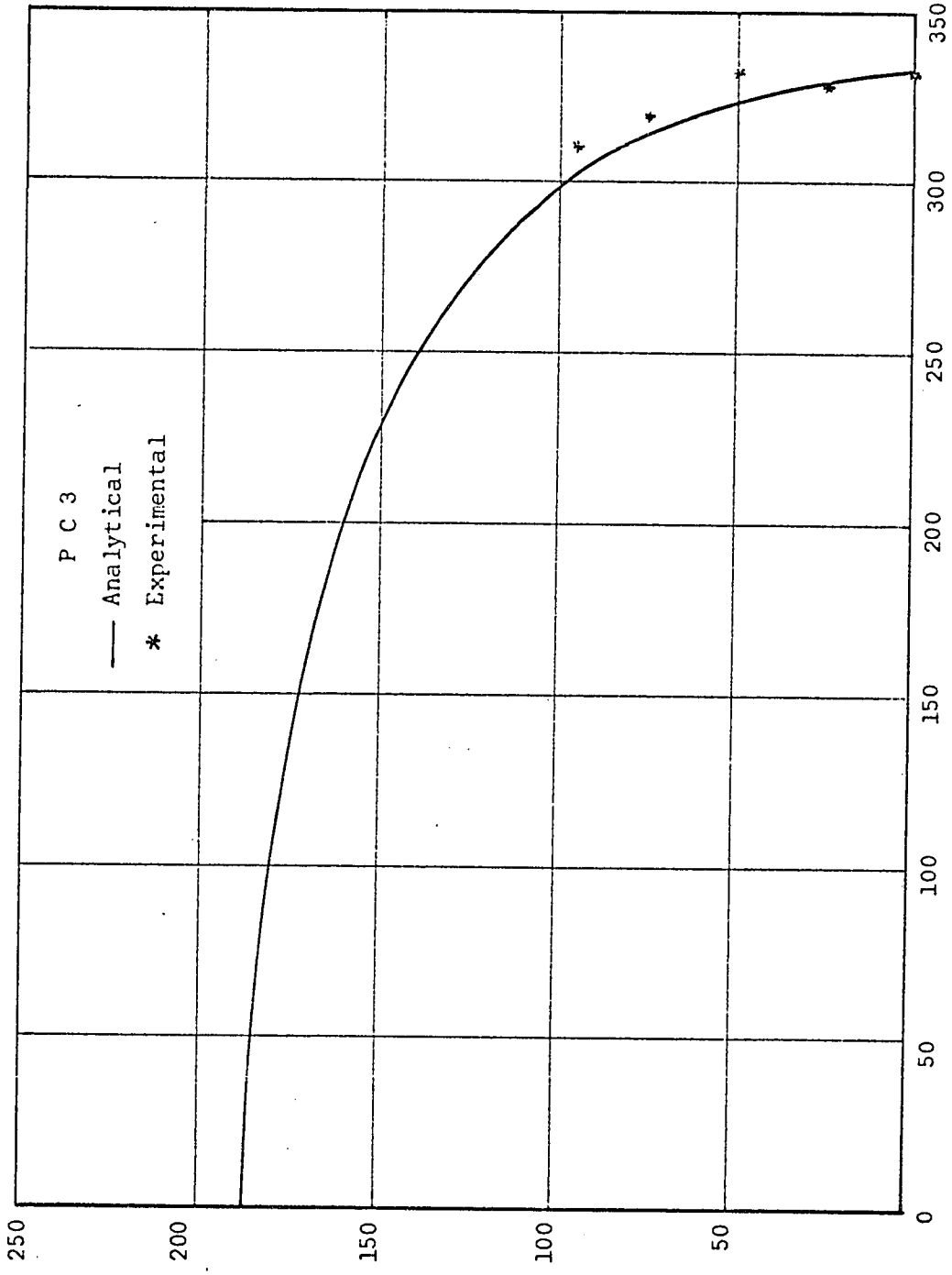

AXIAL THRUST-MOMENT INTERACTION

FIG. 5.23

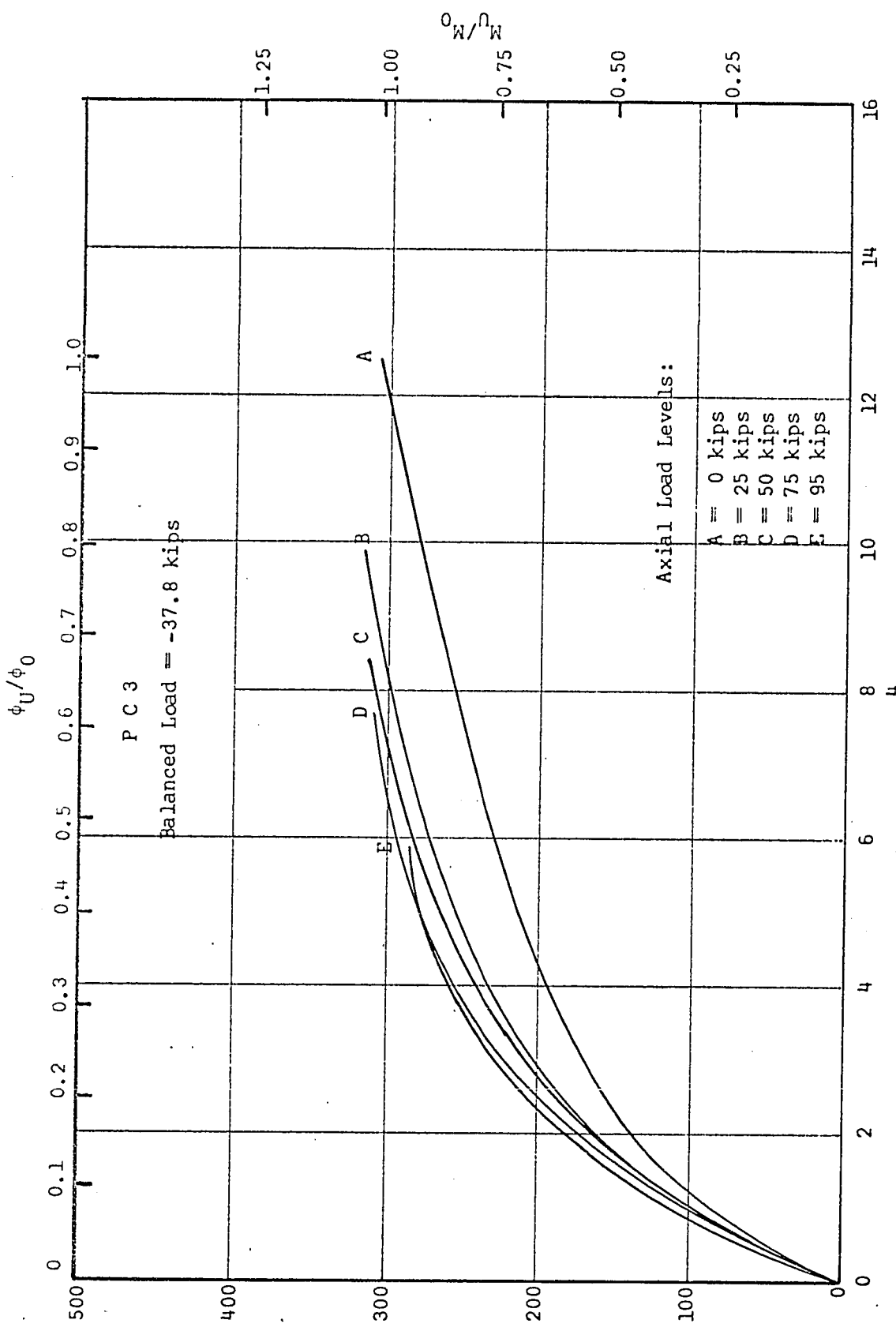

MOMENT-CURVATURE RELATIONSHIP

FIG. 5.24

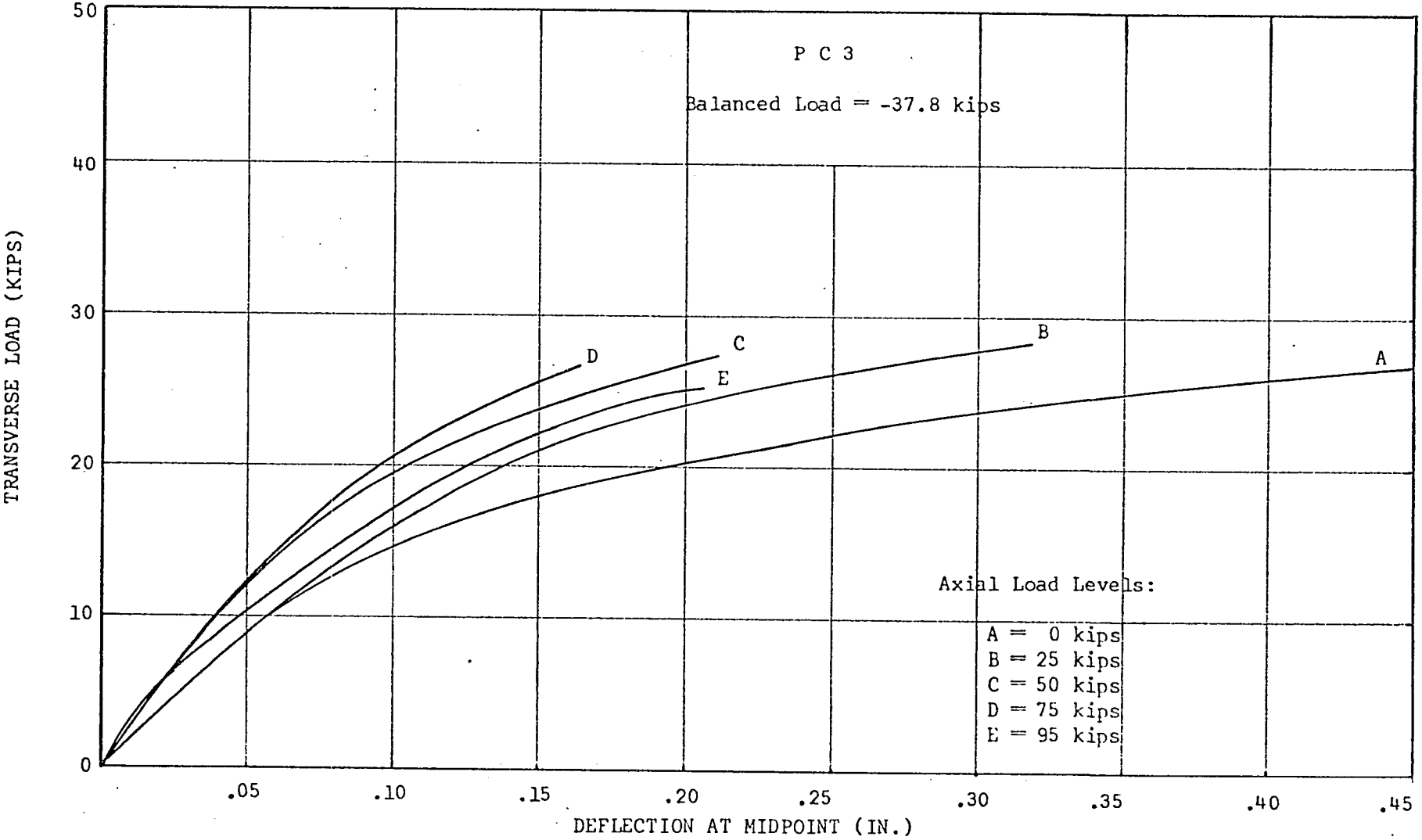

LOAD VS. DEFLECTION AT MIDPOINT RELATIONSHIP

FIG. 5.25

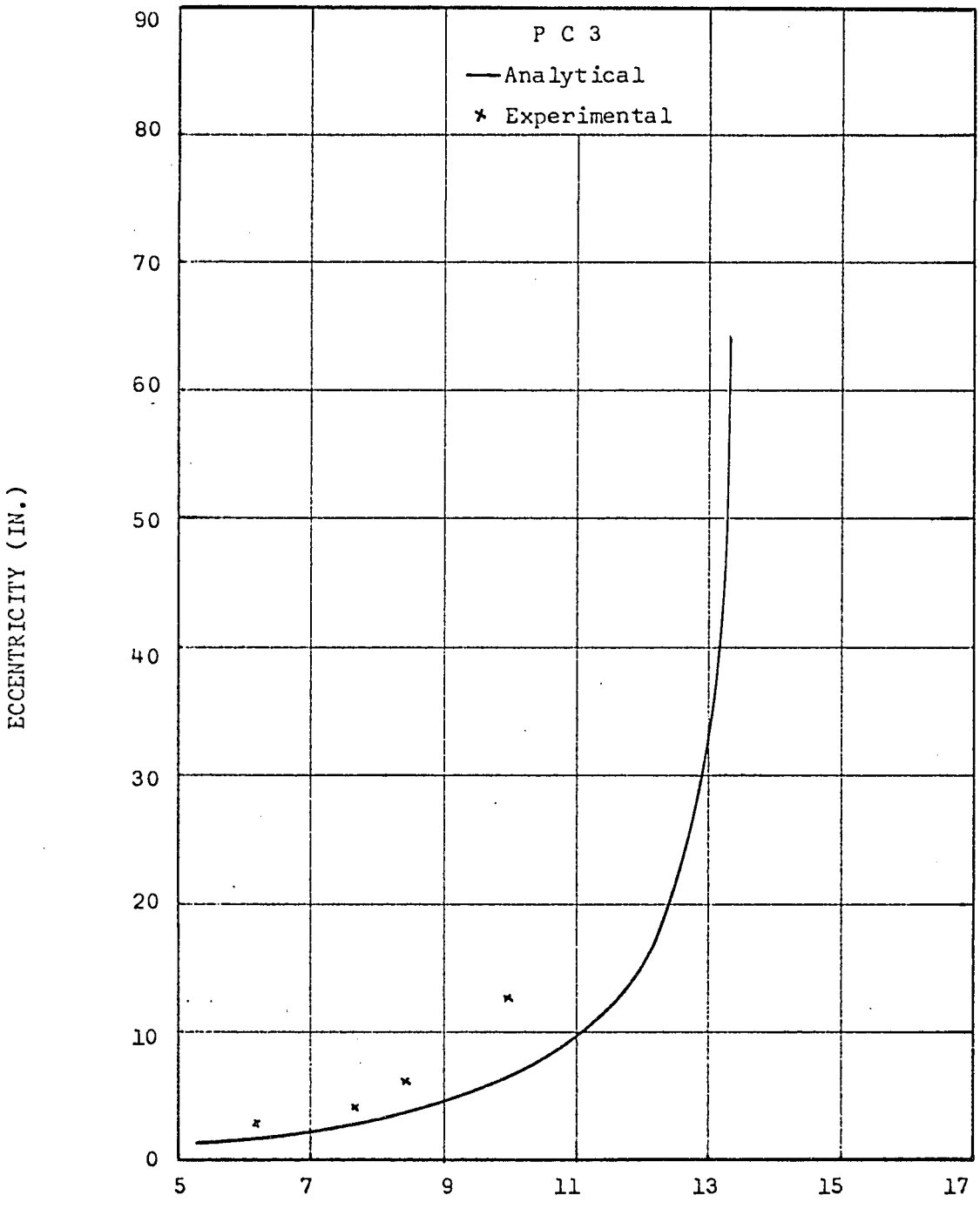

ECCENTRICITY VS. CURVATURE AT THE ULTIMATE LOAD

FIG. 5.26

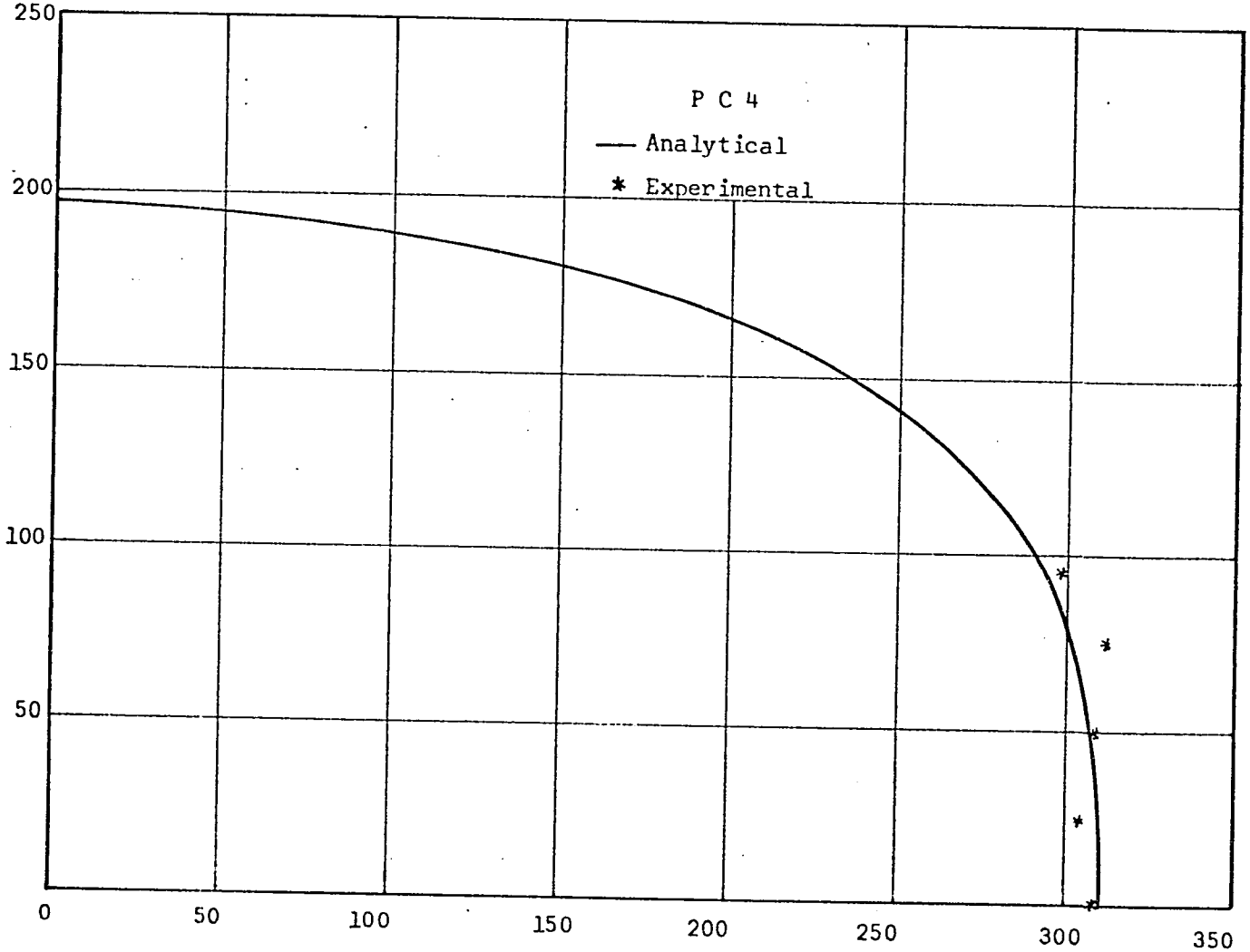

AXIAL THRUST-MOMENT INTERACTION

FIG. 5.27

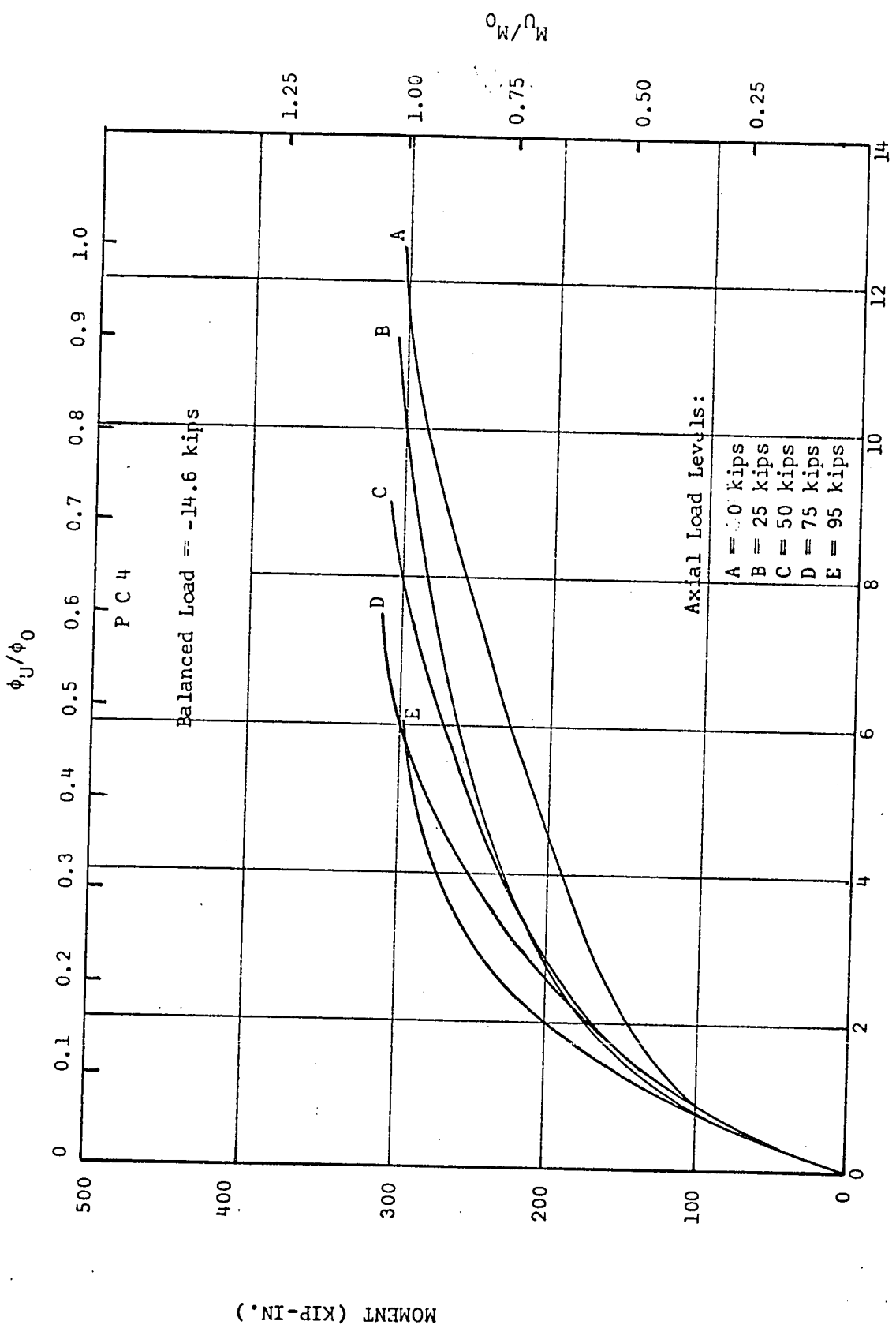

MOMENT-CURVATURE RELATIONSHIP

FIG. 5.28

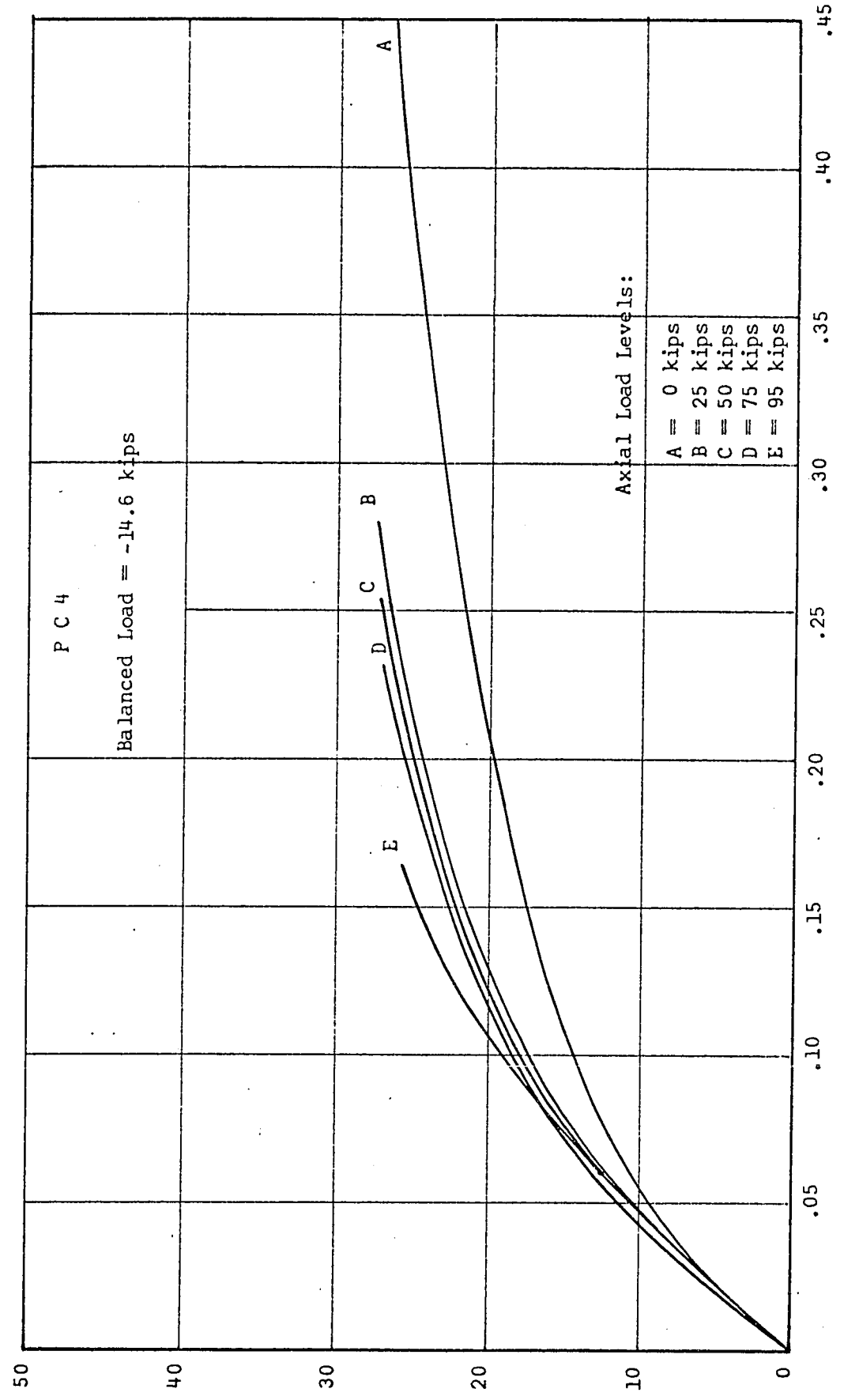

LOAD VS. DEFLECTION AT MIDPOINT RELATIONSHIP

FIG. 5.29

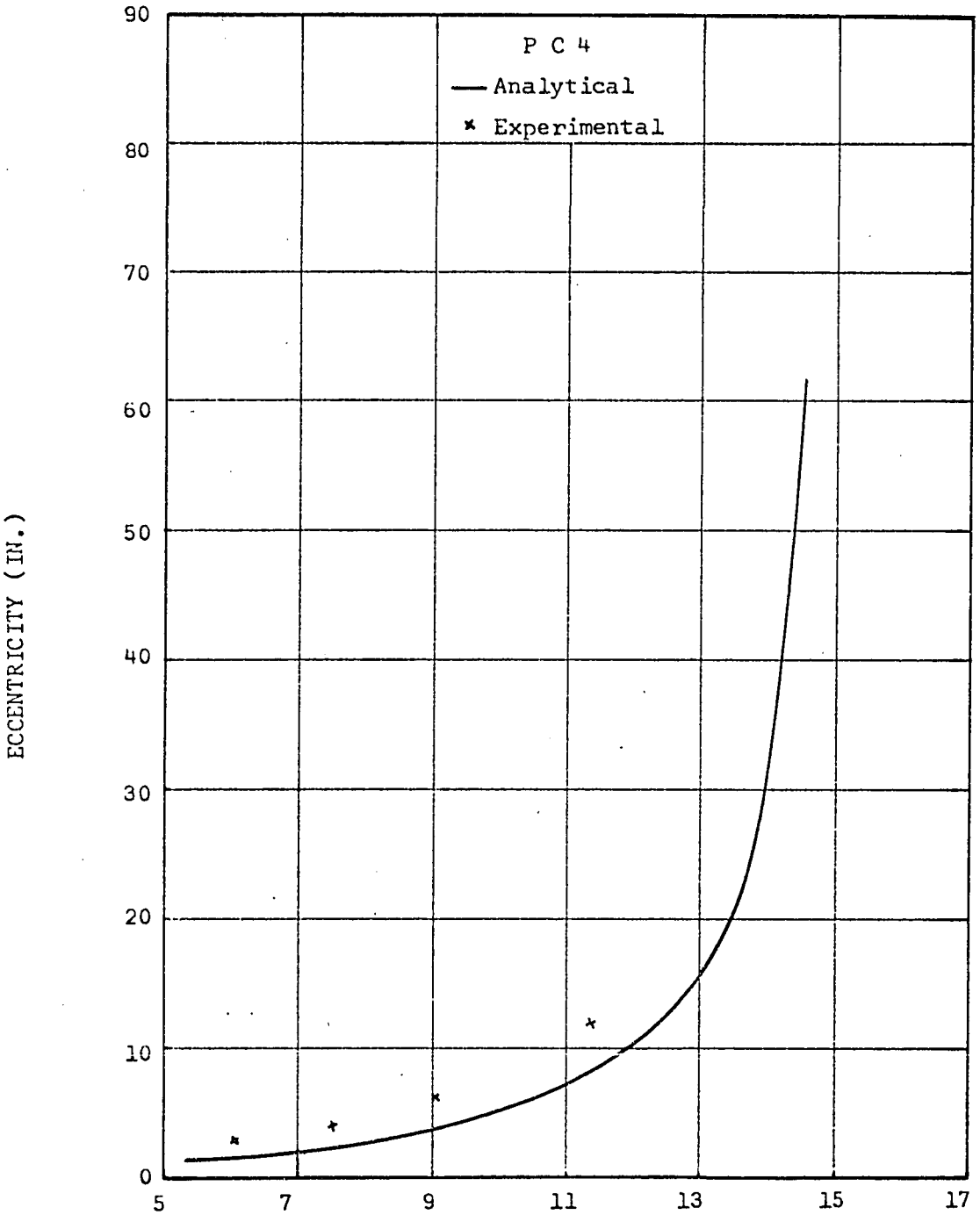

ECCENTRICITY VS. CURVATURE AT THE ULTIMATE LOAD

FIG. 5.30

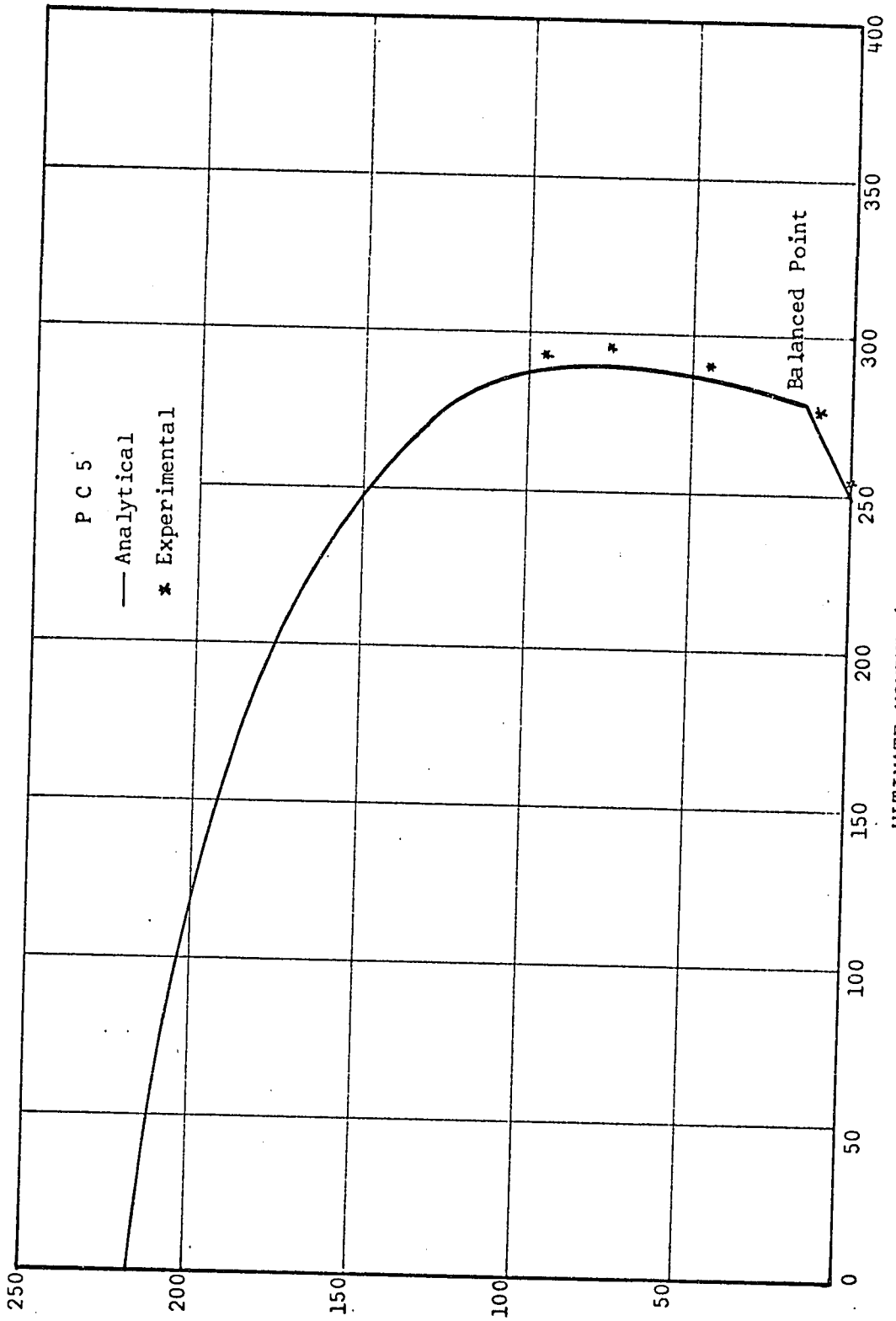

AXIAL THRUST-MOMENT INTERACTION

FIG. 5.31

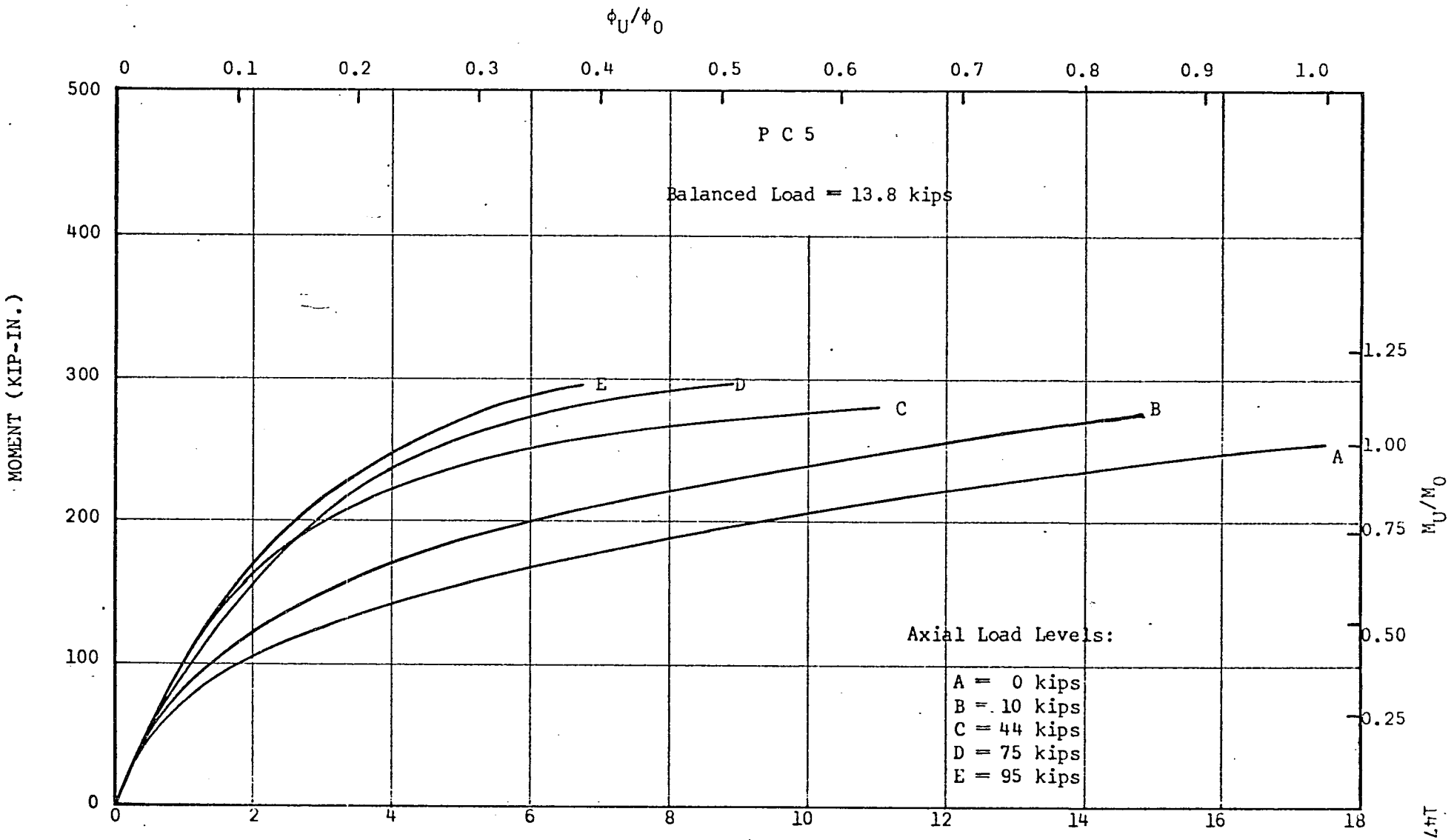

MOMENT-CURVATURE RELATIONSHIP

FIG. 5.32

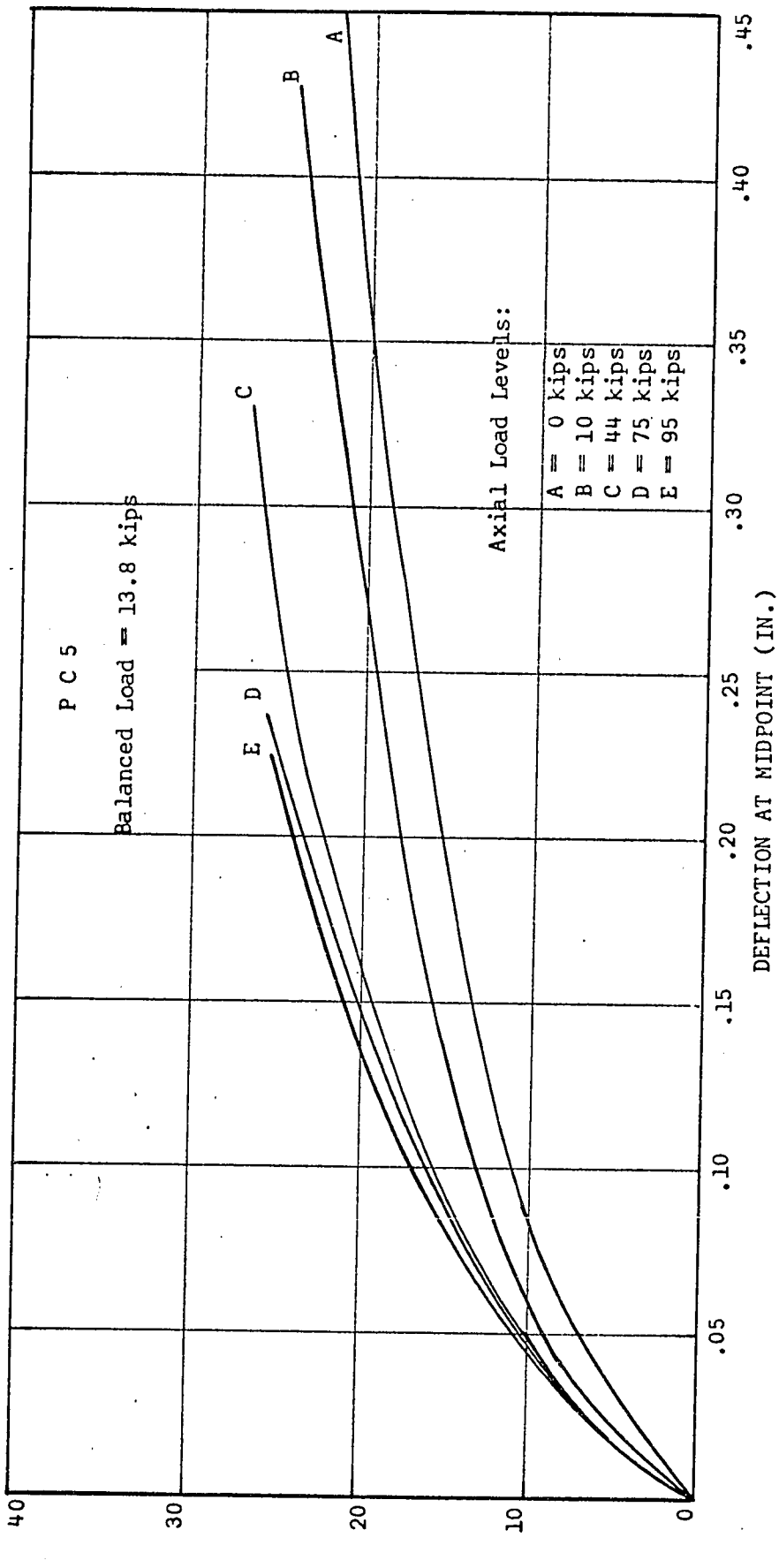

LOAD VS. DEFLECTION AT MIDPOINT RELATIONSHIP

FIG. 5.33

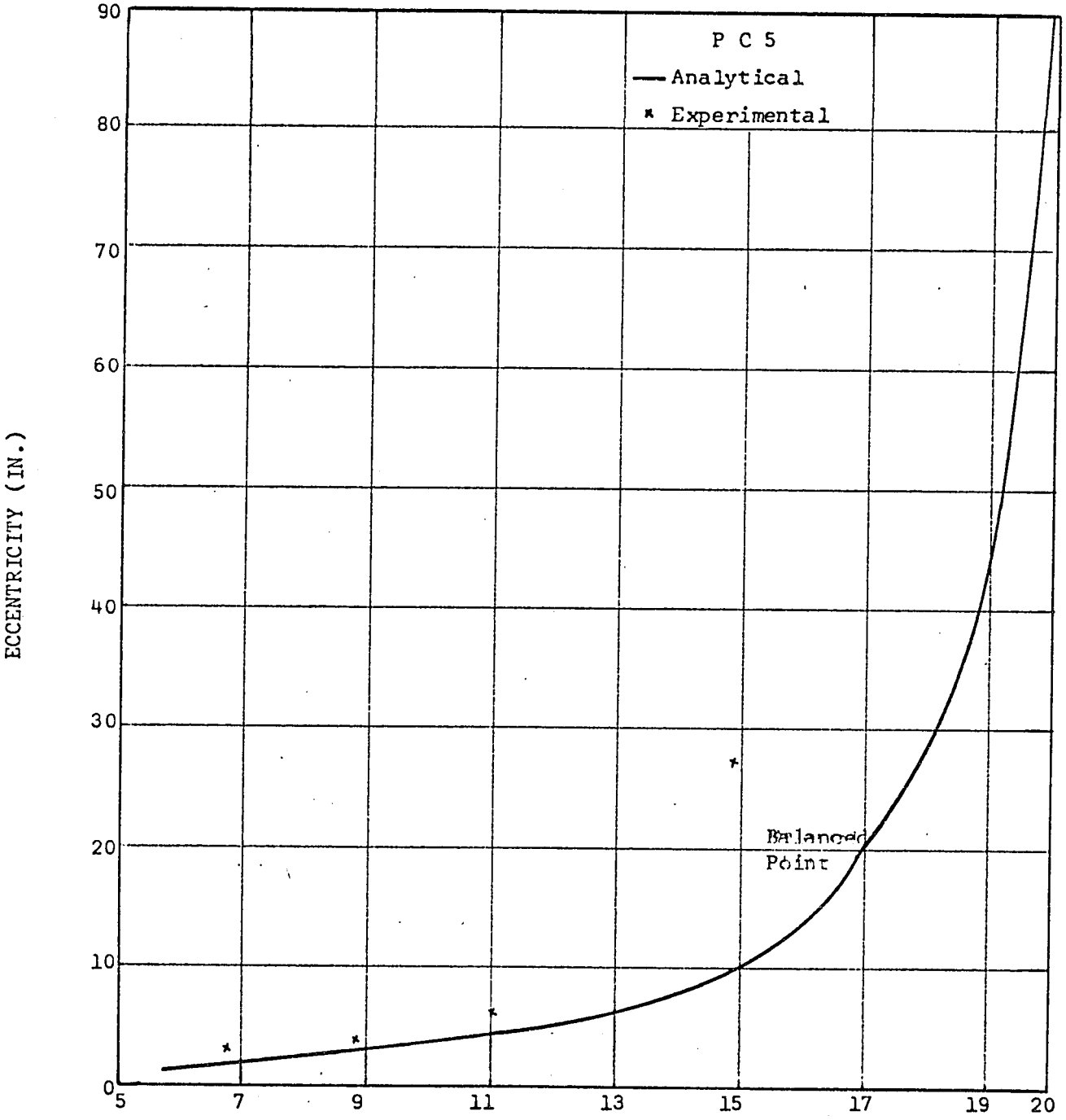

ECCENTRICITY VS. CURVATURE AT THE ULTIMATE LOAD

FIG. 5.34

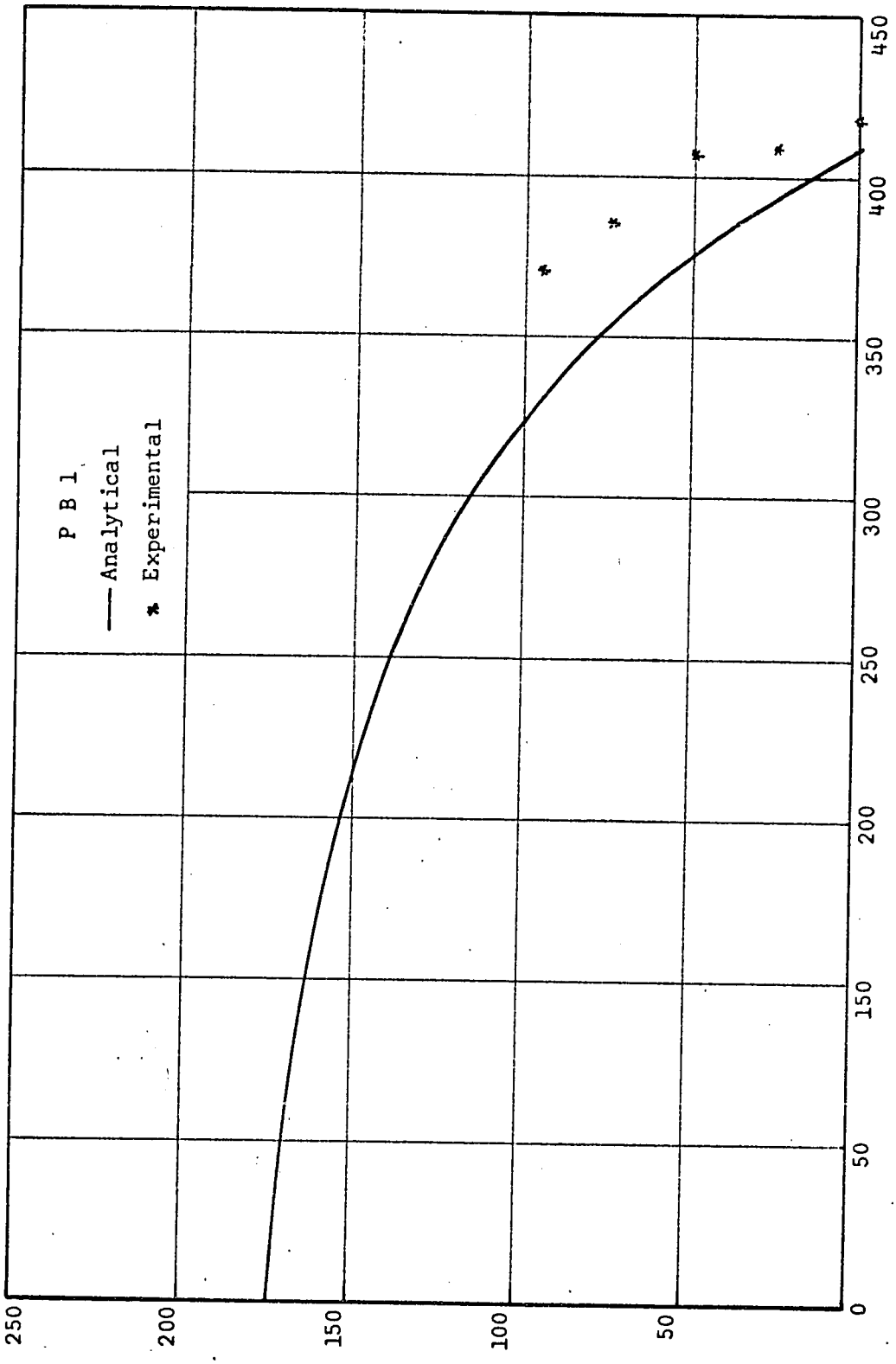

AXIAL THRUST-MOMENT INTERACTION

FIG. 5.35

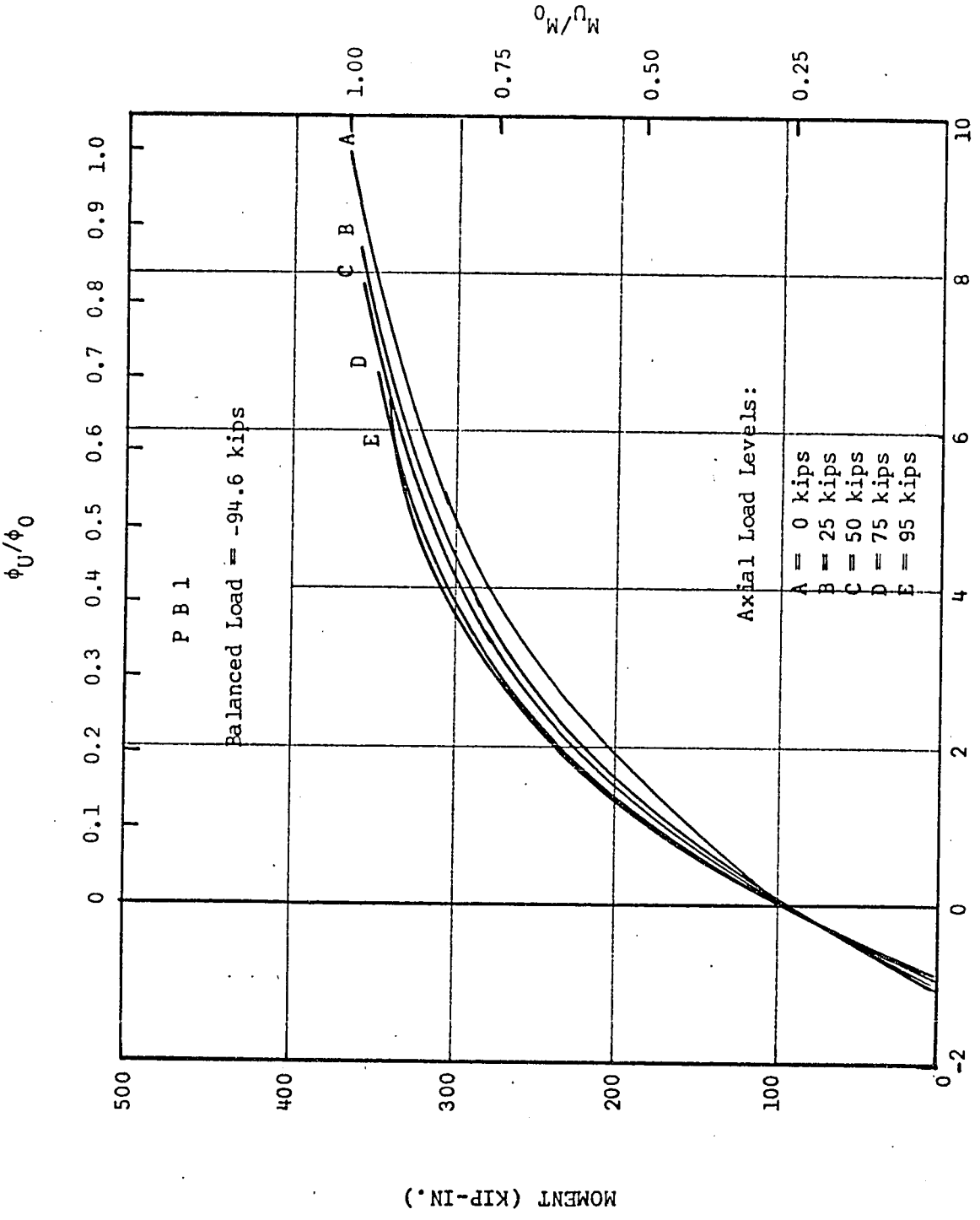

MOMENT-CURVATURE RELATIONSHIP
FIG. 5.36

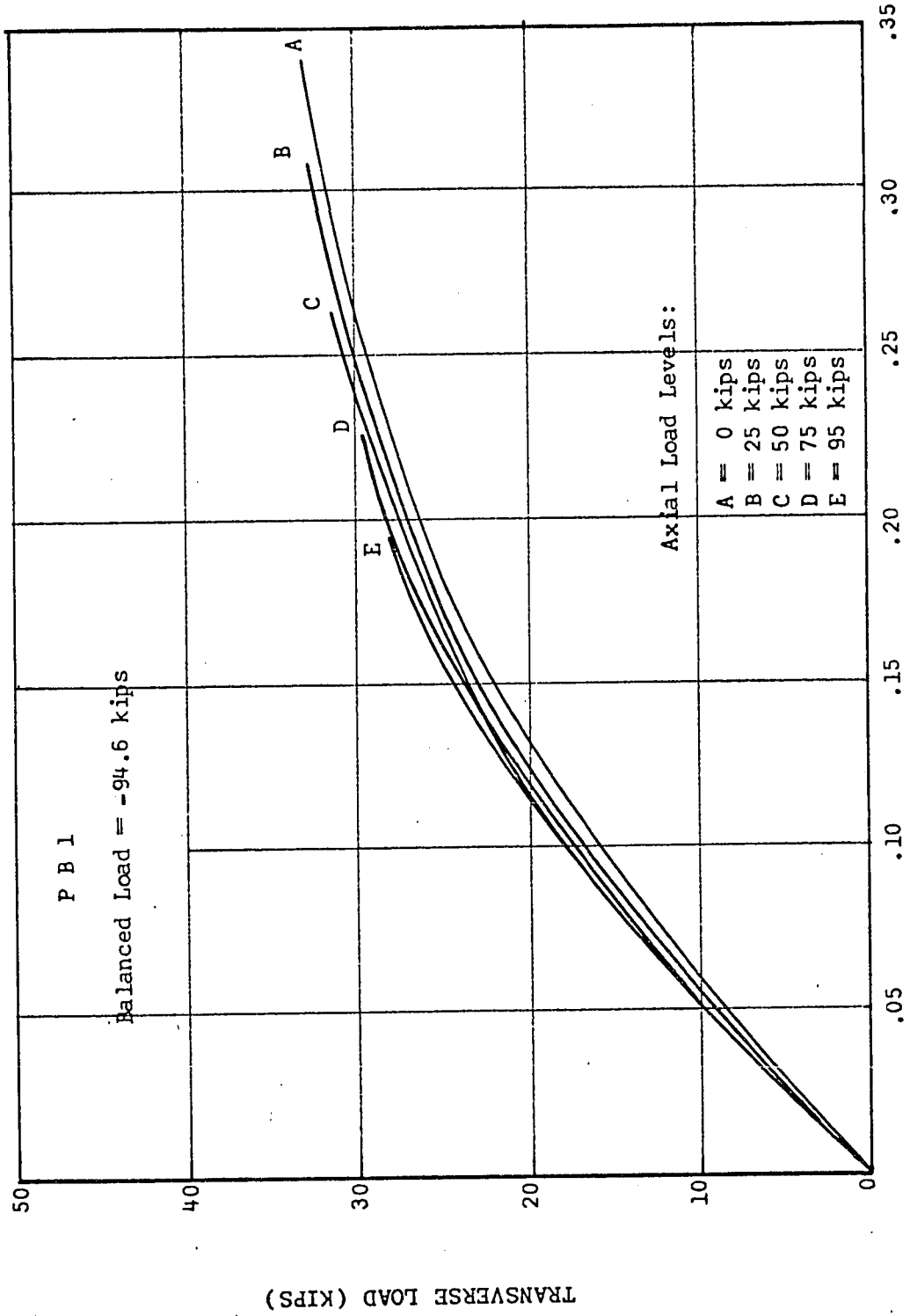

LOAD VS. DEFLECTION AT MIDPOINT RELATIONSHIP

FIG. 5.37

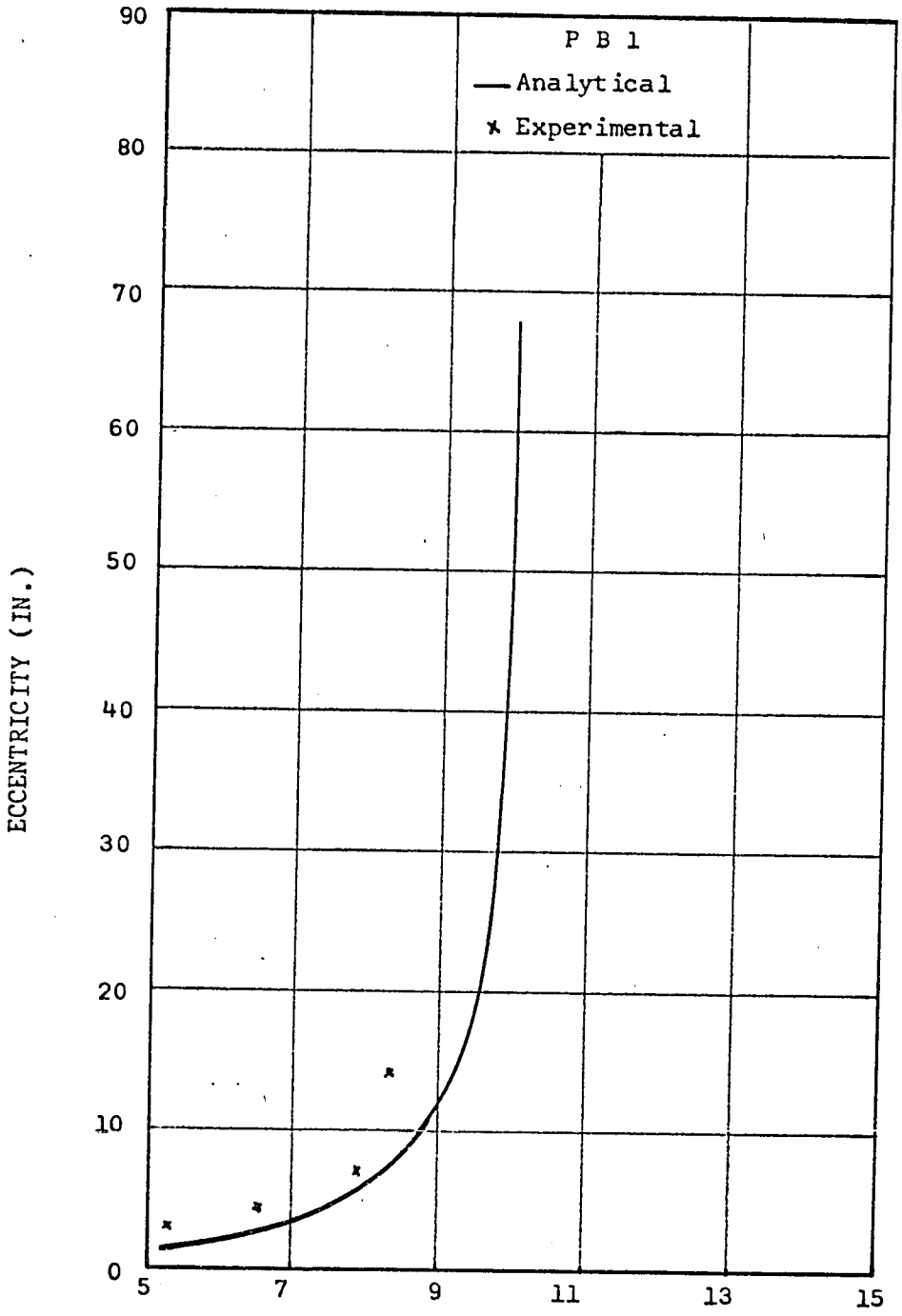

ECCENTRICITY VS. CURVATURE AT THE ULTIMATE LOAD

FIG. 5.38

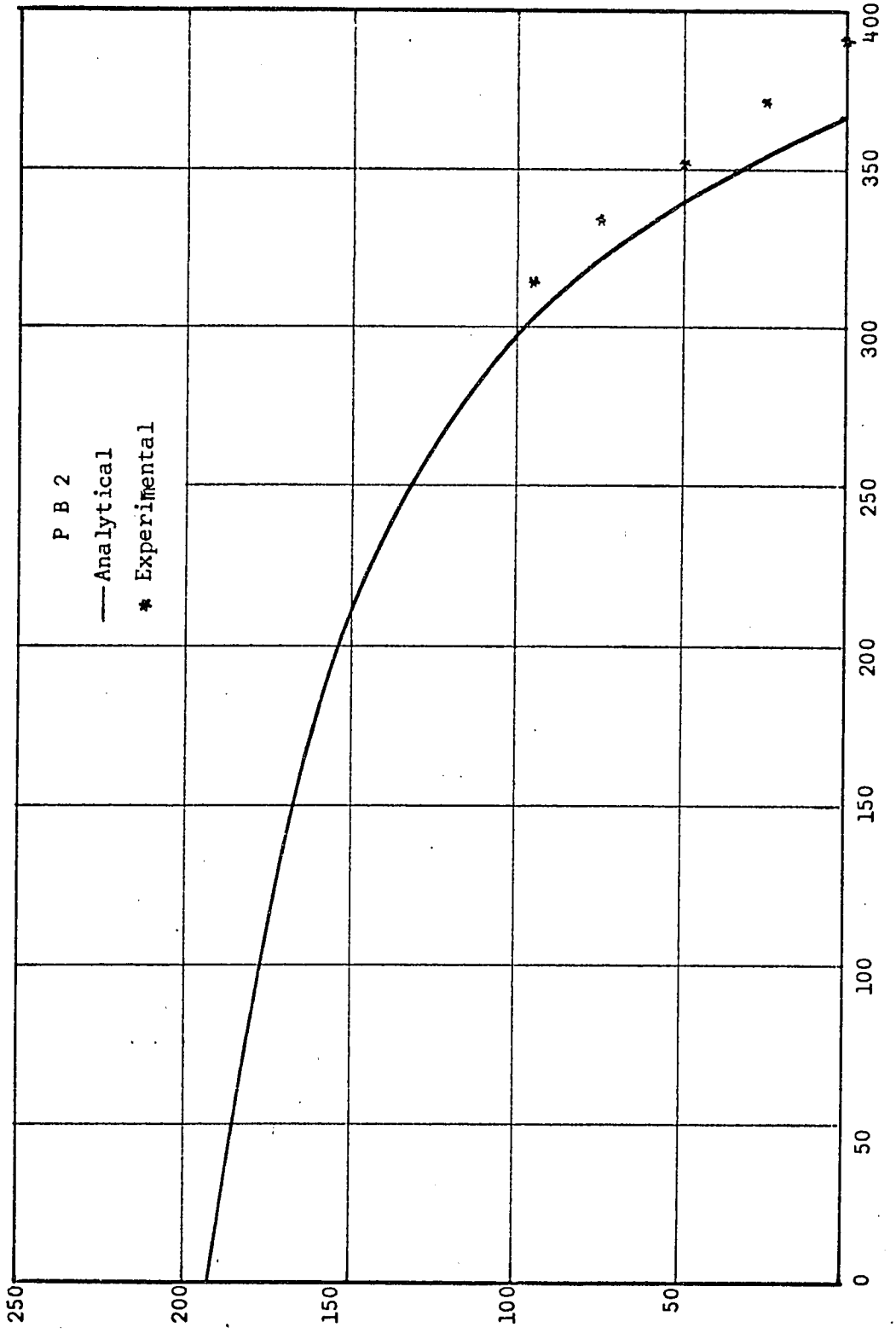

AXIAL THRUST-MOMENT INTERACTION

FIG. 5.39

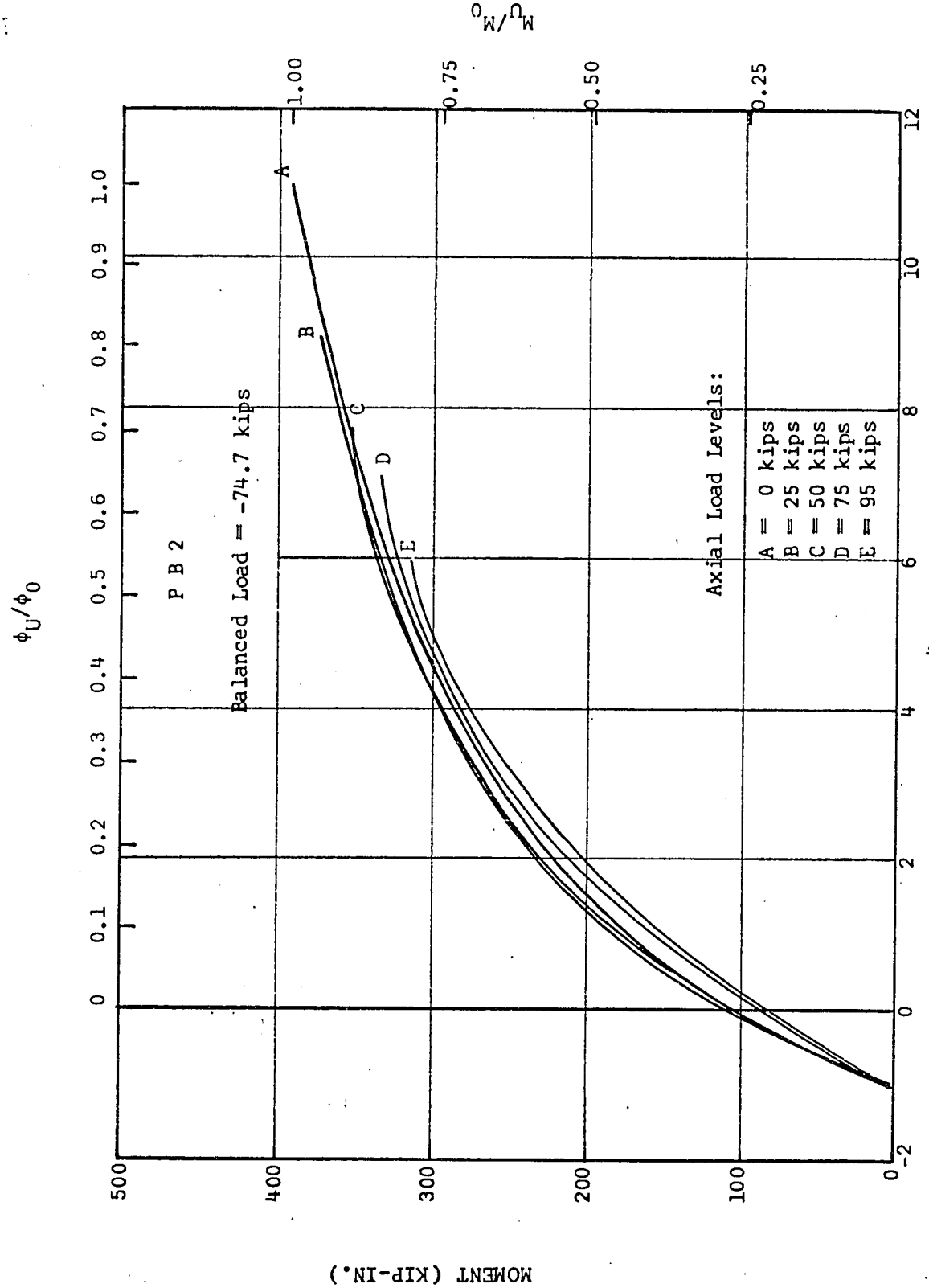

MOMENT-CURVATURE RELATIONSHIP

FIG. 5.40

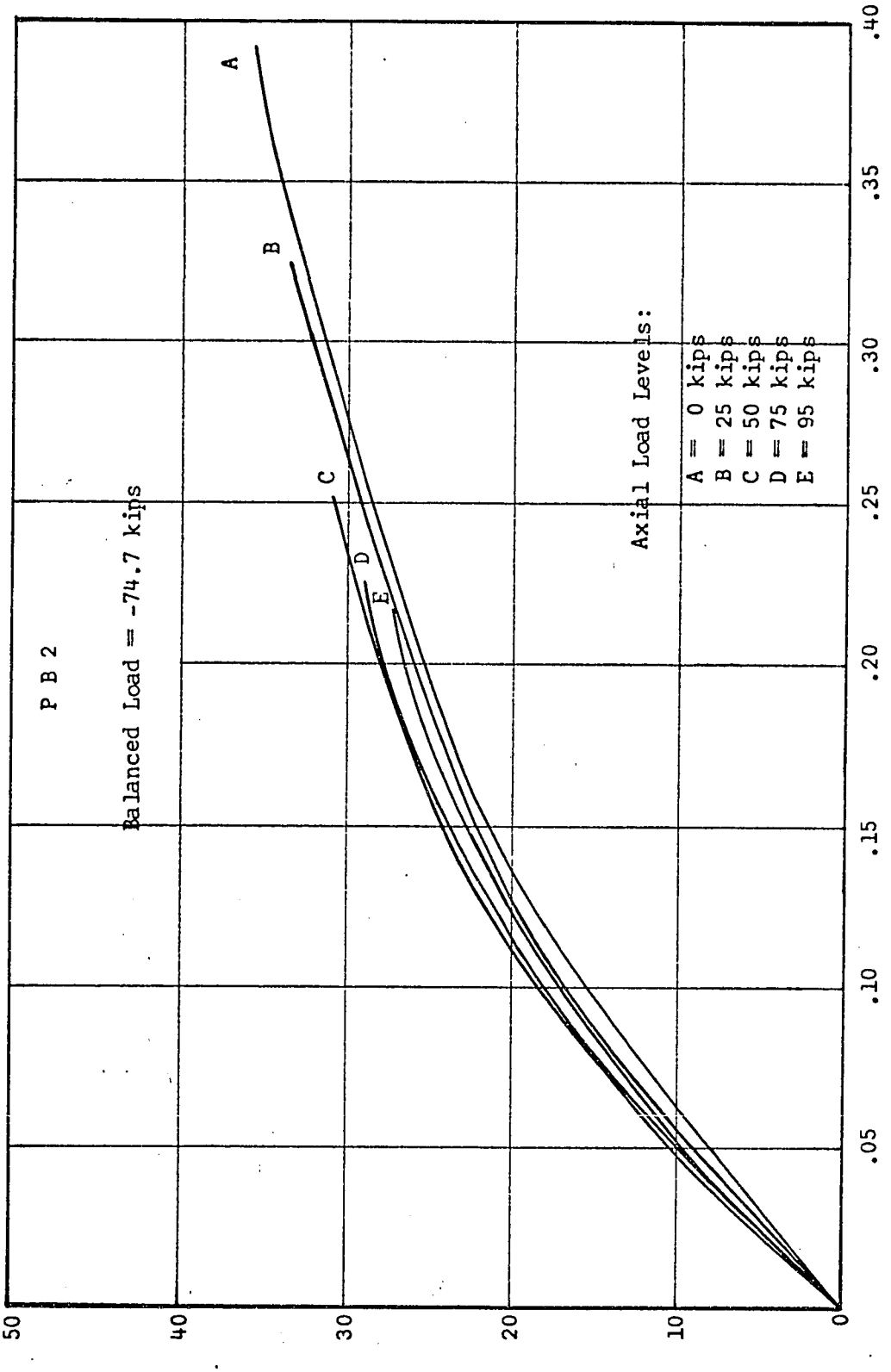

LOAD VS. DEFLECTION AT MIDPOINT RELATIONSHIP

FIG. 5.41

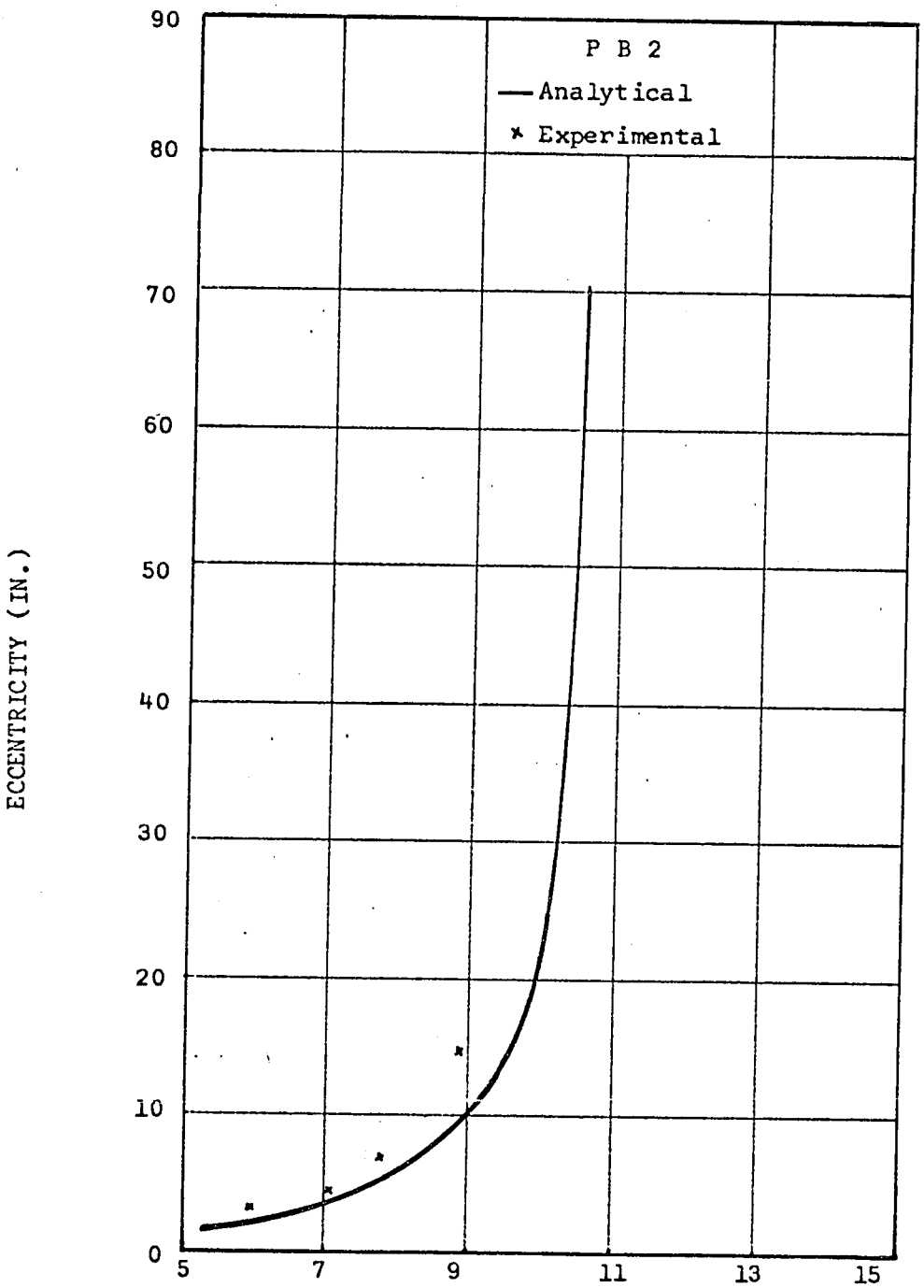

ECCENTRICITY VS. CURVATURE AT THE ULTIMATE LOAD

FIG. 5.42

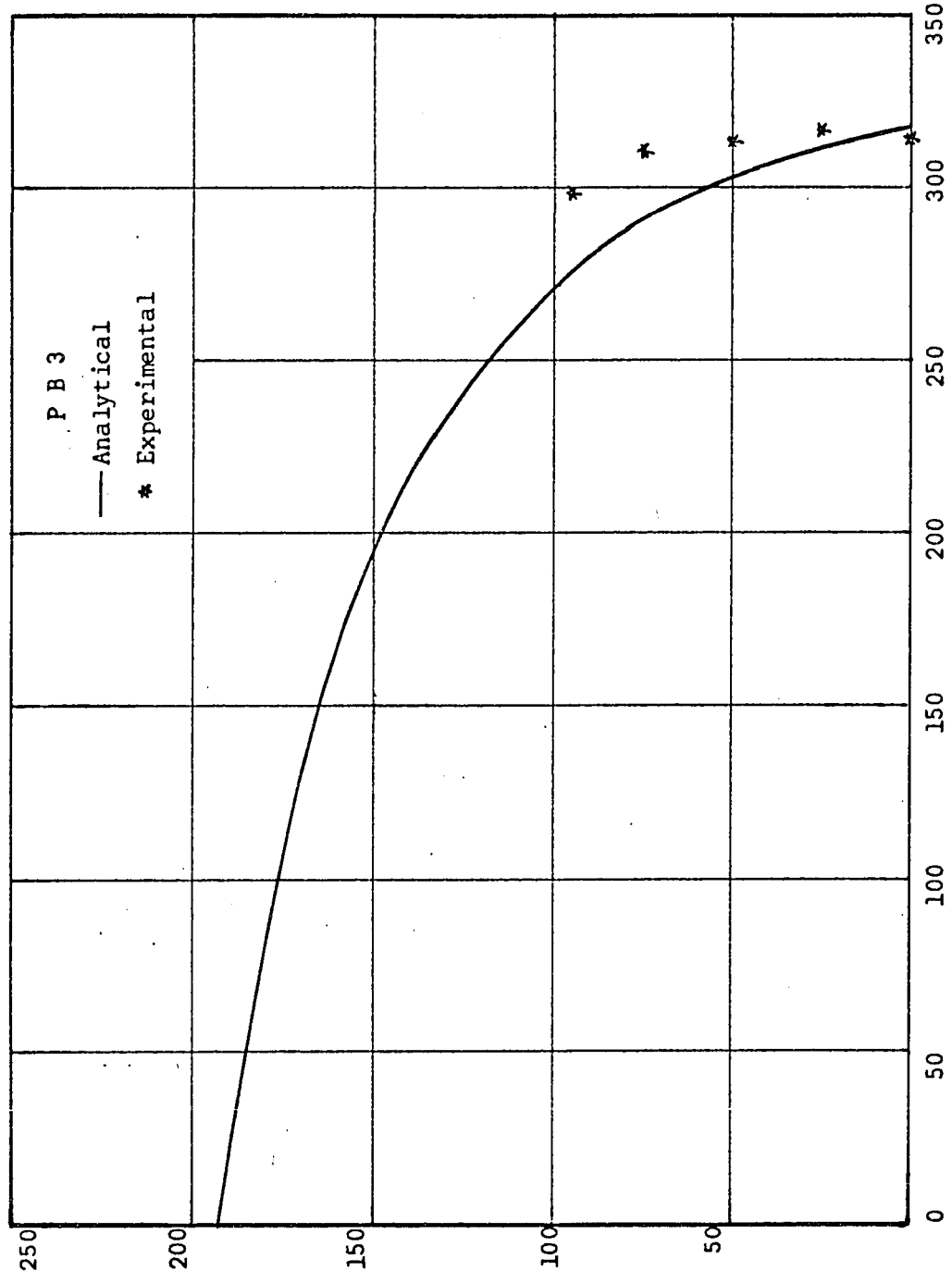

AXIAL THRUST-MOMENT INTERACTION

FIG. 5.43

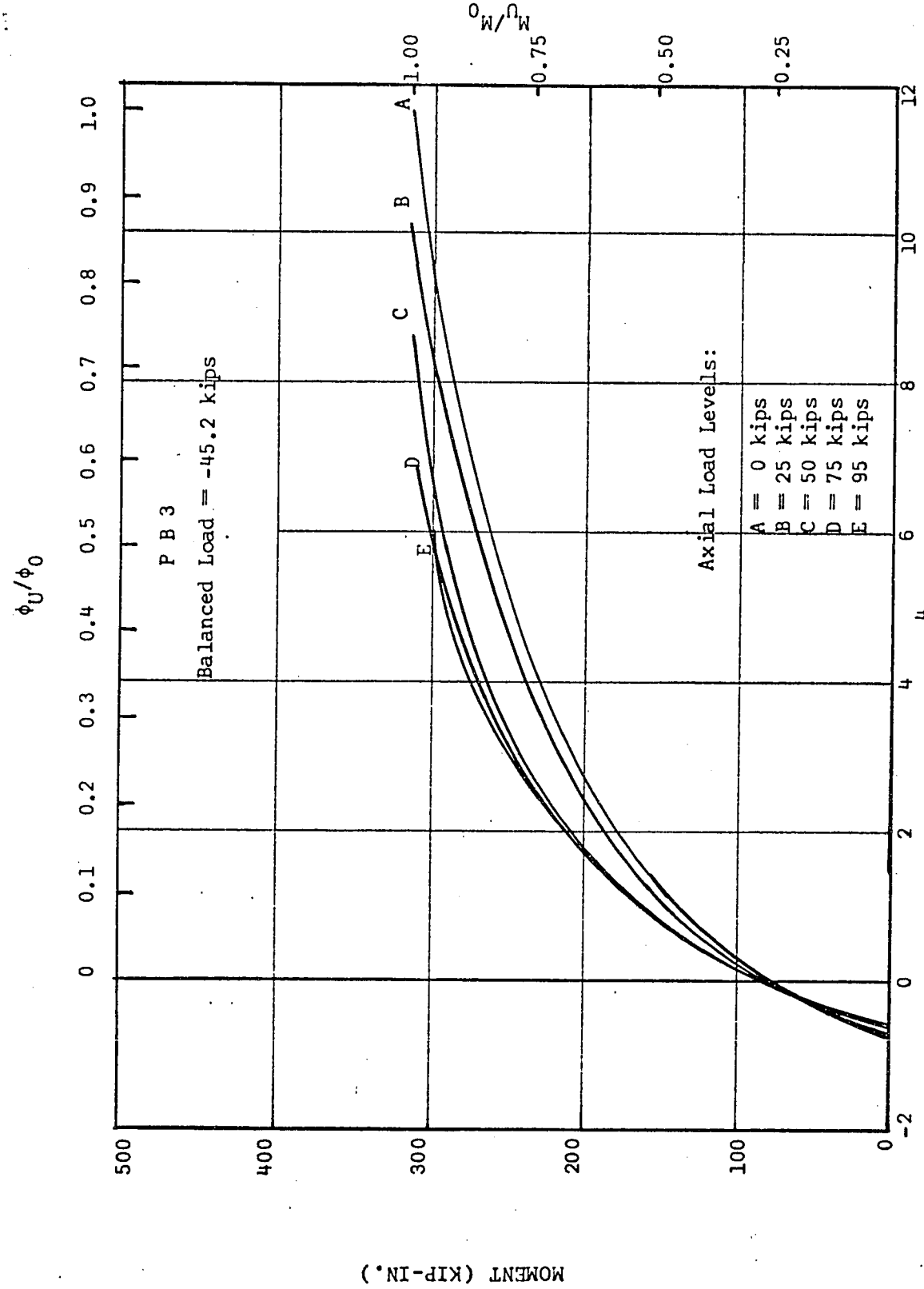

MOMENT-CURVATURE RELATIONSHIP

FIG. 5.44

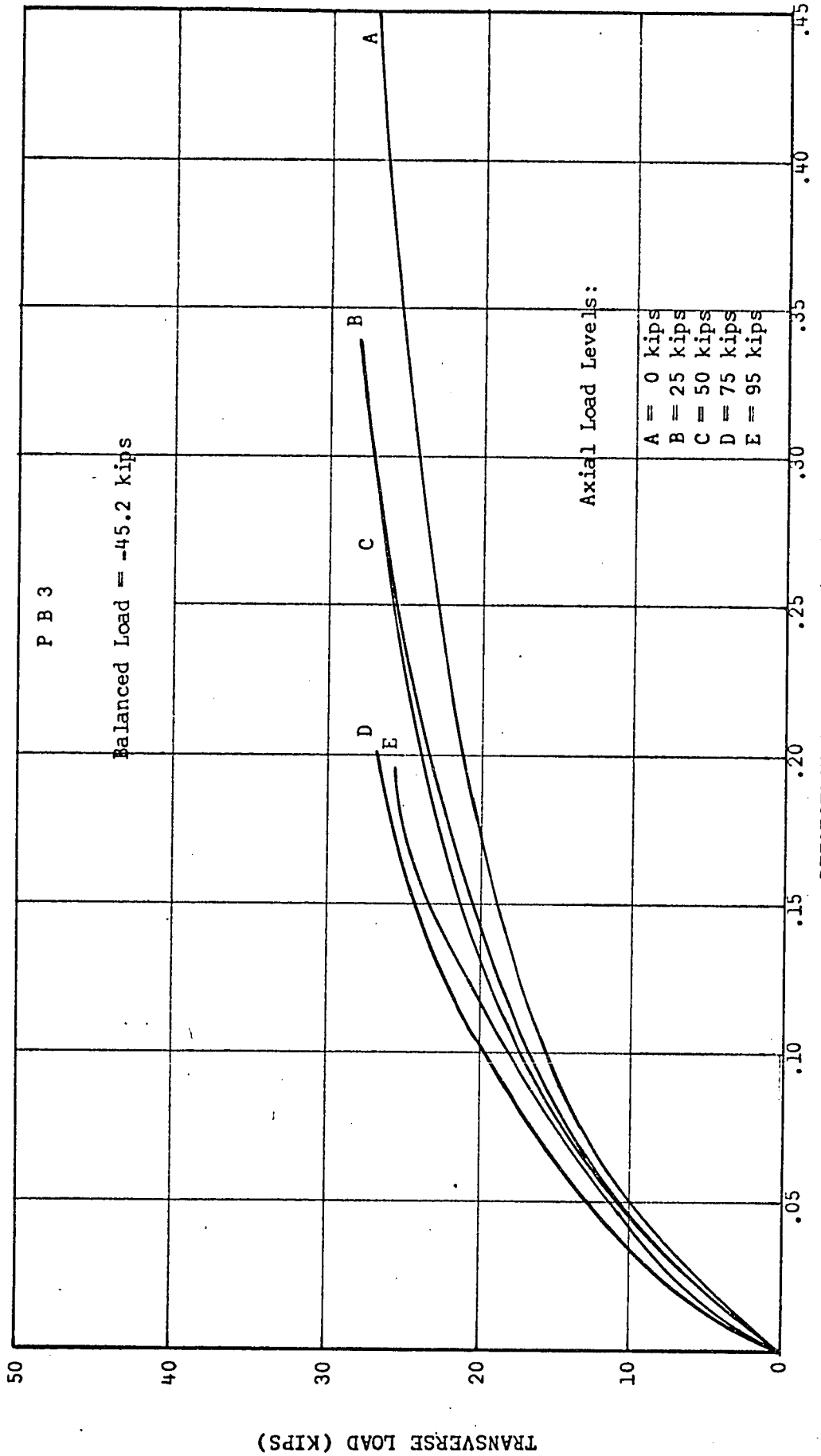

LOAD VS. DEFLECTION AT MIDPOINT RELATIONSHIP

FIG. 5.45

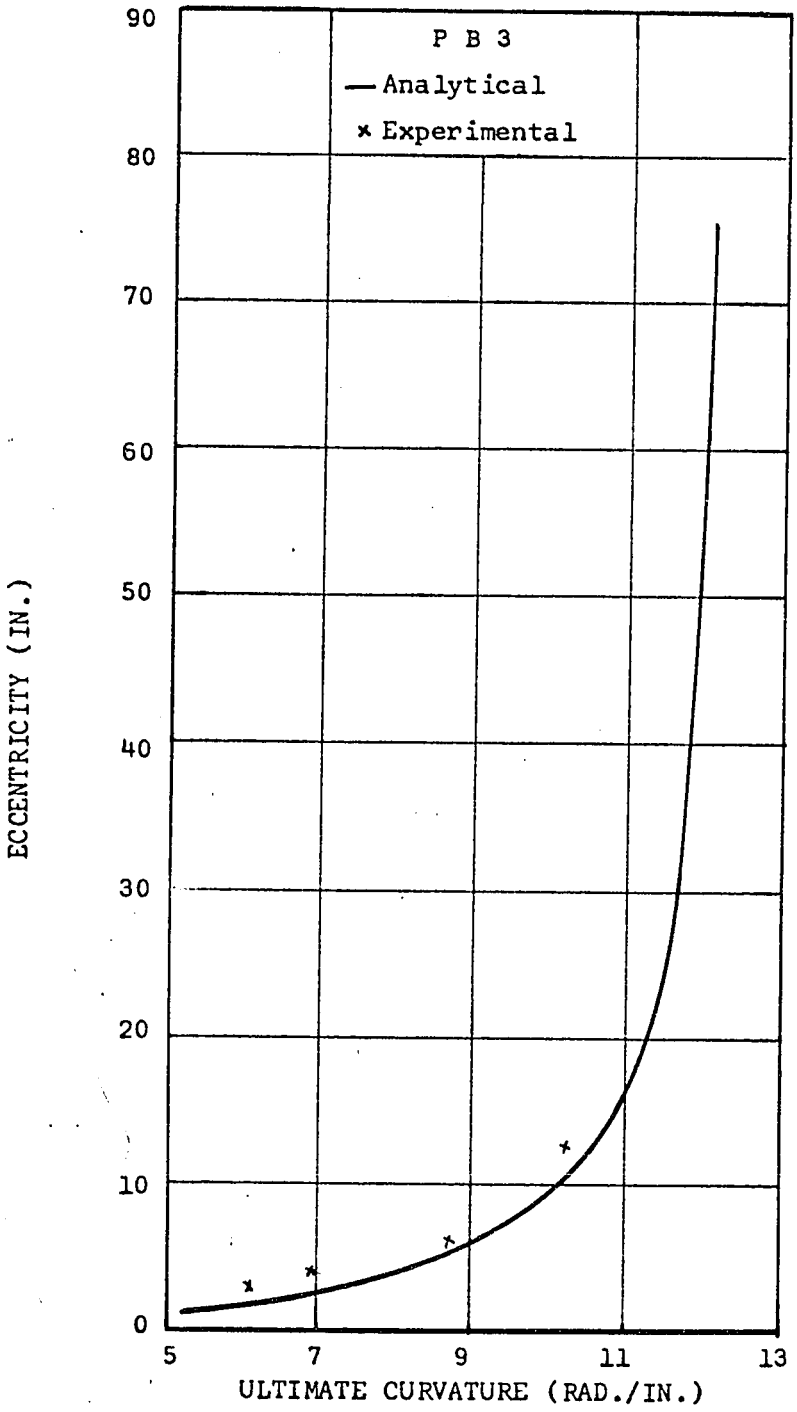

ECCENTRICITY VS. CURVATURE AT THE ULTIMATE LOAD

FIG. 5.46

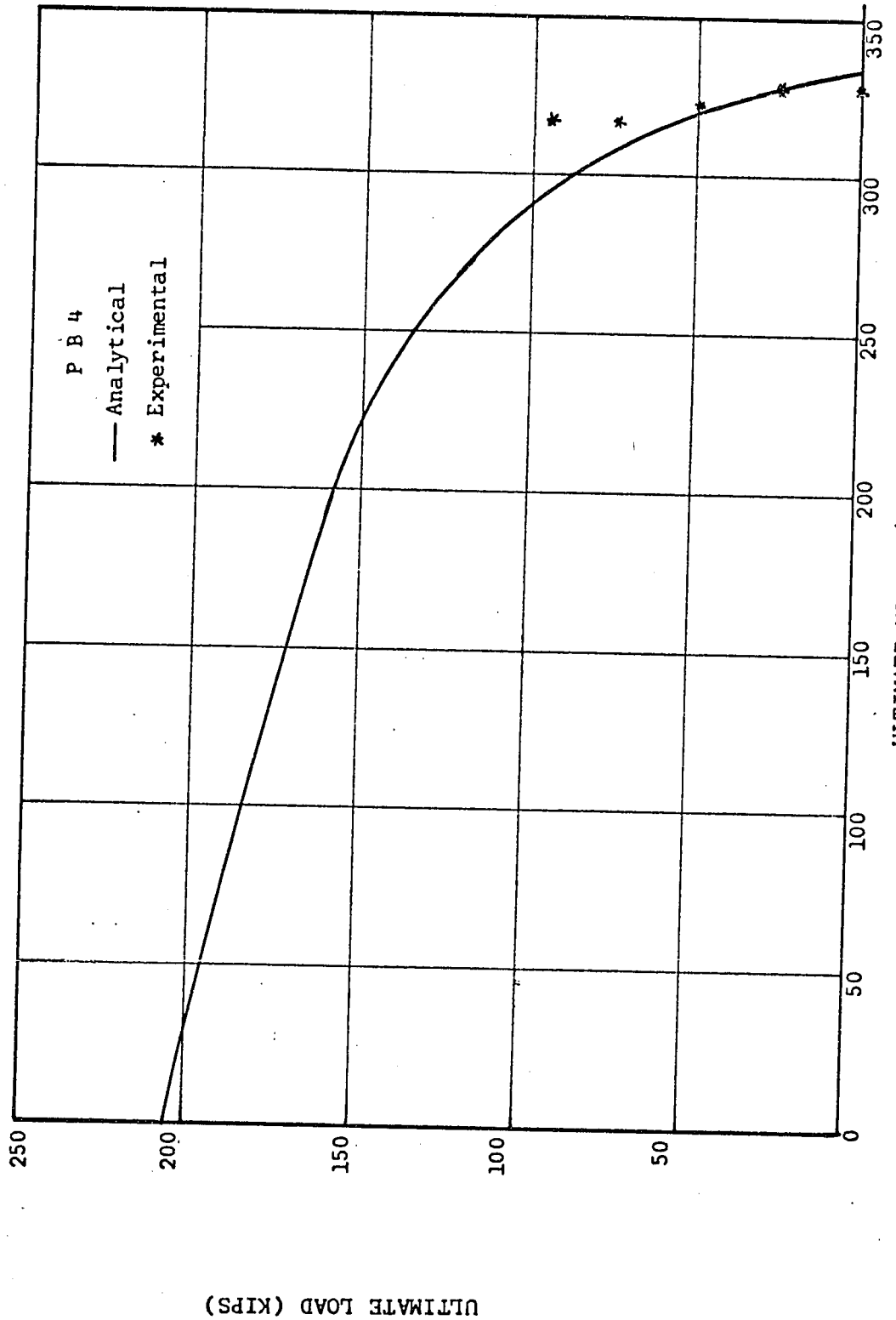

AXIAL THRUST-MOMENT INTERACTION

FIG. 5.47

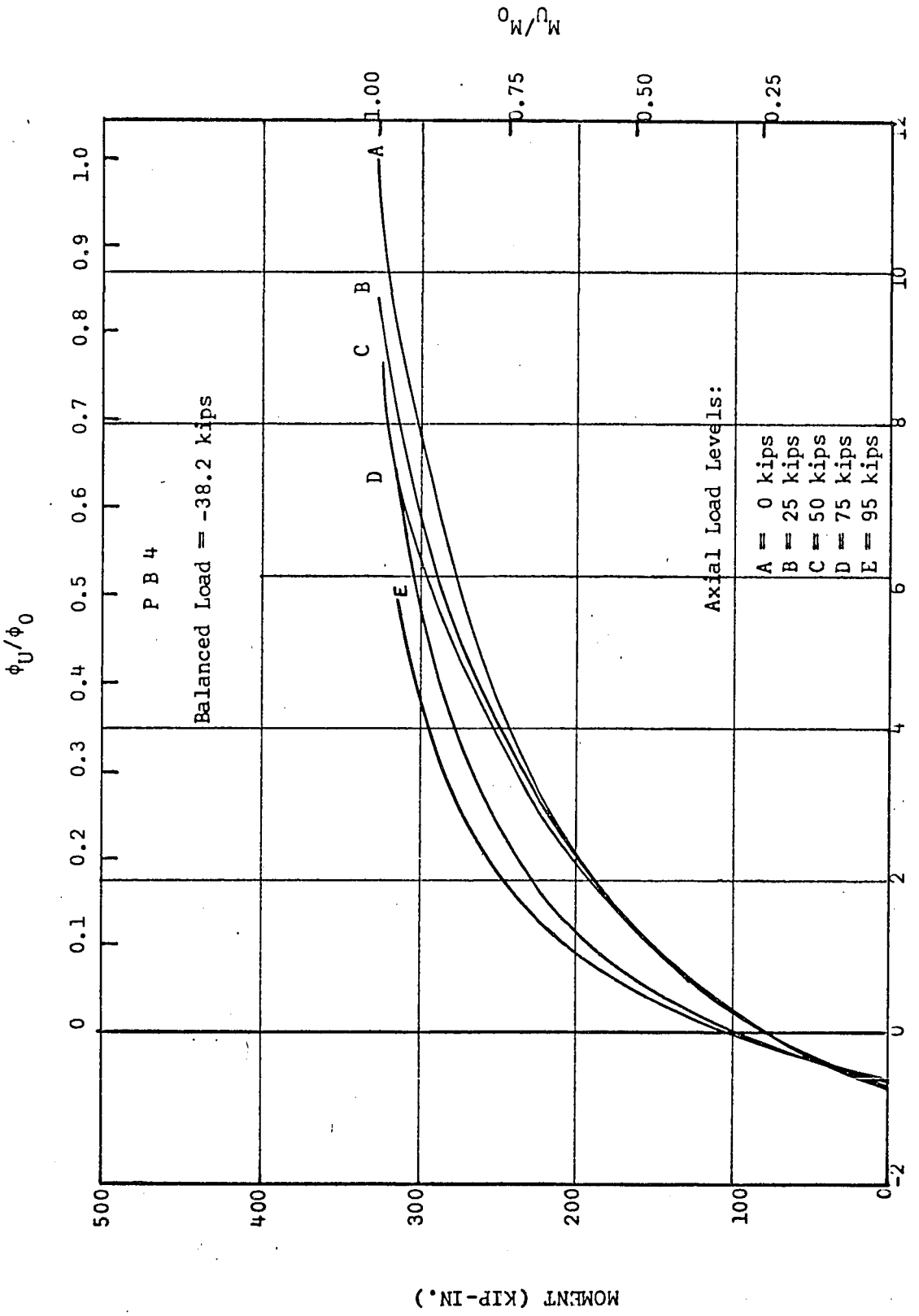

MOMENT-CURVATURE RELATIONSHIP

FIG. 5.48

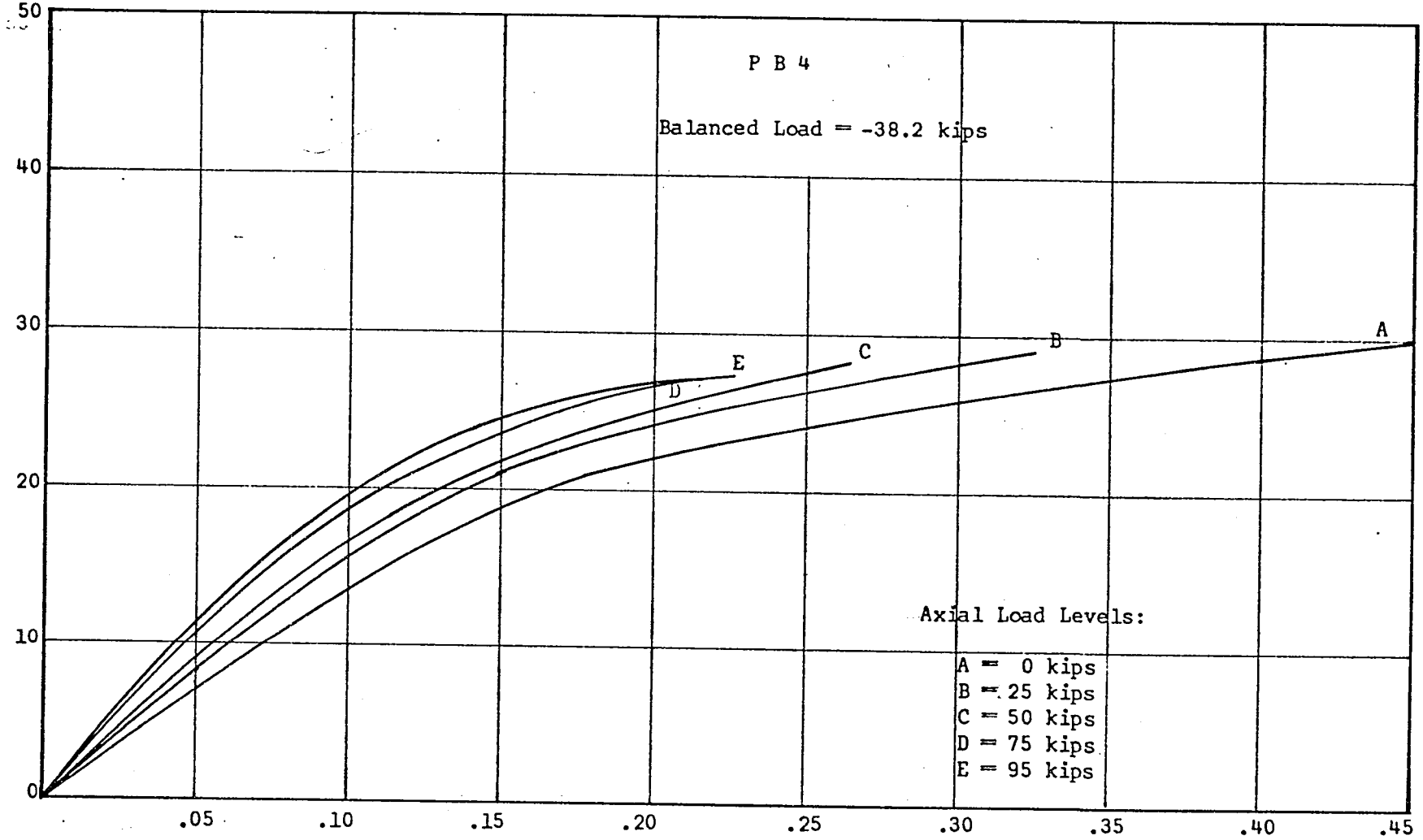

LOAD VS. DEFLECTION AT MIDPOINT RELATIONSHIP
FIG. 5.49

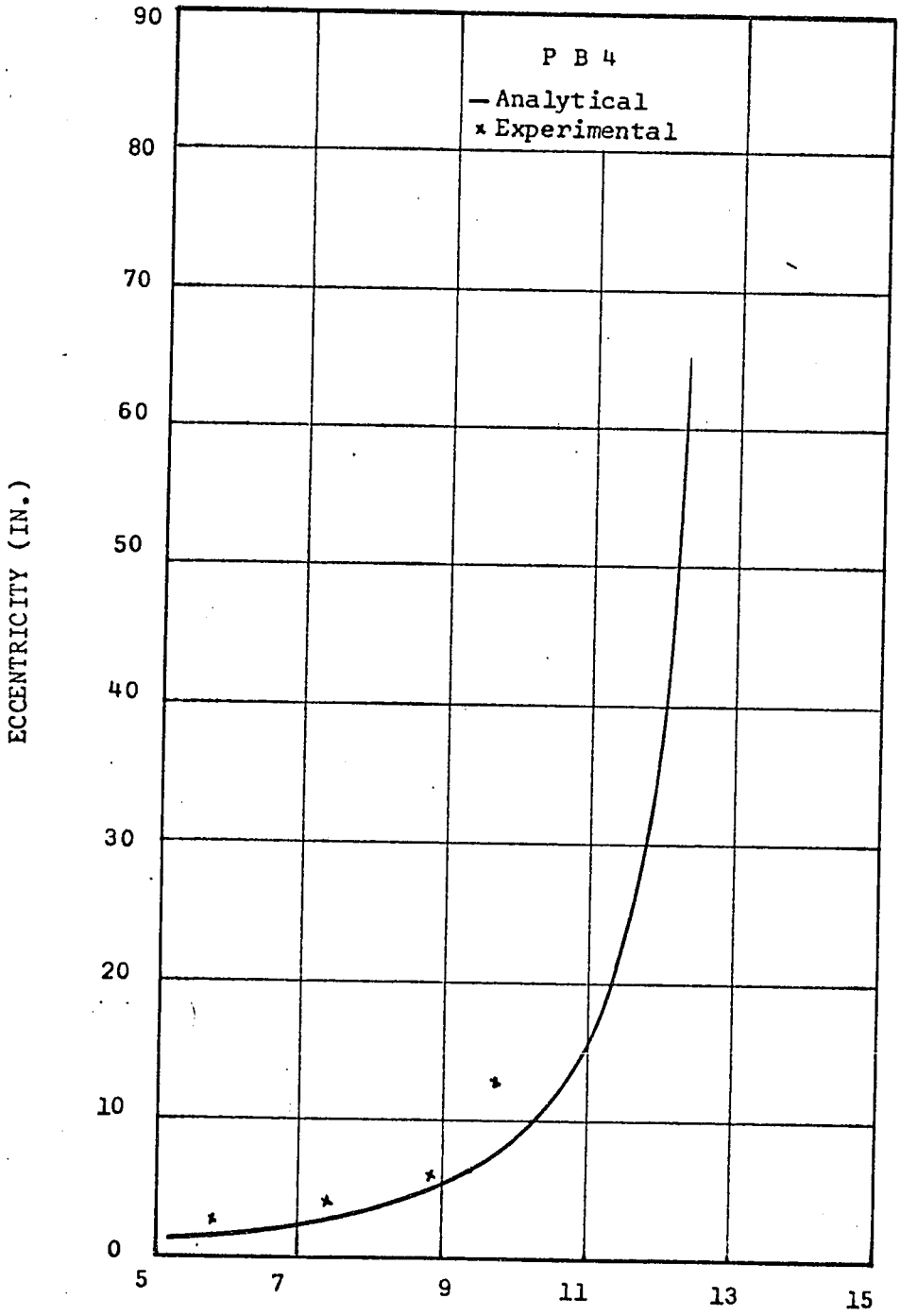

ECCENTRICITY VS. CURVATURE AT THE ULTIMATE LOAD

FIG. 5.50

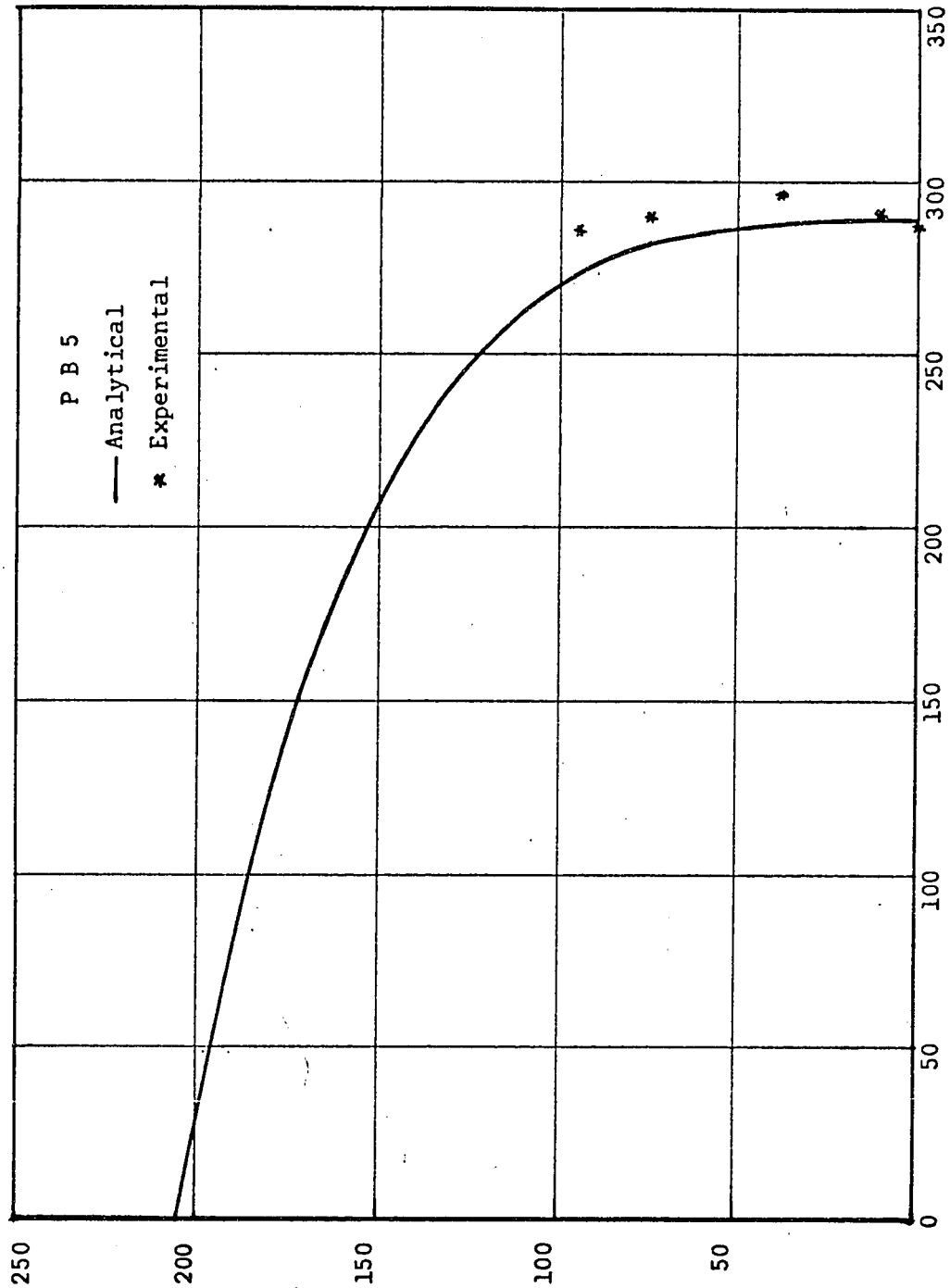

AXIAL THRUST-MOMENT INTERACTION

FIG. 5.51

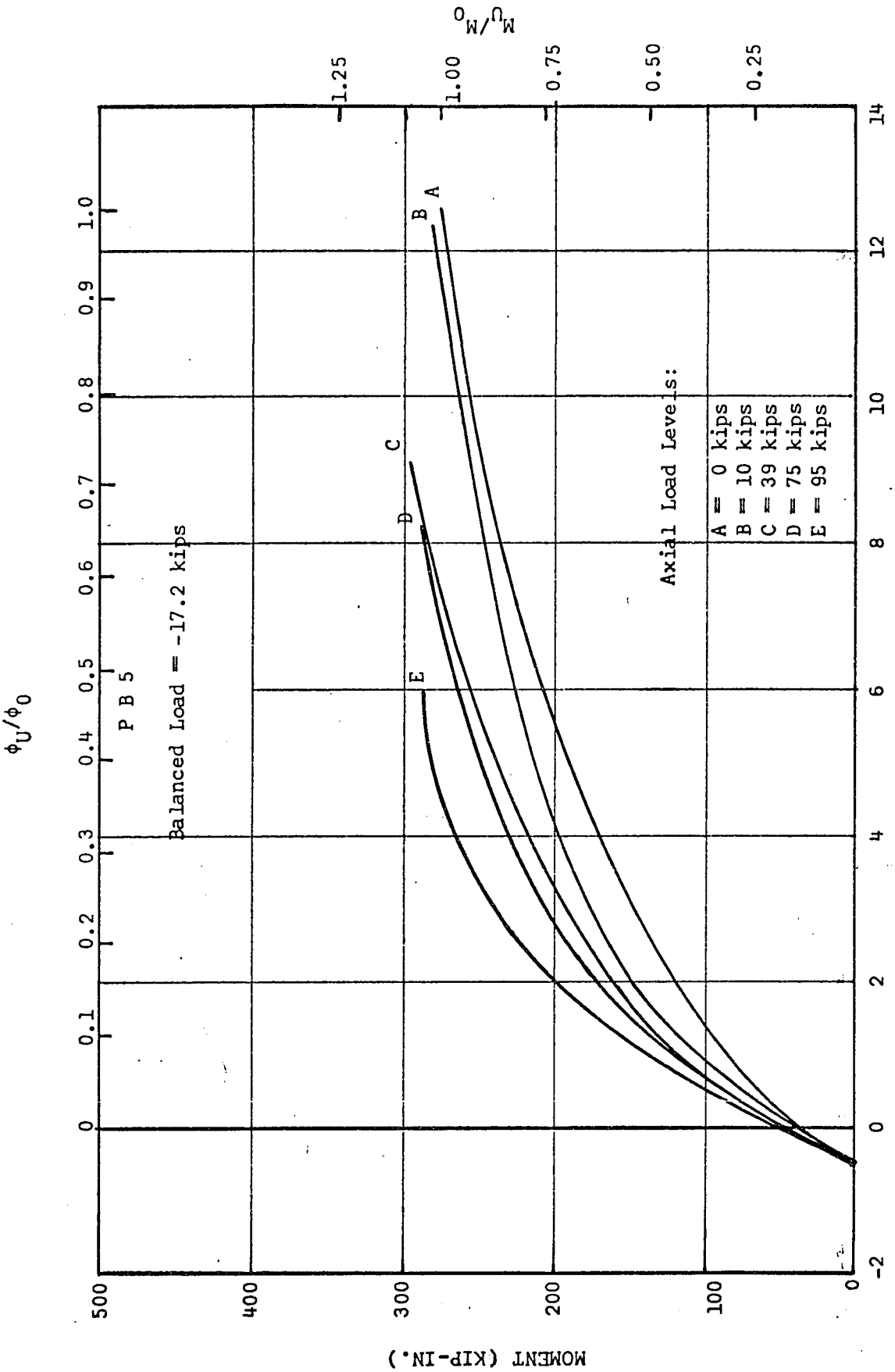

MOMENT-CURVATURE RELATIONSHIP

FIG. 5.52

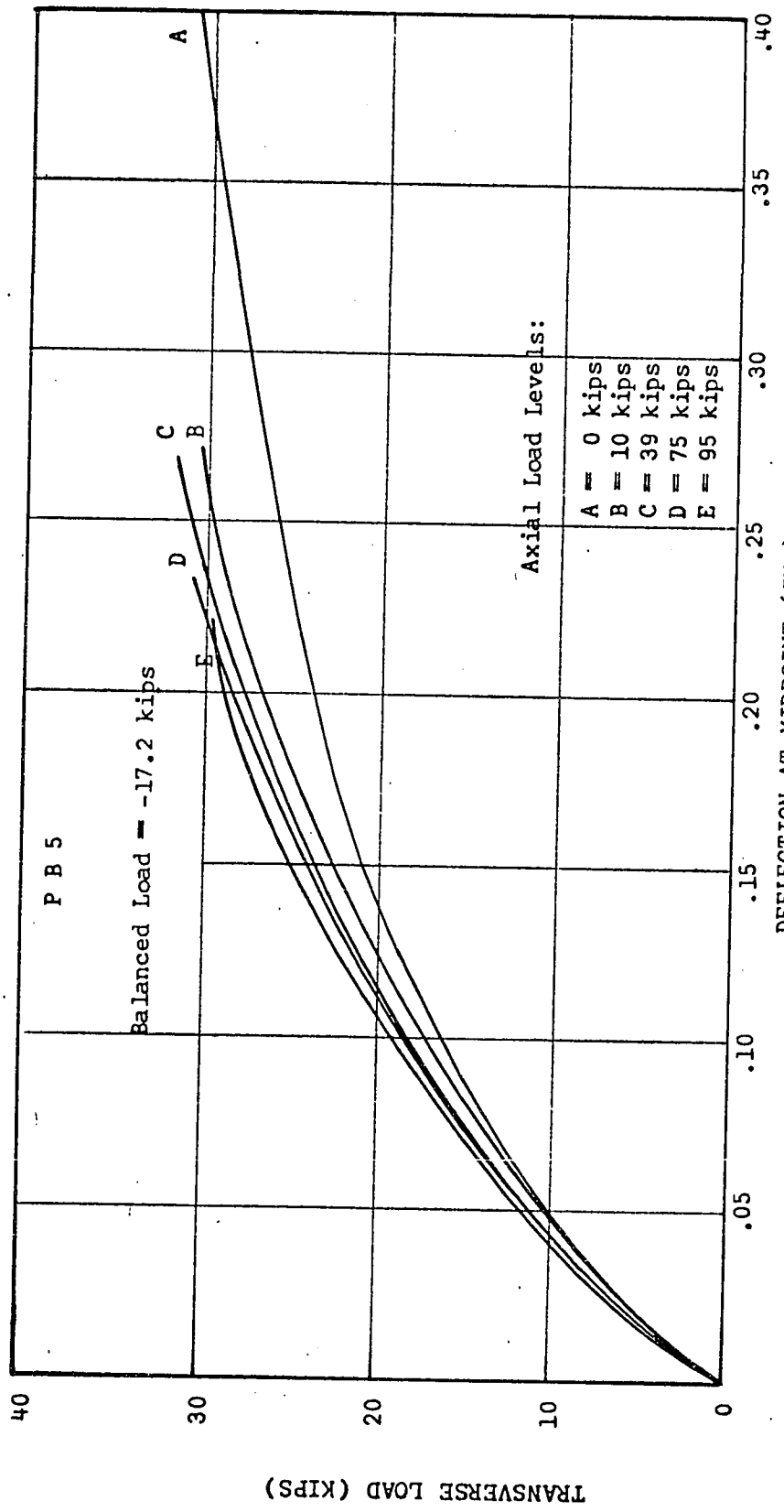

LOAD VS. DEFLECTION AT MIDPOINT RELATIONSHIP

FIG. 5.53

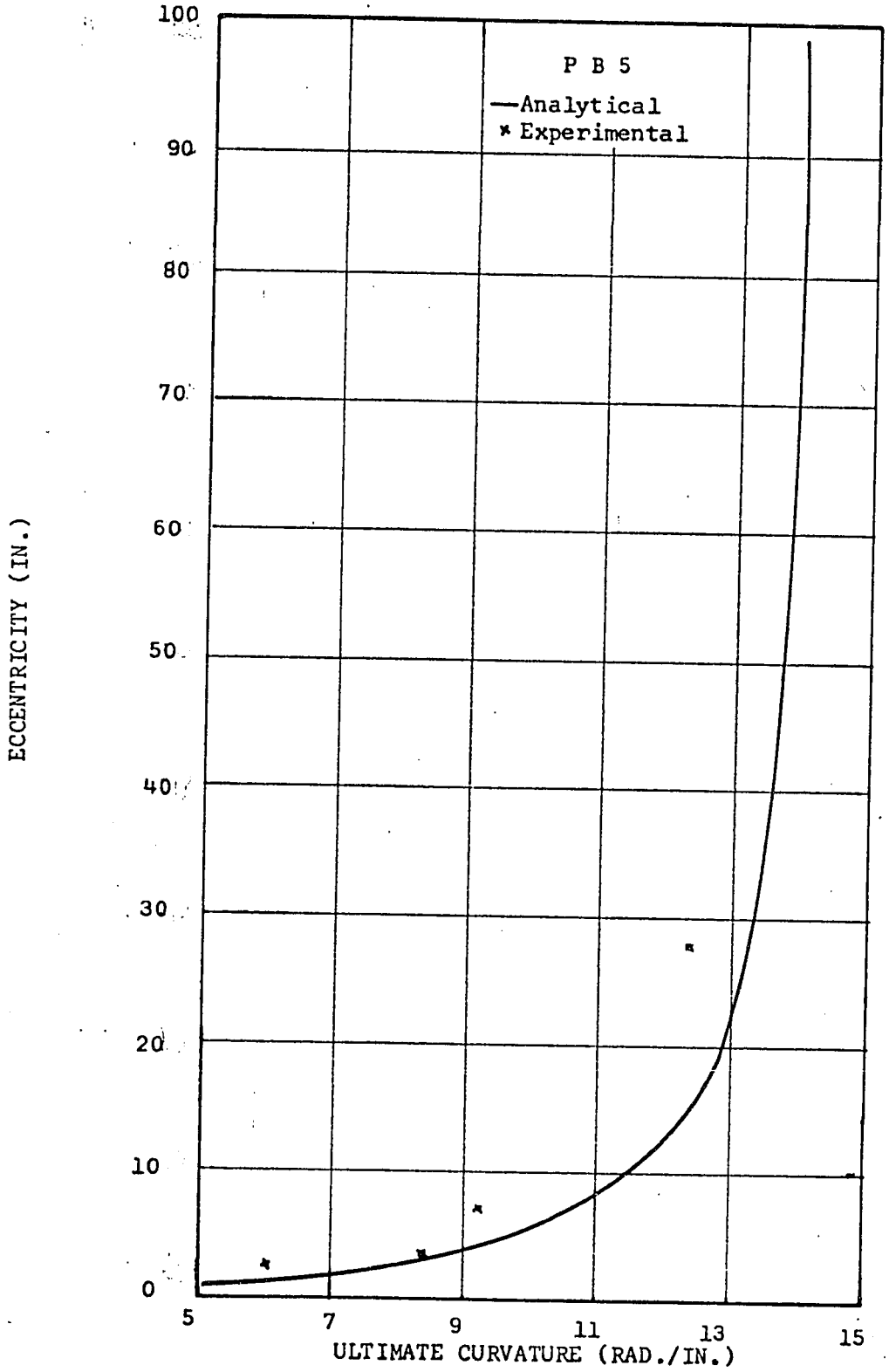

ECCENTRICITY VS. CURVATURE AT THE ULTIMATE LOAD

FIG. 5.54

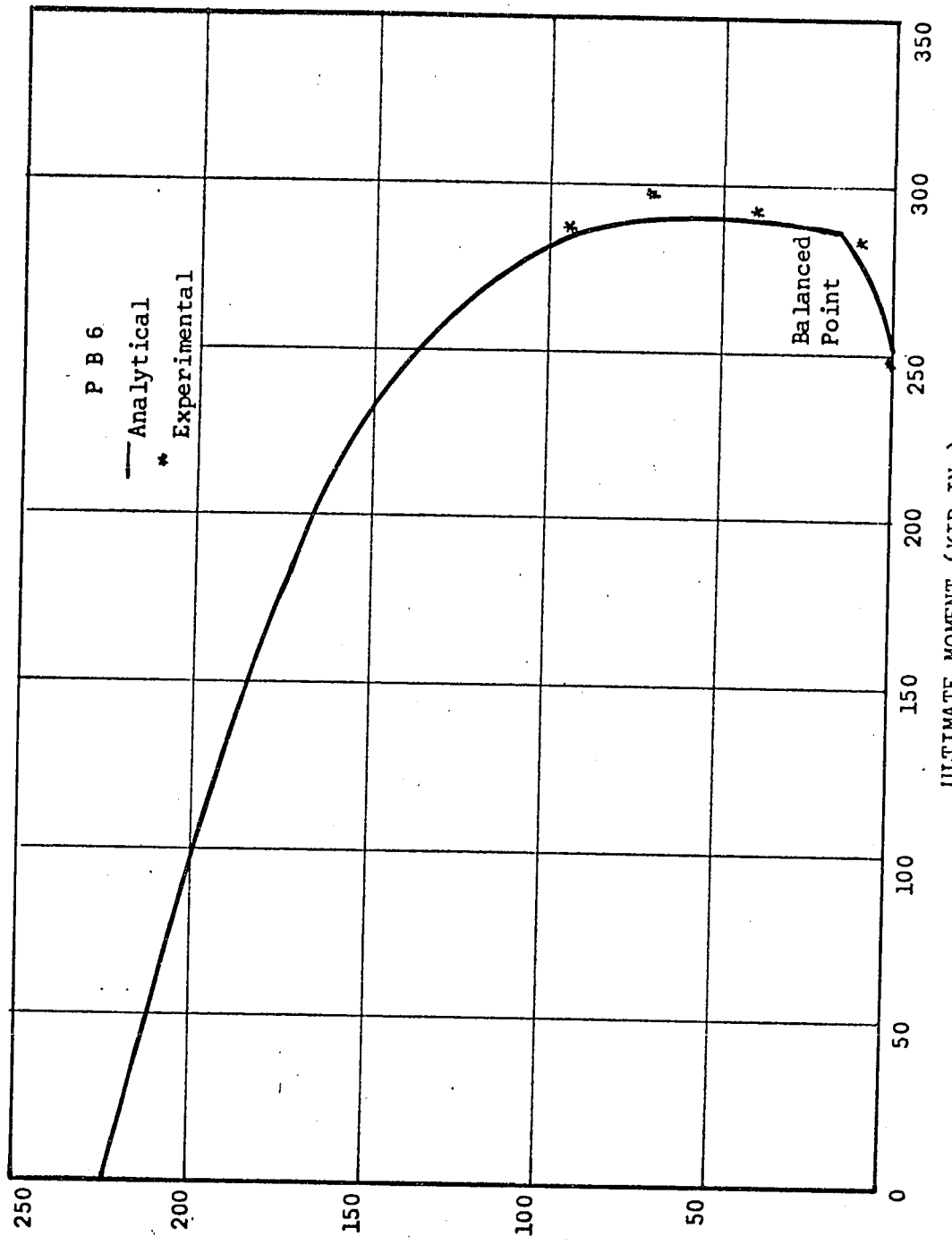

AXIAL THRUST-MOMENT INTERACTION

FIG. 5.55

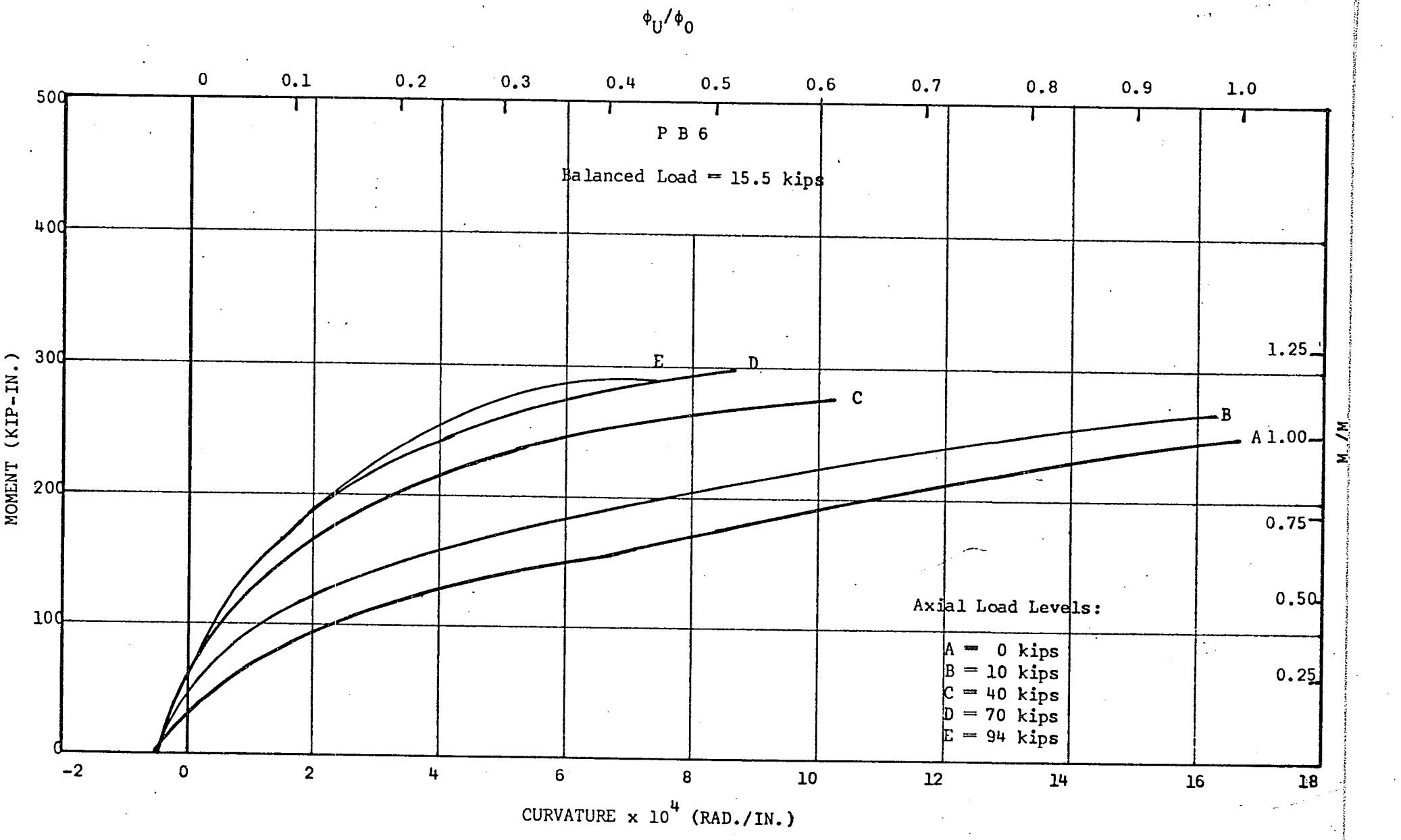

MOMENT-CURVATURE RELATIONSHIP

FIG. 5.56

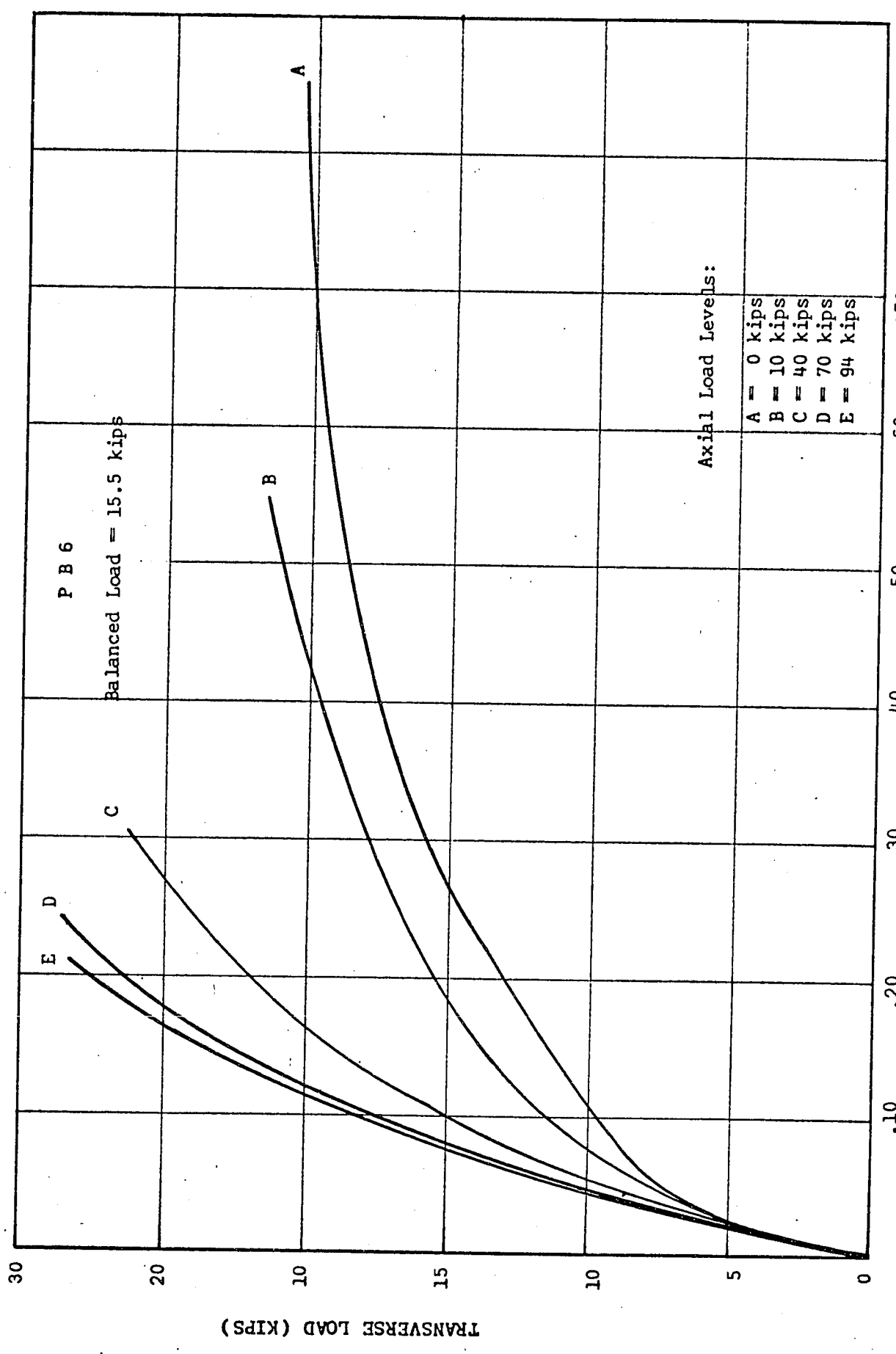

LOAD VS. DEFLECTION AT MIDPOINT RELATIONSHIP

FIG. 5.57

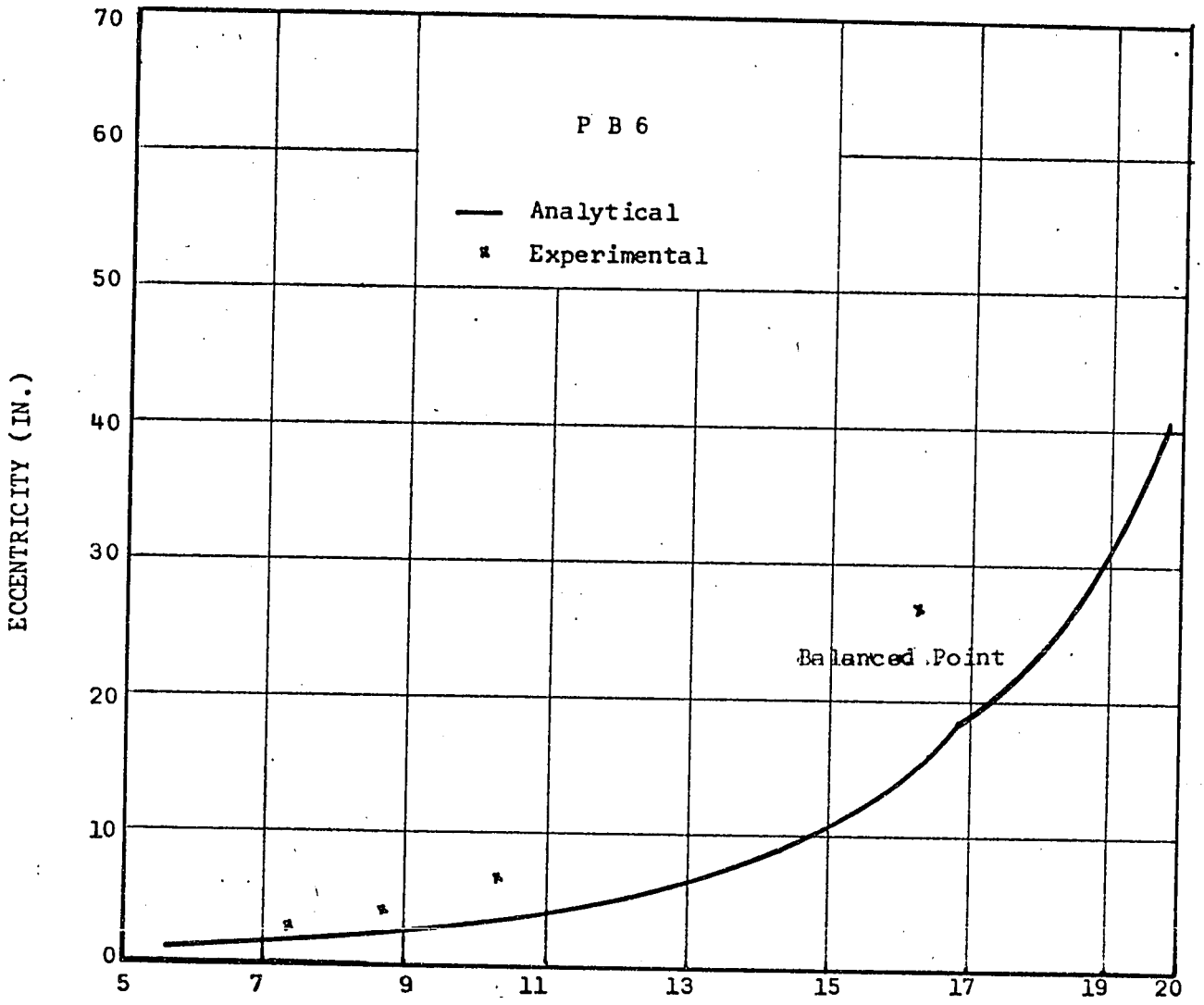

ECCENTRICITY VS. CURVATURE AT THE ULTIMATE LOAD

FIG. 5.58

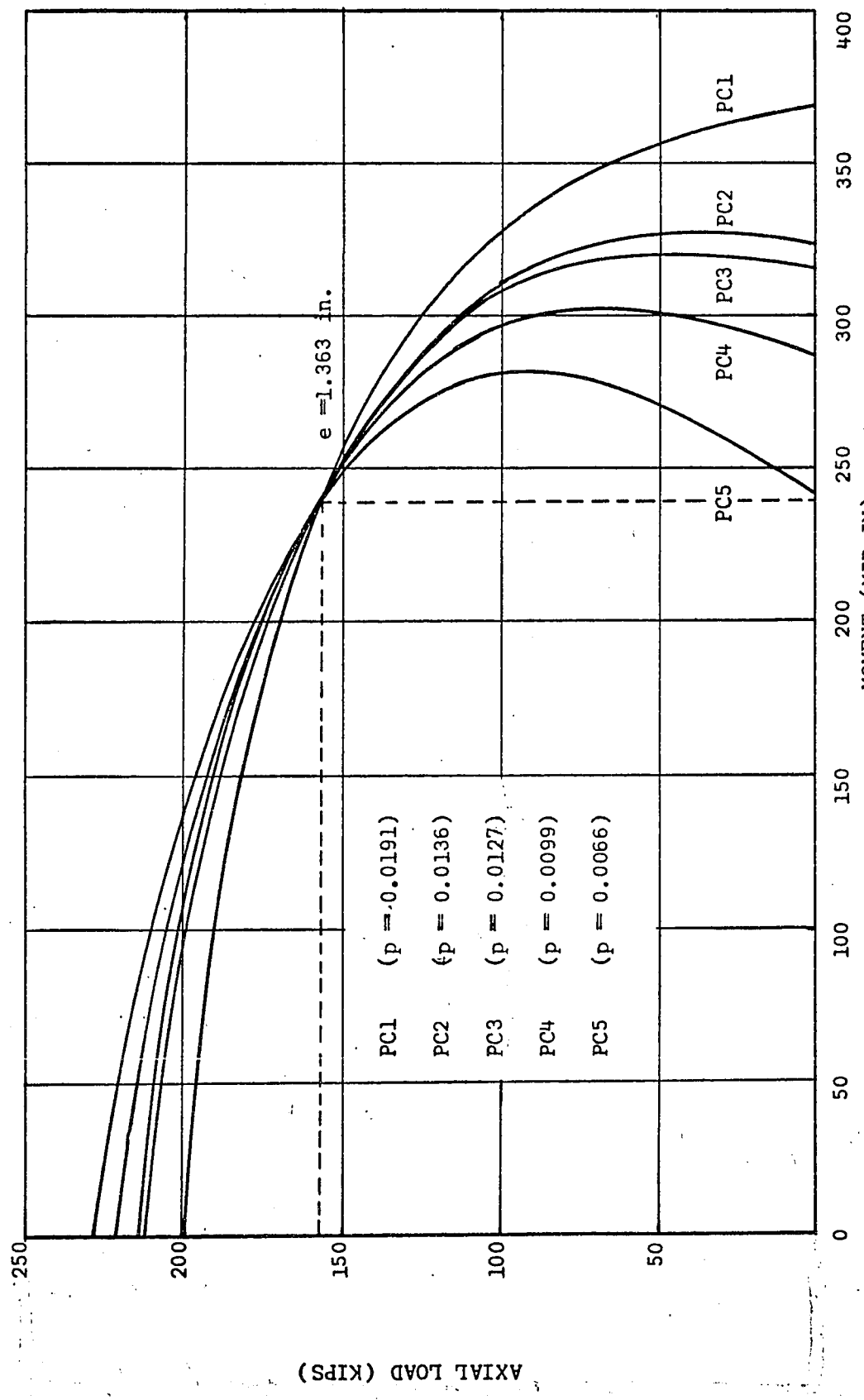

FIG. 6.1: BENDING MOMENT-AXIAL THRUST INTERACTION DIAGRAM FOR THE SYMMETRICALLY PRESTRESSED SERIES.

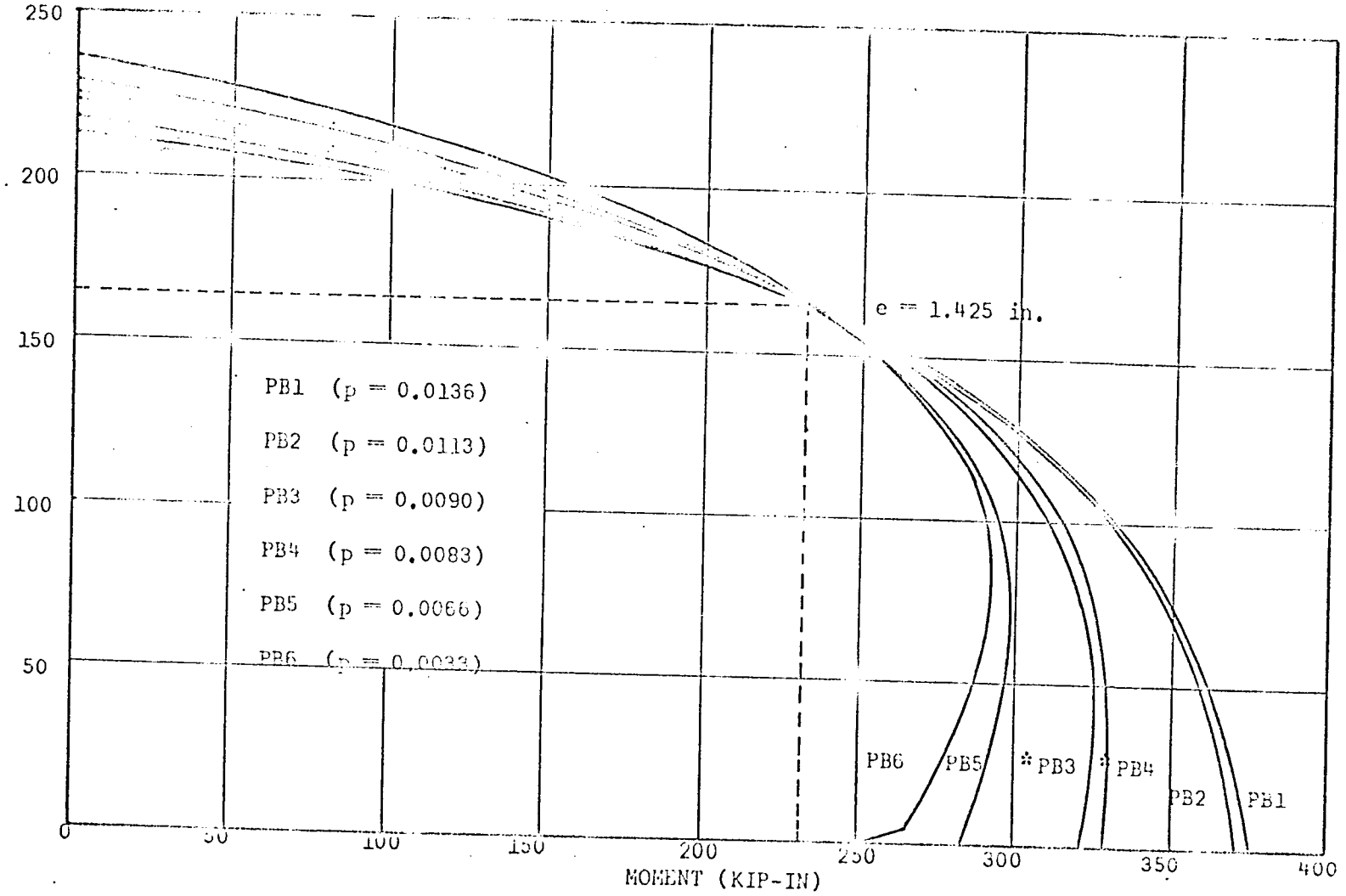

FIG. 6.2: BENDING MOMENT-AXIAL THRUST INTERACTION DIAGRAM FOR THE UNSYMMETRICALLY PRESTRESSED SERIES.
* The total steel ratio of PB3 was more than PB4, but due to the arrangement of steel, the steel area in the bottom layer was more in PB4 than in PB3. The eccentricity of the prestressing tendons in PB4 was therefore more than PB3.

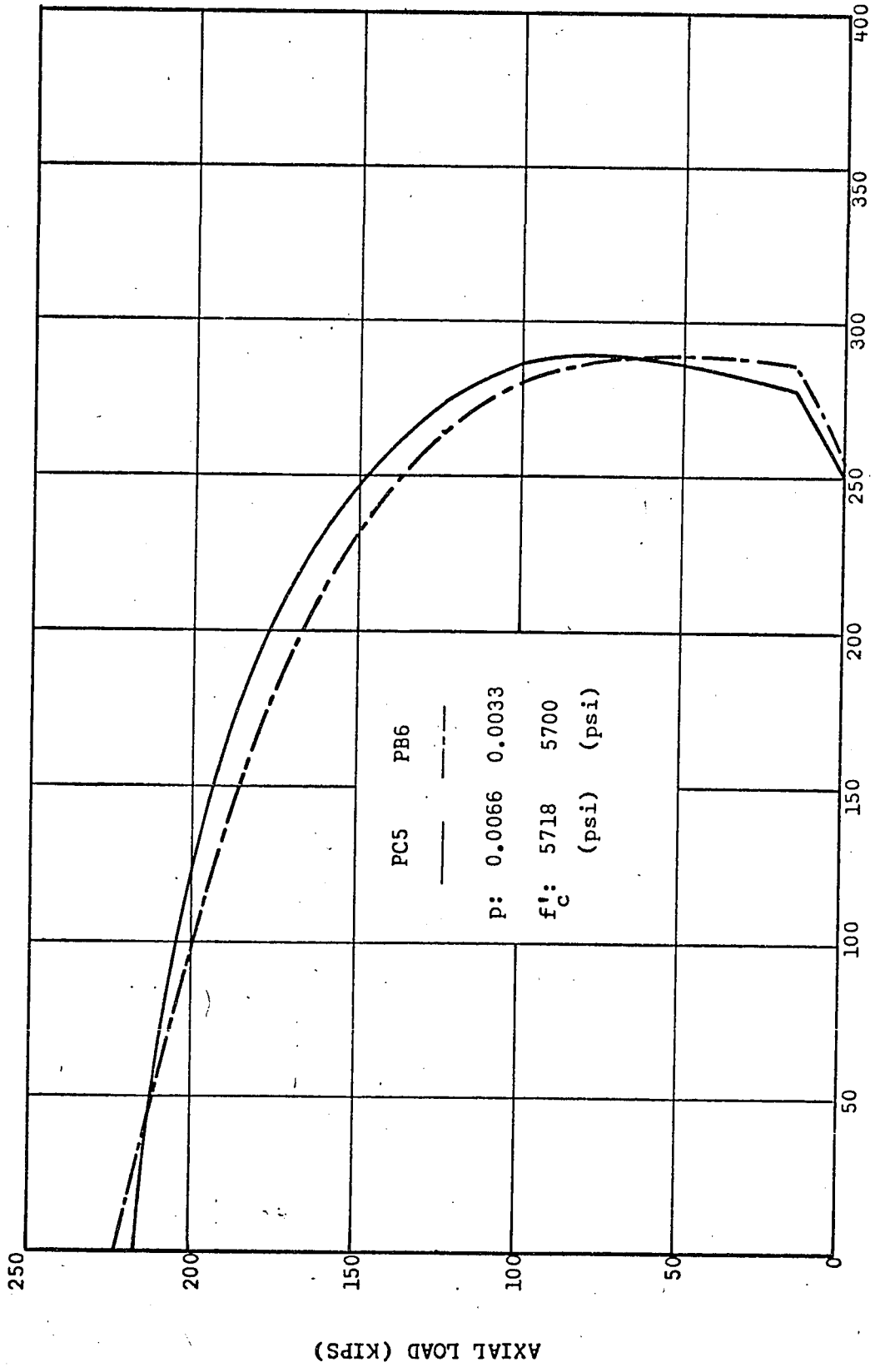

FIG. 6.3: COMPARISON OF LOAD CARRYING CAPACITY OF SYMMETRICALLY AND UNSYMMETRICALLY PRESTRESSED CONCRETE BEAM-COLUMN SPECIMENS.

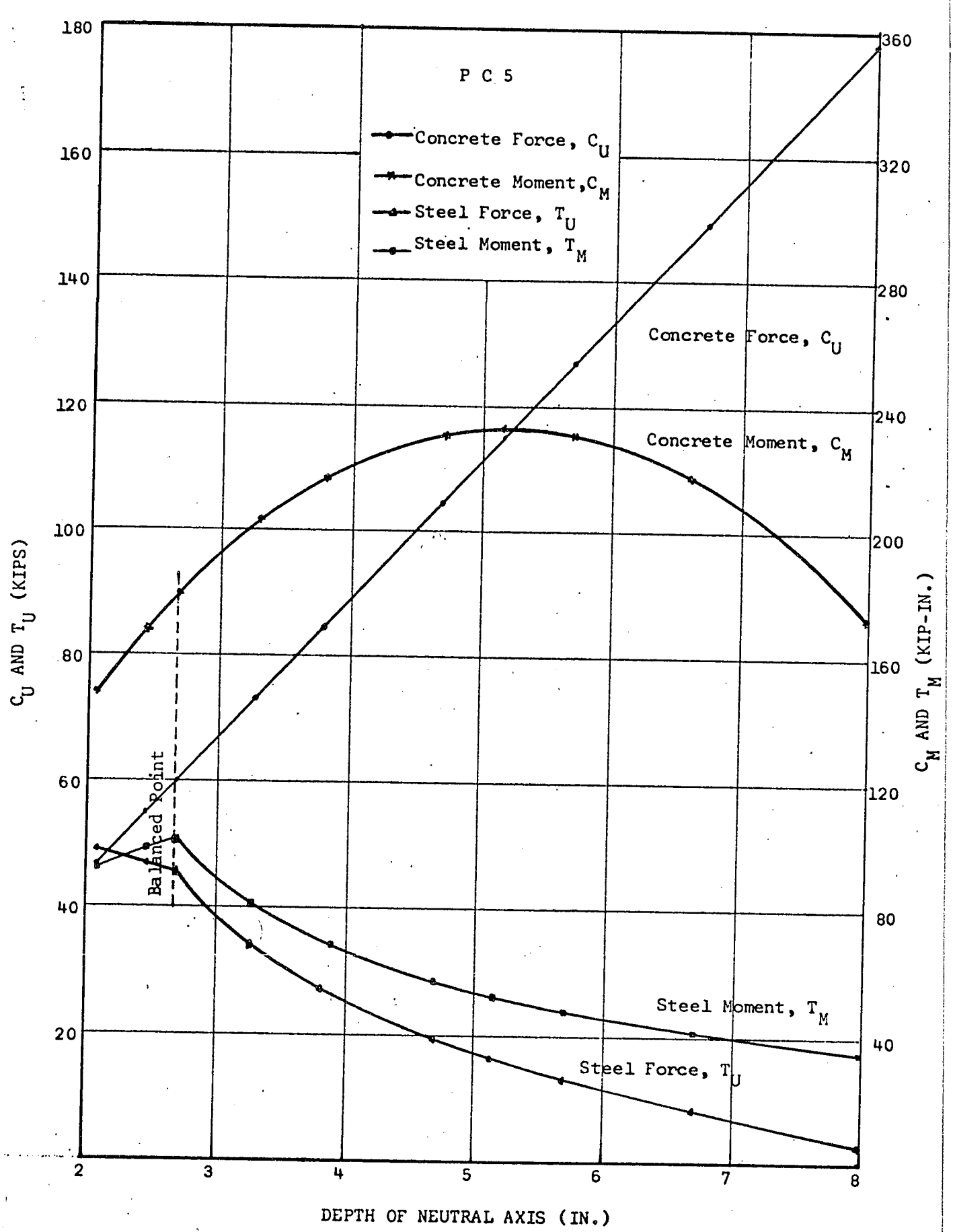

FIG. 6.4: VARIATION OF CONCRETE AND STEEL FORCES AND MOMENTS WITH THE DEPTH OF NEUTRAL AXIS

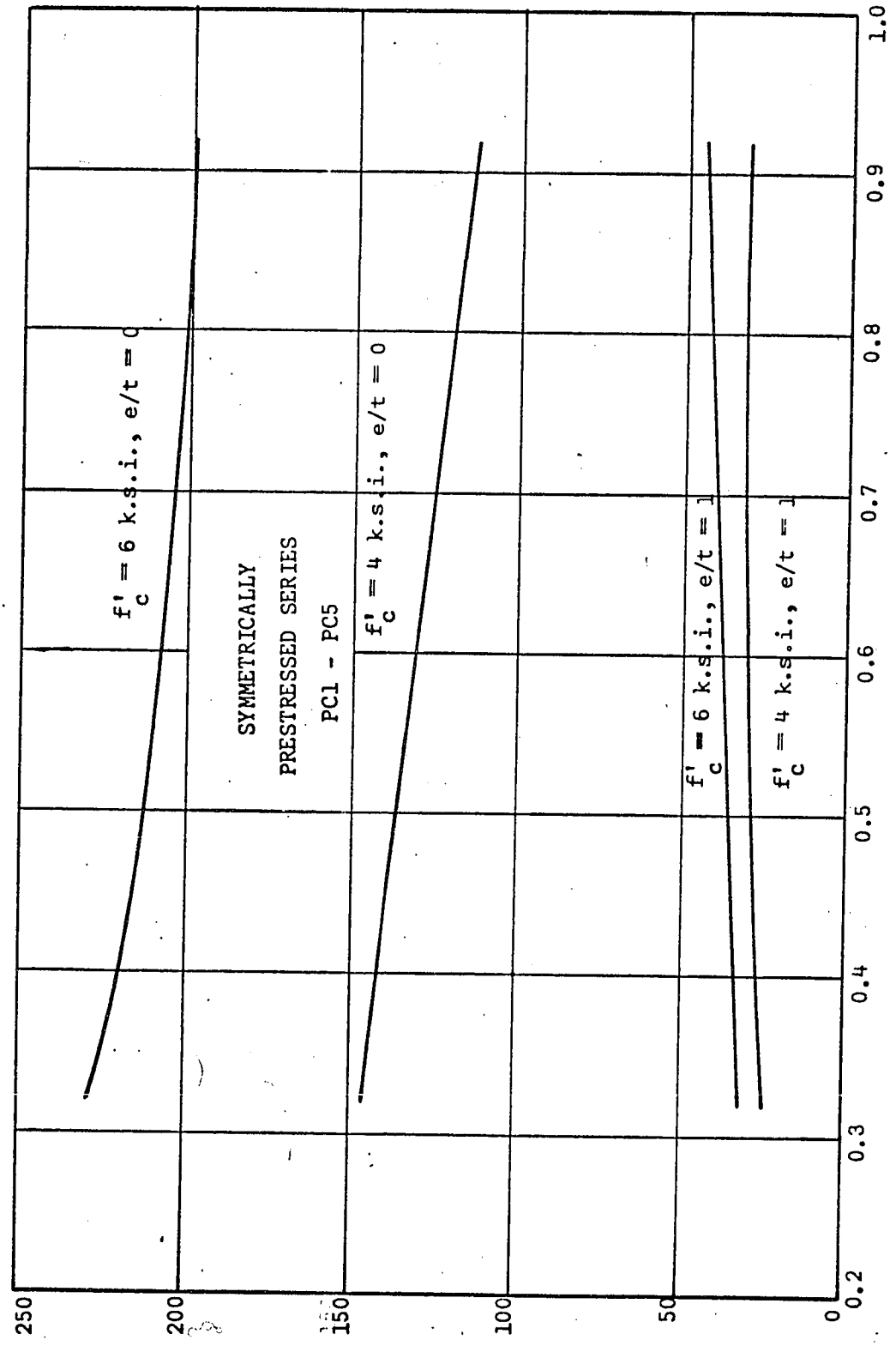

FIG. 6.5: VARIATION OF ULTIMATE LOAD WITH STEEL AREA

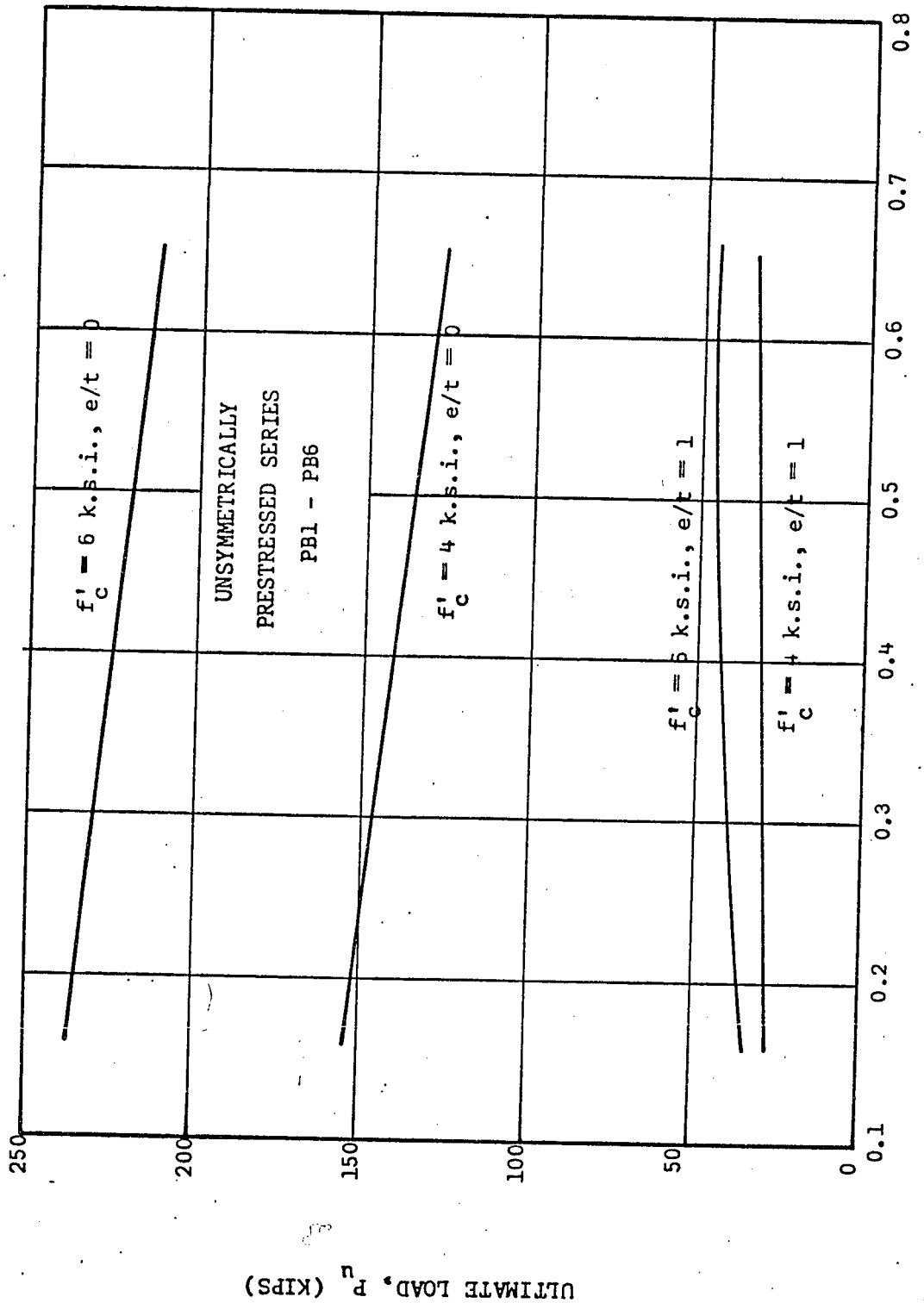

FIG. 6.6: VARIATION OF ULTIMATE LOAD WITH STEEL AREA

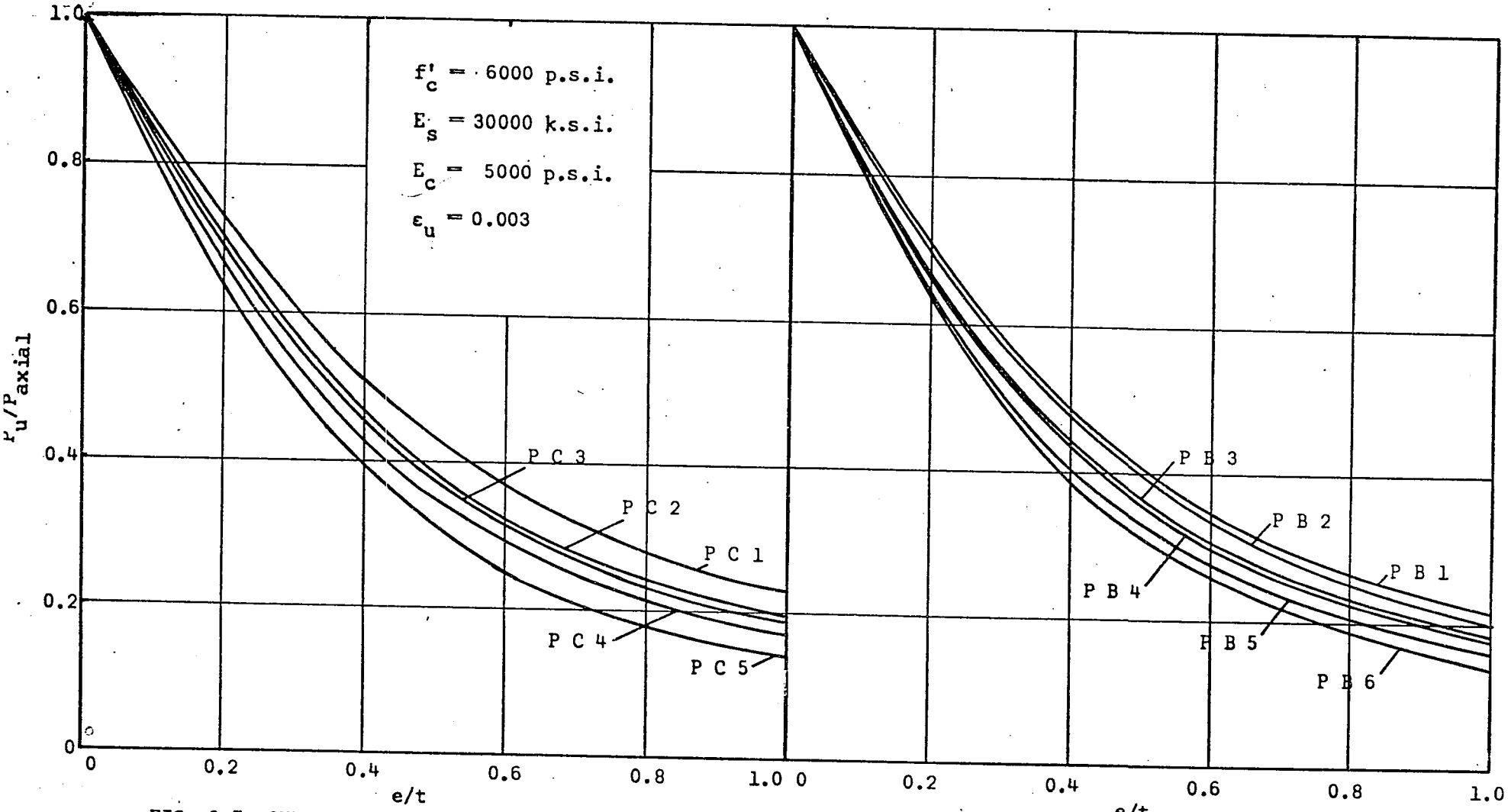

FIG. 6.7: SYMMETRICALLY PRESTRESSED SERIES.

FIG. 6.8: UNSYMMETRICALLY PRESTRESSED SERIES.

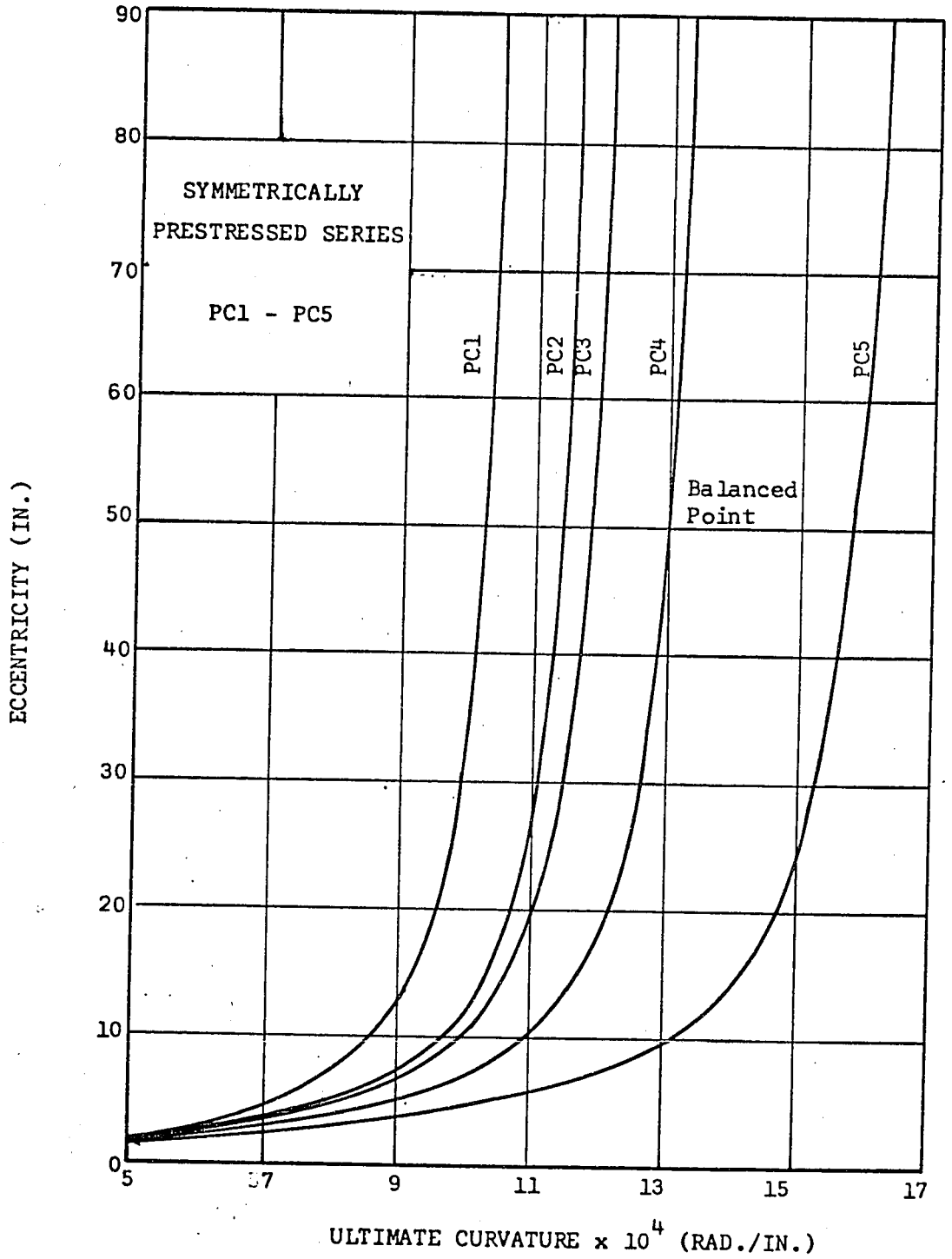

FIG. 6.9: VARIATION OF ULTIMATE CURVATURE WITH ECCENTRICITY OF LOAD

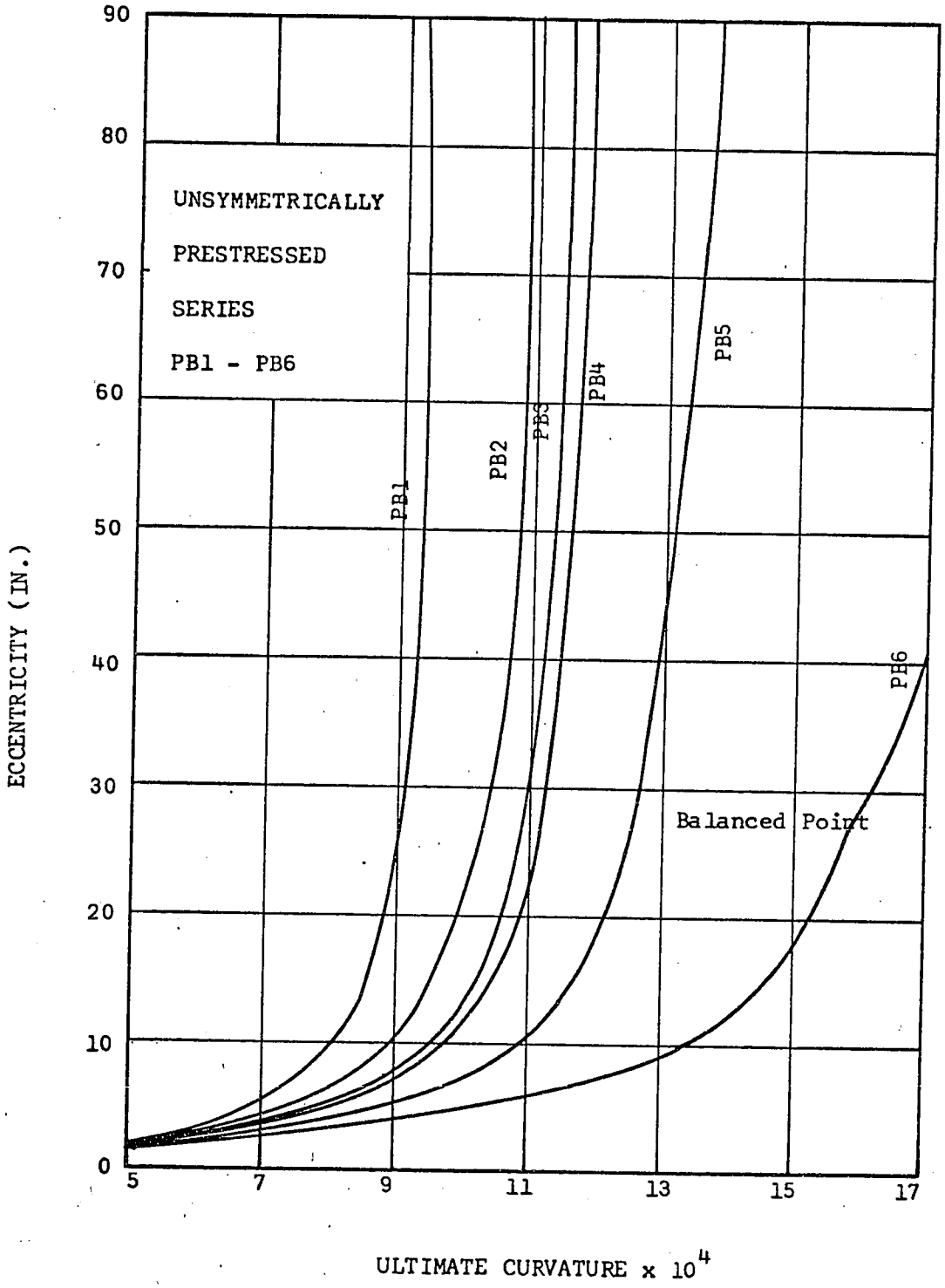

FIG. 6.10: VARIATION OF ULTIMATE CURVATURE WITH ECCENTRICITY OF LOAD.

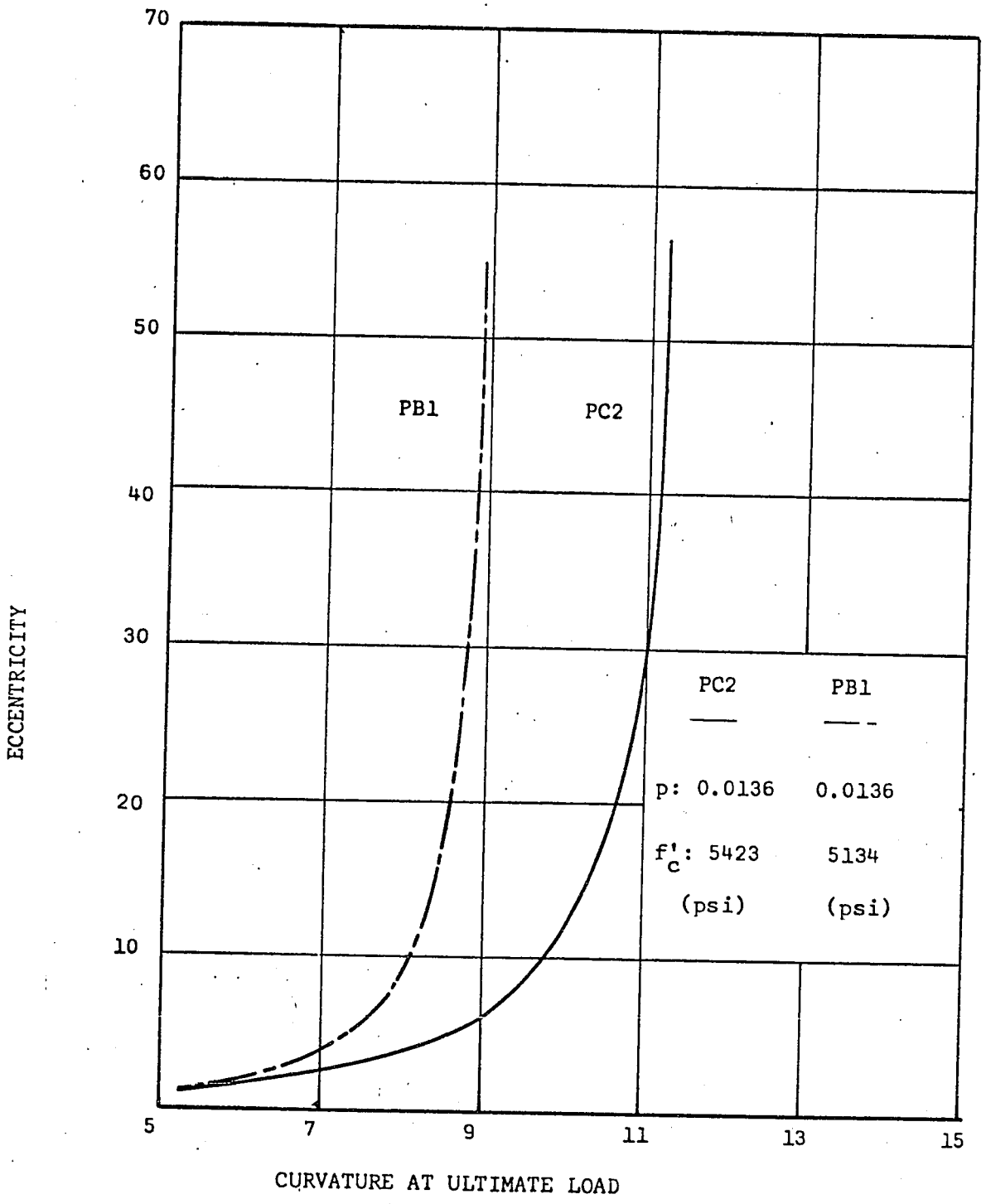

FIG. 6.11: COMPARISON OF DEFORMATION CHARACTERISTICS OF SYMMETRICALLY AND UNSYMMETRICALLY PRESTRESSED BEAM-COLUMN SPECIMENS.

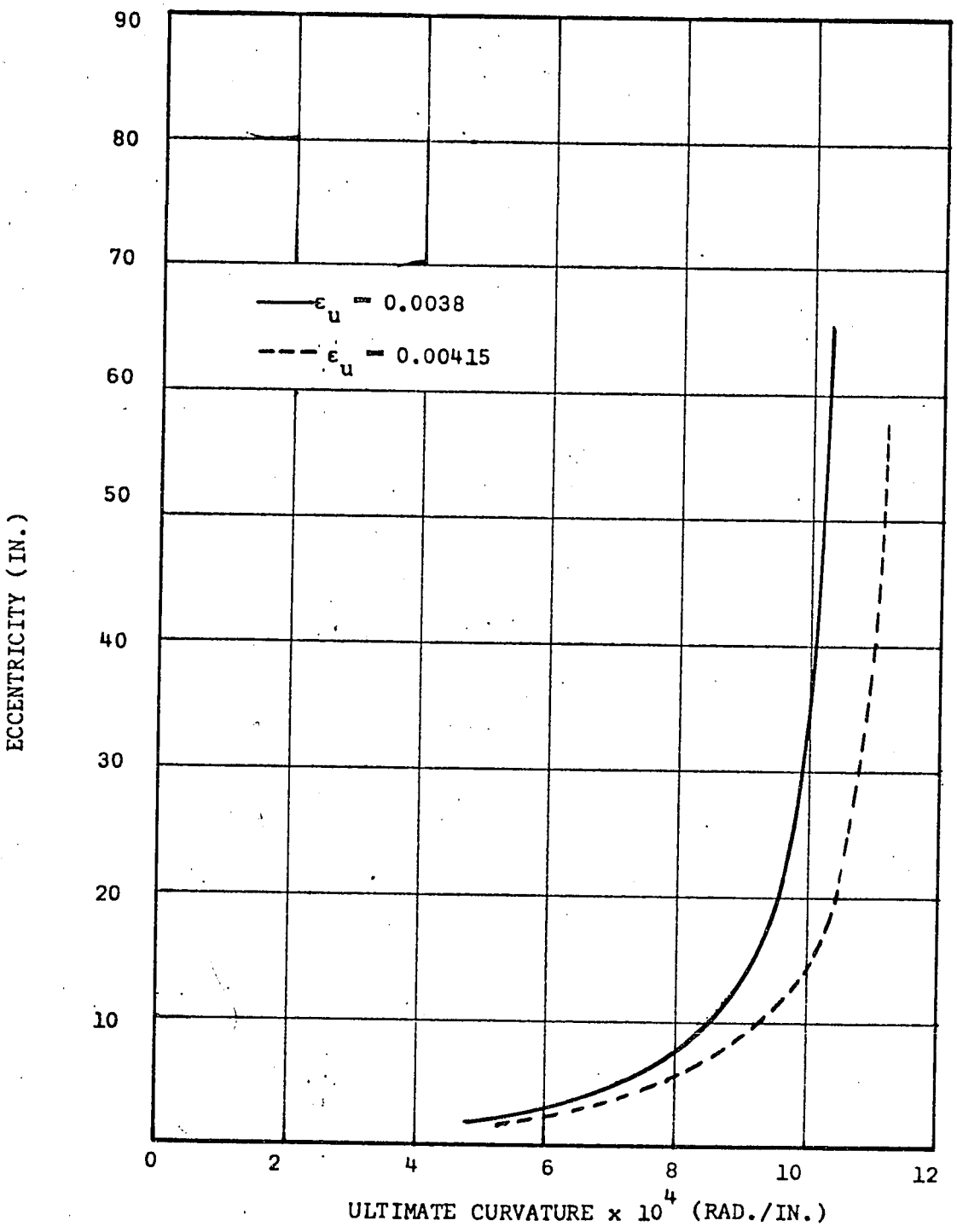

FIG. 6.12: EFFECT OF ULTIMATE CONCRETE STRAIN ON THE DEFORMATION CHARACTERISTICS OF PRESTRESSED CONCRETE BEAM-COLUMNS.

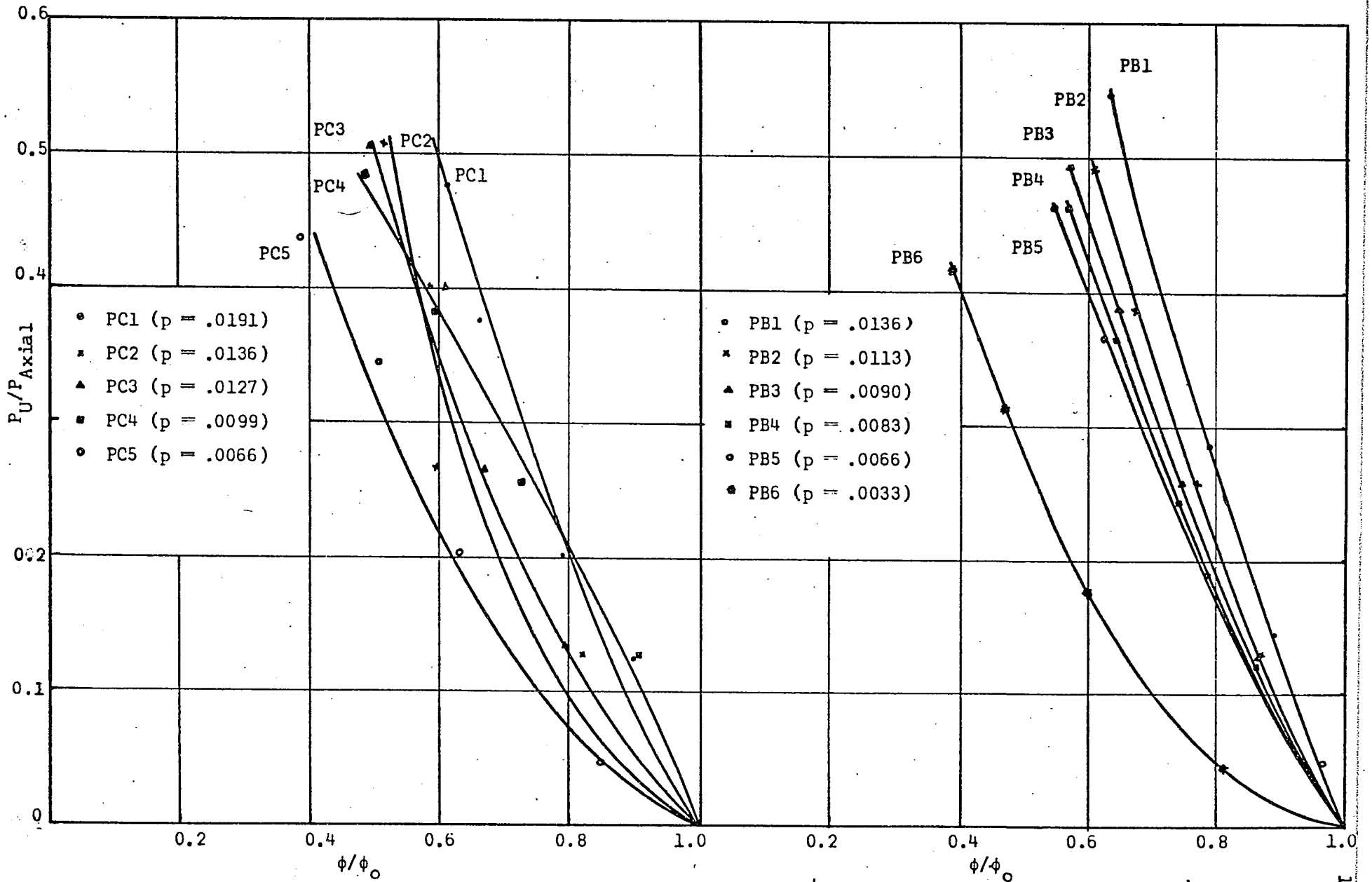

FIG. 6.13: VARIATION OF ϕ/ϕ_o WITH P_U/P_{Axial} FOR THE SYMMETRICALLY PRESTRESSED SERIES.

FIG. 6.14: VARIATION OF ϕ/ϕ_o WITH P_U/P_{Axial} FOR THE UNSYMMETRICALLY PRESTRESSED SERIES.

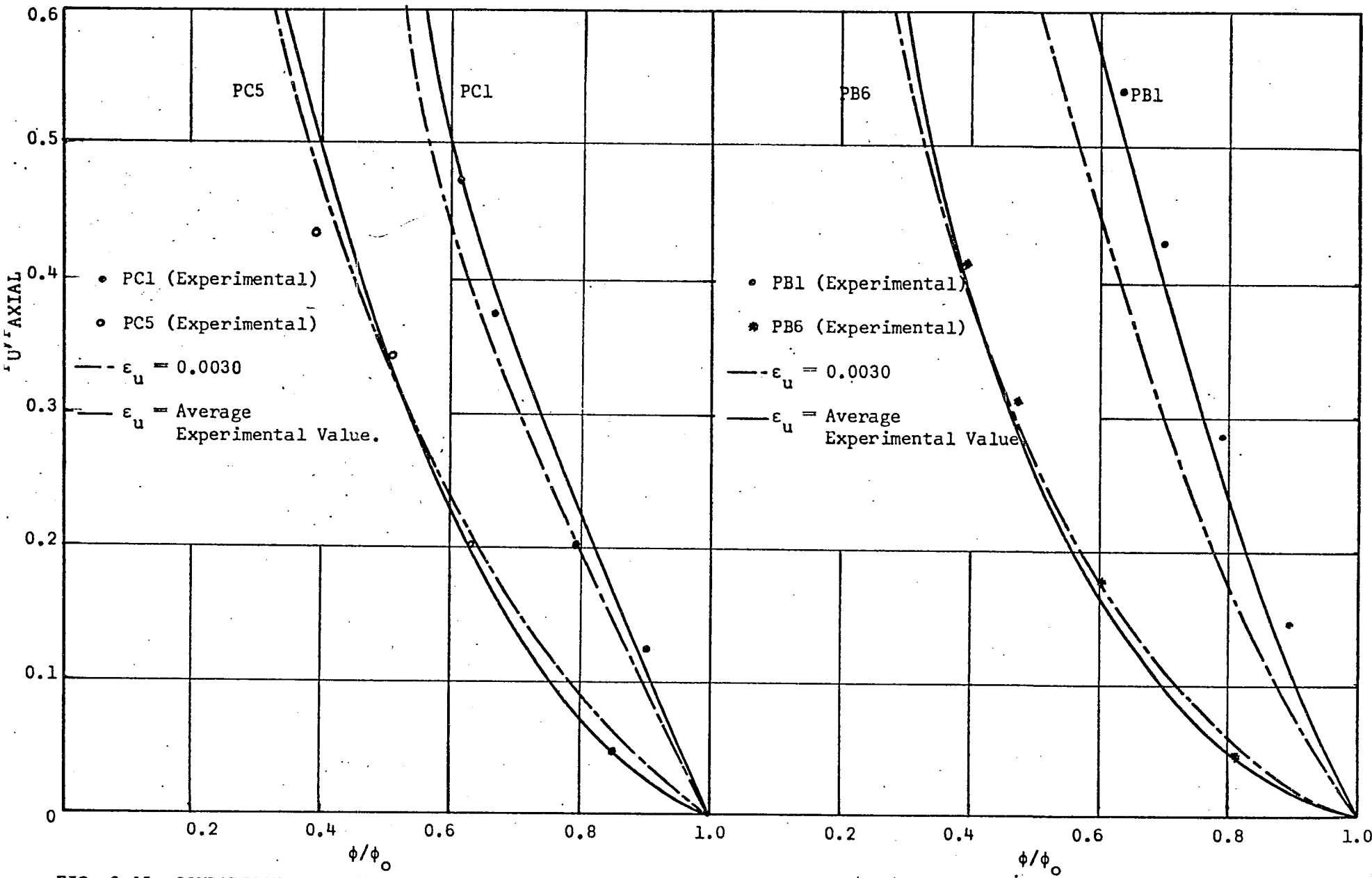

FIG. 6.15: COMPARISON OF TEST AND THEORETICAL VALUES OF P_U/P_{Axial} VS. ϕ/ϕ_o FOR SERIES PC1 AND PC5.

FIG. 6.16: COMPARISON OF TEST AND THEORETICAL VALUES OF P_U/P_{Axial} VS. ϕ/ϕ_o FOR SERIES PB1 AND PB6.

APPENDIX B: TABLES

TABLE 4.1: SECTION PROPERTIES OF THE TEST SPECIMENS

Specimen	A_{s1} (SQ.IN)	A_{s2} (SQ.IN)	A_{s3} (SQ.IN)	A_{s4} (SQ.IN)	f'_c (K.S.I.)	Age (DAYS)
PC1(A - E)	0.4593	-	-	0.4593	6.018	31
PC2(A - E)	0.3267	-	-	0.3267	5.423	31
PC3(A - E)	0.3062	-	-	0.3062	5.394	27
PC4(A - E)	0.2397	-	-	0.2397	5.435	29
PC5(A,D,E)	0.1598	-	-	0.1598	5.718	26
PC5(B,C)	0.1598	-	-	0.1598	5.718	136
PB1(A - E)	-	-	0.3267	0.3267	5.134	24
PB2(A - E)	-	-	0.2178	0.3267	5.417	28
PB3(A - E)	-	-	0.2178	0.2178	5.317	29
PB4(A - E)	-	-	0.1598	0.2397	5.565	33
PB5(A - E)	-	-	0.1598	0.1598	5.447	29
PB6(A - E)	-	-	-	0.1598	5.700	132

TABLE 4.2: SLUMP AND ENTRAINED AIR PERCENTAGE OF THE TEST SPECIMENS.

SPECIMEN NO.	SLUMP (INCHES)	% ENTRAINED AIR
PC1	3	4.6
PC2	2-3/4	4.4
PC3	3	3.9
PC4	2-3/4	3.9
PC5	3	4.5
PB1	3	4.5
PB2	2-3/4	3.9
PB3	3	3.9
PB4	2-3/4	4.4
PB5	3	4.6
PB6	2-3/4	5.0

TABLE 4.3: FEATURES OF MODEL 6204B DC POWER SUPPLY

OUTPUT		INPUT	LOAD REGULATION	LINE REGULATION	TEMP. COEFF.	STABILITY	METER RANGES
D. C VOLTAGE	D. C CURRENT		CONST. VOLTAGE	CONST. VOLTAGE	CONST. VOLTAGE	CONST. VOLTAGE	
0-20V	0-0.6A	105-125/ 210-250 VAC	0.01%	0.01%	0.02%	0.1%	0-5V, 0-50V,
0-40V	0-0.3A	50-400 Hz 0.40A, 24W	PLUS	PLUS	PLUS	PLUS	0-.075A, 0-.75A
			4 MV	4 MV	1 MV/^{o}C	5 MV	

TABLE 5.1: LOAD CELL READING FOR TEST SPECIMEN PC4B

Specimen No: PC4B
Instrument Zero Reading: 0-10
Input Zero Reading: 0-10
Axial Load: 25 K

Date: 30th August, 1968
Zero-Load Cell No. 6: 0-10
Zero-Load Cell No. 5: 0-10
Zero-Load Cell No. 4: 0-10

Reading No.	Load Cell 6	Load Cell 5	Load Cell 4	Remarks
Initial	10	10	10	
1	2000	2000	25000	
2	3850	4000		
3	5670	6000		
4	7510	8000		
5	9360	10000		
6	10270	11000	25120	
7	11220	12000		
8	12000	13000		
9	13020	14000		
10	13970	15000		
11	14790	16000	25240	
12	15670	17000		

TABLE 5.1: LOAD CELL READING FOR TEST SPECIMEN PC4B (CON'D)

Reading No.	Load Cell 6	Load Cell 5	Load Cell 4	Remarks
13	16550	18000		
14	17470	19000		
15	18370	20000		
16	19280	21000		
17	20260	22000		
18	21120	23000		
19	22130	24000		
20	23160	25000		
21	23960	26000		
22	25040	27000		
23	26090	28000		

TABLE 5.2: STRAIN MEASUREMENTS FOR TEST SPECIMEN PC4B

Specimen No. PC4B

Gauge Length = 4 in.

Date: August 30, 1968

Range Reading: 1V

Gate Opening: 1 sec

Vernier Reading: 5

Sensitivity: 0.1V

Reading No.	Transducer No. 1	2	3	4	5	6	7	8	9	10
Initial	34440	29197	35827	39594	39352	37804	31817	28162	34751	29350
1	34743	29348	35829	39812	39745	38104	31730	28454	35140	29851
2	35024	29513	35815	40010	40133	38405	31615	28733	35531	30357
3	35329	29668	35812	40225	40523	38726	31541	29008	35948	30877
4	35672	29846	35800	40446	40912	39036	31414	29296	36394	31421
5	35996	30020	35790	30679	41313	39361	31286	29610	36862	32015
6	36214	30144	35802	40834	41562	39541	31210	29821	37154	32317
7	36321	30179	35808	40959	41743	39702	31133	30002	37432	32660
8	36487	30248	35856	41124	41879	39892	30976	30290	37830	33060
9	36690	30325	35911	41324	42121	40135	30906	30574	38235	33454
10	36889	30393	35993	41552	42518	40321	30794	30786	38637	33931
11	37187	30494	36094	41883	43136	40421	30638	31164	39241	34501

TABLE 5.2: STRAIN MEASUREMENTS FOR TEST SPECIMEN PC4B (CONT'D)

Reading No.	Transducer No. 1	2	3	4	5	6	7	8	9	10
	-	-	-	-	-	-	-	-	-	-
12	37468	30595	36201	42238	43765	40683	30573	31492	39830	35175
13	37828	30717	36320	42661	44517	41377	30506	31802	40401	35834
14	38098	30800	36473	43195	45385	41979	30434	32131	41040	36529
15	38467	30906	36680	43854	46427	42642	40345	32530	41792	37295
16	38867	31032	36890	44508	47479	43491	30293	32904	42566	38060
17	39517	31487	37173	45345	38765	44632	30276	33714	43963	39663
18	40346	31963	37470	46160	50058	45590	30216	34561	45557	41515
19	41379	32557	37872	47266	51726	46835	30101	35596	47349	43621
20	42607	33193	38414	48518	53691	48244	30045	36819	49368	45933
21	44036	34077	38985	49886	55835	49618	29934	38384	51571	48427
22	45685	35375	40641	51372	58161	51098	29776	40277	55568	51174
23	47708	36729	41975	54080	62959	53799	29651	43943	58157	54163

TABLE 5.3: DEFLECTION GAUGE READINGS FOR TEST SPECIMEN PC4B

Specimen No. PC4B

Date: August 30, 1968

Reading No.	1	2	3	4	5	6	7	8	Remarks
Initial	0270	0066	0110	0801	0054	0094	0291	1301	
1	0277	0138	0201	0791	0113	0103	0362	1301	
2	0282	0315	0295	0783	0190	0112	0426	1301	
3	0288	0295	0380	0774	0272	0121	0490	1301	
4	0294	0379	0475	0764	0362	0130	0554	1301	
5	0299	0458	0563	0755	0452	0138	0618	1301	
6	0302	0505	0617	0750	0510	0144	0650	1301	
7	0304	0538	0662	0745	0541	0148	0683	1301	
8	0307	0588	0715	0740	0592	0153	0721	1301	
9	0310	0639	0780	0733	0652	0159	0759	1301	
10	0314	0698	0846	0725	0720	0165	0800	1301	
11	0318	0770	0932	0716	0801	0173	0849	1301	

TABLE 5.3: DEFLECTION GAUGE READING FOR TEST SPECIMEN PC4B (CONT'D)

Specimen No. PC4B

Date: August 30, 1968

Reading No.	1	2	3	4	5	6	7	8	Remarks
12	0323	0845	1016	0707	0872	0181	0900	1301	
13	0326	0920	1105	0697	0971	0190	0954	0923	
14	0331	1000	1200	0687	1061	0199	1010	0923	
15	0336	1100	1309	0675	1162	0208	1070	0923	
16	0341	1200	1420	0663	1272	0219	1133	0923	
17	0348	1305	1553	0649	1403	0231	1210	0923	
18	0354	1412	1680	0636	1522	0243	1280	0923	
19	0362	1550	1835	0619	1678	0257	1364	0923	
20	0370	1700	2020	0600	1861	0274	1469	0923	
21	0380	1850	2200	0581	2060	0292	1576	0760	
22	0390	2040	2435	0555	2290	0311	1689	0760	
23	0404	2280	2740	0522	2620	0338	1850	0760	
24									

TABLE 5.4: CONCRETE STRENGTH AND MODULUS OF ELASTICITY OF SYMMETRICALLY PRESTRESSED BEAM-COLUMN SPECIMENS.

SPECIMEN NO.	ULTIMATE CYLINDER STRENGTH, f'_c	AVE. ULTIMATE CYLINDER STRENGTH, $f'_{c_{ave}}$	INITIAL MODULUS OF ELASTICITY, E_c	AVE. INITIAL MODULUS OF ELASTICITY, $E_{c_{ave}}$	DYNAMIC MODULUS OF ELASTICITY, E_c	AVE. DYNAMIC MODULUS OF ELASTICITY, $E_{d_{ave}}$	INGE-LYSE'S EQUATION $E_c = 1800 + 460f'_c$
	(KSI)	(KSI)	(KSI)	(KSI)	(KSI)	(KSI)	(KSI)
	5.977		4819		4991		
PC1	6.030	6.018		4837		5011	4570
	6.048		4854		5031		
	5.217		4691		4819		
PC2	5.482	5.423		4677		4849	4290
	5.570		4663		4878		
	5.447		4883		4974		
PC3	5.305	5.394		4680		4984	4280
	5.429		4477		4995		
	5.164		4813		4951		
PC4	5.553	5.435		4665		4925	4300
	5.588		4518		4899		
	5.500		4531		4912		
PC5	5.747	5.718		4620		4919	4430
	5.906		4710		4925		

TABLE 5.5: CONCRETE STRENGTH AND MODULUS OF ELASTICITY OF UNSYMMETRICALLY PRESTRESSED BEAM-COLUMN SPECIMENS.

SPECIMEN NO.	ULTIMATE CYLINDER STRENGTH, f'_c	AVE.ULTIMATE CYLINDER STRENGTH, $f'_{c_{ave}}$	INITIAL MODULUS OF ELASTICITY, E_c	AVE. INITIAL MODULUS OF ELASTICITY, $E_{c_{ave}}$	DYNAMIC MODULUS OF ELASTICITY, E_d	AVE.DYNAMIC MODULUS OF ELASTICITY, $E_{d_{ave}}$	INGE-LYSE'S EQUATION $E_c = 1800 + 460f'_c$
	(KSI)	(KSI)	(KSI)	(KSI)	(KSI)	(KSI)	(KSI)
	5.058		4689		4899		
PB1	5.075	5.134		4707		4846	4160
	5.270		4725		4792		
	5.500		4690		4931		
PB2	5.305	5.417		4730		4908	4290
	5.447		4770		4885		
	5.160		4650		4877		
PB3	5.411	5.317		4706		4901	4250
	5.376		4762		4925		
	5.765		4860		4942		
PB4	5.694	5.565		4784		4960	4365
	5.234		4709		4979		
	5.217		4646		4957		
PB5	5.730	5.447		4676		5011	4305
	5.394		4707		5064		
	5.677		4600		4819		
PB6	5.517	5.700		4613		4826	4420
	5.906		4627		4833		

TABLE 6.1: COMPARISON OF EXPERIMENTAL AND THEORETICAL RESULTS OF SYMMETRICALLY PRESTRESSED BEAM-COLUMN SPECIMENS

Specimen No.	P_U (KIPS)	THEORETICAL		EXPERIMENTAL				
		M_U (KIP-IN)	ϕ_U (RAD./IN.)	M_U (KIP./IN.)	ϕ_U (RAD./IN.)	ε_U (IN./IN.)	M_U/M_O	ϕ_U/ϕ_O
PC1A	0	404	0.001150	395	0.001002	0.004221	1.0000	1.0000
B	25	396	0.001015	398	0.000092	0.004120	1.0075	0.9019
C	40	390	0.000935	399	0.000804	0.004253	1.0101	0.7882
D	75	375	0.000788	388	0.000675	0.004027	0.9822	0.6617
E	95	363	0.000720	373	0.000627	0.004221	0.9443	0.6147
PC2A	0	348	0.001325	339	0.001304	0.005170	1.0000	1.0000
B	24	342	0.001148	346	0.001070	0.004794	1.0206	0.8205
C	50	332	0.000977	339	0.000779	0.003908	1.0000	0.5973
D	75	322	0.000842	330	0.000761	0.004329	0.9734	0.5835
E	95	309	0.000755	305	0.000675	0.004151	0.8997	0.5176
PC3A	0	334	0.001362	332	0.001252	0.004588	1.0000	1.0000
B	25	329	0.001178	328	0.000993	0.004469	0.9879	0.7931
C	50	323	0.001014	334	0.000842	0.004271	1.0060	0.6725
D	75	314	0.000865	319	0.000767	0.004349	0.9608	0.6126
E	95	289	0.000770	310	0.000619	0.004337	0.9337	0.4944

TABLE 6.1: COMPARISON OF EXPERIMENTAL AND THEORETICAL RESULTS OF SYMMETRICALLY PRESTRESSED BEAM-COLUMN SPECIMENS (CONT'D)

Specimen No.	P_U (KIPS)	THEORETICAL		EXPERIMENTAL				
		M_U (KIP-IN)	ϕ_U (RAD./IN.)	M_U (KIP./IN.)	ϕ_U (RAD./IN.)	ε_U (IN./IN.)	M_U/M_O	ϕ_U/ϕ_O
PC4A	0	311	0.001482	308	0.001253	0.004216	1.0000	1.0000
B	25	309	0.001263	303	0.001134	0.004710	0.9837	0.9050
C	50	307	0.001060	309	0.000903	0.004441	1.0032	0.7206
D	75	302	0.000895	312	0.000751	0.004017	1.0097	0.5996
E	95	294	0.000790	298	0.000605	0.003929	0.9644	0.4828
PC5A	0	248	0.002086	253	0.001751	0.004838	1.0000	1.0000
B	10	270	0.001762	276	0.001484	0.005082	1.0909	0.8475
C	44	286	0.001325	290	0.001105	0.004469	1.1462	0.6310
D	75	290	0.001049	296	0.000888	0.004548	1.1699	0.5071
E	95	288	0.000908	293	0.000678	0.004093	1.1581	0.3872

TABLE 6.2: COMPARISION OF EXPERIMENTAL AND THEORETICAL RESULTS OF UNSYMMETRICALLY PRESTRESSED BEAM-COLUMN SPECIMENS

Specimen No.	P_U (KIPS)	THEORETICAL		EXPERIMENTAL				
		M_U (KIPS-IN.)	ϕ_U (RAD./IN.)	M_U (KIP./IN.)	ϕ_U (RAD./IN.)	ε_U (IN./IN.)	M_U/M_O	ϕ_U/ϕ_O
PB1A	0	357	0.001028	368	0.000953	0.003979	1.0000	1.0000
B	25	343	0.000916	359	0.000828	0.004055	0.9607	0.8910
C	50	325	0.000812	357	0.000787	0.004391	0.9103	0.7898
D	75	304	0.000716	335	0.000654	0.003996	0.8515	0.6964
E	95	280	0.000651	320	0.000521	0.003818	0.7843	0.6332
PB2A	0	366	0.001090	392	0.001101	0.004529	1.0000	1.0000
B	25	353	0.000950	371	0.000888	0.004225	0.9644	0.8715
C	50	340	0.000841	352	0.000778	0.003951	0.9289	0.7715
D	75	322	0.000735	334	0.000709	0.003932	0.8797	0.6743
E	95	303	0.000663	314	0.000592	0.003726	0.8278	0.6082
PB3A	0	318	0.001228	314	0.001166	0.004016	1.0000	1.0000
B	25	311	0.001065	316	0.001016	0.004082	0.9779	0.8640
C	50	303	0.000916	314	0.000865	0.004120	0.9528	0.7459
D	75	290	0.000789	310	0.000690	0.004147	0.9119	0.6425
E	95	276	0.000700	299	0.000602	0.003793	0.8679	0.5700

TABLE 6.2: COMPARISION OF EXPERIMENTAL AND THEORETICAL RESULTS OF UNSYMMETRICALLY PRESTRESSED BEAM-COLUMN SPECIMENS

Specimen No.	P_U (KIPS)	THEORETICAL		EXPERIMENTAL				
		M_U (KIPS-IN.)	ϕ_U (RAD./IN.)	M_U (KIP./IN.)	ϕ_U (RAD./IN.)	ε_U (IN./IN.)	M_U/M_O	ϕ_U/ϕ_O
PB4A	0	335	0.001262	327	0.001150	0.004317	1.0000	1.0000
B	25	328	0.001088	327	0.000966	0.004065	0.9791	0.8621
C	50	320	0.000934	323	0.000880	0.004181	0.9552	0.7400
D	75	309	0.000810	316	0.000730	0.004184	0.9223	0.6418
E	95	296	0.000718	316	0.000571	0.003699	0.8835	0.5689
PB5A	0	289	0.001364	288	0.001254	0.004005	1.0000	1.0000
B	10	288	0.001320	290	0.001233	0.004559	0.9965	0.9677
C	39	287	0.001075	296	0.000915	0.004280	0.9930	0.7881
D	75	281	0.000852	289	0.000836	0.003773	0.9723	0.6246
E	95	272	0.000745	287	0.000599	0.003570	0.9411	0.5461
PB6A	0	252	0.002284	248	0.001669	0.005857	1.0000	1.0000
B	10	276	0.001852	283	0.001628	0.005348	1.0952	0.8108
C	40	288	0.001364	292	0.001028	0.004013	1.1428	0.5971
D	70	288	0.001064	297	0.000866	0.004353	1.1428	0.4658
E	94	284	0.000890	287	0.000736	0.004012	1.1269	0.3896

TABLE 6.3: VARIATION OF BALANCED LOAD WITH THE STEEL AREA

Specimen No.	Total Compressive Reinforcement (Sq. In.)	Total Tensile Reinforcement (Sq. In.)	Balanced Load (Kips)
PC1	0.4593	0.4593	-98.8
PC2	0.3267	0.3267	-56.4
PC3	0.3062	0.3062	-49.9
PC4	0.2397	0.2397	-28.6
PC5	0.1598	0.1598	- 3.1
PB1	-	0.6534	-100.5
PB2	-	0.5445	-80.3
PB3	-	0.4356	-50.9
PB4	-	0.3995	-46.1
PB5	-	0.3196	-24.6
PB6	-	0.1598	4.8

APPENDIX C: PHOTOGRAPHS

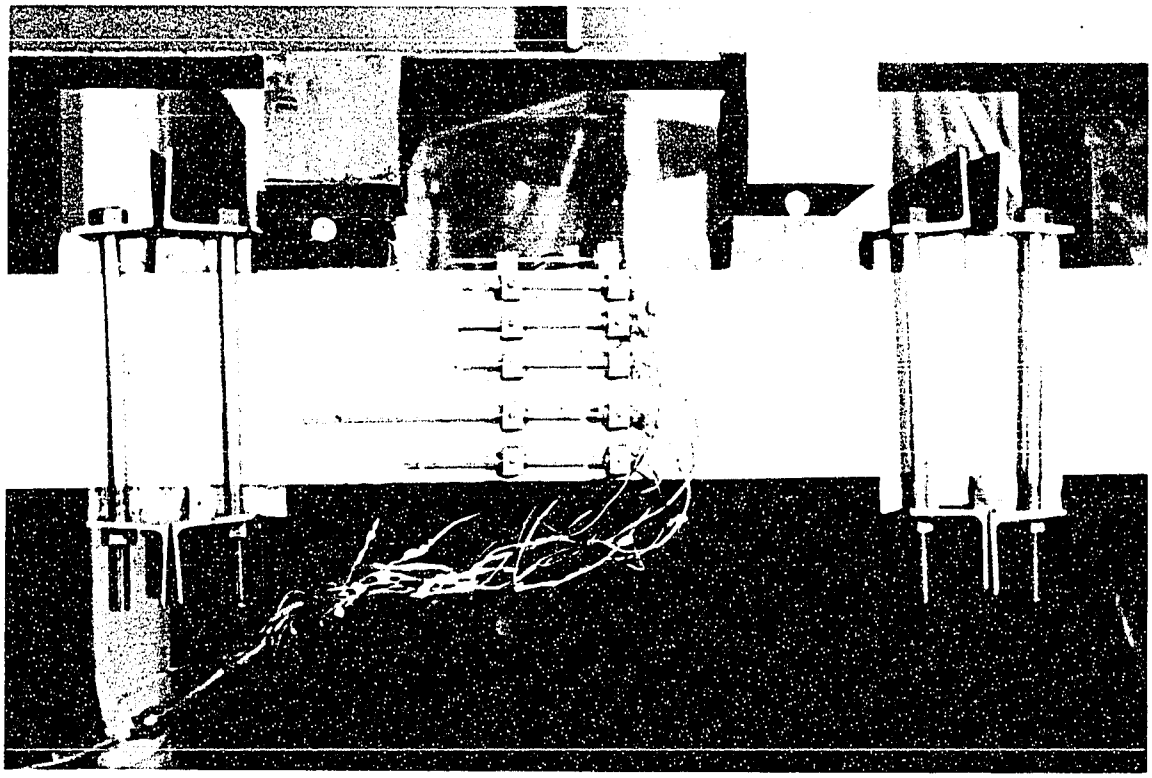

PLATE 4.1 – ARRANGEMENT OF EXTERNAL STIRRUPS, TRANSDUCERS AND LATERAL LOADING.

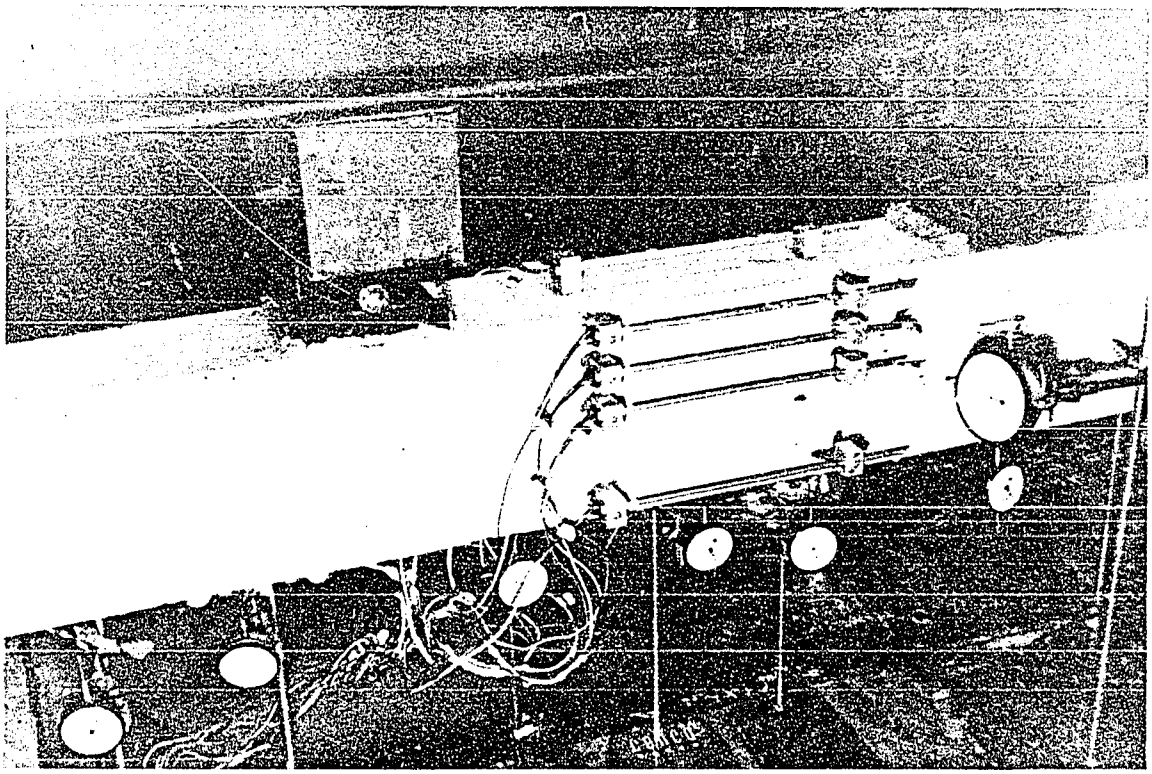

PLATE 4.2 – POSITION OF DEFLECTION BRIDGE.

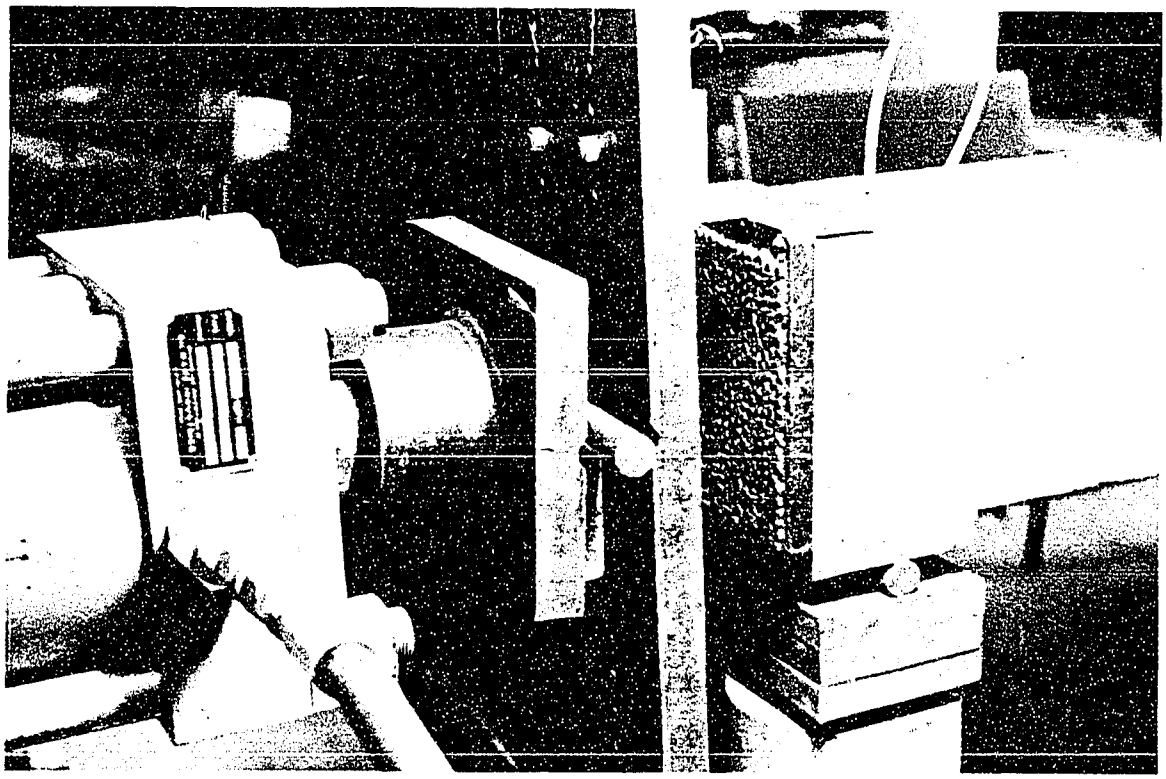

PLATE 4.3 – END CONNECTIONS FOR AXIAL LOADING AT THE HYDRAULIC RAM END.

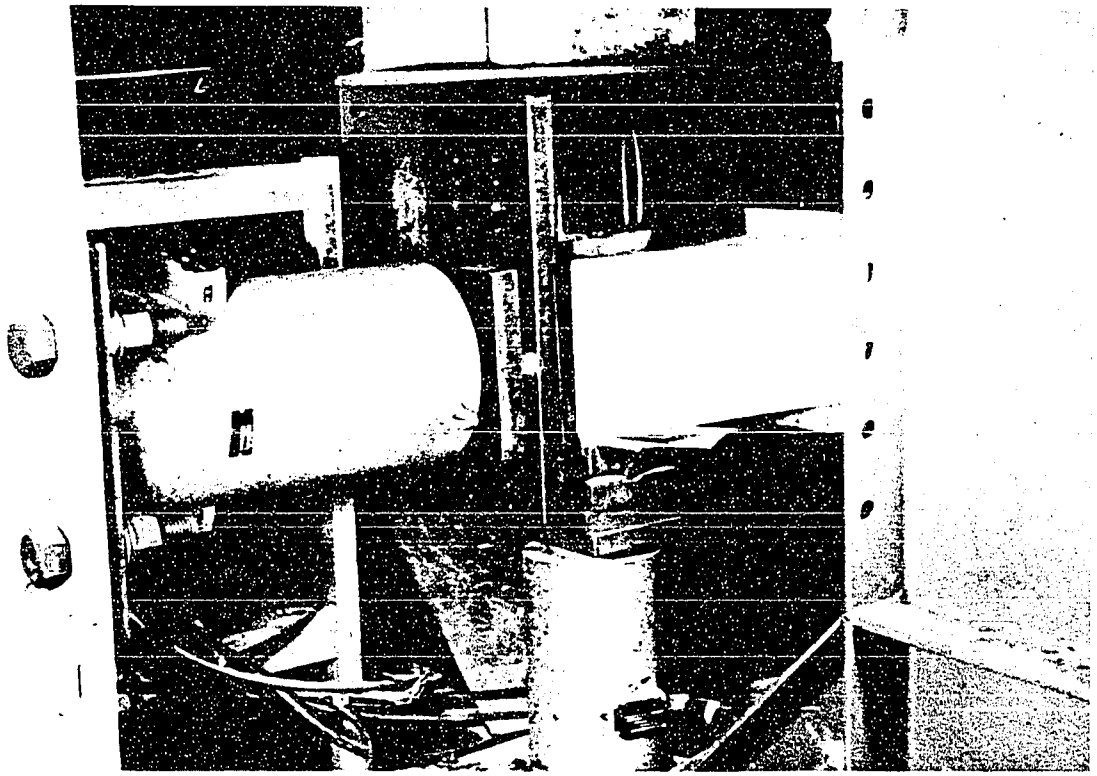

PLATE 4.4 – END CONNECTIONS FOR AXIAL LOADING AT THE LOAD CELL END.

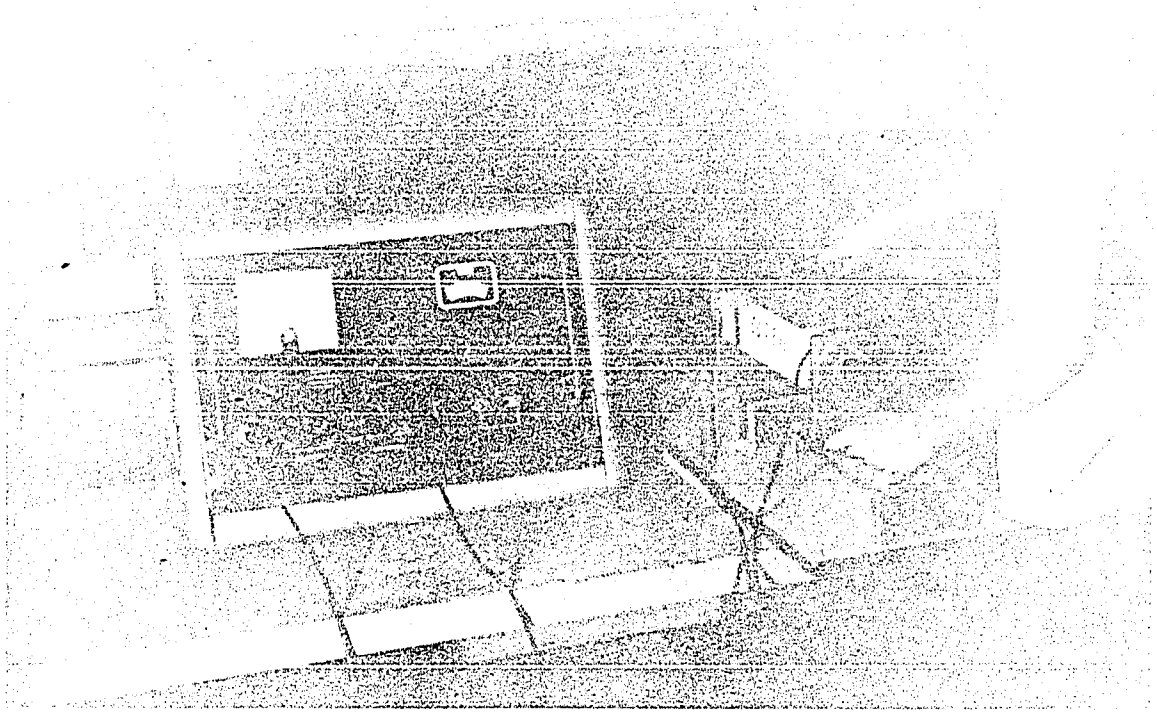

PLATE 4.5 – SONIC TEST OF CONTROL PRISMS IN SCT4 ELECTRODYNAMOMETER.

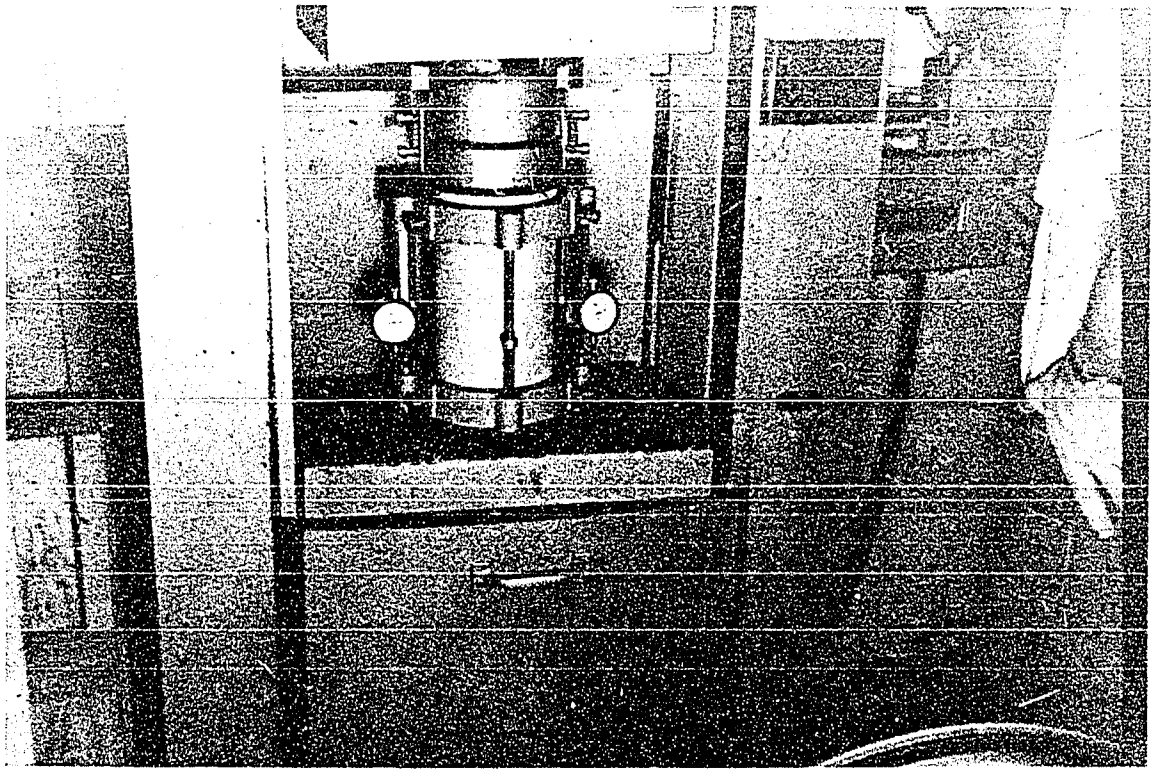

PLATE 4.6 – DEFORMATION TEST FOR CONTROL CYLINDERS.

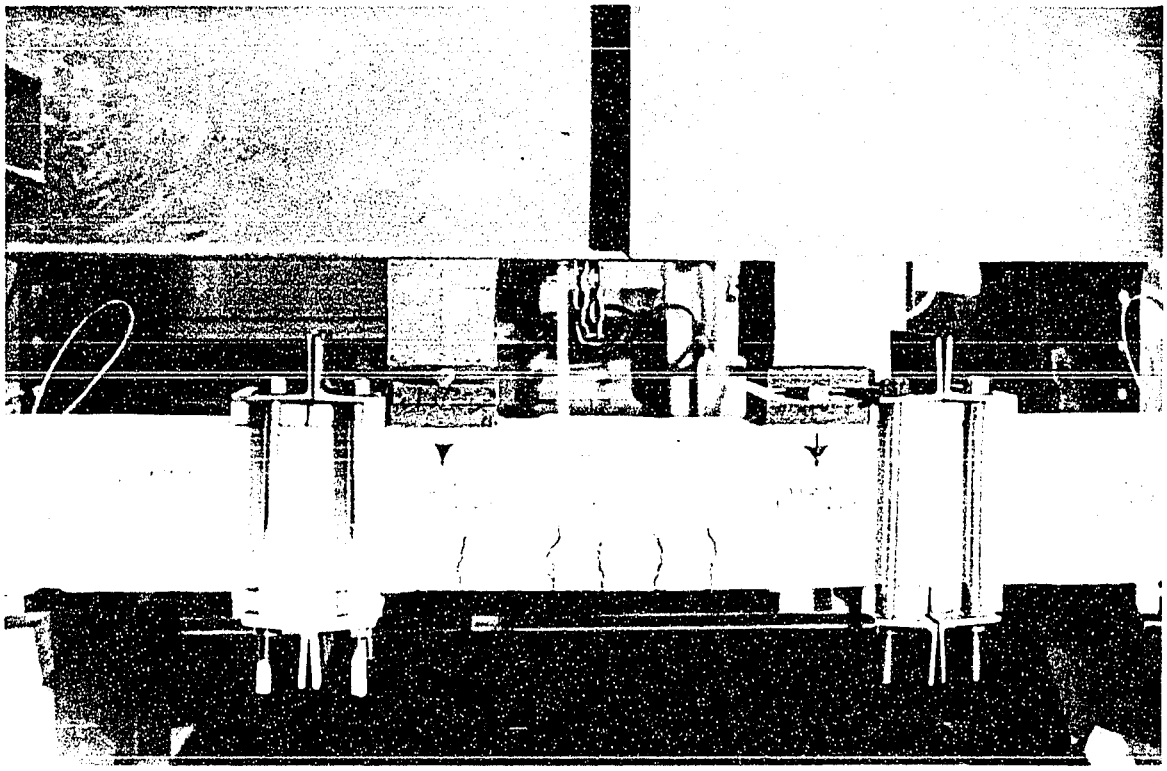

PLATE 6.1 – COMPRESSION FAILURE EXHIBITED BY PBID.

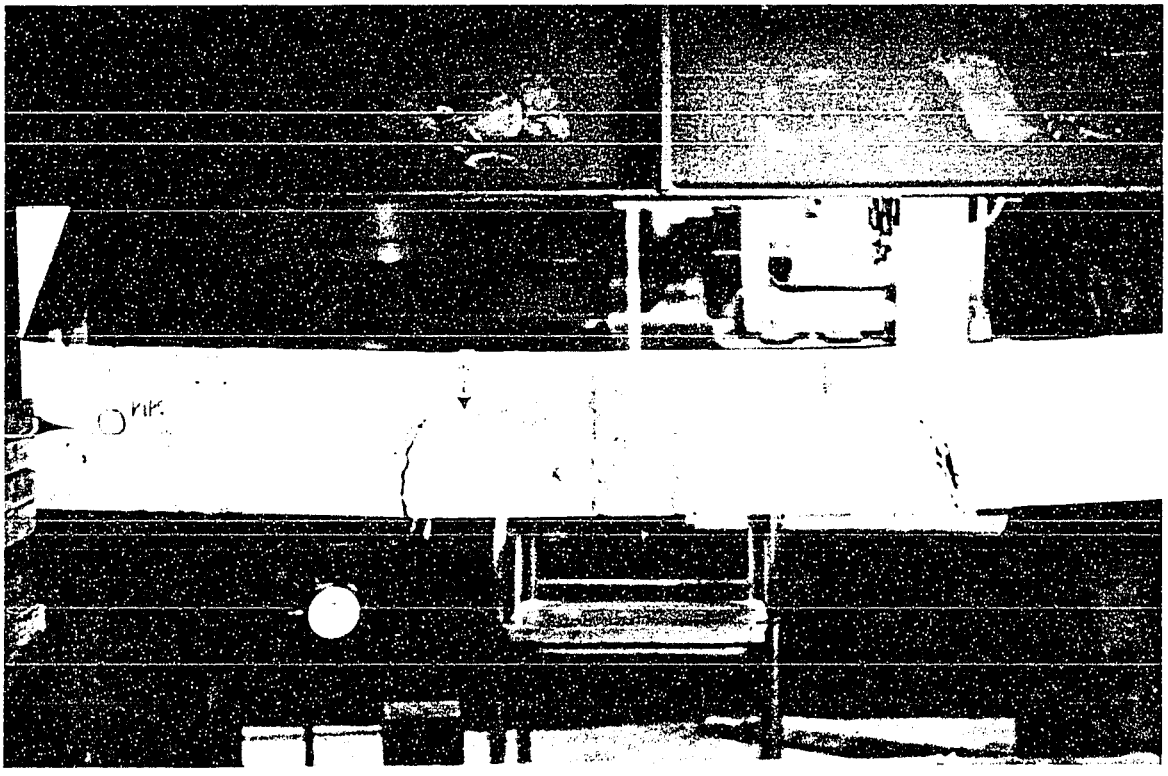

PLATE 6.2 – TENSION FAILURE EXHIBITED BY PB6A.

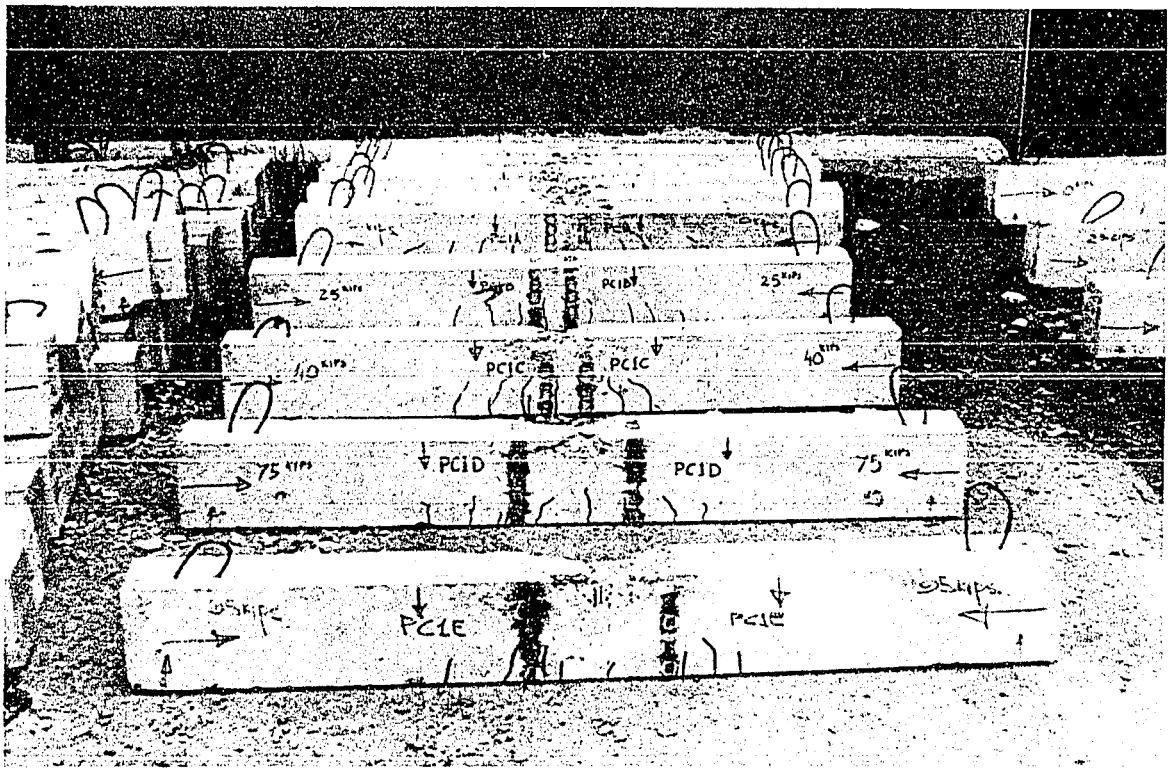

PLATE 6.3 – VARIATION OF CRACK PATTERN WITH AXIAL LOAD IN SERIES PC1.

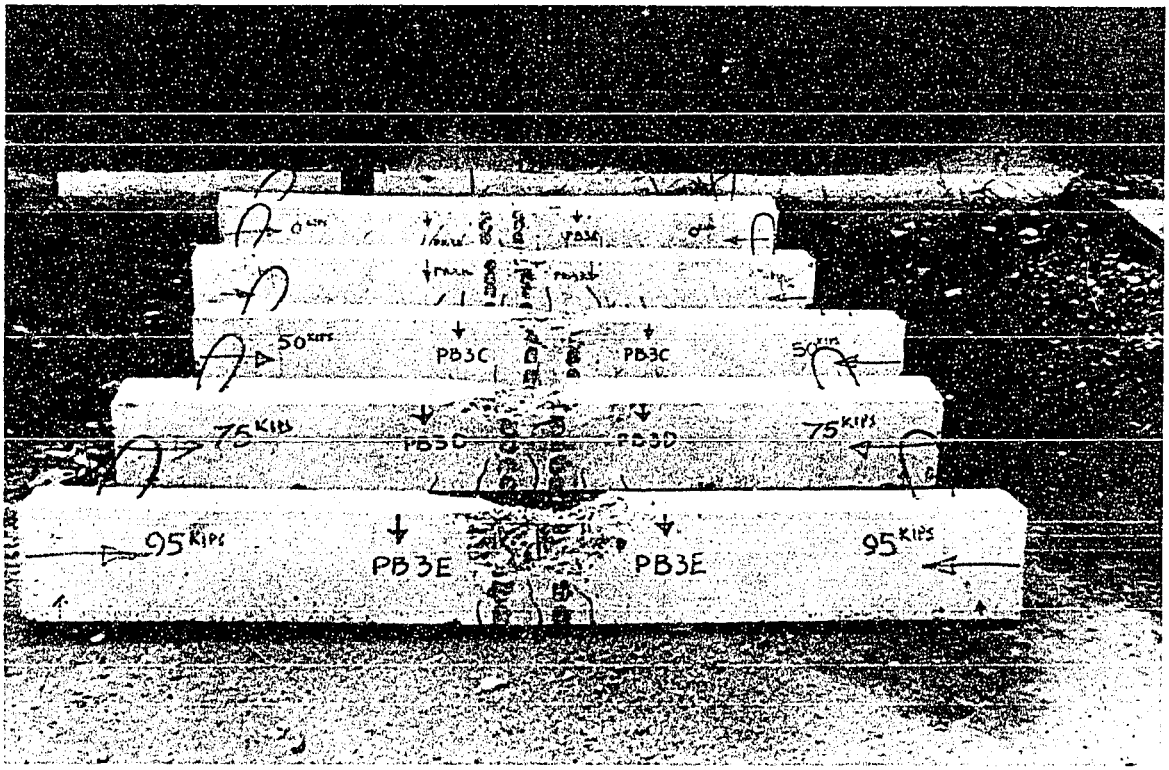

PLATE 6.4 – VARIATION OF CRACK PATTERN WITH AXIAL LOAD IN SERIES PB3.

APPENDIX D: FLOW CHARTS OF COMPUTER PROGRAMMES

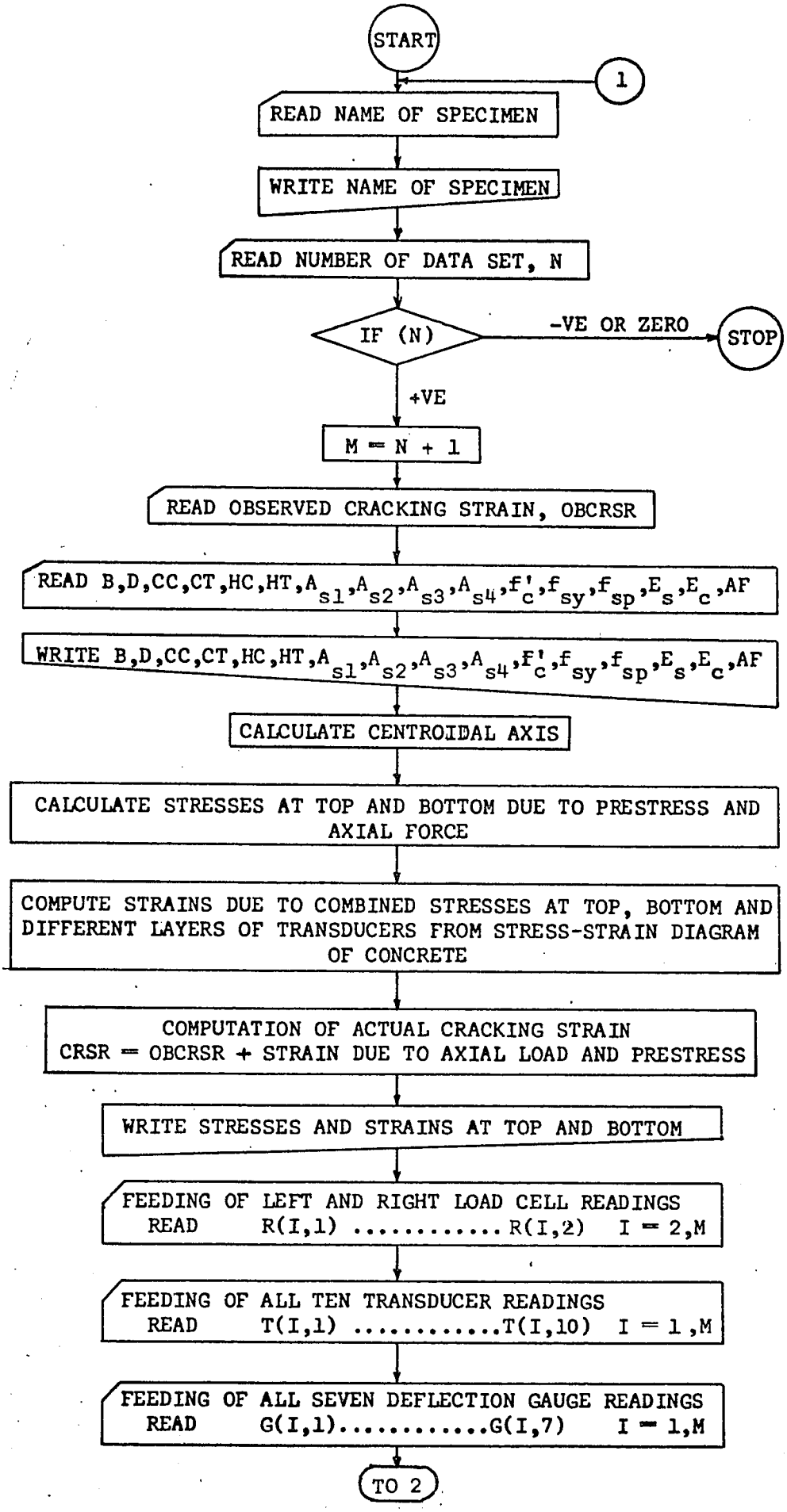

FLOW CHART FOR PROGRAMME B

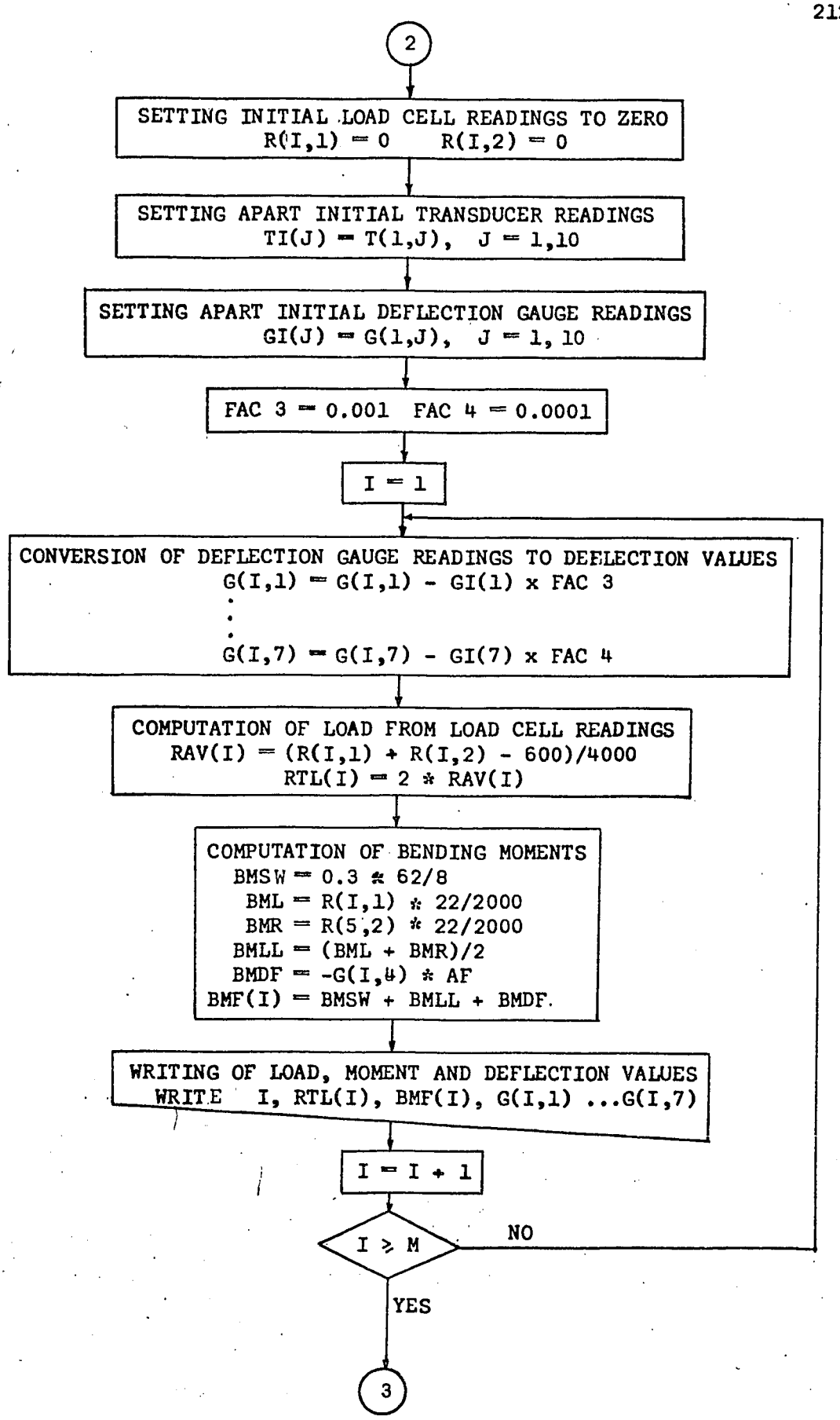

FLOW CHART FOR PROGRAMME B(CONTD.)

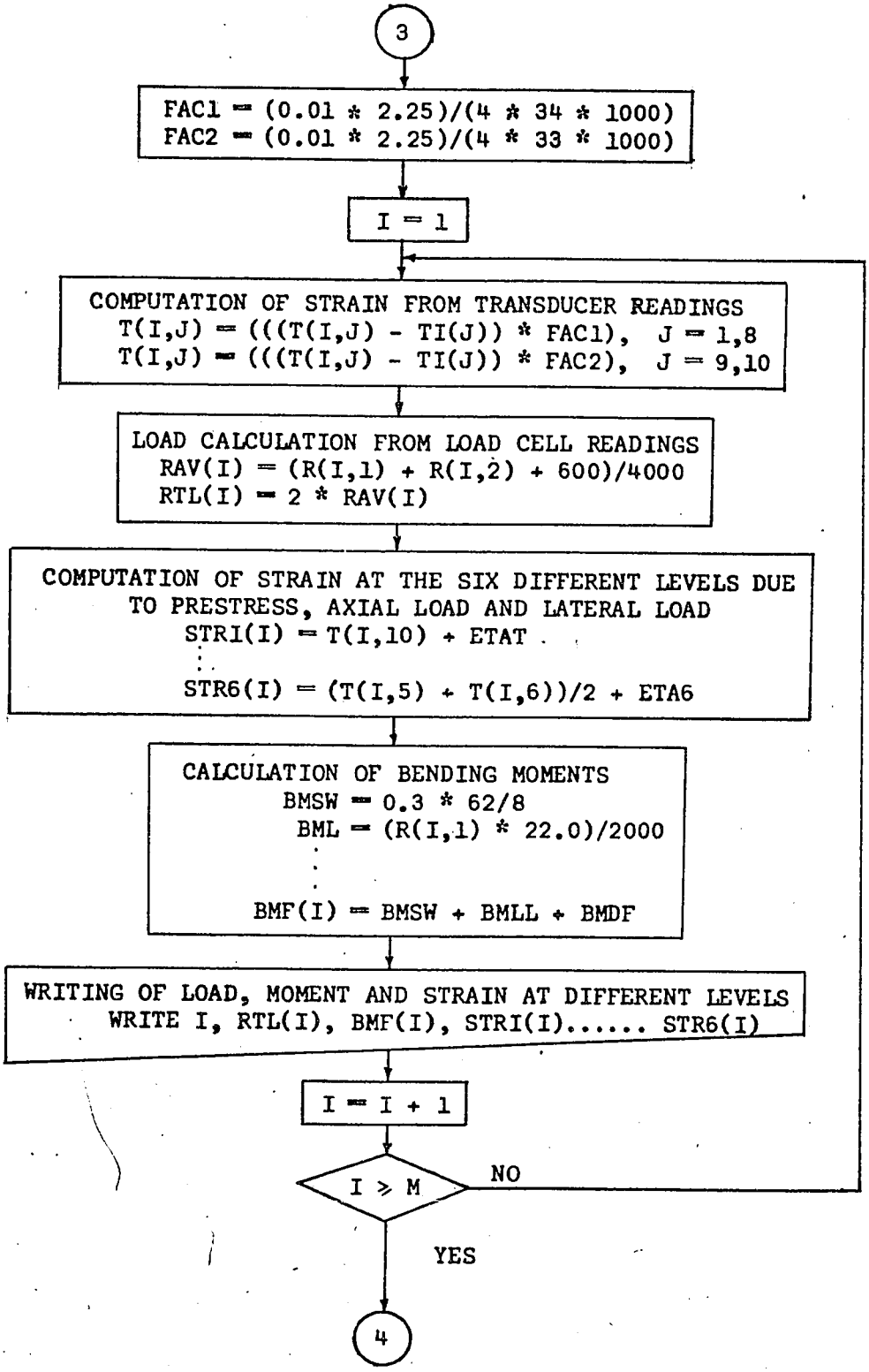

FLOW SHEET FOR PROGRAMME B (CONTD.)

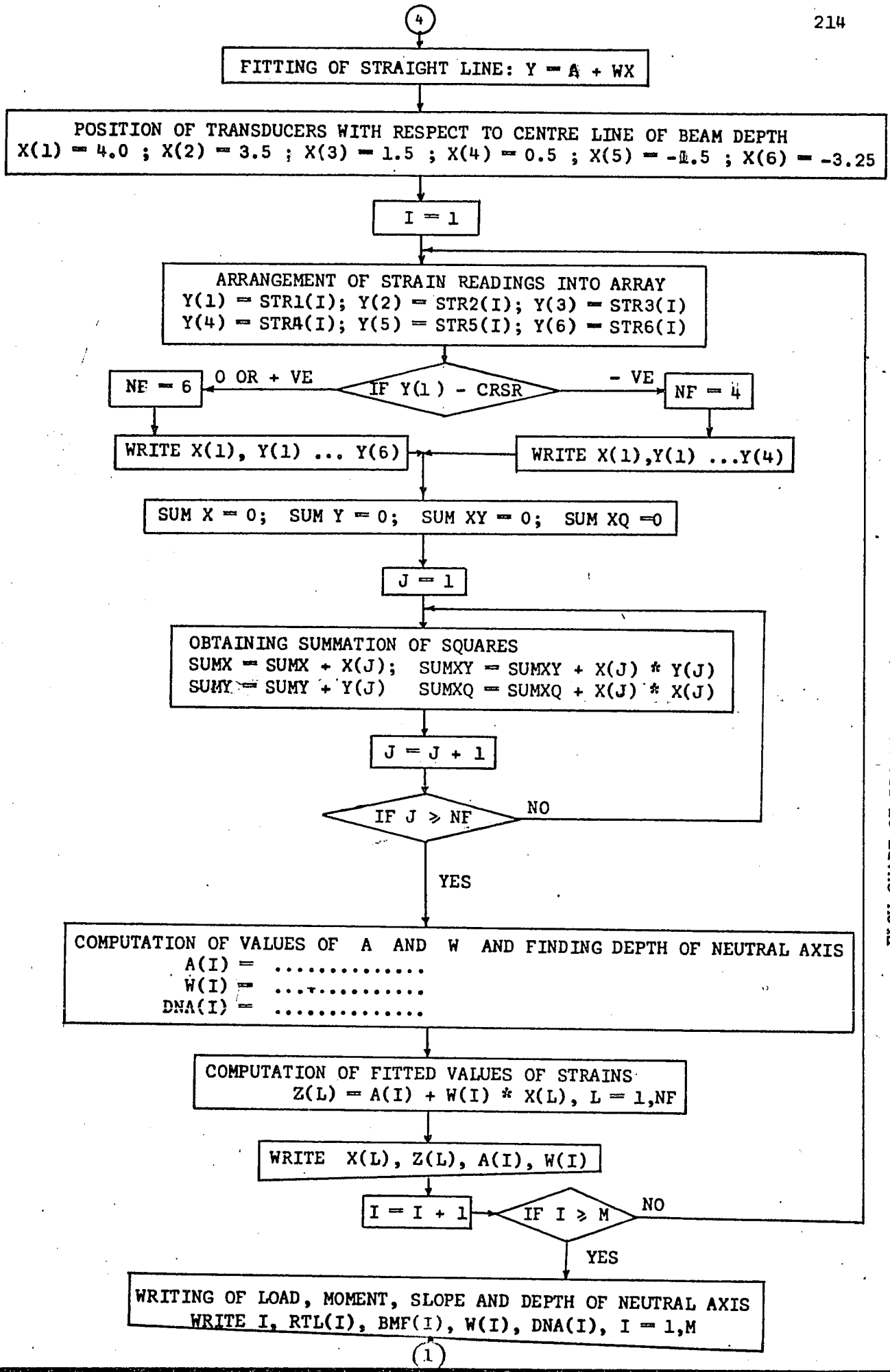

FLOW CHART OF PROGRAMME B (CONTD).

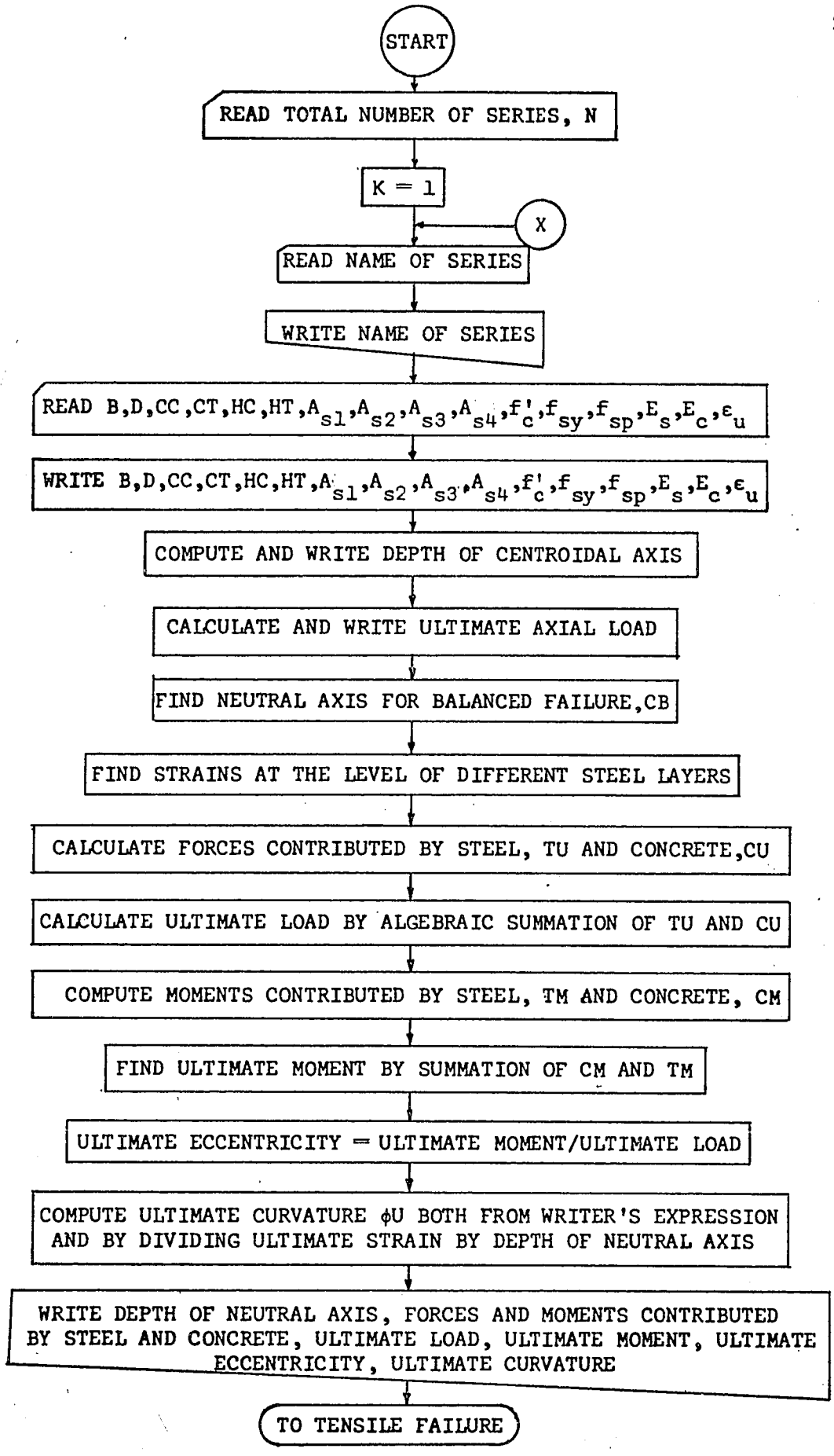

FLOW CHART FOR PROGRAMME C

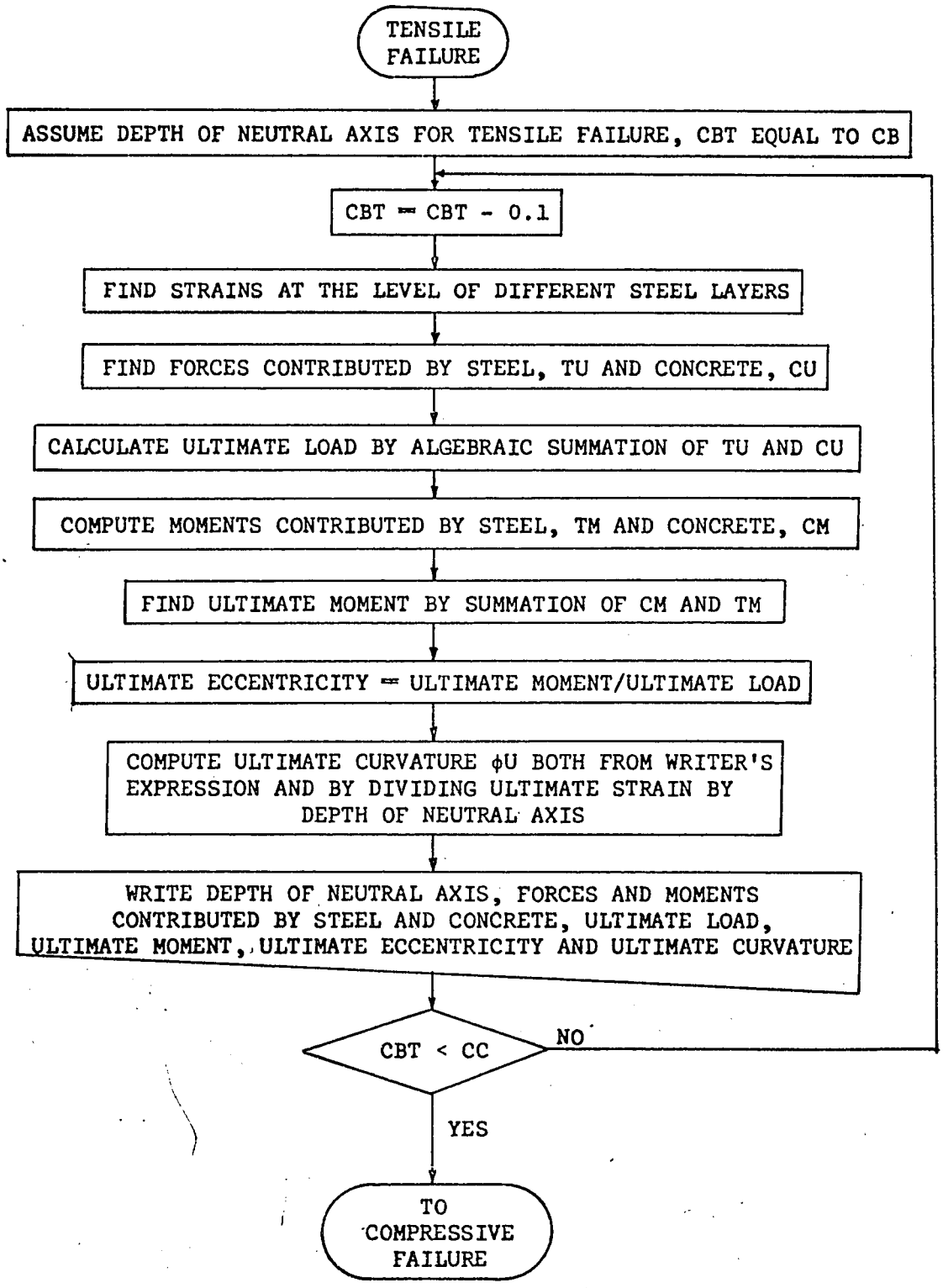

FLOW CHART FOR PROGRAMME C (CONTD)

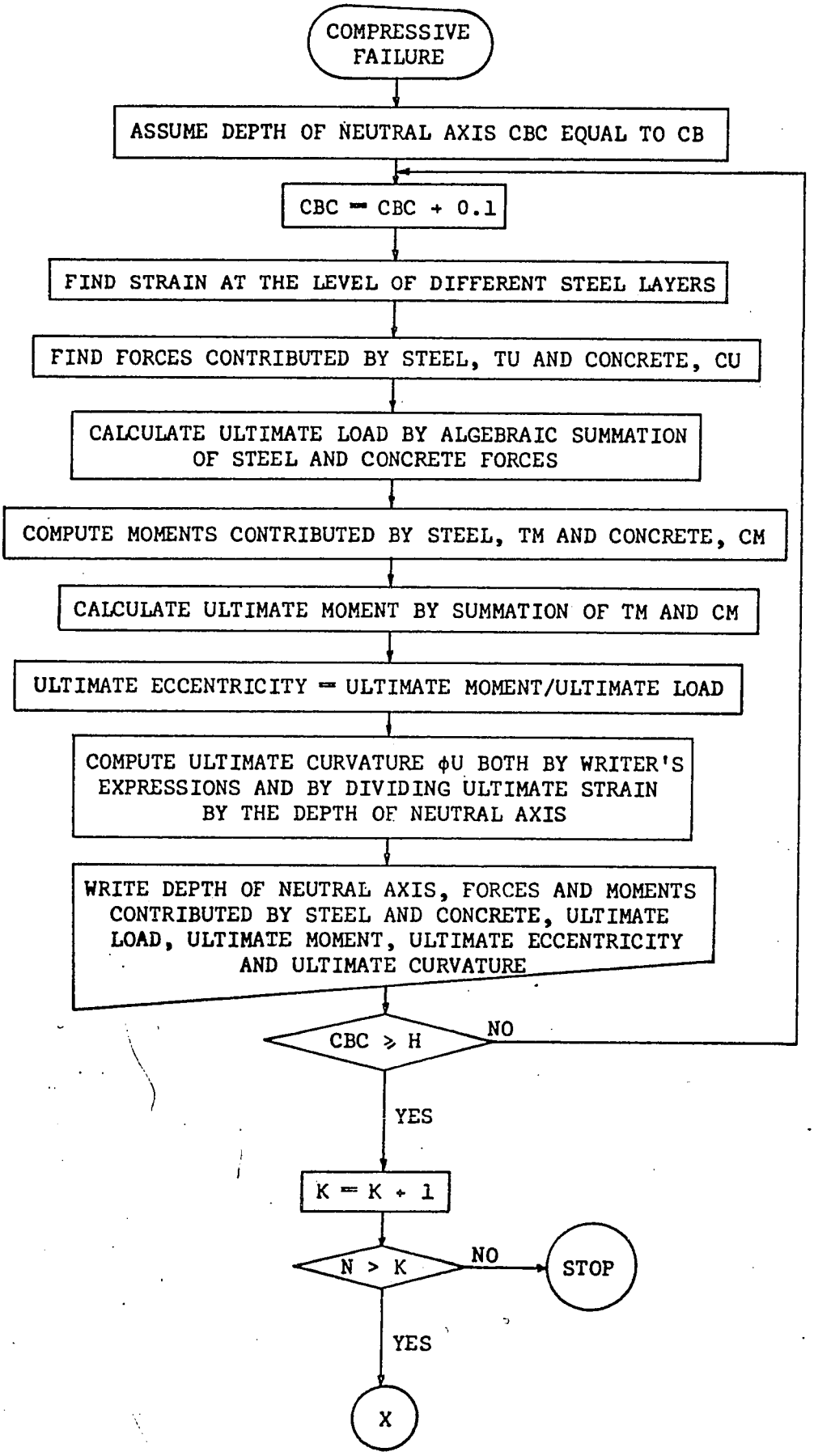

FLOW CHART FOR PROGRAMME C (CONTD)

APPENDIX E: REFERENCES

1. Portland Cement Association

"Ultimate Design of Reinforced Concrete", Modern Developments in Reinforced Concrete No. 11, 1944.

2. Jensen, V.P.

"Ultimate Strength of Reinforced Concrete Beams as Related to the Plasticity Ratio of Concrete", University of Illinois Engineering Experiment Station Bulletin No. 345, June, 1943.

3. Whitney, C.S.

"Design of Reinforced Concrete Members Under Flexure or Combined Flexure and Direct Compression", Proceedings of the American Concrete Institute, V.33, No. 4, 1937, pp. 483-498.

4. Whitney, C.S.

"Eccentrically Loaded Reinforced Concrete Columns", Concrete and Constructional Engineering, V.33, No. 11, Nov. 1938, pp. 549-561.

5. Hognestad, E.

"A Study of Combined Bending and Axial Load in Reinforced Concrete Members", Bulletin No. 1, The Reinforced Concrete Research Council of the Engineering Foundation.

6. Ernst, G.C., JJ. Hromadik and A.R. Riveland

"Inelastic Buckling of Plain and Reinforced Concrete Columns, Plates and Shells", Bulletin No. 3, Nebraska University Engineering Experiment Station, August, 1953.

7. Westergard, H.M. and W.R. Osgood

"Strength of Steel Columns", Transactions, American Society of Mechanical Engineers, V. 51, 1928, pp. 65-80.

8. Broms, B. and I.M. Viest

"Ultimate Strength Analysis of Long Hinged Reinforced Concrete Columns", Journal of the Structural Division, Proceedings of the American Society of Civil Engineers, V. 84, No. ST4, January, 1950.

9. Broms, B. and I.M. Viest

"Design of Long Reinforced Concrete Columns", Journal of the Structural Division, Proceedings of the American Society of Civil Engineers, V. 84, No. ST4, July , 1958.

10. Pfrang, E.O. and C.P. Siess

"Predicting Structural Behaviour Analytically", Journal of the Structural Division, Proceedings of the American Society of Civil Engineers, V. 90, No. ST5, Oct., 1964.

11. Pfrang, E.O. and C.P. Siess

"Behaviour of Restrained Reinforced Concrete Columns", Journal of the Structural Division, Proceedings of American Society of Civil Engineers, V. 90, No. ST5, Oct., 1964.

12. Breckenridge, R.A.

"A Study of the Characteristics of Prestressed Concrete Columns", University of Southern California, Engineering Centre, USCEC Report 18-6, 1953.

13. Ozell, A.M. and A.M. Jerniga

"Some Studies on the Behaviour of Prestressed Concrete Columns", Technical Progress Report No. 3, Supplement V. 10, No. 7, Florida Engineering and Industrial Experiment Station, University of Florida, July, 1956.

14. Zia, Paul Zung-Teh
"Ultimate Strength of Slender Prestressed Concrete Columns", Technical Paper Series No. 131, Florida Engineering and Industrial Experiment Station, V XI, No. 7, July, 1957.

15. Lin, T.Y. and R. Itaya
"A Prestressed Concrete Column Under Eccentric Loading", Journal of the Prestressed Concrete Institute, V. 2, Dec., 1957, pp. 5-17.

16. Itaya, R.
"Design and Uses of Prestressed Concrete Columns", Journal of the Prestressed Concrete Institute, V. 10, No. 3, 1965, pp. 69-91.

17. Lee, Y.C.
"Behaviour of Partially Prestressed Column under Eccentric Loading", Graduate Student Research Report No. 35, Department of Civil Engineering, University of California, Berkeley.

18. Karman, T.V.
"Untersuchungen über Knickfestigkeit", Mifteilungen über Forschungsarbeiten auf dem Gebiete des Ingenieurwessens, No.81, Berlin, Germany, 1910.

19. Lin, T.Y. and T.R. Lakhwara
"Ultimate Strength of Eccentrically Loaded Partially Prestressed Concrete Columns", Journal of the Prestressed Concrete Institute V.11, No. 3, June, 1966, pp. 37-49.

20. Tai, H.
"An Analytical Study of Partially Prestressed Concrete Columns Under Eccentric Loads", Graduate Student Report No. 129, SESM Division, University of California, Berkeley, 1963.

21. Sandrini, L.M.

"Ultimate Strength of Partially Prestressed Concrete Columns Under Eccentric Load - A Computer Analysis", Graduate Student Report No. 146, SESM Division, University of California, Berkeley, 1967.

22. Zia, Paul and F.L. Moreadith

"Ultimate Load Capacity of Prestressed Concrete Columns", Journal of the American Concrete Institute, V. 63, July, 1966.

23. Guillermo, E.C.

"Ultimate Strength of Prestressed Concrete Columns Subjected to Combined Bending and Axial Load", Graduate Student Report No. 185, SESM Division, University of California, Berkeley, 1965.

24. Zia, Paul and E.C. Guillermo

"Combined Bending and Axial Load in Prestressed Concrete Columns", Journal of the Prestressed Concrete Institute, June 1967, pp. 52-59.

25. Aroni, S.

"Slender Prestressed Concrete Columns", thesis presented to the University of California of Berkeley, in Sept. 1966, in partial fulfillment of the requirement for the Degree of Doctor of Philosophy.

26. Hall, A.S.

"Buckling of Prestressed Columns", Symposium on Prestressed Concrete, Cement and Concrete Association of Australia, Sydney, Aug. 1961 (Reprinted in Constructional Review, London, V.K. June 1963, pp. 27-33.

27. Brown, H.R. and A.S. Hall

"Tests on Slender Prestressed Concrete Columns", Symposium on Reinforced Concrete Columns, Special Publication, American Concrete Institute, 1966.

28. Kabaila, A.P. and A.S. Hall

"Analysis of Instability of Unrestrained Prestressed Concrete Columns with End Eccentricities", Symposium of Reinforced Concrete Columns, Special Publication of American Concrete Institute, 1966.

29. Rüsch, H.

"Researches Toward a General Flexural Theory for Structural Concrete", ACI Journal, Proceeding V. 57, No. 1, July, 1960.

30. Brown, K.J.

"The Ultimate Load Carrying Capacity of Prestressed Concrete Columns Under Direct and Eccentric Loading", Civil Engineering and Public Works Review, April, May and June, 1965.

31. Koenan, M.

"Für die Berchnung der Starke der Monierschen Cement platten" Zentralblatt der Bauverwaltung, V. 6, No. 47, Nov. 1886.

32. Hognestad, E.

"Inelastic Behaviour in Tests of Eccentrically Loaded Short Reinforced Concrete Columns", Bulletin No. 2, The Reinforced Concrete Research Council of the Engineering Foundation.

33. Hognestad, E.
"Confirmation of Inelastic Stress Distribution in Concrete", Journal of the Structural Division, Proceedings of the American Society of Civil Engineers, V. 83, No. ST2, March, 1957.

34. Building Code Requirements for Reinforced Concrete (ACI 318-63)

35. Kazinczy, G. Von
"Experiments with Clamped Girders", Betonszemle, 1914.

36. Baker, J.F., M.R. Horne, and J. Heyman
"The Steel Skeleton, Vol. II", Cambridge University Press, Cambridge 1956.

37. Neal, B.G.
"The Plastic Methods, of Structural Analysis", John Wiley and Sons, N.Y. 1957.

38. Seymonds P.S. and B.G. Neal
"Recent Progress in Plastic Methods of Structural Analysis", J. Franklin Institute, 252, 1951.

39. Horne, M.R.
"A Moment Distribution Method for the Analysis and Design of Structures by the Plastic Theory", Proceedings of the Institute of Civil Engineers (London), V. 3(3), 1954.

40. Heyman, J.
"Plastic Design of Portal Frames", Cambride University Press Cambride, 1957.

41. Beedle, L.S., B. Thurlinmann and R.L. Ketter
"Plastic Design in Structural Steel", Lehigh University and American Institute of Steel Construction, N.Y. 1955.

42. Prager, W.

"Minimum Weight Design of a Portal Frame", Proceedings of the ASCE, Journal of the Engineering Mechanics Division, V. 82, 1956.

43. Hodge, P.G.

"Plastic Analysis of Structures", McGraw Hill Book Company, N.Y., 1959.

44. Ernst, G.C.

"Plastic Hinging at the Intersection of Beams and Columns", Proceedings of the American Concrete Institute, V. 53, June 1957, pp. 111-1144.

45. Sawyer, H.A.

"A Proposed Method of Limit Design", ACI-ASCE Joint Committee on Limit Design, May 1960.

46. Baker, A.L.L.

The Ultimate Load Theory Applied to the Design of Reinforced and Prestressed Concrete Frames", Concrete Publication Ltd. (London), 1956.

47. Berwanger, Carl

"Limit Design by Successive Moment Distribution", Journal of the Structural Division, Proceedings of the American Society of Civil Engineers, V. 92, No. ST1, Feb., 1966.

48. Corley, W.G.

"Rotational Capacity of Reinforced Concrete Beams", Journal of the Structural Division, Proceedings of the American Society of Civil Engineers, V. 92, No. ST5, Oct. 1966, pp. 121.

49. Mattock, A.H.

"Rotational Capacity of Hinging Regions in Reinforced Concrete Beams", Proceedings of the International Symposium on Flexural Mechanics of Reinforced Concrete, Miami, Florida, Nov. 10-12, 1964.

50. Pfrang, E.O., C.P. Siess and M.A. Sozen

"Load-Moment-Curvature Characteristics of Reinforced Concrete Cross-Sections", Proceedings of the American Concrete Institute, V. 61, July, 1964.